Nonlinear Finite Element Analysis of Sheet Pile Interlocks

by

Mun Fong Chan

Dissertation submitted to the Faculty of the
Virginia Polytechnic Institute and State University
in partial fulfillment of the requirements for the degree of
DOCTOR OF PHILOSOPHY
in
Civil Engineering

APPROVED:

R.M. Barker (Chairman)

R.A. Heller

S.M. Holzer

K.B. Rojiani

T. Kuppusamy

November, 1985
Blacksburg, Virginia

NONLINEAR FINITE ELEMENT ANALYSIS OF SHEET PILE INTERLOCKS

by

Mun Fong Chan

(ABSTRACT)

A finite element program is developed to depict the behavior of a sheet pile interlock connection in an axial pull test. Two types of sheet piles, PS32 and PSX32, are considered. The thumb and finger in the interlock of a sheet pile will provide three contact points for connection with another sheet pile. The problem is highly nonlinear in nature which involves large deflections and rotations, elastic-plastic material response, and a nonlinear boundary effect due to multi-contact surfaces.

The Updated Lagrangian formulation is adopted in this study. When the response is in elastic range the Updated Lagrangian with Transformation is used while the Updated Lagrangian with Jaumann stress rate is employed when the element starts to yield. An elastic-plastic with isotropic strain hardening material model is used. The yielding of an element is detected by the Von Mises yield criterion. The finite element formulation also includes a moving contact algorithm to incorporate with both geometric and material

nonlinearities. Incremental potential of contact forces for a discretized system is constructed such that geometric compatibilities are maintained between contacting bodies. A method to calculate contact tractions from residual load of internal element stresses is employed. The incremental equilibrium equation is solved by a Newton-Raphson technique. Convergence criteria based on incremental displacement, incremental internal energy of the system, and the changes in contact forces can be chosen to advance or terminate the iteration process.

ACKNOWLEDGEMENTS

The author wishes to express his appreciation to Dr. R.M. Barker for his encouragement and guidance for the past three years. Thanks are also due to Dr. R.A. Heller, Dr. S.M. Holzer, Dr. T. Kuppusamy, and Dr. K.B. Rojiani for reviewing this dissertation and serving on the committee.

The author gives deep gratitude to all his friends in the Shultz Dinning Hall, the Hong Kong Club, and the Virginia Tech Volleyball Club for making his stay in Blacksburg so pleasant and memorable. Special thanks go to

for typing this dissertation and for her friendly and beautiful smiles.

Finally, truly unbounded thanks are due to the author's beloved family for their patience, understanding, and complete devotion.

TABLE OF CONTENTS

ABSTRACT ii

ACKNOWLEDGEMENTS iv

Chapter page

I. INTRODUCTION 1

Purpose and Scope 2
Survey of Literature on Sheet Pile Interlock Analysis 5
Survey of Literature on Nonlinear Finite Element Analysis 7
Survey of Literature on Contact Problems by Finite Element 11

II. FINITE ELEMENT FORMULATION FOR GEOMETRIC AND MATERIAL NONLINEARITIES 16

Geometric Nonlinearity 16
Notations of Variables 17
Incremental Equilibrium Equations 19
Finite Element Discretization 25
Material Nonlinearity 29
Elastic-Plastic Constitutive Model 31
Von Mises Yield Model and Isotropic Strain Hardening 33
Associated Flow Rule 35

III. FINITE ELEMENT FORMULATION FOR CONTACT PROBLEM . . 47

Modeling of Contact Surface 48
Conditions Governing Contact Forces at Contact Node 49
Potential of Contact Forces 50
Contact Potential for Sticking and Sliding Conditions 51
Finite Element Equations Including Contact Effects 54
Evaluations of Sticking and Sliding Conditions . 58
Distributed Traction and Resultant Forces in Contact Segment 60
Calculation of Contact Force Vector 61

IV. NONLINEAR NUMERICAL TECHNIQUE IN GEOMETRIC AND MATERIAL NONLINEAR PROBLEM 71

Solution Process 71
Convergence Criteria 72
Elastic-Plastic Stress Calculation 73
Verification of Geometric and Material Nonlinear Formulation 75
Test Problem 1 76
Test Problem 2 76

V. NUMERICAL TECHNIQUES IN CONTACT ALGORITHM 91

Determination of Contact Location 92
Convergence Criteria 94
Verification of Contact Algorithm 95
Hertz Contact Between Cylinder and Block . . 95
Buried Pipe with Overburden Pressure 98

VI. ANALYSIS OF SHEET PILE INTERLOCKS 119

Sheet Pile Analysis with no Sliding Among Contact Regions 120
Description of Finite Element Model 120
Finite Element Analysis 122
Results of Finite Element Analyses 123
Results of Test Set I 124
Results of Test Set II 125
Results of Test Set III 128
Sheet Pile Analysis with Sliding Among Contact Regions 129
Description of Finite Element Model 129
Finite Element Analysis 130
Results of Finite Element Analyses 131

VII. CONCLUSIONS, DISCUSSIONS, AND RECOMMENDATIONS . . 219

Summary and Discussions of Sheet Pile Analysis with no Sliding Allowed 219
Summary and Discussions of Sheet Pile Analysis with Sliding 221
Recommendations for Future Studies 223

REFERENCES 225

Appendix page

A. CALCULATION OF NODAL CONTACT TRACTIONS 235

VITA 238

LIST OF TABLES

Table — page

3.1. Contact Conditions of a Node as Decided by States of Adjoining Segments 64

4.1. Solution Algorithm for Elastic-Plastic Stress Calculation 78

6.1. Analyses on Sheet Pile Interlocks 138

6.2. Comparisons of Displacements Obtained from the Four-Node and the Eight-Node Element Meshes 139

6.3. Comparison of Axial and Bending Strains at Web (Sec. a-a) for 4-Node and 8-Node Element Meshes . . . 140

6.4. Displacement Versus Load for Three Contact Points on PS32 Sheet Piles 141

6.5. Displacement Versus Load for Three Contact Points on PSX32 Sheet Piles 142

6.6. Comparisons of Stresses for Two Elements which Exhibit Different Yielding Modes in PS32 Sheet Piles (20 k/in) 143

6.7. Comparisons of Stresses for Two Elements which Exhibit Different Yielding Modes in PSX32 Sheet Piles (26 k/in) 144

6.8. Displacement Versus Load for Three Contact Points on PS32 Sheet Piles with Effective Young's Modulus 145

6.9. Displacement Versus Load for Three Contact Points on PSX32 Sheet Piles with Effective Young's Modulus 146

6.10. Longitudinal Displacements at Contact Node Pairs in Case 3 147

6.11. Longitudinal Displacements at Contact Node Pairs in Case 4 148

6.12. Summary of Contact Condition at Maximum Load for PS32 Sheet Piles 149

6.13. Summary of Contact Condition at Maximum Load for PSX32 Sheet Piles 150

6.14. Lateral Displacement at Contactor-Target Nodes 1-6 in Case 1 151

6.15. Lateral Displacement at Contactor-Target Nodes 7-12 in Case 1 152

6.16. Lateral Displacement at Contactor-Target Nodes 13-18 in Case 1 153

6.17. Statics Check at Web Sections of Sheet Piles . . 154

6.18. Statics Check of Contact Forces with Loading . . 155

LIST OF FIGURES

Figure		page
2.1.	Generic Configurations of a System	42
2.2.	Mapping of a Four-Node Element	43
2.3.	Kinematic Strain Hardening	44
2.4.	Isotropic Strain Hardening	45
2.5.	Equivalent Stress Versus Equivalent Plastic Strain Curve	46
3.1.	Representations of Two Bodies in Contact	65
3.2.	Finite Element Discretization in Contact Region	66
3.3.	Interpolations of Contact Forces at Target Nodes	67
3.4.	Schematic Representation of a Contact Point with Definitions of Variables on the Contact Segment	68
3.5.	Calculation of Normal and Tangential Tractions from Nodal Force Vector	69
3.6.	Transformation of Global Tractions to Local Normal and Tangential Tractions	70
4.1.	Newton-Raphson Iteration	79
4.2.	Modified Newton-Raphson Iteration	80
4.3.	Combined Incremental Technique and Newton Raphson Iteration	81
4.4.	Solution Scheme Adopted in Computer Program	82
4.5.	Perforated Tension Strip (Theocaris and Marketos, 1964)	83
4.6.	Finite Element Mesh of Perforated Strip	84
4.7.	Development of Maximum Strain at Point of First Yield in Perforated Strip	85

4.8. Growth of Plastic Zone With Increasing Load in Perforated strip 86

4.9. Cantilever Under Uniformly Distributed Load 87

4.10. Finite Element Models of Cantilever 88

4.11. Tip Deflection Versus Load in Cantilever, Elastic Behavior 89

4.12. Cantilever---Combined Effects of Geometric and Material Nonlinearities (Eight Node Element Mesh) 90

5.1. Local System Used in Defining Target Segment . . . 100

5.2. Determination of Target Segment at which Contact will be Made 101

5.3. Location and Overlap of Contactor Node k 102

5.4. Situations for Different Values of !! 103

5.5. Location and Penetration of Contactor Node k Closest to the First Node of Target Segment 104

5.6. Location and Penetration of Contactor Node k Closest to the Last Node of Target Segment 105

5.7. Hertz Contact Problem Between Cylinder and Block . 106

5.8. Modeling of Hertz Problem by Four-node Elements . 107

5.9. Modeling of Hertz Problem by Eight-node Elements . 108

5.10. Contact Pressure Distributions for Contact Between Elastic Cylinder and Rigid Block 109

5.11. Nondimensional Normal Stress Plots Along Vertical Plane of Symmetry for Contact Between Elastic Cylinder and Block 110

5.12. Contact Pressure Distribution for Contact Between Ealstic-Plastic Cylinder and Rigid Block . . . 111

5.13. Comparison of Normal Stress Distribution Between Elastic and Elastic-Plastic Cases 112

5.14. Finite Element Modeling of Elastic Cylinder and Elastic Block 113

5.15. Contact Pressure Distribution for Contact Between Elastic Cylinder and Elastic Block 114

5.16. Normal Stress Distribution for Contact Between Elastic Cylinder and Elastic Block 115

5.17. Buried Pipe Subjected to Overburden Pressure . . 116

5.18. Finite Element Mesh for Analysis of Buried Pipe . 117

5.19. Computed Tractions Along Pipe-Soil Interface in Analysis of Buried Pipe 118

6.1. Typical Tensile Test of Sheet Pile 156

6.2. Portions of Sheet Piles Modeled for Analysis . . . 157

6.3. Details of Straight Web Piling (U.S. Steel Handbook) 158

6.4. Finite Element Meshes for PS32 and PSX32 Sheet Piles 159

6.5. Four-Node Finite Element Mesh for PSX32 Sheet Piles 160

6.6. Eight-Node Finite Element Mesh for PSX32 Sheet Piles 161

6.7. Locations in Sheet Piles at which Displacements are Tabulated 162

6.8. Sections on Sheet Piles for Statics Check 163

6.9. Locations of Elements in which Equivalent Stresses and Equivalent Strains are Calculated 164

6.10. Comparison of Strain Distributions at Webs for 4-Node and 8-Node Element Meshes 165

6.11. Comparisons of Stress Distributions for 4-Node and 8-Node Element Meshes 166

6.12. Load-Displacement Curve for Tip Deflection (Point 10) in PS32 Sheet Piles 167

6.13. Load-Displacement Curve for Tip Deflection (Point 10) in PSX32 Sheet Piles 168

6.14. Initial and Deformed Shapes of PS32 and PSX32 Sheet Piles 169

6.15. Axial Strain in Web Versus Load for PS32 Sheet Pile 170

6.16. Variations of Bending Strains Along Web with Loads (PS32) 171

6.17. Axial Strain in Web Versus Load for PSX32 Sheet Pile 172

6.18. Variations of Bending Strains Along Web with Loads (PSX32) 173

6.19. Plastic Zones on PS32 Sheet Piles at Different Loadings 174

6.20. Plastic Zones on PSX32 Sheet Piles at Different Loadings 175

6.21. Equivalent Stress Versus Equivalent Strain Plots for Three Typical Elements on PS32 Sheet Piles Model 176

6.22. Equivalent Stress Versus Equivalent Strain Plots for Three Typical Elements on PSX32 Sheet Piles Model 177

6.23. Statics Check at Web Section for PS32 Sheet Pile 178

6.24. Statics Check at Web Section for PSX32 Sheet Pile 179

6.25. Load-Displacement Curve for Tip Deflection (Point 10) in PS32 Sheet Piles with Effective E Value 180

6.26. Load-Displacement Curve for Tip Deflection (point 10) in PSX32 Sheet Piles with Effective E Value 181

6.27. Initial and Deformed Shapes of PS32 and PSX32 Sheet Piles with Effective E Value 182

6.28. Axial Strain Versus Load for PS32 Sheet Pile with Effective E Value 183

6.29. Variations of Bending Strains Along Web with Loads (PS32 With Effective E Value) 184

6.30. Axial Strain Versus Load for PSX32 Sheet Pile with Effective E Value 185

6.31. Variations of Bending Strains Along Web with Loads (PSX32 With Effective E Value) 186

6.32. Finite Element Modeling of Sheet Pile Interlocks 187

6.33. Contact Node Pairs in Sheet Pile Interlocks . . . 188

6.34. Maximum Displacement of PS32 Sheet Pile Interlocks 189

6.35. Maximum Displacement of PSX32 Sheet Pile Interlocks 190

6.36. Longitudinal Displacement Versus Load Plot for Contact Node Pair (5,6) in Case 1 191

6.37. Longitudinal Displacement Versus Load Plot for Contact Node Pair (11,12) in Case 1 192

6.38. Longitudinal Displacement Versus Load Plot for Contact Node Pair (17,18) in Case 1 193

6.39. Longitudinal Displacement Versus Load Plot for Contact Node Pair (5,6) in Case 2 194

6.40. Longitudinal Displacement Versus Load Plot for Contact Node Pair (11,12) in Case 2 195

6.41. Longitudinal Displacement Versus Load Plot for Contact Node Pair (17,18) in Case 2 196

6.42. Deformed Meshes Exhibiting Different Modes of Sliding 197

6.43. Average Lateral Displacement Versus Load Plot for Nodes 1-6 in Case 1 198

6.44. Average Lateral Displacement Versus Load Plot for Nodes 7-12 in Case 1 199

6.45. Average Lateral Displacement Versus Load Plot for Nodes 13-18 in Case 1 200

6.46. Average Lateral Displacement Versus Load Plot for Nodes 1-6 in Case 4 201

6.47. Average Lateral Displacement Versus Load Plot for Nodes 7-12 in Case 4 202

6.48. Average Lateral Displacement Versus Load Plot for Nodes 13-18 in Case 4 203

6.49. Comparison of Deformed Shapes of Sheet Pile Interlocks for Cases 1 and 3 204

6.50. Comparision of Bending Strain in Web 1 of Sheet Piles for Cases 1 and 3 205

6.51. Comparision of Bending Strain in Web 2 of Sheet Piles for Cases 1 and 3 206

6.52. Bending Strain Versus Load Plot for Web 1 of PS32 Sheet Piles 207

6.53. Bending Strain Versus Load Plot for Web 2 of PS32 Sheet Piles 208

6.54. Bending Strain Versus Load Plot for Web 1 of PSX32 Sheet Piles 209

6.55. Bending Strain Versus Load Plot for Web 2 of PSX32 Sheet Piles 210

6.56. Growth of Plastic Zone in PS32 Sheet Piles (Case 3) 211

6.57. Schematic Representation of Statics Check of Contact Forces in Sheet Pile 212

6.58. Normal Contact Force Versus Load for Case 1 . . . 213

6.59. Normal Contact Force Versus Load for Case 3 . . . 214

6.60. Normal Contact Force Versus Load for Case 4 . . . 215

6.61. Tangential Contact Force Versus Load Plot for Case 1 216

6.62. Tangential Contact Force Versus Load Plot for Case 3 217

6.63. Tangential Contact Force Versus Load Plot for Case 4 218

A.1. Contact Tractions and Nodal Forces on a Contact Segment 237

Chapter I

INTRODUCTION

The stability of a cellular cofferdam depends on three types of resistance. The first is shear resistance in a horizontal plane along the base of the cells to prevent sliding. The second is frictional resistance along vertical lines of sheet pile interlocks to prevent tilting or overturning. The final type is the interlock resistance to hoop forces provided by the tensile or pull-out strength of the sheet pile interlocks. The determinations of these resistance components are essentially done by empirical formulae based on past experience and limited experimental testing. In order to evaluate the accuracy of the previous models and to obtain a more cost effective design, an improved analytical procedure is needed.

In previous structural tests on the tensile behavior of sheet pile interlocks performed by Shannon & Wilson (1983), the load-deformation responses of the sheet piles were video taped. The video pictures clearly show a failure mechanism composed of material yielding, followed by deformations associated with the opening of the finger and thumb joint, and final failure when the interlocks slip past each other. An analytical tool is sought to model these complexities in the tensile behavior of the sheet pile interlock connection.

1.1 PURPOSE AND SCOPE

The purpose of this study is to develop an analytical tool that can predict the interlock stability of a cell. To achieve this objective, the tool shall be able to depict the load-displacement behavior of the sheet piles as observed in a laboratory pull test.

Previous modeling of the cell to behave as a perfect vessel underestimates considerably the bulge of the structure. Three factors which contribute to this inaccuracy in the analytical result are: forming of gaps in the interlock connection, misalignment in a cell due to slack in the interlock, and rotation and local yielding of the interlock. The first two factors are caused mainly in manufacturing and installation processes which are very difficult to represent by mathematical models. The presence of these slacks yields extra displacement and rotation other than those caused by straining and sliding of the sheet piles in a pull test. These additional displacement and rotation are responsible for the large displacement as observed in the early going of a tensile test. Modeling of these slacks requires a probabilistic approach to include the variations of the interlock geometry. However, this is beyond the scope of this study. Thus only the rotation, local yielding, and sliding between the interlocks will be considered.

A finite element computer program is developed to analyze the interlock behavior. Both four-node and eight-node isoparametric elements are implemented for generalized plane strain and plane stress conditions. Two types of straight-web sheet piles namely, the regular low carbon PS32 and the high strength PSX32, both manufactured by U. S. Steel, are studied. The straight web sheet pile contains a thumb and finger interlock which provides three contact regions for load transfer. Since significant deformation in the sheet pile may result from rotation and local yielding, the finite element formulation includes large rotation and displacement effects. The Updated Lagrangian approach is adopted for this purpose. The local yielding in the interlock is detected by a Von Mises yield criteria with an isotropic strain hardening rule. The Jaumann stress rate of second Piola-Kirchhoff stress is introduced to update the elasto-plastic stress increment because it is invariant with rotation. Details of both geometric and material nonlinearity modeling is given in Chapter II.

A moving contact algorithm which can be incorporated with the nonlinear material and geometric effects is developed in Chapter III. To include the effect of the contact forces, the total potential of these forces is included in a variational formulation to enforce geometric compatibilities

along the contact surfaces. The contact forces are evaluated from the internal stresses of the contacting bodies. These contact forces will be used later to determine the contact condition of the bodies.

Chapter IV discusses the numerical techniques used in solving the equilibrium equations obtained by geometric and material nonlinear formulation. The convergence criteria adopted and the calculation of the elastic-plastic stresses are also stated in the chapter. The validity of the program is then verified by analyzing two test problems in which the exact solutions are known.

Chapter V explains some of the numerical techniques used in the moving contact algorithm. These include the determination of overlap between two contacting bodies, the location of contact, and the convergence criteria adopted in advancing the incremental equilibrium iteration process. The last part of the chapter is devoted to verification of the contact algorithm by analyzing two test problems.

The computer program is used to model a simple pull-test on the sheet pile interlocks. Two sets of analyses are performed. The first set assumes no sliding among the contact regions in the interlocks while sliding as governed by Coulomb's friction is allowed in the second set of analyses. Chapter VI presents results of the sheet pile interlock ana-

lyses which contain load-deformation behavior, sliding among contact surfaces in the interlocks, and flexural characteristics in the web portion of the sheet pile. The chapter also provides results of elastic-plastic behavior of the interlock connection and statics check of load transfer through the contact areas.

Chapter VII contains conclusions and discussions of the analytical results. From these results a few recommendations are suggested for further studies.

1.2 SURVEY OF LITERATURE ON SHEET PILE INTERLOCK ANALYSIS

In the design of a cellular structure, a variety of methods can be used. These methods include the classical Terzaghi Method; the Tennessee Valley Authority Method; Corps of Engineers, U. S. Army Method; Bureau of Yards and Docks, Department of the Navy Method; Cummings Method; and Hansen's Method. Descriptions of these methods can be found in the paper by Belz (1970). To calculate the interlock tension, all these methods utilize a perfect vessel assumption for the cellular structure.

The TVA Method develops the logic and formulae to describe the maximum interlock forces which takes into account the effect of the arc connections. Rossow (1982) uses the basic hoop tension formula to incorporate with the deforma-

tion of the wye connection and derives the equilibrium equations for that section. The set of equations obtained is nonlinear and is solved numerically.

Only two papers can be found which address the analysis of the local forces in the interlocks subjected to pure tension. Bower (1973) develops the equilibrium equations for some critical sections of the interlocks by simple statics. Experimental results are used to determine the locations of these critical sections. The pull-out strength of the sheet pile is obtained when a failure mechanism of two plastic hinges are formed in the thumb and finger portions in either one of the interlocks. The other paper is a technical report by Kawasaki Steel Company (Nakanishi et al, 1981) which uses the finite element technique to determine the displacement and stress patterns of the interlocks under tensile loading. Constant strain triangular elements are chosen to model the interlocks. For analysis, the material remains in elastic range and the results obtained are used as input data for a shape optimization process.

1.3 SURVEY OF LITERATURE ON NONLINEAR FINITE ELEMENT ANALYSIS

A huge volume of literature has been written on the topic of nonlinear finite element analysis. The following will give a brief review of the recent developments in combined geometric and material nonlinear analyses which are pertinent to this research.

Combining both material and geometric nonlinearities is quite straightforward and can be most efficiently done by an incremental approach. Basically the incremental finite element equation of a continuum can be derived by the principle of virtual work. since geometrical nonlinear behavior is included, the deformed configuration of the system has to be used to derive the equilibrium equation. However, the deformed state is not known beforehand so some other known states have to be chosen as the reference configuration. Depending on the reference state used, different schemes can be distinguished. When all the static and kinematic variables are referred to an initial or undeformed configuration, it is known as the Lagrangian or Total Lagrangian approach. If the current state of the body is chosen as the reference, it is called the Eulerian approach. A third approach replaces the current state by the configuration of the body at the end of the previous step, this is known as the Mixed Lagrangian-Eulerian or Updated Lagrangian method. The Updated

Lagrangian approach is adopted in this research. Only those literatures related to this approach are reviewed below. A more comprehensive list of references on nonlinear analysis is given in books by Zienkeiwicz (1977), Bathe (1982), Oden (1972), and Cook (1974).

One of the early attempts to establish an Updated Lagrangian approach is given by Murray and Wilson (1965) in which a displaced local coordinate system is utilized to transform the nonlinear strain displacement relationship to a geometric transformation. Yaghmai and Popov (1971) derive the incremental equilibrium equation by taking the difference in virtual work done between two consecutive current configurations. Sharifi and Yates (1973) extend the method to include infinitesimal strain but large rotation. Hofmeister et al (1971) and Atluri (1973) form their equations from the principle of virtual work and introduce equilibrium check within each load increment. Gunasekera and Alexander (1972) obtain their equations from the principle of virtual work for a Prandtl-Reuss material but they do not define clearly the stress term used in their formulation. Another ambigious formulation is given by Argyris and Chan (1972) in which the stress and strain terms do not clearly represent a conjugate pair. A different approach is given by Osias and Swedlow (1974) who apply the Galerkin method on the rate

form of equilibrium equations governing the rate of loading upon a deformed solid. They also make use of the invariant Jaumann stress rate to solve large deformation problems. Hutchinson (1973) uses the variational principle on the incremental form of the virtual work done by a system and discusses the finite strain generalization of plastic flow theory. The Jaumann stress rate of second Piola-Kirchhoff stress is used in his work. McMeeking and Rice (1975) follow a similar approach and introduce the formulation for any arbitrary choice of conjugate stress and strain measures. An implicit form of incremental equation can be obtained from simplified kinematic and constitutive relationships (Bathe et al, 1974; Bathe et al, 1975; Stricklin et al, 1971; Stricklin et al, 1972; Stricklin and Haisler, 1974).

According to Bathe (1982), two kinds of formulation are identified for the updated formulation; the Updated Lagrangian with transformation approach (ULT) and the Updated Lagrangian with Jaumann stress rate approach (ULJ). The latter type is more appropriate for solving elastic-plastic problem with large deformations. Wunderlich (1976) has a similar scheme but he omits the initial displacement matrix by dropping some of the nonlinear kinematic terms within the increment. Desai et al (1978) and Banerjee and Fathallah (1979) adopt the ULJ method and apply it on solving geotech-

nical problems. Yamada (1972) and many others (Yamada et al, 1973; Yamada and Sakurai, 1977; Yamada et al, 1977; Yamada and Wifi, 1977) base their formulations on the virtual work equation and derive the stiffness equation which contains the initial stiffness matrix and the load correction factor for pertinent geometrically nonlinear behavior. To correct the effect of rotation of stress field, various definitions of strain and stress rates are introduced. Yamada et al (1973) show in their work that depending on the type of stress rate chosen, the system stiffness matrix may not be symmetrical. They also conclude that the Jaumann stress rate of the second Piola-Kirchoff stress will provide a symmetrical matrix and is suitable for elastic-plastic analyses.

A "natural" approach is developed by Argyris and Kleiber (1977) and refined by Argyris et al (1978) in which they introduce a distinct updated formulation by choosing an intermediate stress free state as the reference configuration. The nonlinear terms from the incremental strain to the incremental displacement relationship are neglected in their work. According to Gadala et al (1980; 1981), a fully nonlinear strain-displacement relationship shall in general be used. However, certain simplifications of the expressions may be achieved in special applications.

1.4 SURVEY OF LITERATURE ON CONTACT PROBLEMS BY FINITE ELEMENT

Because of the highly nonlinear nature involved in the analyses of contact problems, only a few of them have closed-form solutions. With the development of improved finite element techniques, it has become one of the most popular tools for solving the contact problems. Different types of finite element formulations can be found and will be explained in the following paragraphs.

The earliest attempt to use a displacement finite element formulation for solving contact between elastic bodies is given by Wilson and Parsons (1970) in which a differential displacement technique is employed. Ohte (1973) extended their approach to include friction in the contact surface. Chan and Tuba (1971) develop another method in which the contact force is calculated in each iteration by the amount of overlapping or separation of a point on the side of the contacting segment. Tsuta and Yamaji (1973) use equilibrium and compatibility conditions between contact surfaces to relate the incremental equilibrium equations for the contacting bodies. The system stiffness is modified everytime when there is a change in contact condition. A totally different approach of solving contact pressures from flexibility matrices is adopted by Francavilla and Zienkiewicz (1975). Their method is carried further by Sachdeva and Ramakrishnan

(1981) to include coulomb friction. A more general slip criteria to describe the friciton effects has also been studied (Torstenfelt, 1983). Fredriksson (1976) develops a consistent element contact force increment vector and an efficient iteration scheme by using a superelement technique. Gaertner (1977) employs yet another approach in which the nodal unknowns include displacements and their derivatives which are related to strains and stresses. However in his paper, the procedure for including the strains and stresses as unknowns are not clearly explained. Kumar et al (1980) also solve the elastic contact problem but in their algorithm the contact surface has to be known a-priori. Zimmermann and Liu (1980) study elasto-dynamics problems by modifying shape functions in the contact region in order to involve the nodes of the contacting surface. Their approach is unique and has many desirable characteristics in solving contact problems. However, no follow-up of their work can be found yet. For contact between an elastic body with a rigid system, a very simple and direct method is proposed (Rahman et al, 1984). Chang and Salamon (1984) also use a displacement approach to solve elasto-plastic contact problems. A master-slave relationship is employed to include the contact effect.

The second type of formulation for contact problem involves writing the contact conditions as inequality constraints in the total potential of the system. Oden and Kikuchi (1982) use exterior penalty method to solve elastic contact without friction. Oden and Campos (1981) include friction in their work by employing perturbation of the frictional effect to reduce the problem to a variational equality type. Lee and Byung (1984) treat the elasto-plastic contact as a minimization problem. A modified simplex mehtod is used to solve the quadratic programming problem.

In contact surfaces, the contact forces are not known and thus are required to be solved. This can be achieved directly by using the mixed finite element formulation since stresses can be included as unknowns. Pian and Kubomura (1981) introduce the contact tractions as Lagrangian multipliers in the variational formulation. With the change in contact conditions, only those terms in the system stiffness which correspond to the contact surface need to be adjusted. Tseng and Olson (1981) and Olson (1983) use a similar approach and derive multiplicative factors to scale the test load so that a change in the contact condition of one and only one node pair may occur. Ostachowicz (1984) adopts another mixed formulation by using a combination of rigid finite elements, finite elements, and gap elements. More

appropriately, his method should be classified as a displacement formulation with interface element which will be given next.

The usage of an interface element is the favorite approach in analysing soil-structure interaction problems. One of the earliest works is done by Goodman et al (1968) to model jointed rock. Since then both equilibrium and compatible interface elements have been developed. These are summarized in detail by Desai and Phan (1983). Herrmann (1978) derives a fictitious springs for normal and tangential direction at a contact node to study behavior of a reinforced concrete model. Okamoto and Nakazawa (1979) use a psuedo-contact element at which both equilibrium and compatibility conditions are satisfied at the interface. By doing so the unknown contact forces and displacements at contact points can be solved directly from a modified system stiffness which includes the contributions of contact effects. Yogeswaren (1983) utilizes the contact element approach together with a double-node constraint method to solve grouted cylindrical connections with circumferential shear stiffness. Katona (1983) uses a symmetric element constraint matrix and derives a global virtual work statement for the contact surfaces. Like most of the papers above, the algorithm is limited to node-to-node contact

only. In the above works the thickness of the contact element is assumed to be zero. A thin-layer interface element is developed by Desai et al (1985) and is found to be more effective than a zero-thickness element in analyzing contact problems. The choice of the element thickness is also suggested in their work.

So far all the works mentioned above are applicable only to small displacement problems. Petersson (1977) develops an initial-traction matrix due to contact forces and suggests using multi-constraint relations to solve the equilibrium equations. A total Lagrangian scheme is used. However an Updated Lagrangian scheme will give a simpler expression for the initial-traction matrix. Hughes et al (1977) investigate contact-impact problems by introducing a contact element stiffness matrix. Their work is extended by Simo et al (1984) in which a penalty function procedure is used. A tangent operator consistent with the contact/penalty algorithm is developed. A more recent work is presented by Bathe and Chaudhary (1985) who derive the potential of the contact forces which is added to the usual total potential of the systems. A scheme for solving the contact forces from the out-of-balance load vector is proposed. Since their approach allows node-to-internode contact which is desirable in modelling moving contact problem, it is followed quite closely in this study.

Chapter II

FINITE ELEMENT FORMULATION FOR GEOMETRIC AND MATERIAL NONLINEARITIES

In a general finite element analysis, different types of nonlinearities due to geometric, material, and boundary effects are identified. In this chapter, only the first two types of nonlinearities are considered. The geometric nonlinear formulation including both large displacement and large strain will be discussed first. This will be followed by material nonlinear formulation in which an elastic-plastic model is developed.

2.1 GEOMETRIC NONLINEARITY

According to Bathe (1982), the Updated Lagrangian approach is more appropriate in problems involving both large strain and material nonlinear behavior. Hence this approach is adopted in this research. To start the formulation of the Updated Lagrangian approach, it is necessary to define three typical configurations of a continuous system deforming under the application of external loads. Figure 2.1 illustrates the initial configuration of a system (load step 0) and its deformed configurations at steps n and the subsequent step n+1.

It is assumed that all the kinematic and static variables at step n are known. The aim is to establish the incremental finite element equilibrium equations for step n+1 with all variables referred to the configuration at step n. Tensor notations will be used in this chapter and matrix notations will be introduced whenever it is deemed necessary.

2.1.1 Notations of Variables

The coordinates of a generic point P (Fig. 2.1) in a body at the initial configuration are denoted as ${}^{0}x_i$ with i changing from 1 to 3 for a three dimensional space. Similarly the coordinates at the deformed configurations n and n+1 are given as ${}^{n}x_i$ and ${}^{n+1}x_i$ respectively. The notations for the displacements of the body is similar to those for the coordinates; namely, at step n the displacements are ${}^{n}U_i$. The incremental displacements are denoted as ΔU_i and can be written as

$$\Delta U_i = {}^{n+1}U_i - {}^{n}U_i \qquad (2.1)$$

or

$$\Delta U_i = {}^{n+1}x_i - {}^{n}x_i \qquad (2.2)$$

During different deformation stages of the body, its volume, area, specific mass, stresses, and strains are changing continuously. The volume, area, and specific mass at steps 0 and n are denoted as ${}^{0}V$, ${}^{n}V$, ${}^{0}A$, ${}^{n}A$, ${}^{0}\rho$, and ${}^{n}\rho$ respectively. Due to the referential nature of the Updated La-

grangian approach, the notations for the stresses and strains are comprised of three scripts. In analogy to the displacement and coordinate notations, a left superscript indicates the configuration in which the quantity occurs. In addition a left subscript indicates the configuration at which the quantity is measured and finally a right subscript indicates the direction or component of the quantity. For example, the second Piola-Kirchoff stresses at step n+1 measured in the configuration at step n are given as ${}^{n+1}_{n}S_{ij}$ with i and j changing from 1 to 3. However, an exception is made by dropping the left subscript when the quantity under consideration occurs in the same configuration in which it is also measured. For example, the Cauchy stresses will be written as ${}^{n}\tau_{ij}$ instead of ${}^{n}_{n}\tau_{ij}$.

In the formulation of the incremental equilibrium equations, the derivatives of displacements and coordinates are needed. In this report a comma represents differentiation with respect to the coordinate following it, a left superscript indicates the configuration in which the quantity occurs and a left subscript indicates the configuration in which the coordinate is measured, for example

$$ {}^{n+1}_{0}U_{i,j} = \partial {}^{n+1}U_i / \partial {}^{0}x_j \qquad (2.3) $$

and

$$ {}^{n}_{n+1}x_{i,j} = \partial {}^{n}x_i / \partial {}^{n+1}x_j \qquad (2.4) $$

2.1.2 Incremental Equilibrium Equations

The incremental equilibrium equations of a body at two consecutive steps can be derived from the principle of virtual work. Consider a body in equilibrium at step n, the virtual work done by the body is given as

$$\int_{{}^{n}V} {}^{n}\tau_{ij}\delta {}^{n}e_{ij}\, {}^{n}dV = {}^{n}R \tag{2.5}$$

The left hand side is the internal work done where ${}^{n}\tau_{ij}$ is the Cauchy stress tensor and $\delta {}^{n}e_{ij}$ is the variation of the infinitesimal strain tensor which is defined as

$$\delta {}^{n}e_{ij} = \delta\tfrac{1}{2}(\partial\Delta U_i/\partial {}^{n}x_j + \partial\Delta U_i/\partial {}^{n}x_i)$$

$$= \tfrac{1}{2}(\partial\delta\Delta U_i/\partial {}^{n}x_j + \partial\delta\Delta U_j/\partial {}^{n}x_i) \tag{2.6}$$

${}^{n}R$ is the external work done and is given as

$${}^{n}R = \int_{{}^{n}V} {}^{n}f_i^B \delta\Delta U_i\, {}^{n}dV + \int_{{}^{n}S} {}^{n}f_i^S \delta\Delta U_i\, {}^{n}dS \tag{2.7}$$

where ${}^{n}f_i^B$ and ${}^{n}f_i^S$ are components of the externally applied body and surface force vectors respectively, and δU_i is the i component of the virtual incremental displacement vector.

A similar expression can be formed for the body at step n+1

$${}^{n+1}R = \int_{{}^{n+1}V} {}^{n+1}\tau_{ij}\delta {}^{n+1}e_{ij}\, {}^{n+1}dV \tag{2.8}$$

since the volume and area at this configuration are not known, the expression is rewritten with respect to the con-

figuration at step n. To measure the Cauchy stress tensor per unit area in configuration n, the second Piola-Kirchoff stress tensor ${}^{n+1}_{n}S_{ij}$ is used in order to keep the stress tensor symmetric. A detailed derivation can be found in the books by Fung (1965), and Malvern (1969). The transformations between ${}^{n+1}\tau_{ij}$ and ${}^{n+1}_{n}S_{ij}$ are

$$ {}^{n+1}_{n}S_{ij} = ({}^{n}\rho/{}^{n+1}\rho)\cdot {}^{n}_{n+1}x_{i,k}\cdot {}^{n}_{n+1}x_{j,l}\cdot {}^{n+1}\tau_{kl} \qquad (2.9) $$

or

$$ {}^{n+1}\tau_{ij} = ({}^{n+1}\rho/{}^{n}\rho)\cdot {}^{n+1}_{n}x_{i,k}\cdot {}^{n+1}_{n}x_{j,l}\cdot {}^{n+1}_{n}S_{kl} \qquad (2.10) $$

The ratio of the specific mass is obtained by the determinant of the transformation matrix which is essentially a measure of volume change of a continuum at different steps. Thus

$$ {}^{n}\rho/{}^{n+1}\rho = \det\left[{}^{n}_{n+1}J\right] \qquad (2.11) $$

where

$$ \left[{}^{n}_{n+1}J\right] = \left[\partial {}^{n}x_i/\partial {}^{n+1}x_j\right] \qquad (2.12) $$

At this point a Green-Lagrange strain tensor is introduced into the formulation which is energetically conjugate to the second Piola- Kirchoff stress tensor (Hill, 1959), i.e.,

$$ \int_{{}^{n+1}V} {}^{n+1}\tau_{ij}\,\delta\,{}^{n+1}e_{ij} = \int_{{}^{n}V} {}^{n+1}_{n}S_{ij}\,\delta\,{}^{n+1}_{n}\varepsilon_{ij}\,{}^{n}dV \qquad (2.13) $$

where

$$ {}^{n+1}_{n}\varepsilon_{ij} = {}^{n}\varepsilon_{ij} = \frac{1}{2}({}_{n}\Delta U_{i,i} + {}_{n}\Delta U_{j,j} + {}_{n}\Delta U_{k,i}\cdot{}_{n}\Delta U_{k,j}) \qquad (2.14) $$

or

$$ {}^{n}\varepsilon_{ij} = {}^{n}e_{ij} + {}^{n}\eta_{ij} \qquad (2.15) $$

${}^{n}e_{ij}$ is the same infinitesimal strain tensor defined earlier and ${}^{n}\eta_{ij}$ is the nonlinear strain tensor given as

$$ {}^{n}\eta_{ij} = \frac{1}{2}\cdot{}_{n}\Delta U_{k,i}\cdot{}_{n}\Delta U_{k,j} \qquad (2.16) $$

It follows that the variation of the Green-Lagrange strain is

$$ \delta\,{}^{n+1}_{n}\varepsilon_{ij} = \delta\,{}^{n}e_{ij} + \delta\,{}^{n}\eta_{ij} \qquad (2.17) $$

Using second Piola-Kirchoff stress and Green-Lagrange strain tensors, Equation (2.8) can be written as

$$ \int_{{}^{n}V} {}^{n+1}_{n}S_{ij}\,\delta\,{}^{n+1}_{n}\varepsilon_{ij}\,{}^{n}dV = {}^{n+1}R \qquad (2.18) $$

the second Piola-Kirchoff stress term can be arbitrary decomposed into two terms (Yaghmai and Popov, 1971)

$$ {}^{n+1}_{n}S_{ij} = {}^{n}\tau_{ij} + \Delta\,{}^{n}S_{ij} \qquad (2.19) $$

$\Delta\,{}^{n}S_{ij}$ is the incremental second Piola-Kirchoff stress and is related to the incremental Green-Lagrange strain by

$$ \Delta\,{}^{n}S_{ij} = {}^{n}C_{ijrs}\,{}^{n}\varepsilon_{rs} \qquad (2.20) $$

where ${}^{n}C_{ijrs}$ is the fourth order incremental constitutive tensor and will be discussed later in the chapter. Thus, Equation (2.18), together with Equation (2.19), becomes

$$\int_{{}^{n}V} ({}^{n}\tau_{ij} + \Delta^{n}S_{ij})\delta {}^{n+1}_{n}\varepsilon_{ij}\, {}^{n}dV = {}^{n+1}R \tag{2.21}$$

Recall the virtual work equations of the body at step n, Equation (2.5)

$$\int_{{}^{n}V} {}^{n}\tau_{ij}\delta {}^{n}e_{ij}\, {}^{n}dV = {}^{n}R$$

substitute Equation (2.17) in Equation (2.21) and subtract Equation (2.5) from it, the incremental virtual work done is given as

$$\int_{{}^{n}V} ({}^{n}\tau_{ij}\delta {}^{n}\eta_{ij} + \Delta^{n}S_{ij}\delta {}^{n}\varepsilon_{ij})\, {}^{n}dV = {}^{n+1}R - \int_{{}^{n}V} {}^{n}\tau_{ij}\delta {}^{n}e_{ij}\, {}^{n}dV \tag{2.22}$$

The external virtual work done at step n+1 has to be re-written also. For a deformation-independent loading, the law of conservation of mass can be used and ${}^{n+1}R$ is given as

$$\int_{{}^{n+1}V} {}^{n+1}\rho\, {}^{n+1}f_i^B \delta\Delta U_i\, {}^{n+1}dV + \int_{{}^{n+1}S} {}^{n+1}f_i^S \delta\Delta U_i\, {}^{n+1}dS$$

$$= \int_{{}^{0}V} {}^{0}\rho\, {}^{n+1}_{0}f_i^B \delta\Delta U_i\, {}^{0}dV + \int_{{}^{0}S} {}^{n+1}_{0}f_i^S \delta\Delta U_i\, {}^{0}dS \tag{2.23}$$

noting that

$${}^{n+1}\rho\, {}^{n+1}f_i^B\, {}^{n+1}dV = {}^{0}\rho\, {}^{n+1}_{0}f_i^B\, {}^{0}dV \tag{2.24}$$

and

$${}^{n+1}f_i^S\, {}^{n+1}dS = {}^{n+1}_{0}f_i^S\, {}^{0}dS \tag{2.25}$$

where ${}^{n+1}_{0}f_i^B$ and ${}^{n+1}_{0}f_i^S$ denote the body force per unit mass and the surface traction per unit area acting in configuration n+1 but measured in terms of the coordinates in co-

nfiguration 0. If the loading is deformation-dependent such as pressure, Bathe (1982) suggests to approximate the external work done by

$$\int_{{}^{n+1}S} {}^{n+1}f_i^S \delta U_i \, {}^{n+1}dS = \int_{{}^{n+1}S_{(K-1)}} {}^{n+1}f_i^S \delta U_i \, {}^{n+1}dS^{(K-1)} \qquad (2.26)$$

where (K-1) indicates that the integration is performed over the volume and area last calculated in the iteration. A small load step has to be used in order to obtain a good approximation. It has to be pointed out here that a non-symmetrical contribution of the pressure loads to the stiffness matrix is neglected for computation efficiency (Bathe, et al, 1975).

Equation (2.22) cannot be solved directly since it is nonlinear in the displacement increments. However it can be approximated by linearizing the Green-Lagrange strain terms, i.e.,

$$ {}^{n}\varepsilon_{ij} = {}^{n}e_{ij} \qquad (2.27)$$

$$ \delta {}^{n}\varepsilon_{ij} = \delta {}^{n}e_{ij} \qquad (2.28)$$

and

$$ \Delta {}^{n}S_{ij} = {}^{n}C_{ijrs} \, {}^{n}e_{rs} \qquad (2.29)$$

Making use of the above linearizations, Equation (2.22) can be rewritten as

$$\int_{{}^{n}V} {}^{n}\tau_{ij} \delta {}^{n}\eta_{ij} \, {}^{n}dV + \int_{{}^{n}V} {}^{n}C_{ijrs} \, {}^{n}e_{rs} \delta {}^{n}e_{ij} \, {}^{n}dV$$

$$= {}^{n+1}R - \int_{{}^{n}V} {}^{n}\tau_{ij}\delta {}^{n}e_{ij}\, {}^{n}dV \qquad (2.30)$$

Equation (2.30) is the approximate incremental virtual work formulated at the load step n+1 and referred to the configuration n. The equations will be solved for the incremental displacements, strains, and stresses. To improve the accuracy of the solution, equilibrium iterations on the residual load vector are carried out within each load step. The residual load vector is the unbalanced virtual work done by the external and internal loads and is given as

$$ {}^{n+1}R - \int_{{}^{n+1}V(K)} {}^{n+1}\tau_{ij}^{(K)}\delta {}^{n+1}e_{ij}^{(K)}\, {}^{n+1}dV \qquad (2.31)$$

where the right superscript (K) represents results obtained in the Kth iteration. Thus using Updated Lagrangian approach the equations solved repetitively, for K=1,2,3,..., is

$$\int_{{}^{n}V} {}^{n}C_{ijrs}\, {}^{n}e_{rs}^{(K)}\delta {}^{n}e_{ij}\, {}^{n}dV + \int_{{}^{n}V} {}^{n}\tau_{ij}\delta {}^{n}\eta_{ij}^{(K)}\, {}^{n}dV$$

$$= {}^{n+1}R - \int_{{}^{n+1}V(K-1)} {}^{n+1}\tau_{ij}^{(K-1)}\delta {}^{n+1}e_{ij}^{(K-1)}\, {}^{n+1}dV \qquad (2.32)$$

where K=1 corresponds to Equation (2.30), and the displacements are updated as follows

$$ {}^{n+1}U_i^{(K)} = {}^{n+1}U_i^{(K-1)} + \Delta U_i^{(K)} \qquad (2.33)$$

and

$$ {}^{n+1}U_i^{(0)} = {}^{n}U_i \qquad (2.34)$$

A certain convergence criterium is chosen to stop the iterations and this will be discussed later. The whole process is repeated until the last load step is reached.

2.1.3 Finite Element Discretization

For the Updated Lagrangian formulation, the incremental equilibrium equation is given by Equation (2.30) and is copied here

$$\int_{n_V} {}^{n}\tau_{ij}\delta^{n}\eta_{ij}\,{}^{n}dV + \int_{n_V} {}^{n}C_{ijrs}\,{}^{n}e_{rs}\delta^{n}e_{ij}\,{}^{n}dV$$

$$= {}^{n+1}R - \int_{n_V} {}^{n}\tau_{ij}\delta^{n}e_{ij}\,{}^{n}dV$$

Let $\left[{}^{n}_{n}B_{L}\right]$ and $\left[{}^{n}_{n}B_{NL}\right]$ be the linear and nonlinear strain-displacement transformation matrices, $\left[{}^{n}C\right]$ be the incremental constitutive matrix, $\left[{}^{n}\tau\right]$ be the Cauchy stress matrix, and $\left[{}^{n}\hat{\tau}\right]$ be a vector of Cauchy stresses. These matrices will be derived in details later. Then Equation (2.30) can be rewritten as

$$\left(\left[{}^{n}_{n}K_{L}\right] + \left[{}^{n}_{n}K_{NL}\right]\right)\left[U\right] = \left[{}^{n+1}R\right] - \left[{}^{n}F\right] \qquad (2.35)$$

where

$$\left[{}^{n}_{n}K_{L}\right] = \int_{n_V}\left[{}^{n}_{n}B_{L}\right]^{T}\left[{}^{n}C\right]\left[{}^{n}_{n}B_{L}\right]{}^{n}dV \qquad (2.36)$$

$$\left[{}^{n}_{n}K_{NL}\right] = \int_{n_V}\left[{}^{n}_{n}B_{NL}\right]^{T}\left[{}^{n}\tau\right]\left[{}^{n}_{n}B_{NL}\right]{}^{n}dV \qquad (2.37)$$

$$\begin{bmatrix} {}^{n}F \end{bmatrix} = \int_{{}^{n}V} \begin{bmatrix} {}^{n}B_L \end{bmatrix}^T \begin{bmatrix} {}^{n}\hat{\tau} \end{bmatrix} {}^{n}dV \tag{2.38}$$

In this study, the four-node and eight-node elements are used. For simplicity only the matrices for a single four-node element are derived. The same process can be applied on the eight-node element. The assembly process for a system of elements will follow the standard procedures used in general finite element analysis (Bathe, 1982, Zienkiewiez, 1977).

For an element the coordinates and displacements are interpolated by

$${}^{n}x_i = \sum_{j=1}^{4} N_j \, {}^{n}x_i^j \tag{2.39}$$

$${}^{n}U_i = \sum_{j=1}^{4} N_j \, {}^{n}U_i^j \tag{2.40}$$

for i=1 to 2 where ${}^{n}x_i^j$ is the coordinate of nodal point j in direction i at load step n, ${}^{n}U_i^j$ is defined similarly, and N_j is the Lagrange interpolation function given as follows. Consider a typical four-node element (Fig. 2.2), the interpolation functions are

$$N_1 = \tfrac{1}{4}(1-r)(1-s)$$

$$N_2 = \tfrac{1}{4}(1-r)(1+s)$$

$$N_3 = \tfrac{1}{4}(1+r)(1+s) \tag{2.41}$$

$$N_4 = \frac{1}{4}(1+r)(1-s)$$

To obtain $\begin{bmatrix} {}^nB_L \end{bmatrix}$ and $\begin{bmatrix} {}^nB_{NL} \end{bmatrix}$, the following derivatives are required

$$ {}^nU_{i,j} = \sum_{K=1}^{4} ({}^nN_{K,j}) U_i^K \tag{2.42}$$

Since the shape functions N_k refer to the local coordinate system, proper transformation is needed. By chain rule the derivatives are related by

$$\begin{bmatrix} \partial/\partial r \\ \partial/\partial s \end{bmatrix} = \begin{bmatrix} \partial {}^nx_1/\partial r & \partial {}^nx_2/\partial r \\ \partial {}^nx_1/\partial s & \partial {}^nx_2/\partial s \end{bmatrix} \begin{bmatrix} \partial/\partial {}^nx_1 \\ \partial/\partial {}^nx \end{bmatrix} \tag{2.43}$$

Inverting the operator one gets

$$\begin{bmatrix} \partial/\partial {}^nx_1 \\ \partial/\partial {}^nx_2 \end{bmatrix} = \frac{1}{\det|J|} \begin{bmatrix} \partial {}^nx_2/\partial s & -\partial {}^nx_2/\partial r \\ -\partial {}^nx_1/\partial s & \partial {}^nx_1/\partial r \end{bmatrix} \begin{bmatrix} \partial/\partial r \\ \partial/\partial s \end{bmatrix} \tag{2.44}$$

where the determinant of the Jacobian matrix is

$$\det[J] = \frac{\partial {}^nx_1}{\partial r} \cdot \frac{\partial {}^nx_2}{\partial s} - \frac{\partial {}^nx_1}{\partial s} \cdot \frac{\partial {}^nx_2}{\partial r} \tag{2.45}$$

The transformations of integrals are also needed when the matrices are evaluated, this can be achieved by the following

$$\iint_{D(x_1,x_2)} f(x_1,x_2)\,dx_1 dx_2 = \iint_{D(r,s)} f(r,s)\det[J]\,dr\,ds \tag{2.46}$$

where D represents the domain of the integral.

From definitions of ${}^{n}e_{ij}$ and ${}^{n}\eta_{ij}$, the $\left[{}^{n}B_{L}\right]$ and $\left[{}^{n}B_{NL}\right]$ matrices can be constructed. It can be shown easily that

$$\left[{}^{n}e\right] = \left[{}^{n}B_{L}\right]\left[U\right]$$

where

$$\left[{}^{n}B_{L}\right] = \begin{bmatrix} {}^{n}N_{1,1} & 0 & {}^{n}N_{2,1} & 0 & {}^{n}N_{3,1} & 0 & {}^{n}N_{4,1} & 0 \\ 0 & {}^{n}N_{1,2} & 0 & {}^{n}N_{2,2} & 0 & {}^{n}N_{3,2} & 0 & {}^{n}N_{4,2} \\ {}^{n}N_{1,2} & {}^{n}N_{1,1} & {}^{n}N_{2,2} & {}^{n}N_{2,1} & {}^{n}N_{3,2} & {}^{n}N_{3,1} & {}^{n}N_{4,2} & {}^{n}N_{4,1} \end{bmatrix} \tag{2.47}$$

and

$$\left[U\right]^{T} = \left[U_1^1 \; U_2^1 \; U_1^2 \; U_2^2 \; U_1^3 \; U_2^3 \; U_1^4 \; U_2^4\right] \tag{2.48}$$

which is the incremental displacement vector and is given as

$$U_j^k = {}^{n+1}U_j^k - {}^{n}U_j^k = \Delta U_j^k \tag{2.49}$$

For $\left[{}^{n}B_{NL}\right]$, from Equations (2.16) and (2.49), the variation of the nonlinear strain term is

$$\delta\,{}^{n}\eta_{ij} = \delta\left(1/2\,{}^{n}U_{k,i}\cdot{}^{n}U_{k,j}\right) \tag{2.50}$$

After taking the variation the 1/2 term will drop and the expression will be in terms of δU. A more compact way of writing the second term in Equation (2.30) is

$$\int_{n_V} {}^{n}\tau_{ij}\,\delta\,{}^{n}\eta_{ij}\,{}^{n}dV = \left[\delta U\right]^{T}\left(\int_{n_V}\left[{}^{n}B_{NL}\right]^{T}\left[{}^{n}\tau\right]\left[{}^{n}B_{NL}\right]{}^{n}dV\right)\left[U\right] \tag{2.51}$$

where

$$\begin{bmatrix} {}^{n}B_{NL} \end{bmatrix} = \begin{bmatrix} {}^{n}N_{1,1} & 0 & {}^{n}N_{2,1} & 0 & {}^{n}N_{3,1} & 0 & {}^{n}N_{4,1} & 0 \\ {}^{n}N_{1,2} & 0 & {}^{n}N_{2,2} & 0 & {}^{n}N_{3,2} & 0 & {}^{n}N_{4,2} & 0 \\ 0 & {}^{n}N_{1,1} & 0 & {}^{n}N_{2,1} & 0 & {}^{n}N_{3,1} & 0 & {}^{n}N_{4,1} \\ 0 & {}^{n}N_{1,2} & 0 & {}^{n}N_{2,2} & 0 & {}^{n}N_{3,2} & 0 & {}^{n}N_{4,2} \end{bmatrix} \tag{2.52}$$

and

$$\begin{bmatrix} {}^{n}\tau \end{bmatrix} = \begin{bmatrix} {}^{n}\tau_{11} & {}^{n}\tau_{12} & 0 & 0 \\ {}^{n}\tau_{12} & {}^{n}\tau_{22} & 0 & 0 \\ 0 & 0 & {}^{n}\tau_{11} & {}^{n}\tau_{12} \\ 0 & 0 & {}^{n}\tau_{12} & {}^{n}\tau_{22} \end{bmatrix} \tag{2.53}$$

To obtain Equation (2.38), the Cauchy vector is required. The vector is written as $\begin{bmatrix} {}^{n}\hat{\tau} \end{bmatrix}^{T} = \begin{bmatrix} {}^{n}\tau_{11} & {}^{n}\tau_{22} & {}^{n}\tau_{12} & {}^{n}\tau_{33} \end{bmatrix}$.

2.2 MATERIAL NONLINEARITY

After discretization the finite element equilibrium equations contain both the kinematic and constitutive matrices. Therefore it is essential that an appropriate constitutive model is used in order to depict the behavior of the system. In this study an elastic-plastic model is used for steel and its constitutive matrix will be derived in the following

sections. In Bathe's book (1981), other types of material models are discussed.

For hypoelastic material the constitutive matrix relates increments in stresses to increments in strains. That is to say, the total stress depends on the path of deformation. A stress rate is often used to describe this kind of material. When large displacements and rotations are involved, the stress rate chosen must be invariant with respect to rigid body motions. A widely used stress rate is the Jaumann stress rate which, at step n, is defined as

$$ {}^{n}\tau_{ij}^{\ J} = \frac{D}{Dt}{}^{n}\tau_{ij} - {}^{n}\tau_{ip}\,{}^{n}\Omega_{pj} - {}^{n}\tau_{jp}\,{}^{n}\Omega_{pi} \qquad (2.54) $$

where D /Dt denotes the time derivative with constant coordinates. The time derivative in here is the subdivisions of the incremental load step. Also

$$ {}^{n}\Omega_{pj} = \frac{1}{2}\frac{D}{Dt}({}^{n}\Delta U_{j,p} - {}^{n}\Delta U_{p,j}) \qquad (2.55) $$

which is the Cartesian components of the spin tensor. The Jaumann stress rate is related to the infinitesimal strain rate as follows

$$ {}^{n}\tau_{ij}^{\ J} = {}^{n}C_{ijrs}\,\frac{D}{Dt}{}^{n}e_{rs} \qquad (2.56) $$

To implement the stress rate approach, Equation (2.19) is modified as

$$ {}^{n+1}_{n}S_{ij} = {}^{n}\tau_{ij} + D^{n}\tau_{ij} \qquad (2.57) $$

where D signifies 'discrete increment' in , i.e.,

$$D^{n}e_{rs} = {}^{n}e_{rs} \tag{2.58}$$

Rearrange Equation (2.55) together with Equations (2.56) and (2.58)

$$\begin{aligned} D^{n}\tau_{ij} &= {}^{n}\tau_{ij}{}^{J}Dt + ({}^{n}\tau_{ip}{}^{n}\Omega_{pj} + {}^{n}\tau_{jp}{}^{n}\Omega_{pi})Dt \\ &= {}^{n}C_{ijrs}{}^{n}e_{rs} + ({}^{n}\tau_{ip}{}^{n}\Omega_{pj} + {}^{n}\tau_{jp}{}^{n}\Omega_{pi})Dt \end{aligned} \tag{2.59}$$

Substitute Equations (2.57) and (2.59) into Equation (2.30), noting that the term ${}^{n}C_{ijrs}\frac{D}{Dt}{}^{n}e_{rs}$ is much greater than ${}^{n}\tau_{ip}{}^{n}\Omega_{pj}$ terms in general, $D^{n}\tau_{ij}$ can be approximated by ${}^{n}C_{ijrs}{}^{n}e_{rs}$. It should be pointed out that the full expression Equation (2.59) is used when the plastic stresses are updated. After the substitutions and approximation, the incremental equilibrium equation remains identical to Equation (2.30). This formulation is named as the ULJ approach by Bathe et al (1974) and is appropriate for large strain condition also (Bathe,1981).

2.2.1 Elastic-plastic Constitutive Model

In this study the generalized Hooke's law is used for a body behaving in the elastic range. The material matrix is formed from two elastic constants E and ν, which are Young's modulus and Poisson's ratio, respectively. In a general two dimensional problem, the stress and strain are related as follows

$$[\sigma] = [C][e] \tag{2.60}$$

where

$$[\sigma] = \begin{bmatrix} \sigma_{11} \\ \\ \sigma_{22} \\ \\ \sigma_{12} \\ \\ \sigma_{33} \end{bmatrix} \quad \text{and} \quad [e] = \begin{bmatrix} e_{11} \\ \\ e_{22} \\ \\ e_{12} \\ \\ e_{33} \end{bmatrix} \tag{2.61}$$

and

$$[C] = \frac{E}{(1+\nu)} \begin{bmatrix} \frac{1-\nu}{1-2\nu} & \frac{\nu}{1-2\nu} & 0 & \frac{\nu}{1-2\nu} \\ \\ \frac{\nu}{1-2\nu} & \frac{1-\nu}{1-2\nu} & 0 & \frac{\nu}{1-2\nu} \\ \\ 0 & 0 & \frac{1}{2} & 0 \\ \\ \frac{\nu}{1-2\nu} & \frac{\nu}{1-2\nu} & 0 & \frac{1-\nu}{1-2\nu} \end{bmatrix} \tag{2.62}$$

It is clear that $\begin{bmatrix} {}^{n}C \end{bmatrix}$ is constant in elastic analysis and is given by Equation (2.62). To obtain the constitutive matrix for plane strain analysis, one can simply cross out the row and column corresponding to the strain ε_{33}. This will leave a 3x3 upper left matrix in Equation (2.62). For plane

stress analysis, static condensation is used on the stress to obtain the required 3x3 matrix (Bathe et al, 1974).

In the theory of plasticity, three criteria are used to describe the plastic behavior of a continuum. They are

1) A yield function which specifies the stress state at which the material yields

2) A flow rule which relates the plastic strain increments to the stress increments during the event of plastic flow

3) A hardening rule which modifies the yield surface during plastic flow

Each criterion has many different theories and it is not the intention of this report to present these. Only those which are applied in this study will be discussed. Additional information on plasticity can be found in books by Drucker (1960), Hill (1950), and Washizu (1977).

2.2.2 Von Mises Yield Model and Isotropic Strain Hardening

The Von Mises model is used in this study because of its simplicity and its relevance in metal plasticity. Mathematically, the yield criterion is defined by a yield surface with the function

$$F({}^{n}\sigma, {}^{n}e^{P}) = 1/2({}^{n}S_{ij}{}^{d} - {}^{n}\alpha_{ij})({}^{n}S_{ij}{}^{d} - {}^{n}\alpha_{ij}) - {}^{n}\mu \qquad (2.63)$$

where the deviatoric stresses are given as

$${}^{n}S_{ij}{}^{d} = {}^{n}\sigma_{ij} - \frac{{}^{n}\sigma_{mm}}{3}\delta_{ij} \qquad (2.64)$$

δ_{ij} is the Kronecker delta and is defined as

$$\delta_{ij} = 0 \quad \text{for} \quad i = j \qquad (2.65)$$
$$= 1 \qquad\qquad i = j$$

and

$$^{n}\mu = \frac{1}{3}\,{}^{n}\sigma_y{}^{2} \qquad (2.66)$$

with $^{n}\sigma_y$ as the yield stress in simple tension and is a function of the plastic work done.

In Equation (2.63), $^{n}\alpha_{ij}$ is a strain hardening parameter which governs the translation of the yield surface. There are two types of strain hardening rules: kinematic hardening and isotropic hardening. For kinematic hardening material, the yield surface only translates with the yield surface shape remaining constant (Fig.2.3). Isotropic hardening occurs when the yield surface expands uniformly but without translation and rotation (Fig.2.4). In this study the isotropic hardening rule is used for both the regular and high strength steels. It is clear that for isotropic hardening, including elastic perfectly plastic case, the $^{n}\alpha_{ij}$ term will vanish. Thus, Equation (2.63) reduces to

$$F = \frac{1}{2}\,{}^{n}S_{ij}{}^{d}\,{}^{n}S_{ij}{}^{d} - \frac{1}{3}\,{}^{n}\sigma_y{}^{2} \qquad (2.67)$$

when yielding occurs, the function F and its differential form are both zero, i.e.,

$$\frac{1}{2}\,{}^{n}S_{ij}{}^{d}\,{}^{n}S_{ij}{}^{d} = \frac{1}{3}\,{}^{n}\sigma_y{}^{2} \qquad (2.68)$$

and

$$ {}^{n}S_{ij}{}^{d}\, d{}^{n}S_{ij}{}^{d} = \frac{2}{3}\, {}^{n}\sigma_{y}\, d{}^{n}\sigma_{y} \tag{2.69} $$

2.2.3 Associated Flow Rule

A basic assumption in incremental theory of plasticity is that during plastic deformation, the material is incompressible, i.e., (Popov, 1981)

$$ de_{11}{}^{P} + de_{22}{}^{P} + de_{33}{}^{P} = 0 \tag{2.70} $$

Define

$$ de_{ij}{}'^{P} = de_{ij}{}^{P} - \frac{1}{3}\, de_{kk}{}^{P}\delta_{ij} \tag{2.71} $$

as the deviatoric plastic strain increment, it is obvious from Equation (2.70) that

$$ de_{ij}{}'^{P} = de_{ij}{}^{P} \tag{2.72} $$

The general flow rule is given as

$$ de_{ij}{}^{P} = d\lambda(\partial F/\partial {}^{n}\sigma_{ij}) \tag{2.73} $$

Equation (2.73) is the associated flow rule when it is used with the Von Mises criterion. $d\lambda$ is an unknown scalar. It can be shown that

$$ \partial F/\partial {}^{n}\sigma_{ij} = {}^{n}S_{ij}{}^{d} \tag{2.74} $$

then Equation (2.73) becomes

$$ d{}^{n}e_{ij}{}^{P} = d\lambda\, {}^{n}S_{ij}{}^{d} \tag{2.75} $$

and is known as the Prandtl-Reuss flow rule. This flow rule will be used to derive the elastic-plastic constitutive matrix for the material. To keep the derivation general, a three dimensional body with isotropic strain hardening will be discussed. Then the two dimensional plane strain model will be extracted from the general matrix.

Consider an elastic model, the generalized Hooke's law can be written in terms of deviatoric stresses and strains

$$ {}^{n}S_{ij}{}^{d} = 2G\,{}^{n}e_{ij}{}^{'E} \tag{2.76} $$

where G is the shear modulus and is given as

$$ G = \frac{E}{2(1+\nu)} \tag{2.77} $$

The rate form then becomes

$$ d^{n}e_{ij}{}^{'E} = \frac{d^{n}S_{ij}{}^{d}}{2G} \tag{2.78} $$

The total rate of deformation is given by the sum of the elastic and plastic components.

$$ d^{n}e_{ij}{}^{'T} = d^{n}e_{ij}{}^{'E} + d^{n}e_{ij}{}^{'P} \tag{2.79} $$

From Equations (2.72), (2.75), and (2.78), the total strain rate is

$$ d^{n}e_{ij}{}^{'T} = \frac{d^{n}S_{ij}{}^{d}}{2G} + d\lambda\,{}^{n}S_{ij}{}^{d} \tag{2.80} $$

To obtain $d\lambda$, square both sides of Equation (2.75), then

$$ d^{n}e_{ij}{}^{P}\,d^{n}e_{ij}{}^{P} = d\lambda^{2}\,{}^{n}S_{ij}{}^{d}\,{}^{n}S_{ij}{}^{d} \tag{2.81} $$

By definitions of equivalent stress and strain

$$ {}^{n}S_{ij}{}^{d}\,{}^{n}S_{ij}{}^{d} = \frac{2}{3}\,{}^{n}\bar{\sigma}^{2} \tag{2.82} $$

and

$$ d{}^{n}e_{ij}{}^{P}d{}^{n}e_{ij}{}^{P} = \frac{2}{3}\,{}^{n}d\bar{e}^{P2} \tag{2.83} $$

It can be seen that ${}^{n}\bar{\sigma}$ is same as ${}^{n}\sigma_{y}$ in Von Mises model. Equation (2.81) can be solved for $d\lambda$ as follows

$$ d\lambda^{2} = \frac{3}{2}(1/{}^{n}\bar{\sigma}^{2})(\frac{2}{3}d{}^{n}e_{ij}{}^{P}d{}^{n}e_{ij}{}^{P}).\frac{3}{2} $$

$$ = (\frac{3}{2}(1/{}^{n}\bar{\sigma})\,{}^{n}d\bar{e}^{P})^{2} $$

Thus

$$ d\lambda = \frac{3}{2}(1/{}^{n}\bar{\sigma})\,{}^{n}d\bar{e}^{P} \tag{2.84} $$

Define ${}^{n}H$ as the slope of the equivalent stress-equivalent plastic strain curve (Fig. 2.5)

$$ {}^{n}H = {}^{n}d\bar{\sigma}/{}^{n}d\bar{e}^{P} \tag{2.85} $$

Recall Equation (2.69), replacing ${}^{n}\sigma_{y}$ by ${}^{n}\bar{\sigma}$ together with Equation (2.85), it becomes

$$ {}^{n}S_{ij}{}^{d}d{}^{n}S_{ij}{}^{d} = \frac{2}{3}\,{}^{n}\bar{\sigma}\,{}^{n}d\bar{\sigma} $$

$$ = \frac{4}{9}\,{}^{n}\bar{\sigma}^{2}\,{}^{n}Hd\lambda \tag{2.86} $$

From Equation (2.80), multiplying both sides by ${}^{n}S_{ij}{}^{d}$ and using Equations (2.82) and (2.86)

$$ {}^{n}S_{ij}{}^{d}(2Gd{}^{n}e_{ij}{}^{'T}) = {}^{n}S_{ij}{}^{d}d{}^{n}s_{ij}{}^{d} + 2Gd\lambda\,{}^{n}S_{ij}{}^{d}\,{}^{n}S_{ij}{}^{d} $$

$$ = \frac{4}{9}\,{}^{n}\sigma^{2}\,{}^{n}H d\lambda + \frac{4G}{3}({}^{n}\sigma^{2}d\lambda) $$

$$ = \frac{4G}{3}\,{}^{n}\sigma^{2}d\lambda\left(1 + \frac{{}^{n}H}{3G}\right) \qquad (2.87) $$

or

$$ {}^{n}S_{ij}{}^{d}d{}^{n}e_{ij}{}^{'T} = {}^{n}\beta d\lambda \qquad (2.88) $$

where

$$ {}^{n}\beta = \frac{2}{3}\,{}^{n}\sigma^{2}\left(1 + \frac{{}^{n}H}{3G}\right) \qquad (2.89) $$

Equation (2.88) can be written as

$$ d\lambda = {}^{n}S_{ij}{}^{d}d{}^{n}e_{ij}{}^{'T}/{}^{n}\beta \qquad (2.90) $$

Consider the term

$$ {}^{n}S_{ij}{}^{d}d{}^{n}e_{ij}{}^{'T} = {}^{n}S_{ij}{}^{d}(d{}^{n}e_{ij}{}^{T} - (d{}^{n}e_{kk}{}^{T}/3)\delta_{ij}) \qquad (2.91) $$

let $m = d{}^{n}e_{kk}{}^{T}/3$, then Equation (2.91) becomes

$$ {}^{n}S_{ij}{}^{d}d{}^{n}e_{ij}{}^{'T} = {}^{n}S_{ij}{}^{d}d{}^{n}e_{ij}{}^{T} - {}^{n}S_{kk}{}^{d}m \qquad (2.92) $$

but

$$ {}^{n}S_{kk}{}^{d} = {}^{n}S_{11}{}^{d} + {}^{n}S_{22}{}^{d} + {}^{n}S_{33}{}^{d} = 0 \qquad (2.93) $$

therefore

$$ {}^{n}S_{ij}{}^{d}d{}^{n}e_{ij}{}^{'T} = {}^{n}S_{ij}{}^{d}de_{ij}{}^{T} \qquad (2.94) $$

Substitute the above into Equation (2.90)

$$ d\lambda = {}^{n}S_{ij}{}^{d}de_{ij}{}^{T}/{}^{n}\beta \qquad (2.95) $$

Replacing Equation (2.94) for $d\lambda$ in Equation (2.80), then

$$d^{n}S_{ij}{}^{d} = 2G(d^{n}e_{ij}{}^{'T} - {}^{n}S_{ij}{}^{d}\,{}^{n}S_{kl}{}^{d}d^{n}e_{kl}{}^{T}/{}^{n}\beta) \qquad (2.96)$$

To obtain the required constitutive matrix, all the deviatoric terms have to be changed back to normal definitions of stress and strains. Since

$${}^{n}S_{ij}{}^{d} = {}^{n}\sigma_{ij} - \frac{{}^{n}\sigma_{mm}}{3}\delta_{ij} \qquad (2.64)$$

Recall Equation (2.64) and from theory of elasticity

$${}^{n}\sigma_{kk} = 3K^{n}e_{mm} \qquad (2.97)$$

where

$$K = \frac{E}{3(1-2\nu)} \qquad (2.98)$$

The rate form of the deviatoric stress can be expressed as

$$d^{n}S_{ij}{}^{d} = d^{n}\sigma_{ij} - \frac{E}{3(1-2\nu)}de_{mm}{}^{T} \qquad (2.99)$$

also

$$d^{n}e_{ij}{}^{'T} = d^{n}e_{ij}{}^{T} - \frac{d^{n}e_{mm}{}^{T}}{3}\delta_{ij} \qquad (2.100)$$

Putting Equation (2.99) into Equation (2.96), it can be shown easily that

$$d^{n}\sigma_{ij} = \frac{E}{(1+\nu)}(d^{n}e_{ij}{}^{T} + \frac{\nu}{(1-\nu)}d^{n}e_{mm}{}^{T}\delta_{ij} - {}^{n}S_{ij}{}^{d}\,{}^{n}S_{kl}{}^{d}d^{n}e_{kl}{}^{T}/{}^{n}\beta) \qquad (2.101)$$

or in matrix form

$$\begin{bmatrix} d\sigma^{n} \end{bmatrix} = \begin{bmatrix} {}^{n}C^{EP} \end{bmatrix}\begin{bmatrix} d^{n}e^{T} \end{bmatrix} \qquad (2.102)$$

which is the incremental constitutive matrix required in the finite element formulation. For a general case

$$\begin{bmatrix} {}^{n}C^{EP} \end{bmatrix} = E/(1+\nu) \begin{bmatrix} C_{11} & C_{12} & C_{13} & C_{14} \\ C_{12} & C_{22} & C_{23} & C_{24} \\ C_{13} & C_{23} & C_{33} & C_{34} \\ C_{14} & C_{24} & C_{34} & C_{44} \end{bmatrix} \qquad (2.103)$$

where

$$C_{11} = \frac{1-\nu}{1-2\nu} - {}^{n}S_{11}{}^{d2}/{}^{n}\beta$$

$$C_{12} = \frac{\nu}{1-2\nu} - {}^{n}S_{11}{}^{d}\,{}^{n}S_{22}{}^{d}/{}^{n}\beta$$

$$C_{13} = - {}^{n}S_{11}{}^{d}\,{}^{n}S_{12}{}^{d}/{}^{n}\beta$$

$$C_{14} = \frac{\nu}{1-2\nu} - {}^{n}S_{11}{}^{d}\,{}^{n}S_{33}{}^{d}/{}^{n}\beta$$

$$C_{22} = \frac{1-\nu}{1-2\nu} - {}^{n}S_{22}{}^{d2}/{}^{n}\beta$$

$$C_{23} = - {}^{n}S_{22}{}^{d}\,{}^{n}S_{12}{}^{d}/{}^{n}\beta$$

$$C_{24} = \frac{\nu}{1-2\nu} - {}^{n}S_{22}{}^{d}\,{}^{n}S_{33}{}^{d}/{}^{n}\beta$$

$$C_{33} = \frac{1}{2} - {}^{n}S_{12}\, d^{2}/{}^{n}\beta$$

$$C_{34} = - {}^{n}S_{33}\, d\, {}^{n}S_{12}\, d/{}^{n}\beta$$

$$C_{44} = \frac{1-\nu}{1-2\nu} - {}^{n}S_{33}\, d^{2}/{}^{n}\beta$$

and

$$\left[d^{n}\sigma\right] = \begin{bmatrix} d^{n}\sigma_{11} \\ d^{n}\sigma_{22} \\ d^{n}\sigma_{12} \\ d^{n}\sigma_{33} \end{bmatrix} \quad \text{and} \quad \left[d^{n}e^{T}\right] = \begin{bmatrix} d^{n}e_{11} \\ d^{n}e_{22} \\ 2d^{n}e_{12} \\ d^{n}e_{33} \end{bmatrix} \qquad (2.104)$$

To obtain the C^{EP} matrices for plane strain and plane stress problems, the same procedure stated in Section 2.2.1 can be used. The matrices are also derived by Yamada et al (1968). The above theory is applicable for small strain condition. However, since the deformed configuration of the body is used in the ULJ approach, the above result can be used for large deformation also. Two other theories (Green and Nagdhi, 1965; Lee, 1969) have been proposed but they are difficult to implement (Desai et al, 1978).

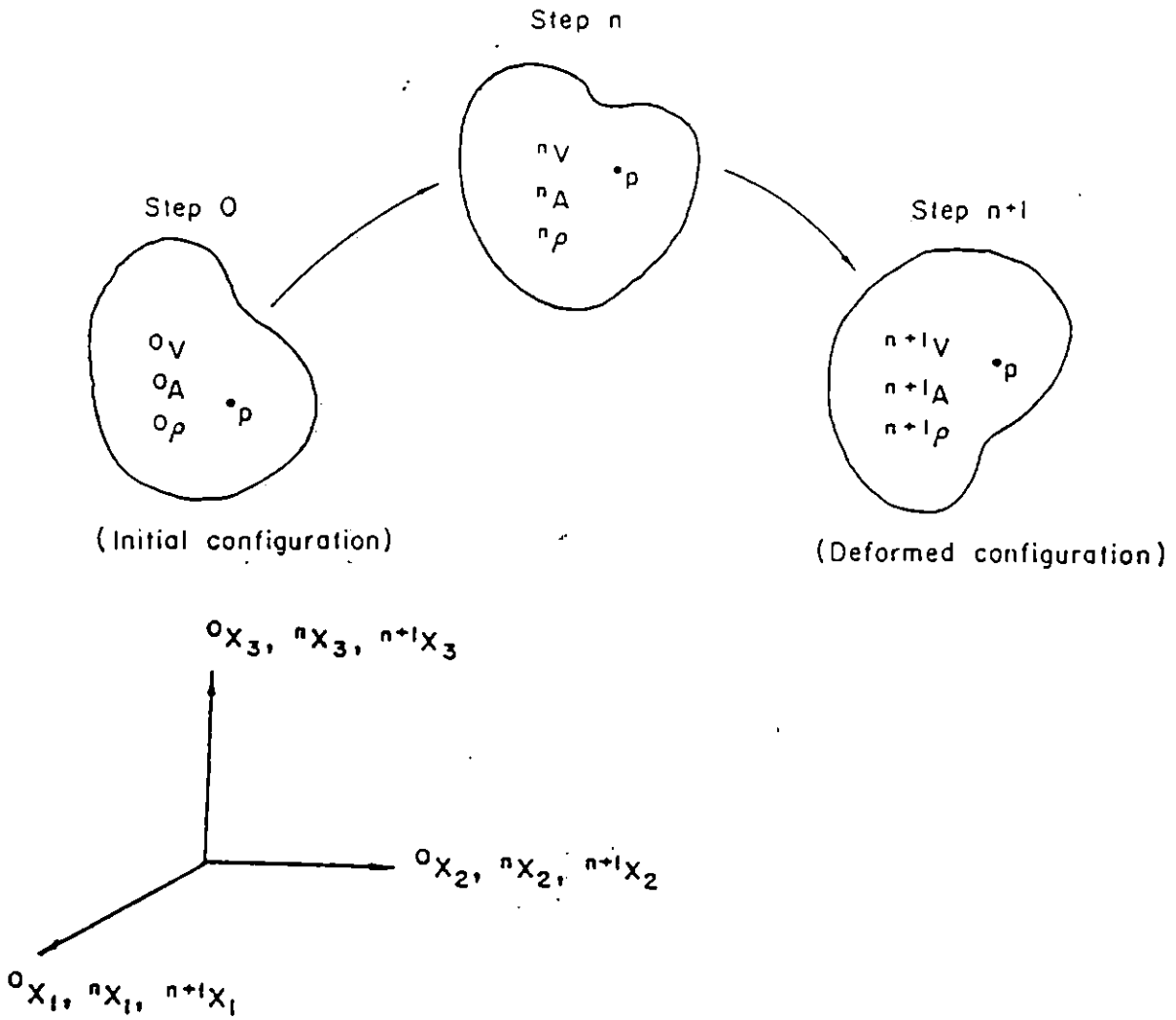

Figure 2.1: Generic Configurations of a System

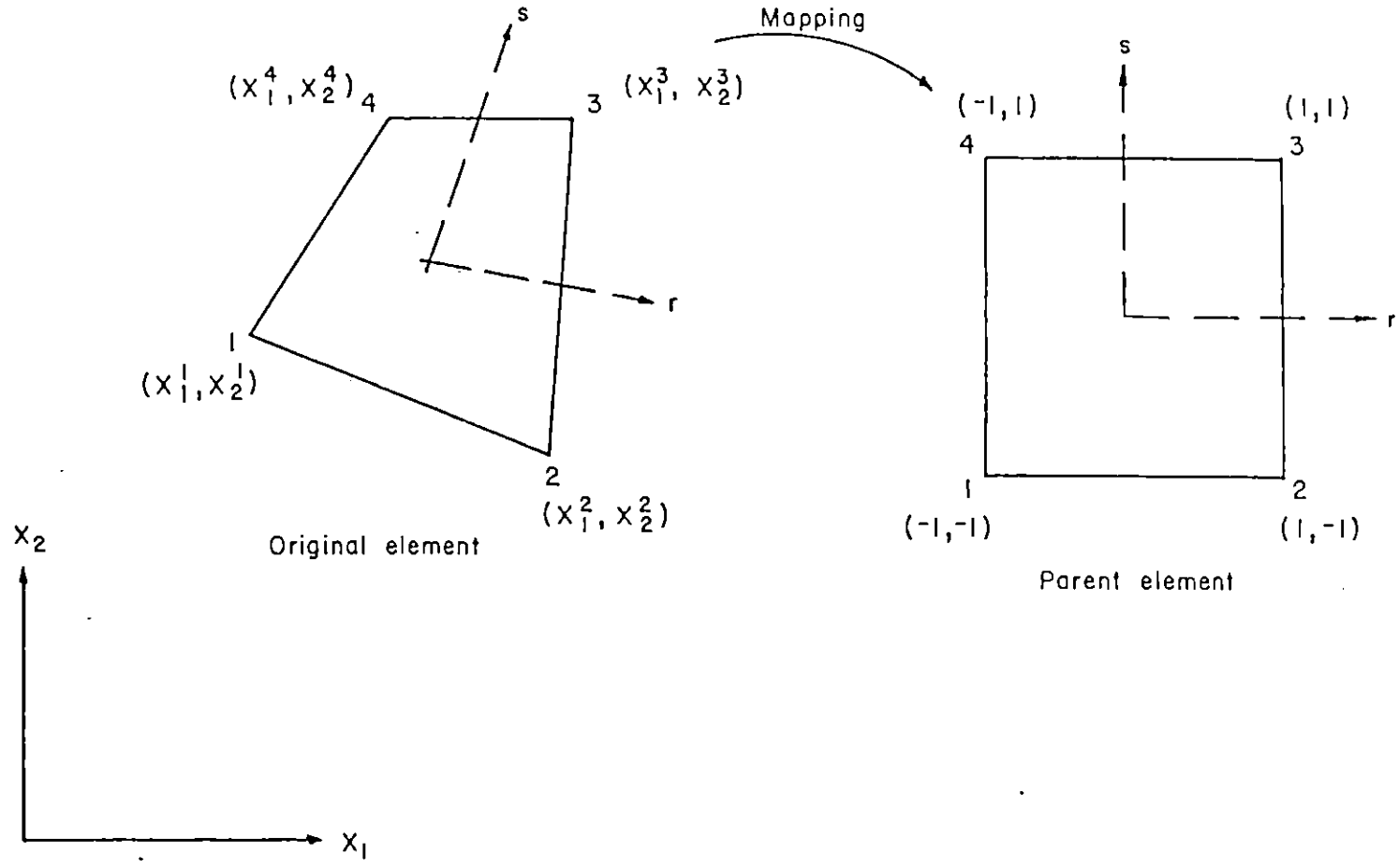

Figure 2.2: Mapping of a Four-Node Element

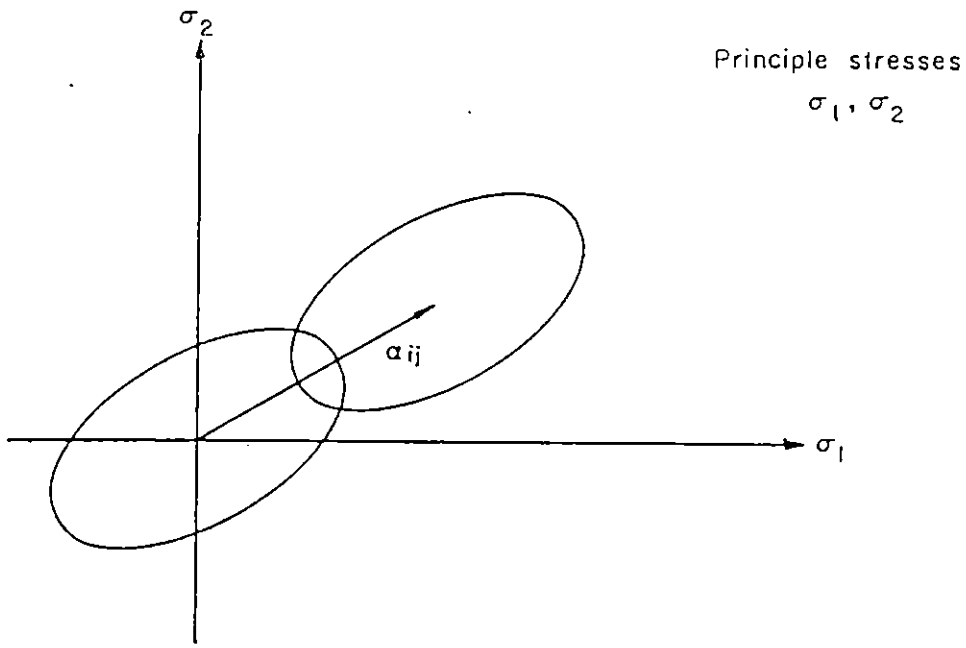

Figure 2.3: Kinematic Strain Hardening

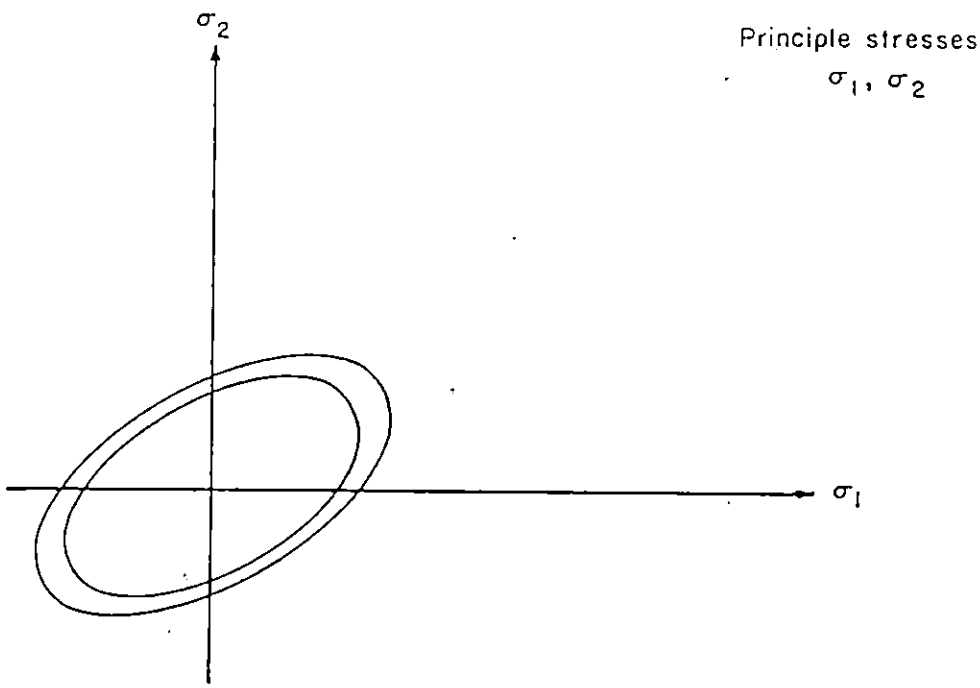

Figure 2.4: Isotropic Strain Hardening

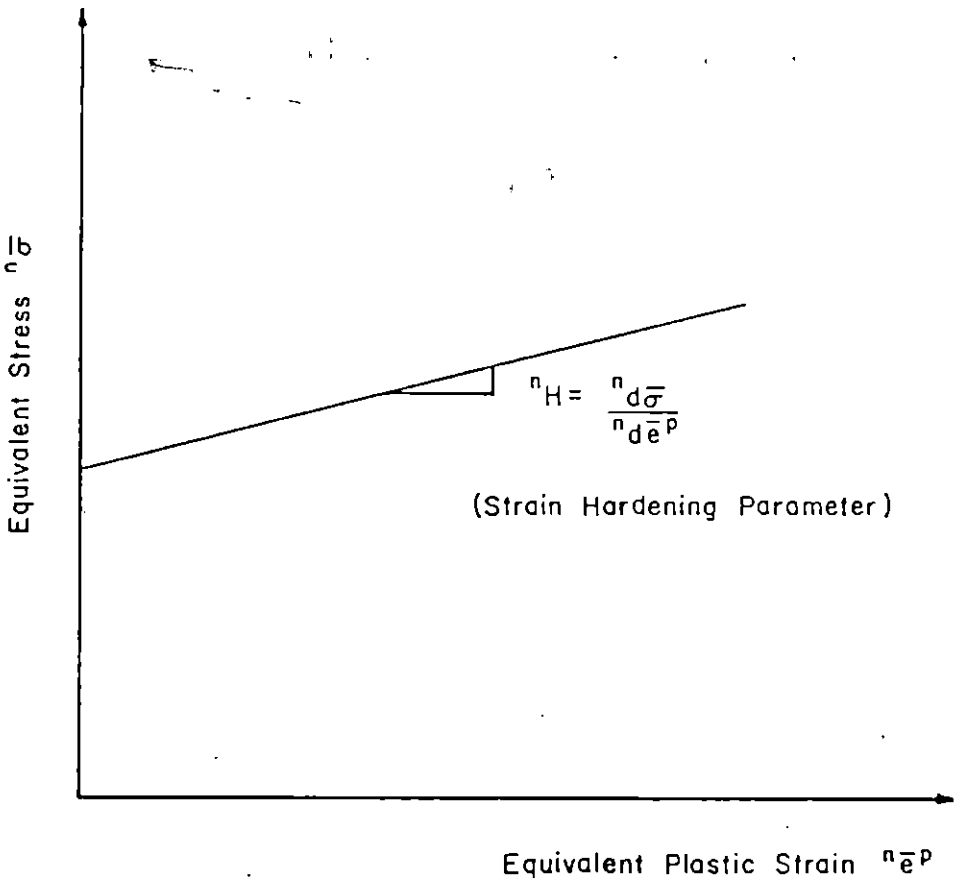

Figure 2.5: Equivalent Stress Versus Equivalent Plastic Strain Curve

Chapter III

FINITE ELEMENT FORMULATION FOR CONTACT PROBLEM

The incremental virtual work done by a continuum system is derived in previous chapter. Using an Updated Lagrangian approach the result obtained is rewritten herein

$$\int {}^{n}_{V} {}^{n}\Delta S_{ij} \, {}^{n}dV + \int {}^{n}_{V} {}^{n}\tau_{ij} \delta {}^{n}\eta_{ij} \, {}^{n}dV = {}^{n+1}R - \int {}^{n}_{V} {}^{n}\tau_{ij} \delta {}^{n}e_{ij} \, {}^{n}dV \qquad (3.1)$$

or in matrix form

$$\left(\begin{bmatrix} {}^{n}K_{L} \end{bmatrix} + \begin{bmatrix} {}^{n}K_{NL} \end{bmatrix} \right) \begin{bmatrix} \Delta U \end{bmatrix} = \begin{bmatrix} {}^{n+1}R \end{bmatrix} - \begin{bmatrix} {}^{n}F \end{bmatrix} \qquad (3.2)$$

Details of the terms can be found in Sections 2.1.2 and 2.1.3. To account for the effect of contact forces, the total potential of these forces is included in the variational formulation to enforce the geometric compatibilities along the contact surface. However it is easier to derive the incremental virtual work equation for a contact surface without referring to a potential function of a continuum. This approach is adopted in this study and will be explained in details in the following sections.

3.1 MODELING OF CONTACT SURFACE

For clarity of presentation only two generic bodies are shown in Figure 3.1 to represent the contact problem considered. The bodies are arbitrarily chosen as the contactor and target. These bodies are discretized into finite elements. A subset of boundary nodes on ${}^{n}B^{1}$ is designated as candidate contact nodes and a subset of segments or nodes on ${}^{n}B^{2}$ is designated as the target surface. These subsets should include all possible contact points throughout the loading history of the systems. These are shown schematically in Figure 3.2. It is noted that the contactor nodes are restricted from penetrating into the target surface. However this is not the case for the target nodes. This will violate the physical condition of contact considered in this study. Thus care must be taken when modelling a problem with the use of the contact algorithm. For each contactor node k, there is a contact force vector λ_k associated with it. The contact forces acting on the corresponding target surface are interpolated linearly from λ_k as shown in Figure 3.3. It has to be pointed out that for problems with a multi-contact surface, such as the sheet-pile interlock problem, it will be advantageous to designate part of the boundary of a body as contactor and part of it as target. Thus the term contactor or target from now on does not

represent a whole body. Instead only a subset of boundary nodes is referred to by that term. As mentioned in the beginning of this section, only two bodies are shown in the problem, the contact algorithm developed is applicable to any number of contacting bodies.

3.2 CONDITIONS GOVERNING CONTACT FORCES AT CONTACT NODE

When a contact node comes into contact with the target surface, the contact force on the node is always compressive. Thus if during an iteration a tensile force is found acting on the contact node, debonding occurs and the contact force is set to be zero.

In most engineering problems, friction has to be included in order to have a realistic result. The development of friciton laws and the mechanics using these laws to predict motion along contact surface are of major concerns to many researchers (Dieterich, 1978; Oden and Pires, 1983). In this study the motion of the contact bodies is governed by Coulomb's law of friction, with μ_s the coefficient of static friction and μ_k the coefficient of kinetic friction.

Consider a node initially at contact to a target surface. Suppose a tangential traction t_t is developed along the contact surface. The motion of the contact point depends on the magnitude of t_t as well as t_n which is the compressive

normal traction. This is indicated by the following equations.

Sticking $$|t_t| < \mu_s t_n \tag{3.3}$$

Sliding $$|t_t| = \mu_k t_n \tag{3.4}$$

The direction of the tangential traction will always be opposite to the direction of sliding. If t_t drops below the kinetic friction, sticking is said to take place again.

3.3 POTENTIAL OF CONTACT FORCES

As mentioned in the introduction of this chapter, the incremental total potential of the contact forces is added to the usual variational functional. That is

$$\pi_1 = \pi - \sum_k W_k \tag{3.5}$$

where π is the usual incremental total potential leading to the incremental equilibrium equation (Equation 3.1) and $\sum_k W_k$ is the incremental potential of the contact forces. It is noted that this term is obtained after the system is discretized instead of treating as a continuum. This approach greatly facilitates the above formulation because it does not involve the reference of a total potential function for the contact surface. The following sections concentrate on evaluating W_k for each contact node in sticking and sliding conditions.

Since equilibrium iteration is used within each load increment, the value of W_k is written for iteration (i) in load step n+1 where the response of the system at step n has been calculated and that (i-1) iterations have been performed for the solution at step n+1. After W_k is established, a first variation of the potential is carried out. The corresponding contributions will give additional terms to Equation (3.1). However, the terms in Equation (3.1) remain unaltered. Thus the extra terms due to contact conditions can be interpreted as a Lagrangian multiplier contributions to the system.

3.3.1 Contact Potential for Sticking and Sliding Conditions

A node k is said to come into contact with a segment AB when penetration occurs within the target. This is illustrated in Figure 3.4. The location of contact on surface AB is assumed to be the normal projection of the node k on AB. This is indicated as point C in the figure. Other terms which are necessary in the derivation of the contact potential are also summarized in the following

1. ${}^{n+1}x_A^{(i-1)}$, ${}^{n+1}x_B^{(i-1)}$, ${}^{n+1}x_k^{(i-1)}$: current global coordinates of nodes A, B, and, k respectively after iteration (i-1).
2. $\Delta_k^{(i-1)}$: overlap of node k on target segment AB.

3. $d^{(i-1)}$: length of segment AB.

4. n_T, n_N: unit vector along local axes on target segment with respect to global reference frame; updated during each iteration.

5. $\beta^{(i-1)}$: nondimensional parameter to locate contact point C.

Also associated with node k is a contact force ${}^{n+1}\lambda_k^{(i-1)}$ or in component form

$$ {}^{n+1}\lambda_k^{(i-1)} = {}^{n+1}\lambda_{kx}^{(i-1)} i + {}^{n+1}\lambda_{ky}^{(i-1)} j \tag{3.6} $$

From geometry of the contact condition

$$ \Delta_k^{(i-1)} = ({}^{n+1}x_k^{(i-1)} - {}^{n+1}x_A^{(i-1)}) \cdot n_N \tag{3.7} $$

$$ \beta^{(i-1)} = ({}^{n+1}x_k^{(i-1)} - {}^{n+1}x_A^{(i-1)}) \cdot n_T/d^{(i-1)} \tag{3.8} $$

and

$$ d^{(i-1)} = \|{}^{n+1}x_B^{(i-1)} - {}^{n+1}x_A^{(i-1)}\| \tag{3.9} $$

The contact forces for target segment AB are interpolated as stated in Figure 3.3 and are repeated here

$$ {}^{n+1}\lambda_A^{(i-1)} = -(1-\beta^{(i-1)}){}^{n+1}\lambda_k^{(i-1)} \tag{3.10} $$

$$ {}^{n+1}\lambda_B^{(i-1)} = -\beta^{(i-1)}\,{}^{n+1}\lambda_k^{(i-1)} \tag{3.11} $$

To construct the contact potential, the incremental displacements at nodes A, B, and k in iteration (i) are $\Delta U_A^{(i)}$, $\Delta U_B^{(i)}$, and $\Delta U_k^{(i)}$ respectively. These displacements are

such that the overlap $\Delta_k^{(i-1)}$ is eliminated. For a sticking condition, the contact point remains unchanged, hence

$$\beta^{(i)} = \beta^{(i-1)} \tag{3.12}$$

The potential W_k due to the contact forces at nodes A, B, and k is

$$W_k = {}^{n+1}\lambda_k^{(i)T}(\Delta U_k^{(i)} + \Delta_k^{(i-1)}) + {}^{n+1}\lambda_A^{(i)T}\Delta U_A^{(i)} + {}^{n+1}\lambda_B^{(i)T}\Delta U_B^{(i)} \tag{3.13}$$

The contact force at node k can be written as

$${}^{n+1}\lambda_k^{(i)} = {}^{n+1}\lambda_k^{(i-1)} + \Delta\lambda_k^{(i)} \tag{3.14}$$

where $\Delta\lambda_k^{(i)}$ is the change in the contact force. Combining Equations (3.10)-(3.14), W_k is rewritten as

$$W_k = {}^{n+1}\lambda_k^{(i-1)T}\left[(\Delta U_k^{(i)} + \Delta_k^{(i-1)}) - (1-\beta^{(i-1)})\Delta U_A^{(i)} - \beta^{(i)}\Delta U_B^{(i)}\right] + \Delta\lambda_k^{(i)T}\left[(\Delta U_k^{(i)} + \Delta_k^{(i-1)}) - (1-\beta^{(i-1)})\Delta U_A^{(i)} - \beta^{(i)}\Delta U_B^{(i)}\right] \tag{3.15}$$

For a sliding condition

$$\beta^{(i)} = \beta^{(i-1)} + \Delta\beta^{(i)} \tag{3.16}$$

Also

$$\Delta\lambda_k^{(i)} = -\Delta\lambda_N^{(i)} n_N \tag{3.17}$$

where $\Delta\lambda_N^{(i)}$ is the change in magnitude of the normal component of ${}^{n+1}\lambda_k^{(i-1)}$. The negative sign is there because di-

rection of the normal component is opposite to the direction of $^{n}n_N$. The potential W_k now is

$$W_k = {}^{n+1}\lambda_k^{(i)T}\left[(\Delta U_k^{(i)} + \Delta_k^{(i-1)}) - (1-\beta^{(i)})\Delta U_A^{(i)} - \beta^{(i)}\Delta U_B^{(i)}\right] \quad (3.18)$$

Bathe and Chaudhary (1985) suggest in their work that $\Delta\beta^{(i)}$ can be neglected since it is the change of β within an iteration. Also this will retain the symmetry of the stiffness matrix. Thus using Equations (3.14), (3.17), and (3.18) together with the assumption on $\beta^{(i)}$, W_k can be written as

$$W_k = {}^{n+1}\lambda_k^{(i-1)T}\left[(\Delta U_k^{(i)} + \Delta_k^{(i-1)}) - (1-\beta^{(i-1)})\Delta U_A^{(i)} - \beta^{(i-1)}\Delta U_B^{(i)}\right]$$

$$+ \Delta\lambda_N^{(i)} - n_N^{T}\left[(\Delta U_k^{(i)} + \Delta_k^{(i-1)}) - (1-\beta^{(i-1)}\Delta U_A^{(i)}) - \beta^{(i-1)}\Delta U_B^{(i)}\right] \quad (3.19)$$

Equations (3.15) and (3.19) are considered for all nodes which are in sticking and sliding contact respectively.

3.3.2 Finite Element Equations Including Contact Effects

To construct the finite element equations for contacting systems, the stationarity of the contact potential is invoked. Since there are two variables involved, ΔU and $\Delta\lambda$, two sets of Euler equations are obtained. For illustrative purpose only the equations corresponding to nodes A, B, and k are derived. To include other nodes, the standard assembly process used in finite element analysis can be adopted.

For sticking contact, the variationals of π_1 with respect to ΔU and $\Delta\lambda$ are performed. The Euler equations obtained are discretized into finite element equations and can be given as

$$\left\{\begin{bmatrix} {}^{n+1}K_T^{(i-1)} & 0 \\ 0 & 0 \end{bmatrix} + \begin{bmatrix} {}^{n+1}K_C^{(i-1)} \end{bmatrix}\right\}\begin{bmatrix} \Delta U^{(i)} \\ \Delta\lambda^{(i)} \end{bmatrix}$$

$$= \begin{bmatrix} {}^{n+1}R \\ 0 \end{bmatrix} - \begin{bmatrix} {}^{n+1}F^{(i-1)} \\ 0 \end{bmatrix} + \begin{bmatrix} {}^{n+1}R_C^{(i-1)} \\ {}^{n+1}\Delta_C^{(i-1)} \end{bmatrix} \tag{3.20}$$

where

$${}^{n+1}R_C^{(i-1)} = \begin{bmatrix} {}^{n+1}\lambda_{kx}^{(i-1)} \\ {}^{n+1}\lambda_{ky}^{(i-1)} \\ -(1-\beta^{(i-1)})^{n+1}\lambda_{kx}^{(i-1)} \\ -(1-\beta^{(i-1)})^{n+1}\lambda_{ky}^{(i-1)} \\ -\beta^{(i-1)n+1}\lambda_{kx}^{(i-1)} \\ -\beta^{(i-1)n+1}\lambda_{ky}^{(i-1)} \end{bmatrix} \tag{3.21}$$

$${}^{n+1}\Delta_C^{(i-1)} = \begin{bmatrix} \Delta_{kx}^{(i-1)} \\ \Delta_{ky}^{(i-1)} \end{bmatrix} \tag{3.22}$$

and

$$
{}^{n+1}K_C^{(i-1)} = \begin{bmatrix}
 & -1 & 0 \\
 & 0 & -1 \\
 & 1-\beta^{(i-1)} & 0 \\
0 & 0 & 1-\beta^{(i-1)} \\
 & \beta^{(i-1)} & 0 \\
 & 0 & \beta^{(i-1)} \\
 & 0 & 0 \\
\text{Sym.} & & 0
\end{bmatrix} \tag{3.23}
$$

with the corresponding unknown vector as

$$
\begin{bmatrix} \Delta U^{(i)} \\ \Delta\lambda^{(i)} \end{bmatrix} = \begin{bmatrix}
\Delta U_{kx}^{(i)} \\
\Delta U_{ky}^{(i)} \\
\Delta U_{Ax}^{(i)} \\
\Delta U_{Ay}^{(i)} \\
\Delta U_{Bx}^{(i)} \\
\Delta U_{By}^{(i)} \\
\Delta\lambda_{kx}^{(i)} \\
\Delta\lambda_{ky}^{(i)}
\end{bmatrix} \tag{3.24}
$$

After standard assembly procedure, the dimension of matrix K_T is NEQ X NEQ whereas K_C has a dimension of NEQT X NEQT. The terms NEQ and NEQT are defined as follow:

1. NEQ = total number of displacement degree of freedom of the system
2. NEQT = NEQ plus total unknown contact nodal forces associated with all contactor nodes

For the remaining parts of Equation (3.20), ΔU, R, F, and R_C are vectors of dimension NEQ while $\Delta\lambda$ and Δ_C are of the order NEQT-NEQ.

For sliding contact, only the penetration in the normal direction needs to be restrained. Thus

$$ {}^{n}\Delta_C^{(i-1)} = -n_N \Delta_k^{(i-1)} = (-n_{Nx}\Delta_{kx}^{(i-1)} - n_{Ny}\Delta_{ky}^{(i-1)}) \qquad (3.25) $$

The modification in the contact stiffness term is obtained similarly and it can be seen easily that it has the following form

$$ {}^{n+1}K_C^{(i-1)} = \begin{bmatrix} & & n_{Nx} \\ & & n_{Ny} \\ 0 & & -(1-\beta^{(i-1)})n_{Nx} \\ & & -(1-\beta^{(i-1)})n_{Ny} \\ & & -\beta^{(i-1)}n_{Nx} \\ & & -\beta^{(i-1)}n_{Ny} \\ \text{Sym.} & & 0 \end{bmatrix} \qquad (3.26) $$

The corresponding solution vector is

$$\begin{bmatrix} \Delta U^{(i)} \\ \Delta \lambda^{(i)} \end{bmatrix} = \begin{bmatrix} \Delta U_{kx}^{(i)} \\ \Delta U_{ky}^{(i)} \\ \Delta U_{Ax}^{(i)} \\ \Delta U_{Ay}^{(i)} \\ \Delta U_{Bx}^{(i)} \\ \Delta U_{By}^{(i)} \\ \Delta \lambda_{N}^{(i)} \end{bmatrix} \qquad (3.27)$$

It can be noted that two constraint equations are associated with a stick condition while there is only one constraint equation for a sliding case. The vector ${}^{n+1}R_C^{(i-1)}$ has yet to be derived. This will be done in the next section. To solve Equation (3.20), full Newton- Raphson iteration is found to yield best results (Bathe and Chaudhary, 1985).

3.4 EVALUATIONS OF STICKING AND SLIDING CONDITIONS

An essential step in a contact algorithm is to update the contact condition of a node. The algorithm has to be able to decide if contact has taken place or not. If contact does occur, it has to determine whether the node sticks or slides on the target segment. Once the type of contact is

known, the contact force vector ${}^{n+1}R_C$ can be evaluated. This will be given later in this chapter.

A most direct way to find out the contact condition of a node is based on the total contact point forces. However the determination of these forces can lead to numerical difficulties. It is more effective to establish the contact condition of a node by considering the conditions of its adjacent segments.

Recall Equation (3.20), the contact forces at a node k are given as λ_k and can be determined from summing up all the $\Delta\lambda_k^{(i)}$ obtained in the solution. However it is found that the use of $\Delta\lambda_k$ on a contact problem can yield inaccurate results. An alternate approach is to evaluate the contact forces from the vector $\Delta R^{(i-1)}$ defined as

$$\Delta R^{(i-1)} = {}^{n+1}F^{(i-1)} - {}^{n+1}R \qquad (3.28)$$

which is the negative of the out-of-balance load vector encountered in nonlinear analysis. This approach is used by Bathe and Chaudhary (1985).

The following sections will consider the conditions for sticking and sliding contacts and the evaluation of the contact force vector ${}^{n+1}R_C$. During an iteration in which there is a change from no contact to contact condition, sticking is assumed for the contact node. Based on this assumption, new contact forces are calculated and the contact condition is modified accordingly.

3.4.1 Distributed Traction and Resultant Forces in Contact Segment

The distributed tractions in a contactor segment can be determined from the nodal force vector ΔR. Figure 3.5 illustrates the calculation of the contact force from ΔR. In the figure, t_x^k and t_y^k are the magnitudes of distributed tractions at the node k while t_n^k and t_t^k are the magnitudes of the normal and tangential tractions with reference to a set of local coordinate system. A discontinuity is observed in these normal and tangential tractions at the nodes.

Using a "consistent" approach, the tractions are related to the nodal point forces by a linear displacement interpolation. For plane stress and plane strain analyses,

$$\begin{bmatrix} \Delta R_{kx}^{(i-1)} \\ \Delta R_{ky}^{(i-1)} \end{bmatrix} = h \begin{bmatrix} t_x^{k-1} & t_x^k & t_x^{k+1} \\ t_y^{k-1} & t_y^k & t_y^{k+1} \end{bmatrix} \begin{bmatrix} d_{j-1}^{(i-1)}/6 \\ (d_{j-1}^{(i-1)} + d_j^{(i-1)})/3 \\ d_j^{(i-1)}/6 \end{bmatrix} \quad (3.29)$$

where h is the uniform thickness of the element. With proper rearrangement the nodal contact tractions can be solved easily. The details are given in Appendix A. To evaluate the normal and tangential tractions, the usual transformation procedure is used and is given in Figure 3.6. Note that the normal traction is positive when acting from node k to node k+1.

To determine the contact condition, the resultant normal and tangential forces on each segment are needed. These are given by the area under the distributed normal and tangential tractions respectively. That is

$$T_n^j = hd_j^{(i-1)}(t_n^k + t_n^{k+1})/2 \tag{3.30}$$

$$T_t^j = hd_j^{(i-1)}(t_t^k + t_t^{k+1})/2 \tag{3.31}$$

where T_n^j and T_t^j are normal and tangential contact forces on segment j. With T_n^j and T_t^j the contact condition is established by the following:

(1) If $T_n^j < 0$, the segment is assumed to experience tension release and T_n^j is set equal to zero.

(2) If $T_t^j \leq \mu_s T_n^j$, sticking occurs.

(3) If $T_t^j > \mu_s T_n^j$, sliding occurs and T_t^j is set equal to $\mu_k T_n^j$.

After the contact condition of each segment is known, the contact condition at the contact node can be found. These conditions are summarized in Table 3.1.

3.4.2 Calculation of Contact Force Vector

The evaluation of the contact force vector ${}^{n+1}R_C$ depends on the contact state of the adjoining segments. Assume segment in previous iteration was in sticking contact, then two situations can arise in the current iteration:

Case 1. Segment continues to stick.

Case 2. Segment changes to sliding contact.

For Case 1 ${}^{n+1}R_C$ is calculated as the consistent nodal loads from the normal and tangential tractions on the segment. If segments j-1, j, and j+1 all have the conditions indicated by Case 1, the nodal loads at point k and k+1 are simply the values in ΔR (Fig. 3.4).

In Case 2 only the tangential traction is modified in calculating the consistent nodal loads. A uniformly distributed tangential traction with its value scaled down to equal the frictional capacity is used on a sliding segment. The magnitude is given as

$$(t_t^k)_{mod.} = (t_t^k + t_t^{k+1})|T_f^j/T_t^j|/2 \qquad (3.32)$$

where

$$T_f^j = \mu_s T_n^j \qquad (3.33)$$

For tension release both normal and tangential tractions on the segment are set to be zero.

A different situation arises when the segment was in sliding contact in the previous iteration. A procedure similar to the above can be used. Case 1 now corresponds to a change from sliding to sticking mode. For Case 2 the segment will continue to slide. However, to find the frictional capacity of the segment (Equation 3.33), μ_k is used instead. With ${}^{(i-1)}R_C$ vector calculated, together with the

appropriate contact stiffness terms and overlap vector $\Delta_C^{(i-1)}$, Equation (3.20) can now proceed with the iteraiton i until a certain convergence criteria is met. This will be addressed in another chapter.

TABLE 3.1

Contact Conditions of a Node as Decided by States of Adjoining Segments

State of Adjoining Segments		State
One Adjoining Segment	Other Adjoining Segment	of Node
sticking	sticking sliding no contact	sticking
sliding	sliding no contact	sliding
no contact	no contact	no contact

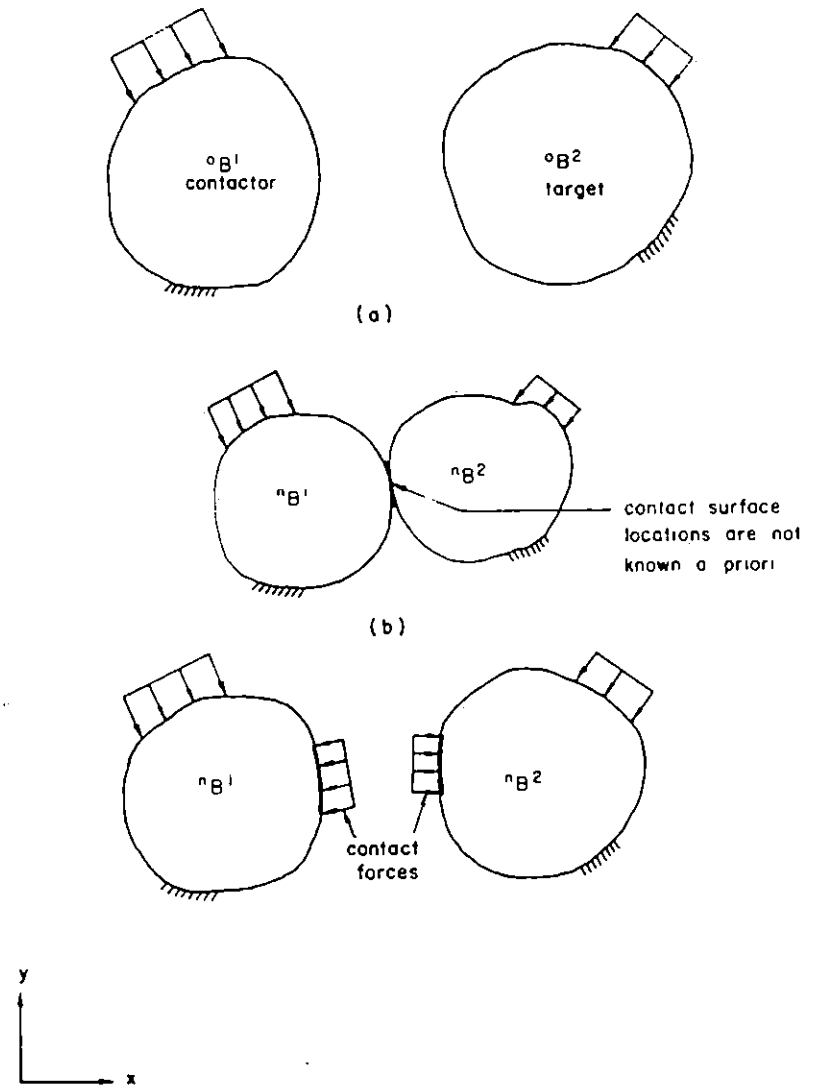

Figure 3.1: Representations of Two Bodies in Contact

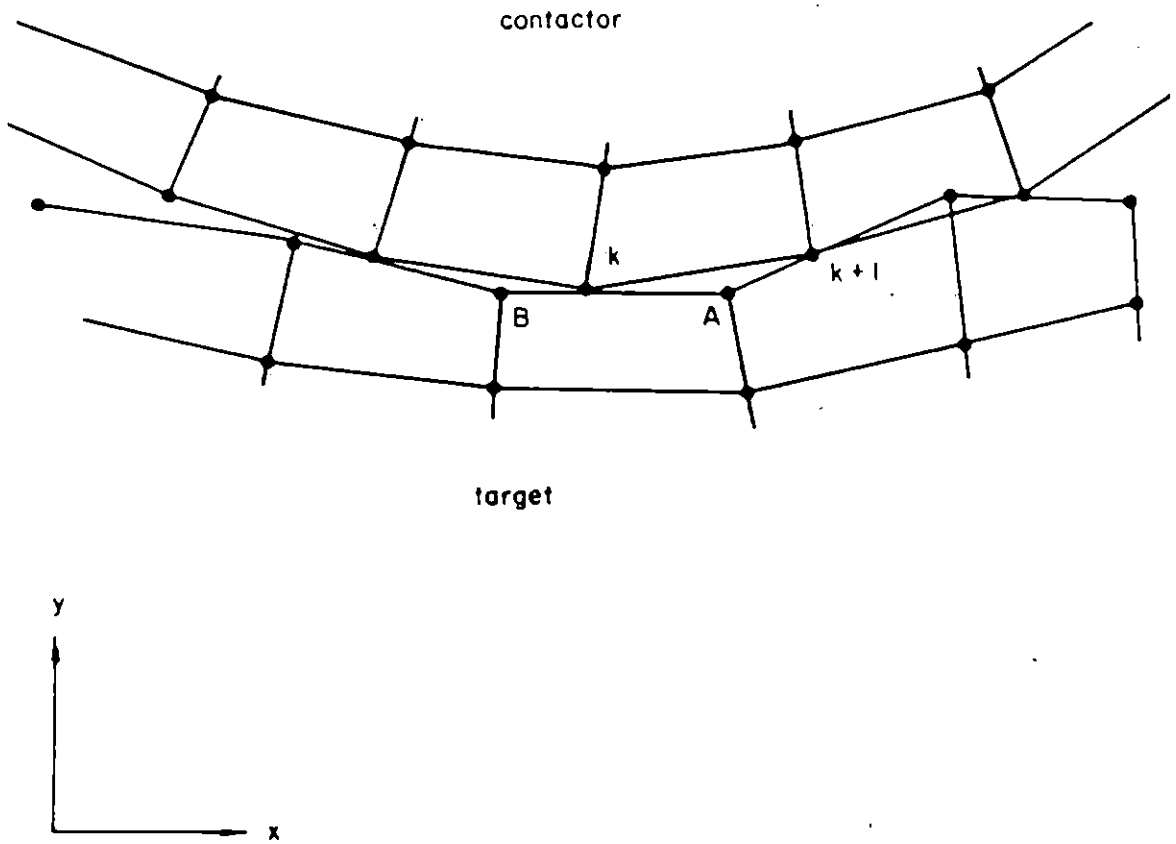

Figure 3.2: Finite Element Discretization in Contact Region

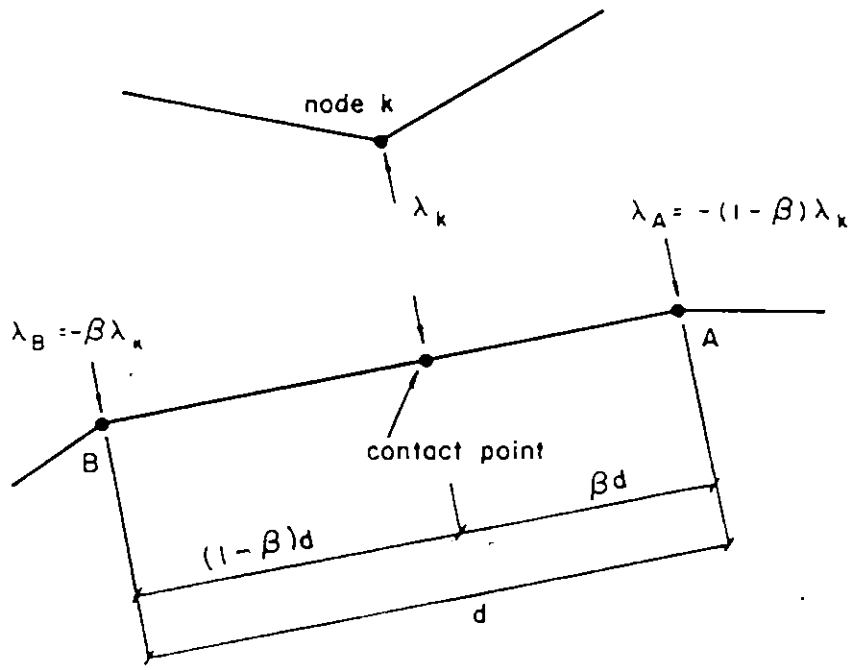

Figure 3.3: Interpolations of Contact Forces at Target Nodes

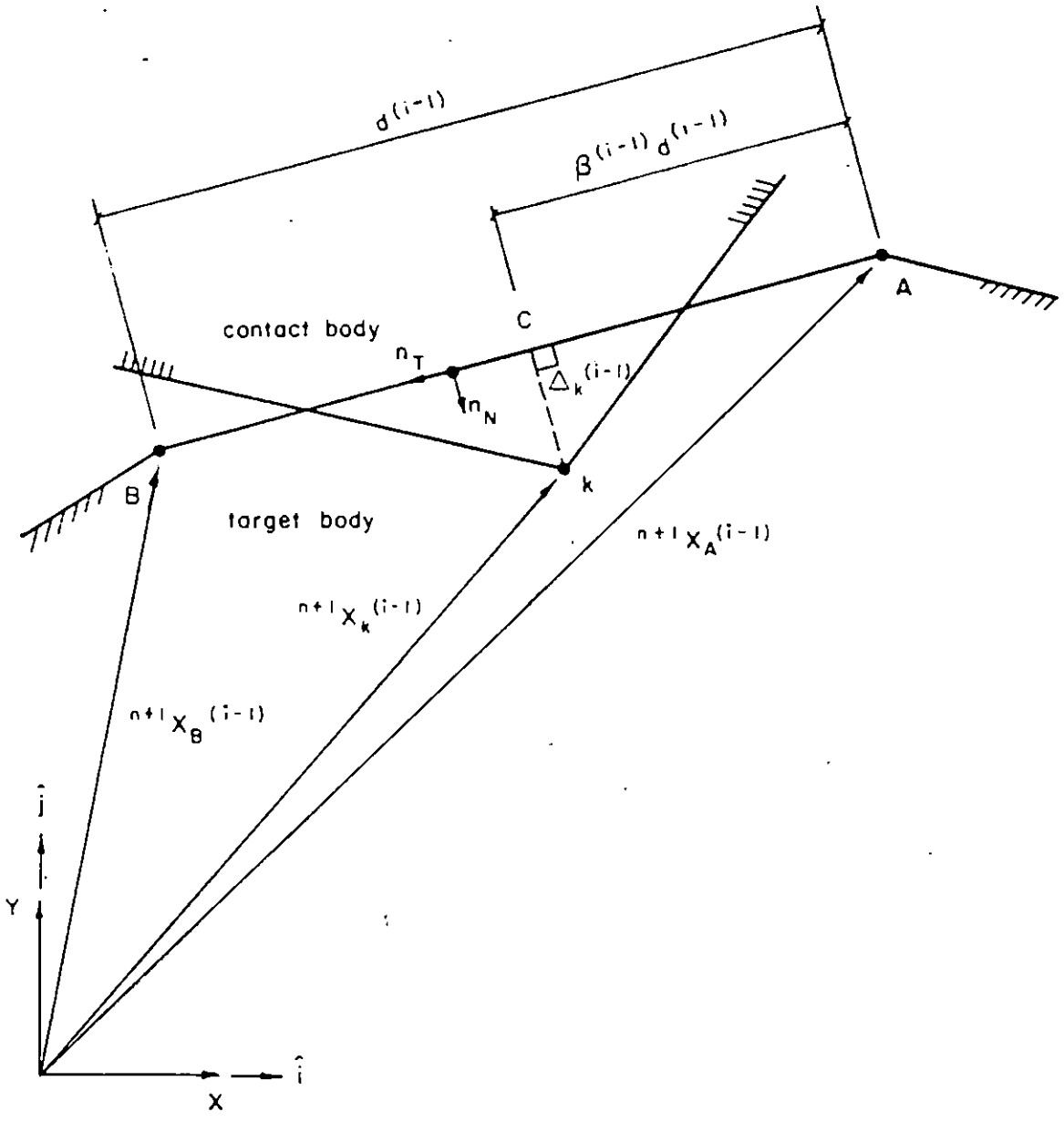

Figure 3.4: Schematic Representation of a Contact Point with Definitions of Variables on the Contact Segment

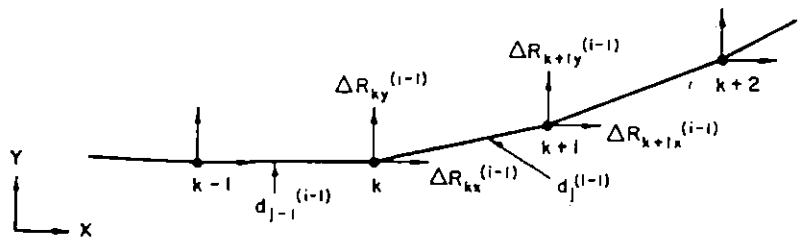

(a) Nodal Forces on Contactor Body

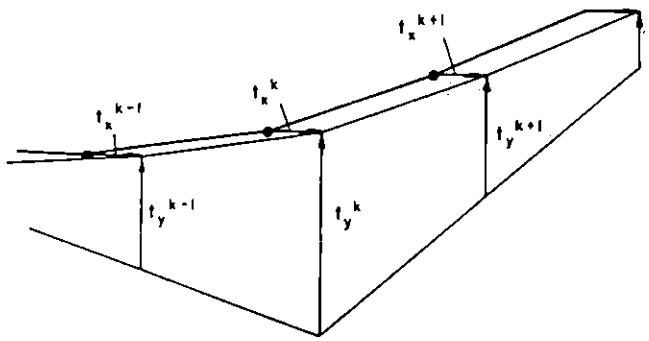

(b) Traction Acting on Contactor Body

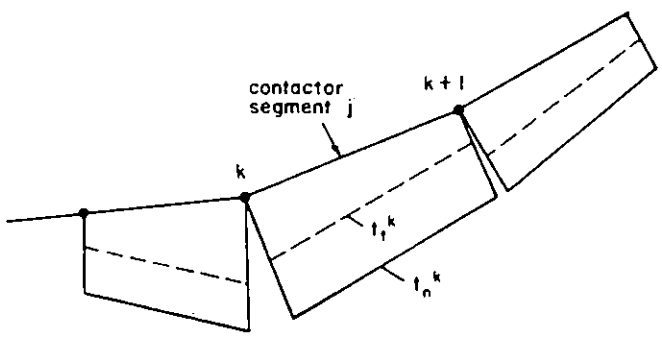

(c) Normal and Tangental Tractions on Contactor Body

Figure 3.5: Calculation of Normal and Tangential Tractions from Nodal Force Vector

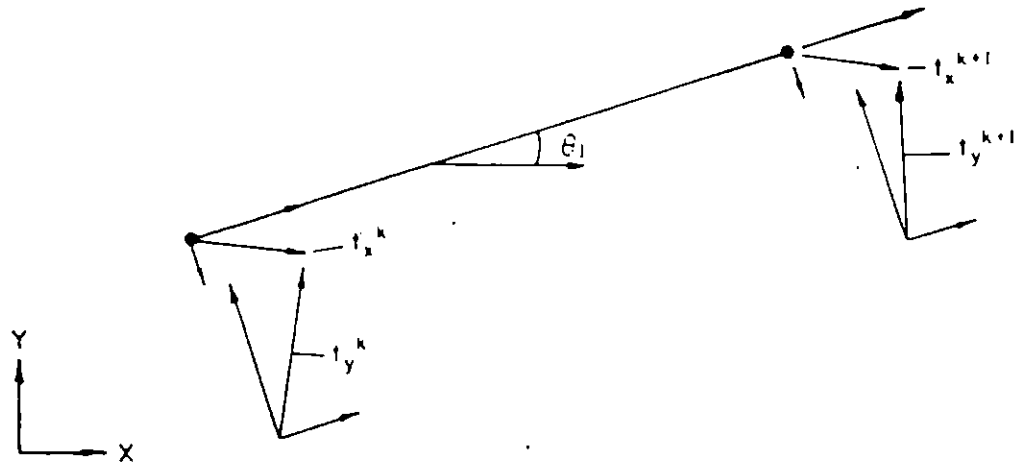

$$\begin{bmatrix} t_n^k \\ t_t^k \\ t_n^{k+1} \\ t_t^{k+1} \end{bmatrix} = \begin{bmatrix} -S & C & 0 & 0 \\ C & S & 0 & 0 \\ 0 & 0 & -S & C \\ 0 & 0 & C & S \end{bmatrix} \begin{bmatrix} t_x^k \\ t_y^k \\ t_x^{k+1} \\ t_y^{k+1} \end{bmatrix}$$

$$S = \sin \theta_j$$

$$C = \cos \theta_j$$

Figure 3.6: Transformation of Global Tractions to Local Normal and Tangential Tractions

Chapter IV

NONLINEAR NUMERICAL TECHNIQUE IN GEOMETRIC AND MATERIAL NONLINEAR PROBLEM

In nonlinear problems it is essential to have a good computational scheme in numerical analysis. The incremental scheme and iterative scheme are widely used in finite element methods. In large deformation analysis with plasticity, a combination of these two techniques is needed because neither one alone will be adequate to obtain an accurate result. The formulations and discussions of these techniques are given elsewhere (Desai, 1979; Stricklin and Hailer, 1974). Only the technique used in this study is presented next.

4.1 SOLUTION PROCESS

Recall the general finite element equation to be solved, Equation (2.35) together with equilibrium iterations in each load step, the equation can be written as

$$\left(\left[{}^{n}K_{L}^{(i)}\right] + \left[{}^{n}K_{NL}^{(i)}\right]\right)\left[U^{(i+1)}\right] = \left[{}^{n+1}R\right] - \left[{}^{n}F^{(i)}\right] \qquad (4.1)$$

where i is the iteration number. It is obvious from this equation that a combination of incremental and iterative techniques is required to solve it. The Newton-Raphson method is probably the most popular approach to handle a nonli-

near problem. The steps of using the Newton-Raphson method are shown in Figure 4.1. For computational efficiency, very often a constant tangent stiffness is used (Fig. 4.2). This is known as the modified Newton-Raphson method. The Newton-Raphson technique, together with the incremental scheme (Fig. 4.3), can be used to solve Equation (4.1). In the computer program written in this study, the user is able to specify the number of iterations with constant stiffness before the stiffness is updated (Fig. 4.4).

4.2 CONVERGENCE CRITERIA

In an iterative process, a realistic criterion is a must for the termination of the iteration. If a loose convergence tolerance is used, the results can be inaccurate. On the other hand if a tight convergence tolerance is used, it will become computationally ineffective. In general, three solution variables can be served as termination criteria (Bathe and Cimento, 1980). They are the displacements, the out of balance forces, and the internal energy. Since the displaced configuration at load step n+1 is sought, it is natural to use the displacements as the convergence check. Hence, a realistic convergence criterion is

$$\|\Delta U^{(i)}\| / \|^{n+1}U\| \leq \varepsilon_D \qquad (4.2)$$

where ε_D is a displacement convergence tolerance and $\|\Delta U^{(i)}\|$ and $\|^{n+1}U\|$. are the norms of the incremental displacements and the total displacements at step n+1. The norm of a variable is given as

$$\|\Delta U^{(i)}\| = \left[\sum_{k=1}^{M} (\Delta U_k^{(i)})^2\right]^{1/2} \tag{4.3}$$

where M is the total number of degrees of freedom in the system. But ^{n+1}U is not known in advance, it can be approximated by $^{n+1}U^{(i)}$. Thus the criterion becomes

$$\|\Delta U^{(i)}\| / \|^{n+1}U^{(i)}\| \leq \varepsilon_D \tag{4.4}$$

In this study ε_D is chosen as 0.001 which is recommended by Bathe and Cimento (1980). Of course the choice of ε_D can be affected by the divisions of load steps. If a very small step is used, the criterion can be relaxed to a larger value.

4.3 ELASTIC-PLASTIC STRESS CALCULATION

In elastic-plastic analysis, the constitutive matrix depends on the current conditions of the stresses, strains, and other state variables. Since the rate forms of stresses and strains are used, Equations (2.20) and (2.59), an integration process is needed to obtain an accurate response prediction. After solving Equation (4.1) the incremental displacements, and thus the incremental strains, can be found. The stresses at load step n+1 are calculated by

$$ {}^{n+1}\tau_{ij} = {}^{n}\tau_{ij} + \int_{n_e}^{n+1_e} {}^{n}C^{EP}_{de} \qquad (4.5) $$

When equilibrium iteration is performed, Equation (4.5) can be generalized as

$$ {}^{n+1}\tau_{ij}^{(i-1)} = {}^{n}\tau_{ij} + \int_{n_e}^{n+1_e(i-1)} {}^{n}C^{EP}_{de} \qquad (4.6) $$

Various numerical integration schemes can be used to solve the above. For elastic-plastic case the Euler forward integration method is adopted for its simplicity. Table 4.1 summarizes the use of the method to solve Equation (4.6). (See step g) The steps in the table are self-explanatory, however, a few words are added for steps (e) and (g) in the following.

To determine the variable RATIO, a linear interpolation method can be used (Hatt, 1974). Suppose F0 is the value of the yield function at step n and F0 is less than 0. After the stresses are updated the new value of yield function is F1 and F1 is greater than 0. The interpolation factor RATIO is given as

$$ \text{RATIO} = - \frac{F0}{F1 - F0} \qquad (4.7) $$

It is important to point out here that the value RATIO is admissible when the loading increment is small. Nayak and Zienkiewicz (1972) give a more accurate procedure to determine RATIO for large load increment. In this study the load

increment is quite small and the usage of Equation (4.7) is found to be adequate.

For step (g) the elastic-plastic strains are subdivided into DDEP. The size of the subdivision will affect the accuracy of the results. The choice of the size is such that the results will be sufficiently accurate and the computational cost will be economical. In this report, DEP is divided into 30 equal increments which is within the range recommended by the program NONSAP (Bathe et al, 1973). Of course when the load increment is reduced, a larger increment can be used to subdivide DEP.

4.4 VERIFICATION OF GEOMETRIC AND MATERIAL NONLINEAR FORMULATION

A computer program is written to handle both nonlinear plane strain and plane stress problems. The Updated Lagrangian with Transformation scheme is used when the body behaves elastically and the Updated Lagrangian with Jaumann stress rate scheme is used when the response is in the plastic range. Two simple problems were analyzed by the computer program to illustrate its features.

4.4.1 Test Problem 1

A perforated strip subjected to tensile loading (Fig. 4.5) was modeled by four-node plane stress elements (Fig. 4.6). The mesh was quite coarse compared to the one used by Zienkiewicz et al (1969) who analyzed the same problem. The results obtained (Fig. 4.7) agreed well with the theoretical results by Theocaris and Marketos (1964). In Figure 4.8, the growth of plastic zone with increasing load is plotted. The largest zone corresponded to a p value of 0.872 σ_y. To obtain zones for higher loading, a very small loading increment was required. For the purpose of the test, this was not done. The spread of plastic zone had a similar pattern to the one obtained by Zienkiewicz et al mentioned above.

4.4.2 Test Problem 2

A cantilever beam with uniform loading (Fig. 4.9) was modeled by both the four-node and eight-node elements (Fig. 4.10). First a very large yield strength was used to keep the beam in elastic range. The results obtained (Fig. 4.11) were compared to the analytical solution by Holden (1972). The eight-node elements gave a very accurate result. For the four-node element, even though more elements and larger degree of freedom were allowed, the results were not as good. This verified the fact that the eight-node element is supe-

rior to the four-node element in modeling flexural behavior. To see the combined effect of geometric and material nonlinearities, a small yield strength of 750 psi was used for the eight-node element mesh in the second run. The results are shown in Figure 4.12. As expected the tip deflection increased when the beam started to yield. The counter effect of geometric and material nonlinearities can be seen from load step 80 to 90. Beyond load step 90, material nonlinear behavior governs, the displacement increased drastically and the solution fails to converge.

TABLE 4.1

Solution Algorithm for Elastic-Plastic Stress Calculation

Given: SIG = total stresses at step n
TAU = total stresses at step n+1
DELPS = incremental strains

a) Calculate the stress increments DSIG using elastic material matrix
DSIG = C * DELPS

b) Calculate TAU
TAU = SIG + DSIG

c) With TAU as the state of stress, determine the value of the yield function by Equation (2.67).

d) If f(TAU) ≤ 0, behavior is elastic and procedure is stopped. Hence the stresses at step n+1 are given by TAU.

e) If f(TAU) > 0 and the previous state of stress indicates elastic behavior, there is a transition from elastic to plastic. A variable RATIO, which is the portion of incremental strain taken elastically, is determine as follows
f(SIG + RATIO * DSIG) = 0
If the previous state of stress is plastic, RATIO is set 0 and proceed to step f.

f) Redefine TAU as the stress at start of yield
TAU = SIG + RATIO * DSIG
and calculate the elastic-plastic strain increment
DEP = (1 - RATIO) * DELPS

g) To obtain the final stresses, the stress increments due to the elastic-plastic strain DEP are added to TAU. Since the material is path dependent, DEP is subdivided into subincrements DDEP and TAU is updated for each interval by the increments in stresses corresponding to the strain increments. In the calculation, the constitutive matrix corresponding to the latest available stress condition is used, i.e.,
TAU = TAU + C * DDEP
for all subincrements DDEP.

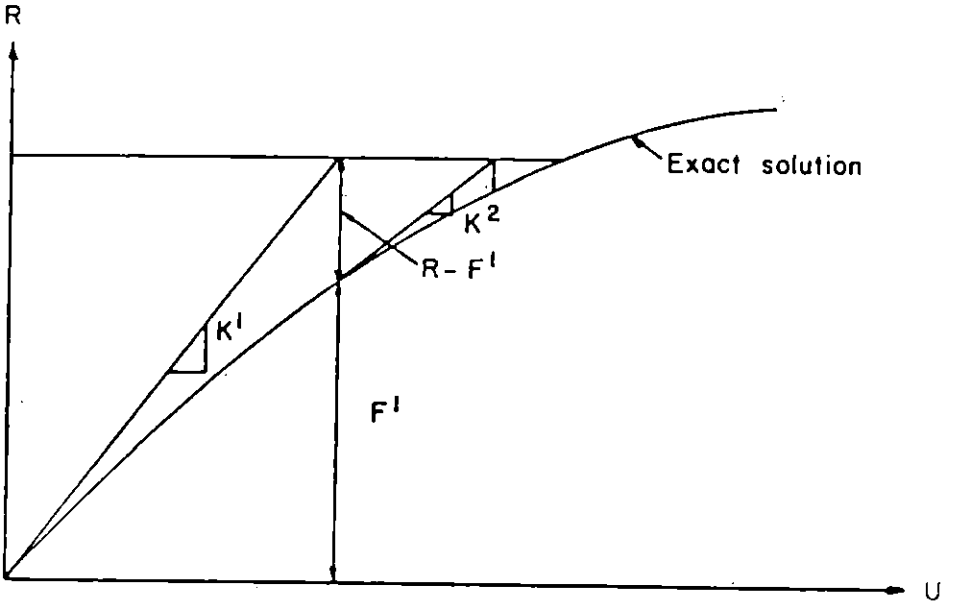

Figure 4.1: Newton-Raphson Iteration

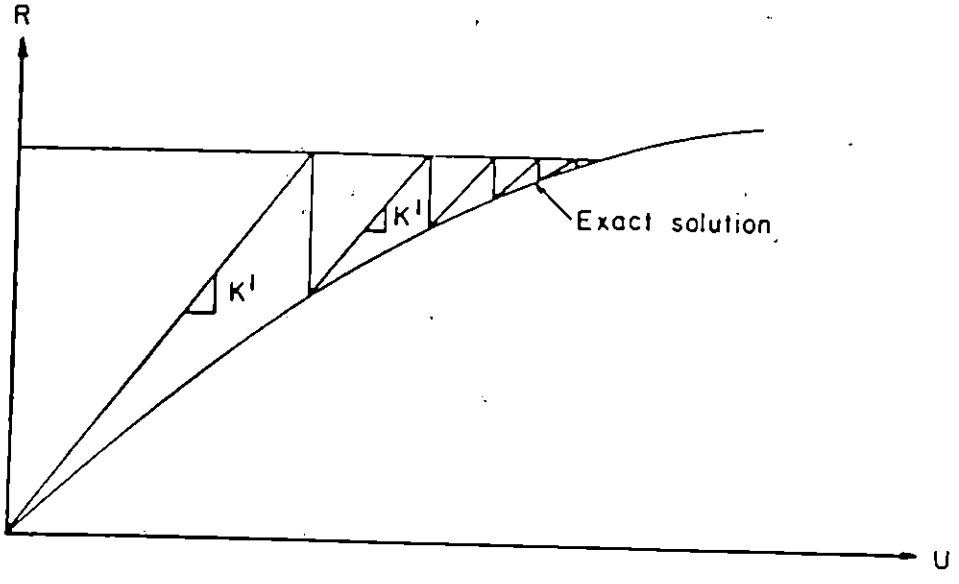

Figure 4.2: Modified Newton-Raphson Iteration

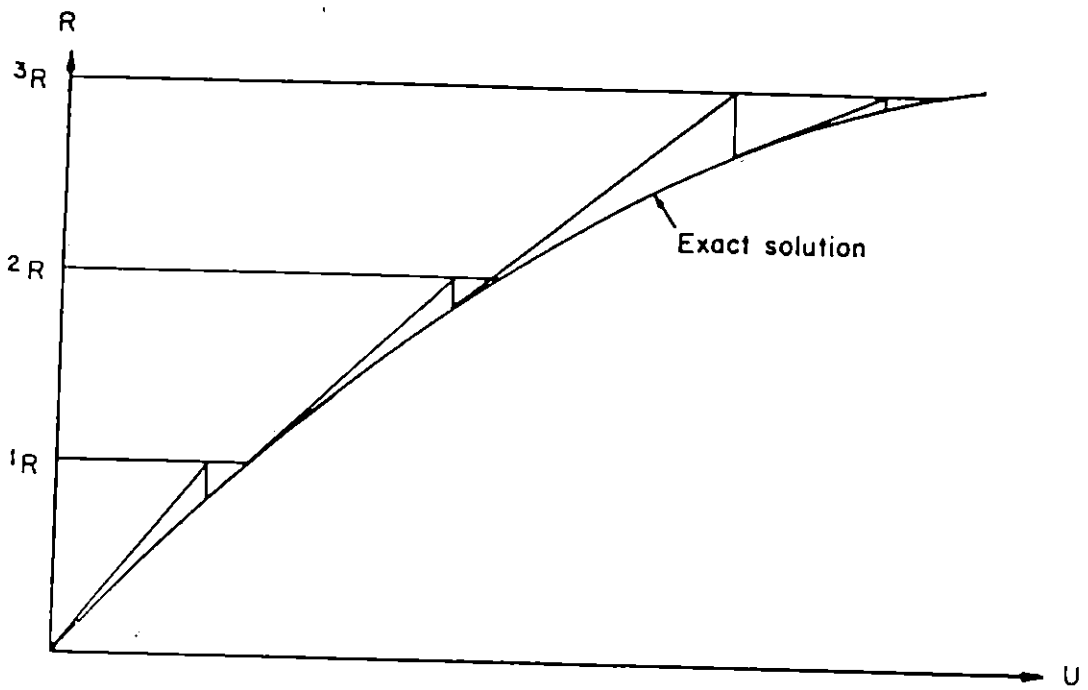

Figure 4.3: Combined Incremental Technique and Newton Raphson Iteration

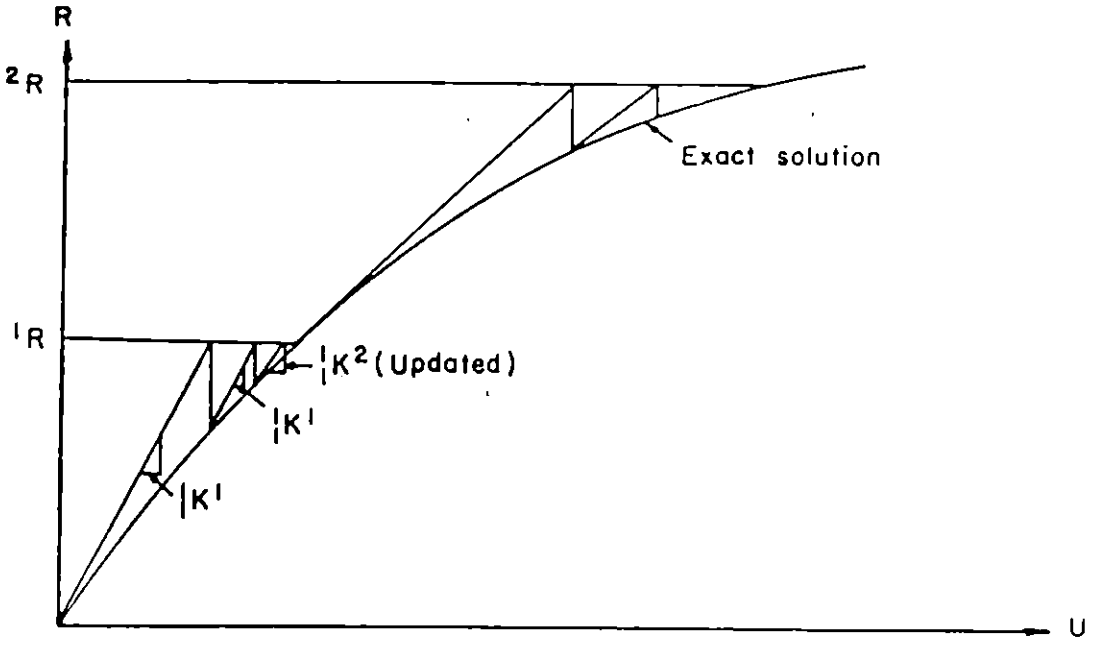

Figure 4.4: Solution Scheme Adopted in Computer Program

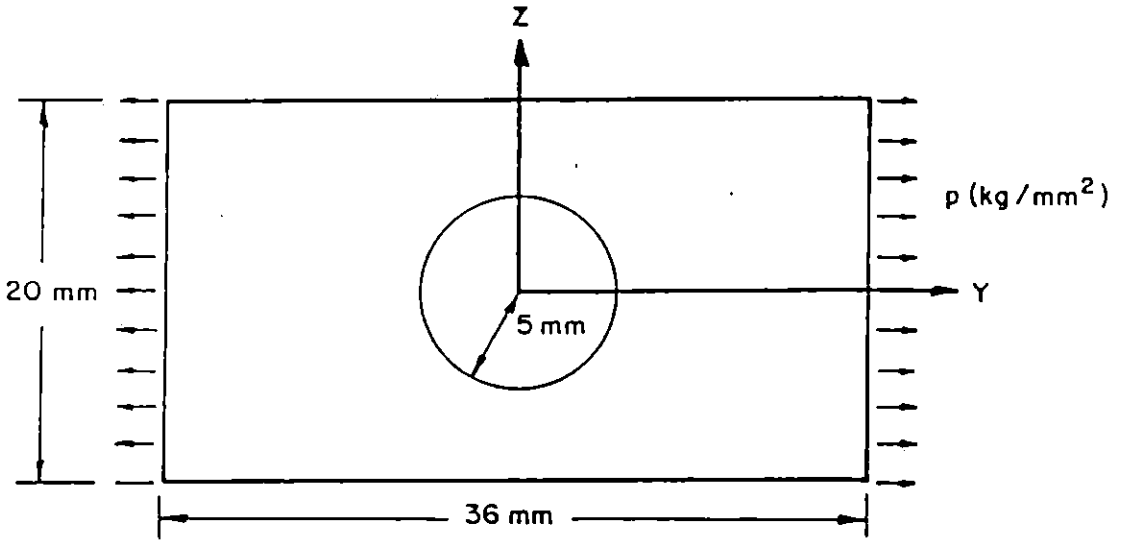

ELASTIC-PLASTIC ISOTROPIC HARDENING MATERIAL,
VON MISES YIELD CONDITION

$E = 7000$ kg/mm^2

$\nu = 0.2$

$\sigma_y = 2.43$ kg/mm^2

$E_T = 225$ kg/mm^2

Figure 4.5: Perforated Tension Strip (Theocaris and Marketos, 1964)

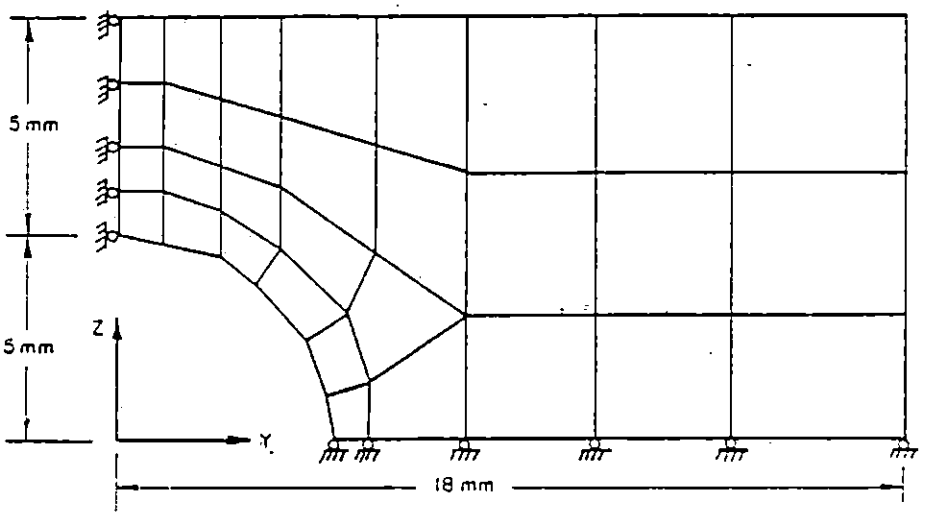

Figure 4.6: Finite Element Mesh of Perforated Strip

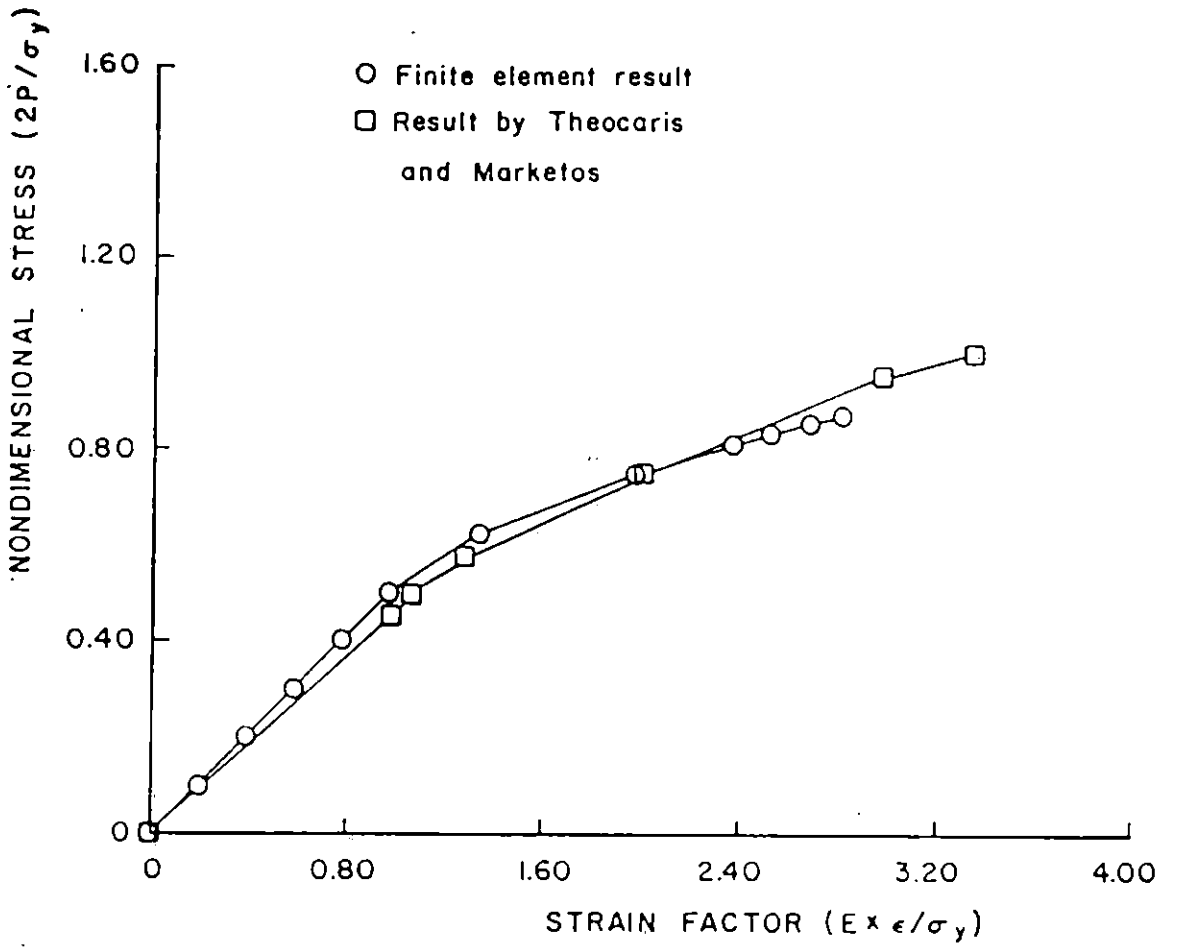

Figure 4.7: Development of Maximum Strain at Point of First Yield in Perforated Strip

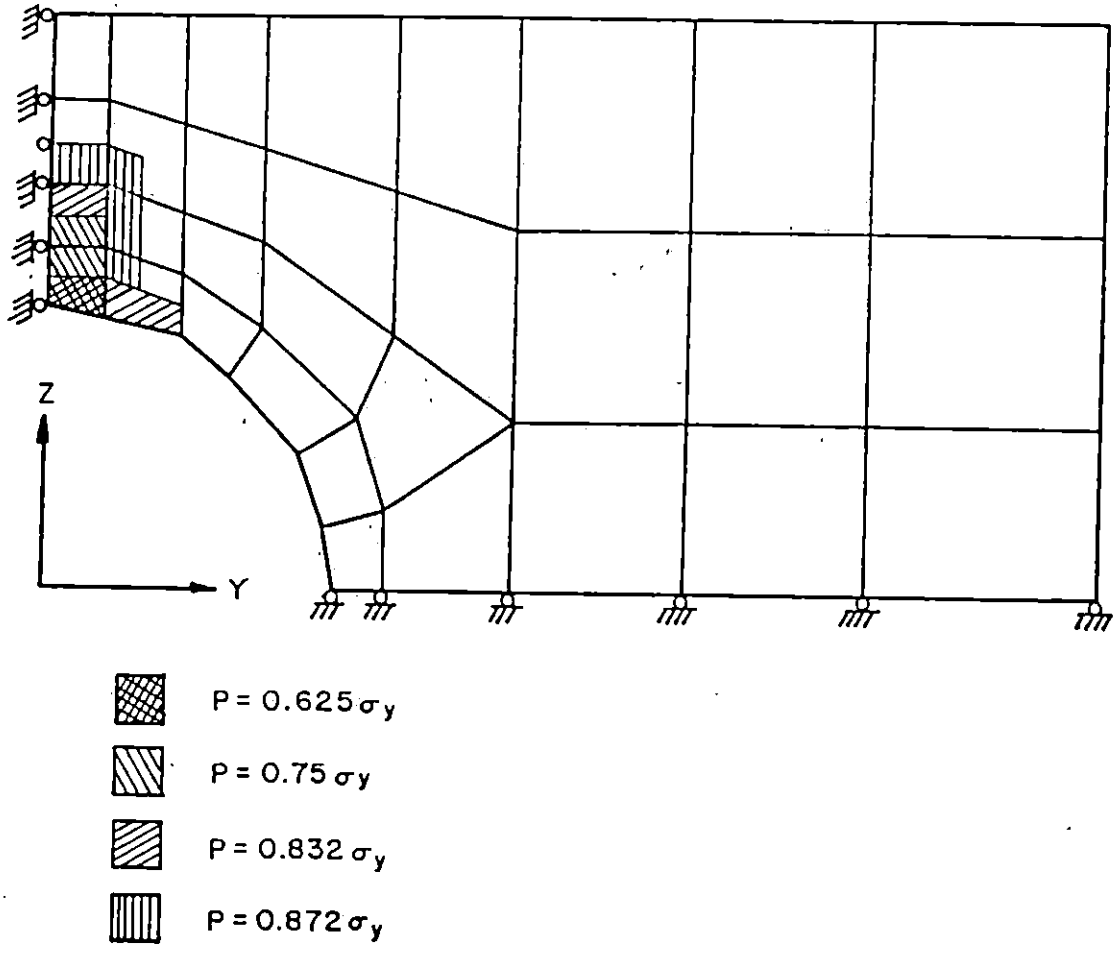

Figure 4.8: Growth of Plastic Zone With Increasing Load in Perforated strip

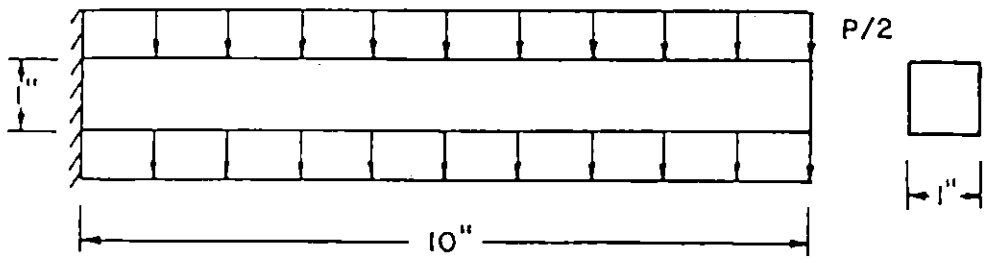

$E = 1.2 \times 10^4$ lb/in^2 $\quad f_y = 1200$ lb/in^2

$\nu = 0.2$

$P_{max} = 10$ lb/in

Figure 4.9: Cantilever Under Uniformly Distributed Load

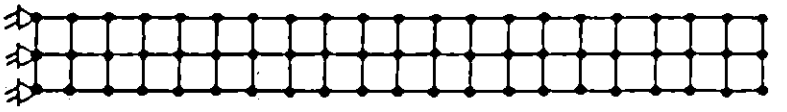

D.O.F. = 120

40 four - node elements

no. of load steps = 100 (with equilibrium iterations)

(a) Four - node Element Mesh

(fy = 750 lb/in^2 for material nonlinear test)

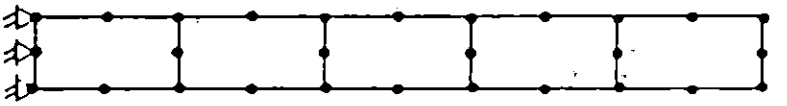

D:O.F. = 50

5 eight - node elements

no of load steps = 100 (without equilibrium iterations)

(b) Eight - node Element Mesh

Figure 4.10: Finite Element Models of Cantilever

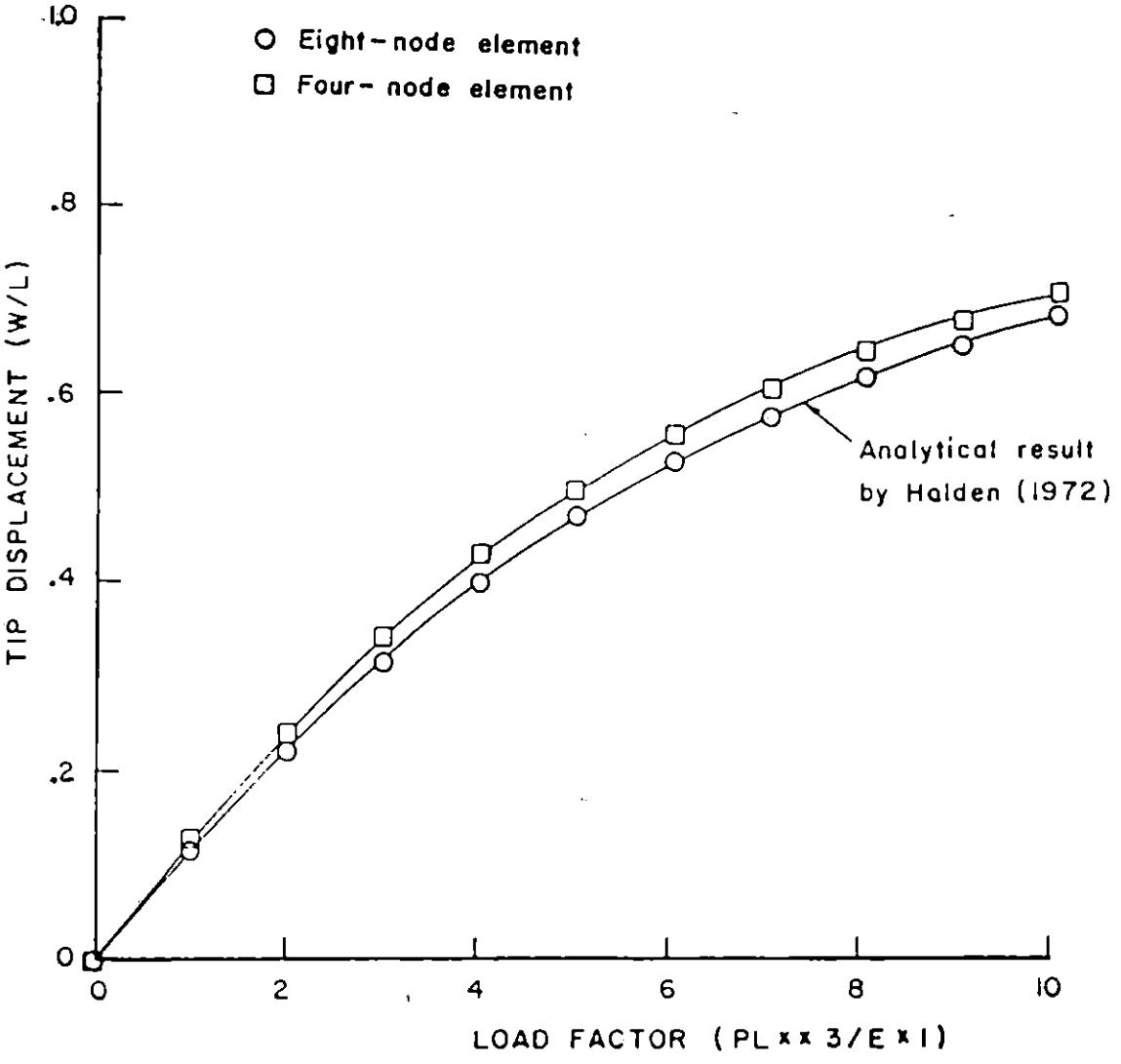

Figure 4.11: Tip Deflection Versus Load in Cantilever, Elastic Behavior

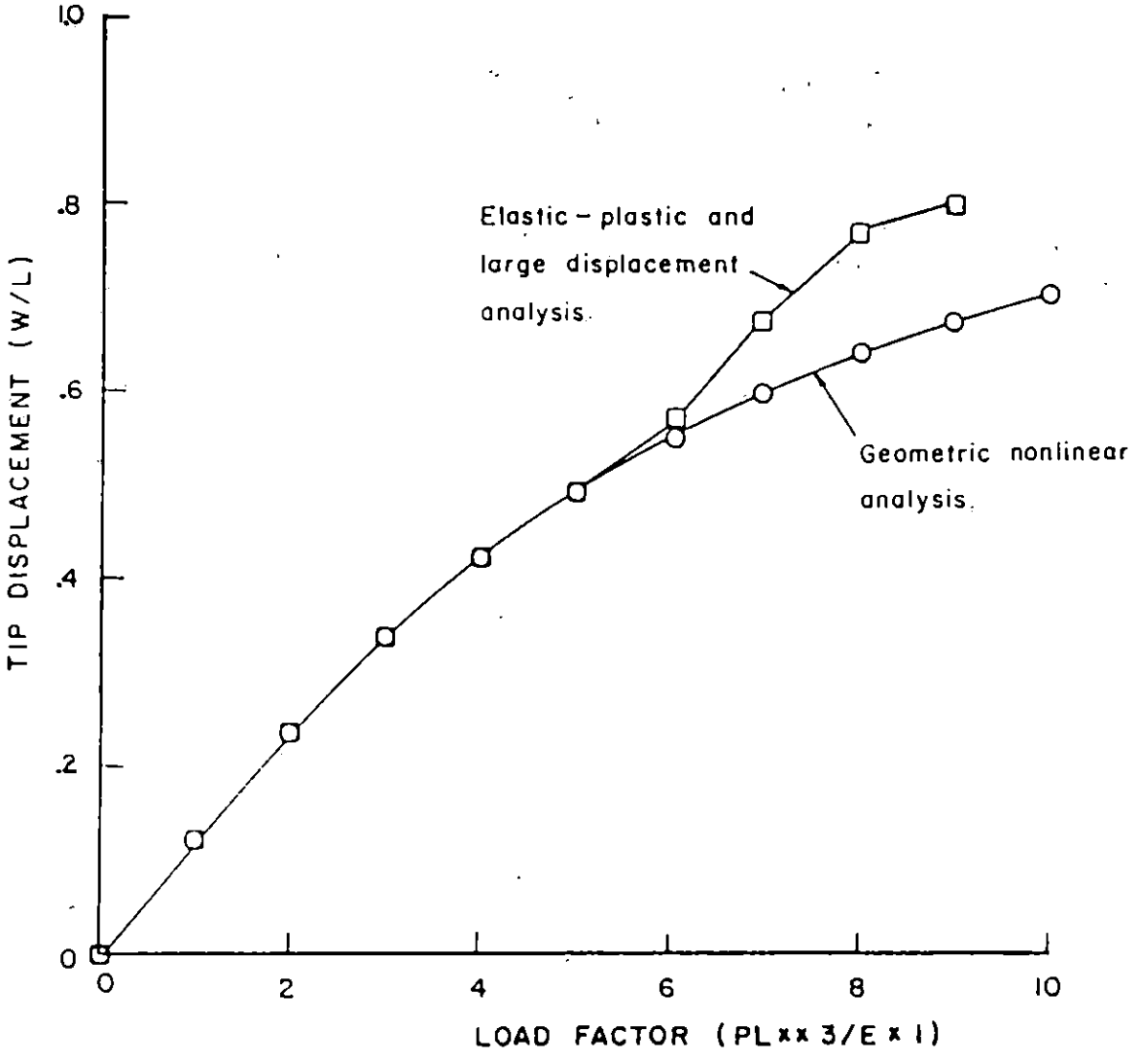

Figure 4.12: Cantilever---Combined Effects of Geometric and Material Nonlinearities (Eight Node Element Mesh)

Chapter V

NUMERICAL TECHNIQUES IN CONTACT ALGORITHM

In Chapter III, the basic formulation for the contact problem is presented. Because of the highly nonlinear contact conditions involved in the analyses, care must be taken with respect to the details of the formulation.

In the evaluations of nodal penetration Δ and the nondimensional location factor β, dot products with respect to the local coordinate system of the target segment are needed (Equations 3.7 and 3.8). Thus a consistent definition of these unit vectors is adopted in order to avoid confusion and to facilitate program implementation. Figure 5.1 represents the nature of input data when the contact element side is described. For instance, if contact is possible at side 1 of the element as shown, the target side is defined by going in counter-clockwise direction from node 1 to node 2. The unit tangential vector will also point from nodes 1 to 2. Thus unit normal vector will always point into the target element. Recall that in Chapter III the same convention is used for defining positive tractions. With this local coordinate system the location factor β is always measured from the first node of the target segment. For instance, β is measured from node 1 in the above example. In the fol-

lowing sections, all the equations derived for determination of contact and its location follow the same reference system given above.

5.1 DETERMINATION OF CONTACT LOCATION

At the end of each iteration, the new locations of all contact points are required to determine the amount of penetration by the contactor nodes and their positions on the corresponding target segments. These will enable the construction of the contact stiffness and the contact force vector which are used for the next iteration. Thus a vital step in the contact algorithm is the procedure to trace the relative positions of the contactor nodes with respect to the target segments. An inherent assumption is that the incremental displacement is small compared to the size of the target segment. To achieve this, first, a search is needed for each contactor node to locate a target node which is closest to it. In Figure 5.2, it is assumed that the contactor node is determined to be nearest to target node i. It is clear from the figure that contact can be made either at segment d_{i-1} or segment d_i. Thus the next step is to decide at which segment the node k will contact. To do this a line passing through node i which is perpendicular to the line joining nodes i-1 and i+1 is constructed. Figure 5.2

shows a convex and concave target segment and the lines described above.

Define

$$n_i = (X_{i+1} - X_{i-1})/\|X_{i+1} - X_{i-1}\| \tag{5.1}$$

which is the unit vector pointing from node i-1 to node i+1. The upper case X represents a position vector. Then

$$l_o = (X_i - X_{i-1}) \cdot n_i \tag{5.2}$$

and

$$l = (X_k - X_{i-1}) \cdot n_i \tag{5.3}$$

If

$$\begin{aligned} l < l_o &\quad \text{then contact at } d_{i-1} \\ l = l_o &\quad \text{contact at node i} \\ l > l_o &\quad \text{contact at } d_i \end{aligned} \tag{5.4}$$

The final step is to decide whether contact has taken place. This is done by calculating the overlap of node k (Fig. 5.3). From the figure, Δ_k is calculated as

$$\Delta_k = (X_k - X_i) \cdot n_N \tag{5.5}$$

If

$$\begin{aligned} \Delta_k = \quad > 0 &\quad \text{contact} \\ < 0 &\quad \text{no contact} \end{aligned} \tag{5.6}$$

and

$$\beta_k = (X_k - X_i) \cdot n_T/d_{i-1} \tag{5.7}$$

where

$$0 < \beta_k < 1 \tag{5.8}$$

It is possible that the calculated value for β_k is greater than 1, in that case it is set as 1 (Fig. 5.4). Some modifications are required when node i is the first or the last node in the contact segment. These are given schematically in Figures 5.5 and 5.6.

5.2 CONVERGENCE CRITERIA

In the analysis of contact problem, both the nodal displacements and contact forces are formulated as unknowns in the solution process. Thus a realistic convergence check shall include both the displacement and force effects. Bathe and Chaudhary (1985) suggest usages of the convergence criteria on incremental energy and the change in contact forces in their work. To measure the convergence in incremental energy, a tolerance ETOL is chosen such that

$$\frac{\Delta U^{(i)T}\left({}^{n+1}R + {}^{n+1}R_C^{(i-1)} - {}^{n+1}F^{(i-1)}\right)}{\Delta U^{(1)T}\left({}^{n+1}R + {}^{n}R_C - {}^{n}F\right)} < ETOL \tag{5.9}$$

The recommended value for ETOL is 0.001. For the convergence in contact forces, it is measured by the following equations

where

$$\|\Delta R^{(i-1)} - \Delta R^{(i-2)}\| / \|\Delta R^{(i-1)}\| < \text{RCTOL} \qquad (5.10)$$

and $\|\Delta R\|$ is the norm of all the components in ΔR corresponding to the contact forces. A typical value for RCTOL is 0.01.

5.3 VERIFICATION OF CONTACT ALGORITHM

To illustrate the validity of the contact algorithm, two sets of problems are analysed. The first set contains Hertz contact between a cylindrical body and a flat block. Three different cases are studied under these topics: contact between an elastic cylinder and a rigid block, contact between an elastic-plastic cylinder and a rigid block, and contact between an elastic cylinder and an elastic block. The second set of problems investigates the contact behavior of a buried pipe with overburden pressure. Details are given in the following sections.

5.3.1 Hertz Contact Between Cylinder and Block

A cylindrical body with a radius of 10 inches is subjected to a concentrated load at its center. (Figure 5.7) Because of double symmetry, only a quarter of the cylinder needs to be modelled. Also given in the figure are the load

magnitudes and material properties of the cylinder and the block for the three different analysis cases mentioned previously. Results obtained are compared with the exact solution derived by Hertz (Timoshenko and Goodier, 1970) and are presented separately. Convergence criteria based on incremental displacement is used in these examples.

a) Elastic cylinder and rigid block

Both the four-node and eight-node elements are used to model this problem. The four-node element mesh has 161 degrees of freedom while the eight-node element mesh contains 237 degrees of freedom (Figures 5.8 and 5.9). The contact pressure distributions along different contact lengths are plotted in Figure 5.10 for both meshes. Good agreement with the exact solution can be concluded for both elements. The calculated contact lengths differ from the known solution by less than 4 percent in all cases. With more degrees of freedom in the mesh, the eight-node element yields a more accurate result than the four-node element mesh. To show its superiority over the four-node element, the normal stress distribution along the vertical line of symmetry is plotted in Figure 5.11. Excellent results are obtained from the eight-node elements, on the other hand, the results by the four-node elements are somewhat erratic.

b) Elastic-plastic cylinder and rigid block

The problem is also analysed by both the four-node and eight-node elements. However the four-node element mesh fails to converge because of high stress concentration when penetrations occur between part of the contactor and target surfaces. This is due to the fact that the element stresses are not calculated accurately by the mesh. The eight-node element mesh is not impaired by the same problem. This amplifies once more the advantages of using eight-node elements.

The contact pressure distribution obtained from the eight-node elements is given in Figure 5.12. No exact solution is available for the elastic-plastic cylinder case. However the responses are compared with the elastic cylinder case (Figs. 5.12 and 5.13) to justify the correctness of the results. From these figures it can be seen that a redistribution of load carried occurs because of yielding of the tip element. More load is taken by the elements adjacent to the tip which is physically explainable as an increase of loading carried by the more stiff unyielded elements. Thus it can be concluded the results obtained are physically sound.

c) Elastic cylinder and elastic block

Only the eight-node element is used in this case (Fig 5.14). There is a total of 375 degrees of freedom. Figure

5.15 shows the theoretical contact distribution (Timoshenko and Goodier, 1970) and calculated results. Because of the mesh used, only one point can be compared with the known solution. However, an excellent statics check is noted for the loading and the normal contact force. For P equal to 571.25 lbs., the normal contact force obtained is 571.44 lbs. To obtain more points on the curve, a finer mesh is required. However this was not done in this testing phase. The normal stress distribution along a vertical section through the center of the cylinder is given in Figure 5.16. No exact solution is available for comparison but it is obvious that the curve follows a similar pattern as the results obtained in case (a) of this test set (Fig. 5.11).

5.3.2 Buried Pipe with Overburden Pressure

The buried pipe analysed is shown in Figure 5.17 with the material properties of both the pipe and the surrounding soil. Both materials are assumed to be linear elastic media even though a nonlinear material model is more realistic for soils in general applications. The objective in this test set is to predict tractions along the pipe-soil interface under different frictional conditions. The weight of the soil is assumed to be small compared to the overburden pressure.

The same problem was studied by Bathe and Chaudhary (1985) and a finite element mesh similar to theirs is adopted (Fig 5.18). However the curve beam element used in their work is not available in the present study and an eight-node element is used instead. To model the problem correctly, a good estimate on the thickness of the pipe is required. This is done by back-calculation from the given moment of inertia for the curve beam element and the thickness thus chosen is 0.01 meter. (Note the exact value from calculation is 0.014m and 0.01m is used for convenience.) Three cases of frictional effects are investigated and the results are shown in Figure 5.19. For convergence a check on the incremental internal energy and contact force components is used. The total overburden pressure is divided into four equal load steps.

As seen from the figure, the calculated results differ slightly from the results by Bathe and Chaudhary. This is due to the fact that the stiffness of the pipe is underestimated in this study. However, very similar patterns of responses can be observed in all cases. For the purpose of testing, no further effort is spent here to match exactly the pipe stiffness by changing its thickness.

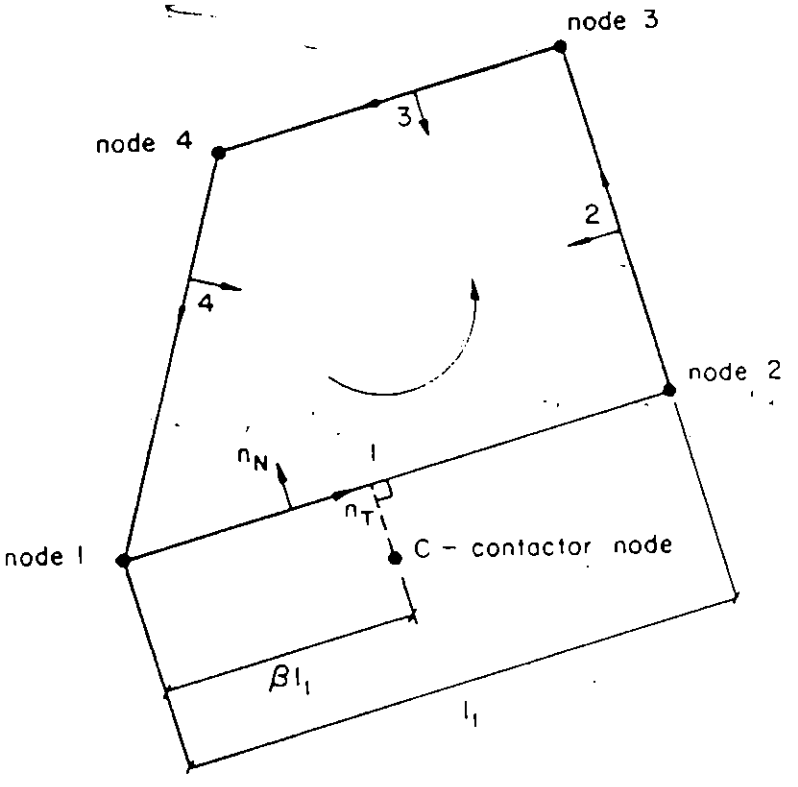

Figure 5.1: Local System Used in Defining Target Segment

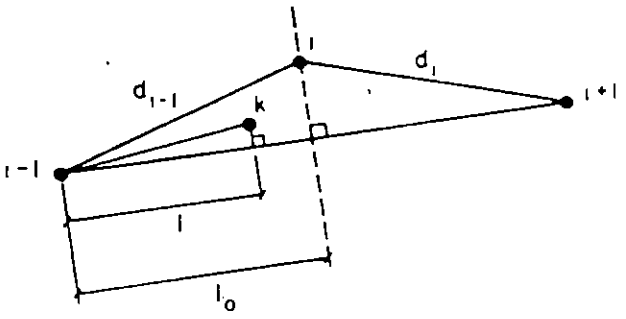

a) convex target surface

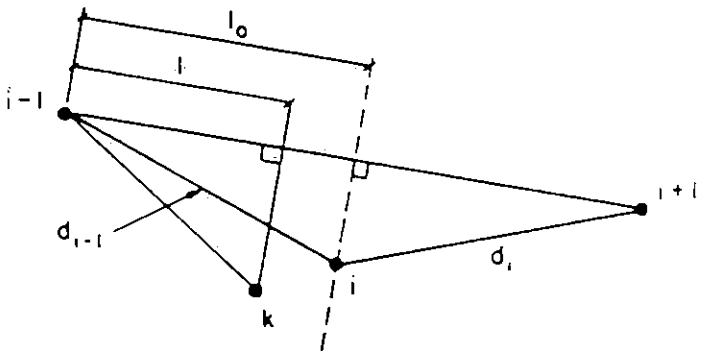

b) concave target surface

Figure 5.2: Determination of Target Segment at which Contact will be Made.

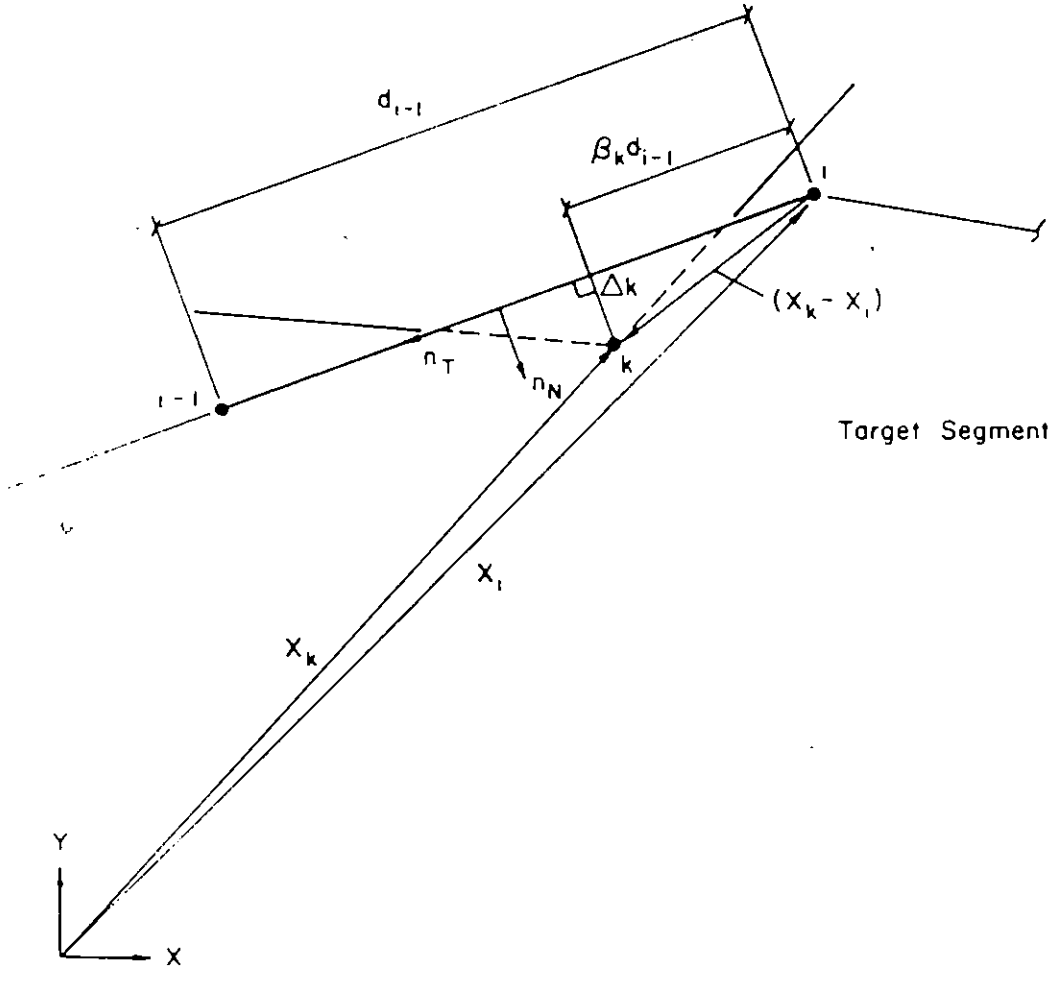

Figure 5.3: Location and Overlap of Contactor Node k

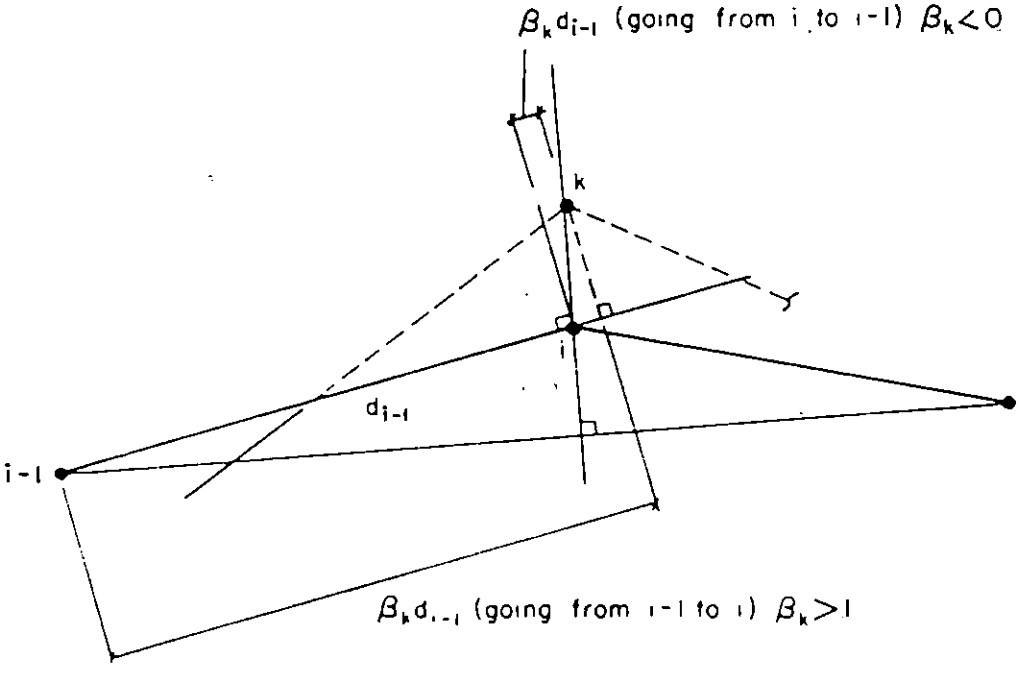

Figure 5.4: Situations for Different Values of β

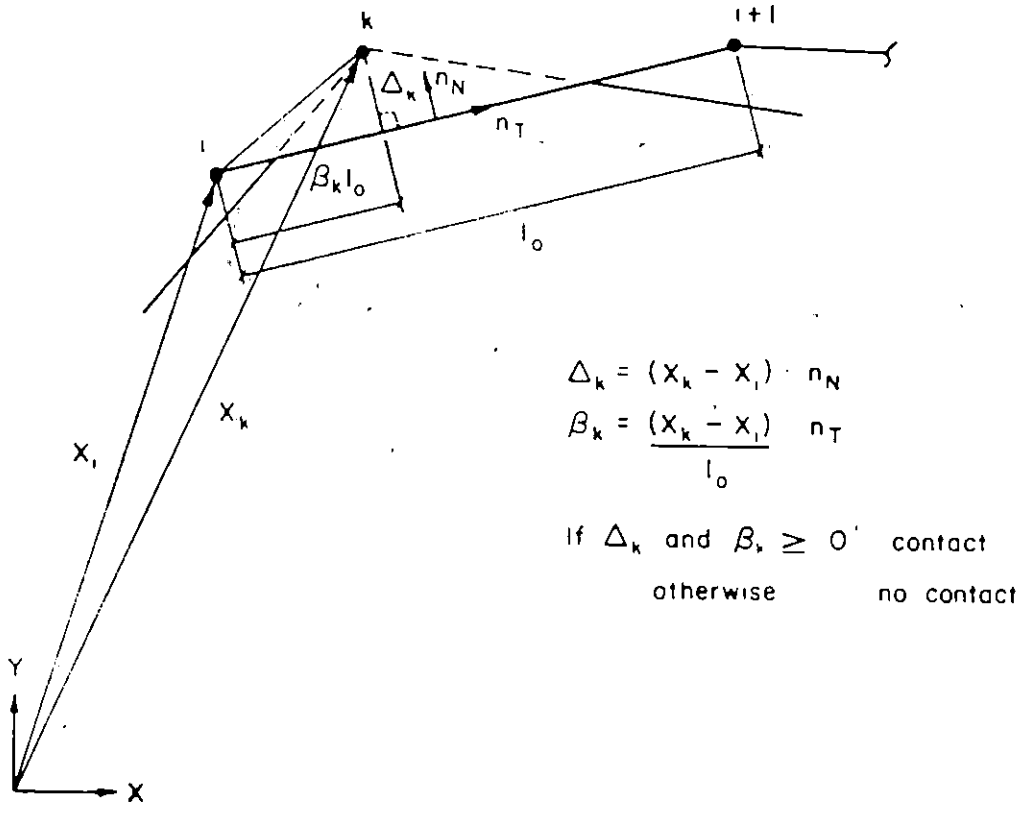

Figure 5.5: Location and Penetration of Contactor Node k Closest to the First Node of Target Segment

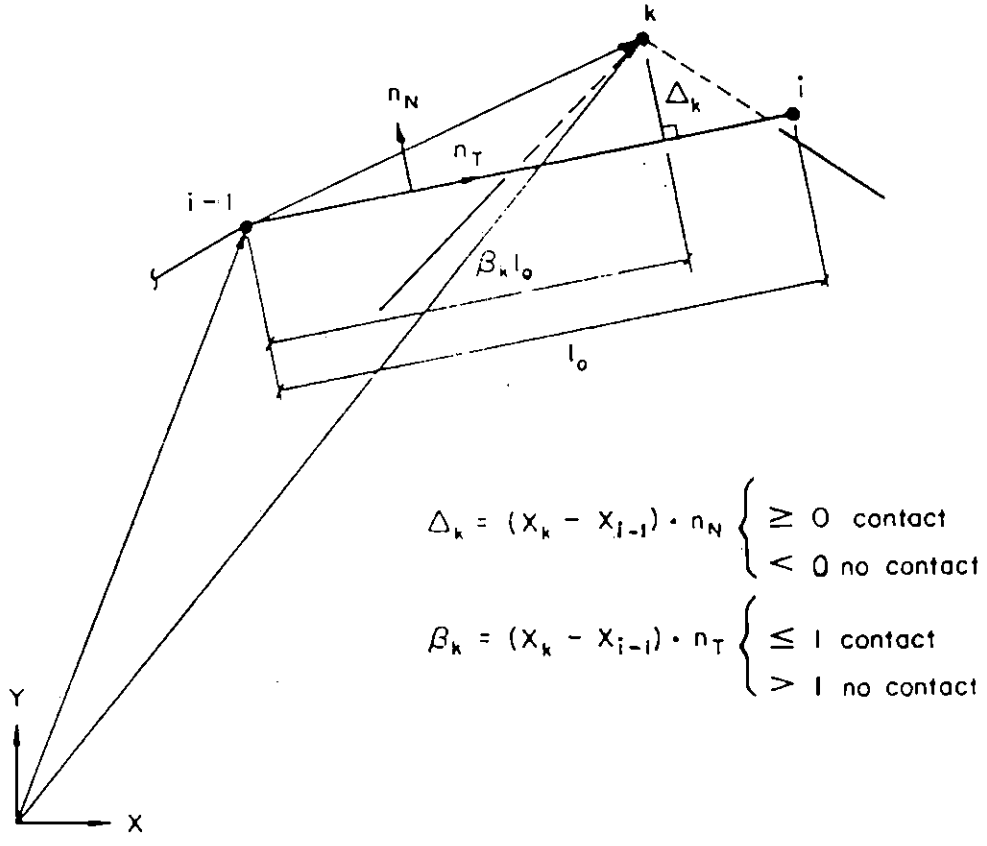

Figure 5.6: Location and Penetration of Contactor Node k Closest to the Last Node of Target Segment

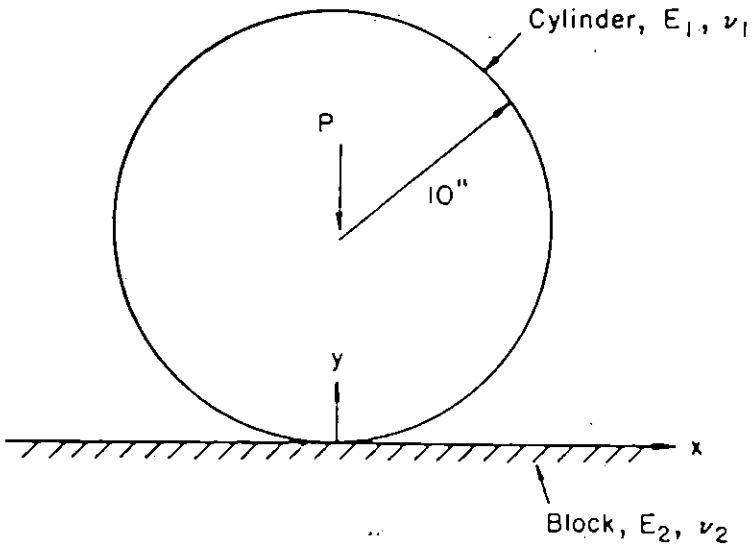

Case (a) P = 2500 lbs

E_1 = 30000 psi ν_1 = 0.25

E_2 = 900000000 psi ν_2 = 0.2

Case (b) P = 2500 lbs

E_1 = 30000 psi ν_1 = 0.5

yield stress = 800 psi

strain hardening parameter = 3000 psi

E_2 = 900000000 psi ν_2 = 0 2

Case (c) P = 571 25 lbs

E_1 = 30000 psi ν_1 = 0 25

E_2 = 300000 psi ν_2 = 0.25

Figure 5.7: Hertz Contact Problem Between Cylinder and Block

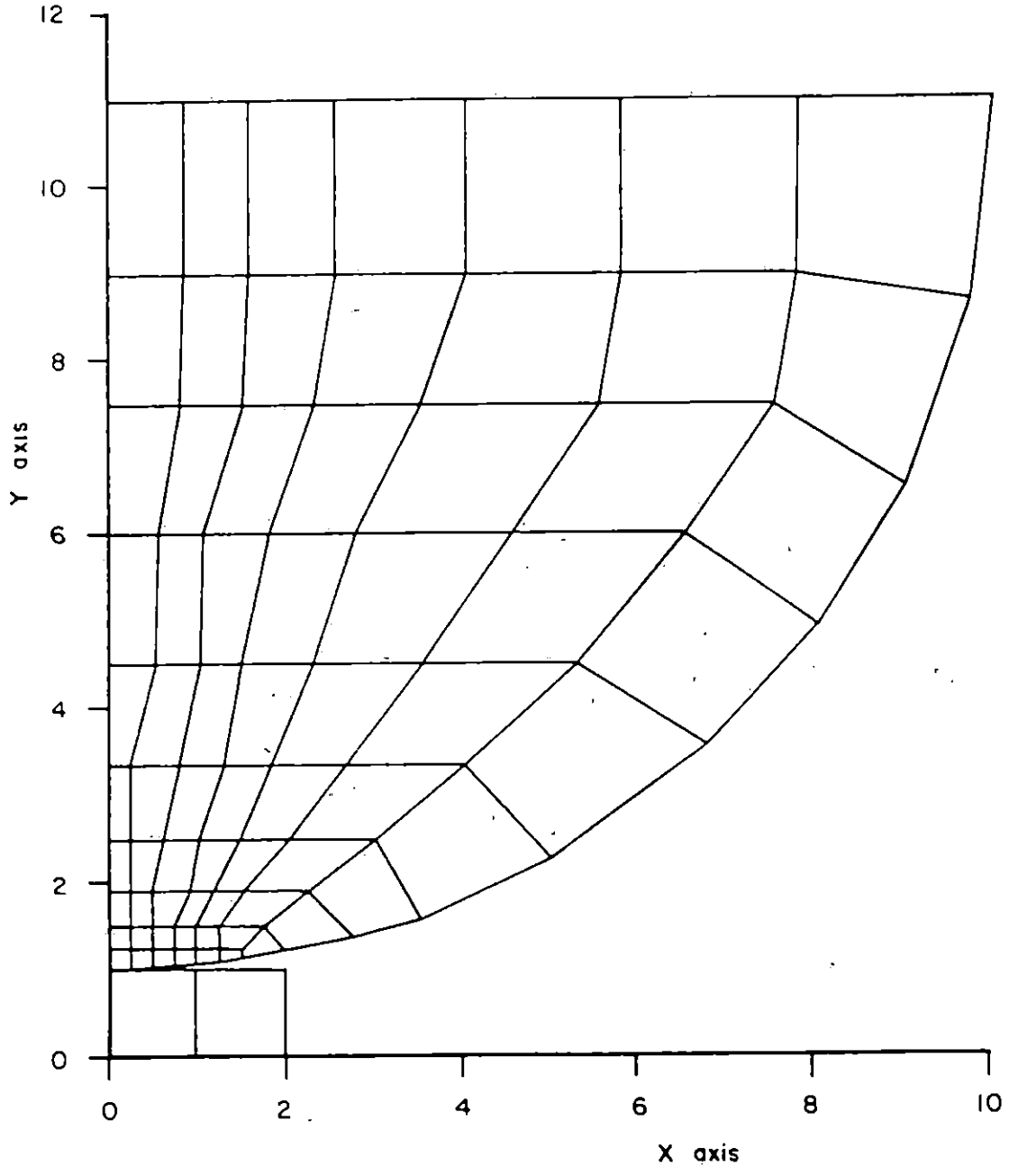

Figure 5.8: Modeling of Hertz Problem by Four-node Elements

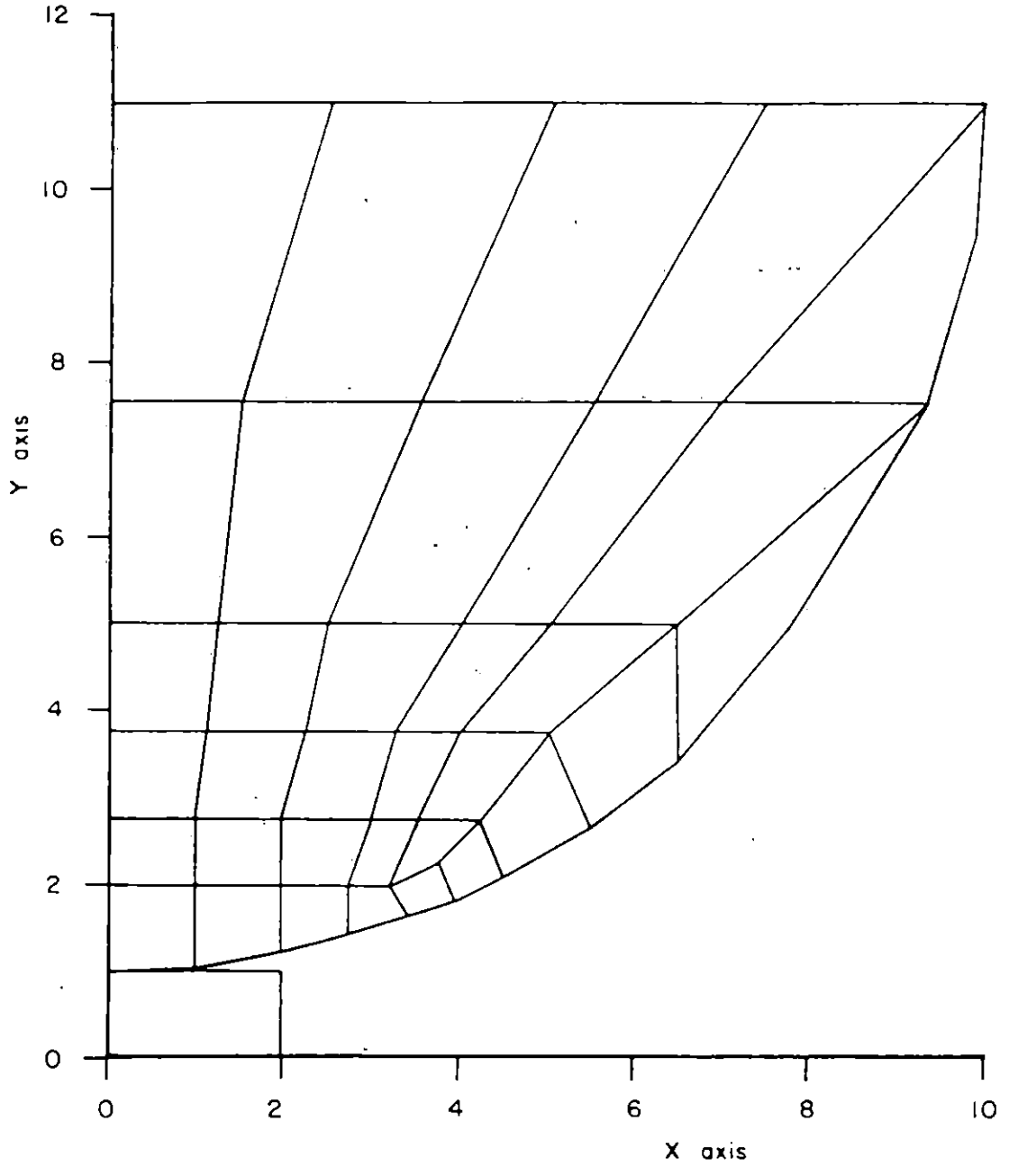

Figure 5.9: Modeling of Hertz Problem by Eight-node Elements

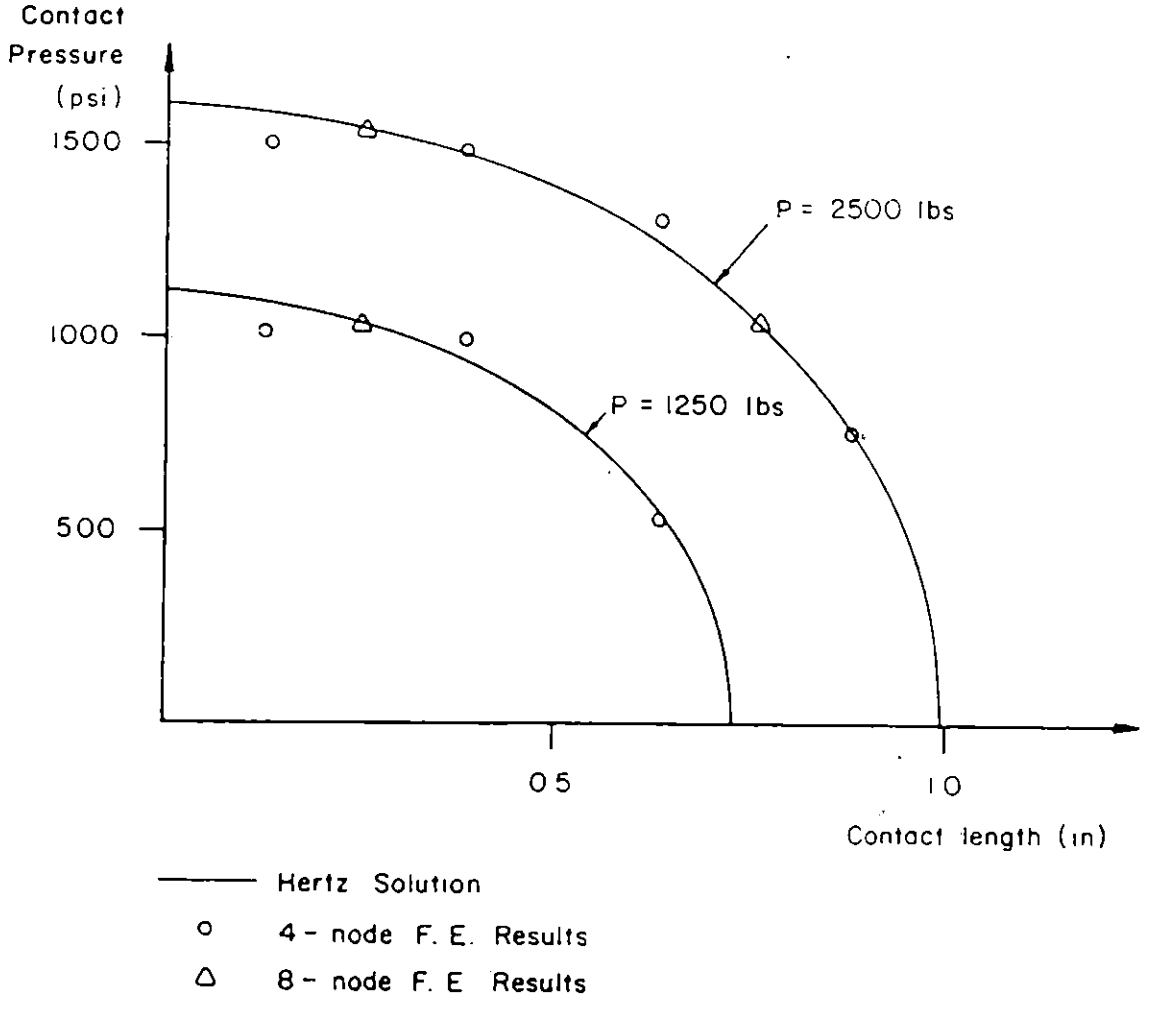

Figure 5.10: Contact Pressure Distributions for Contact Between Elastic Cylinder and Rigid Block

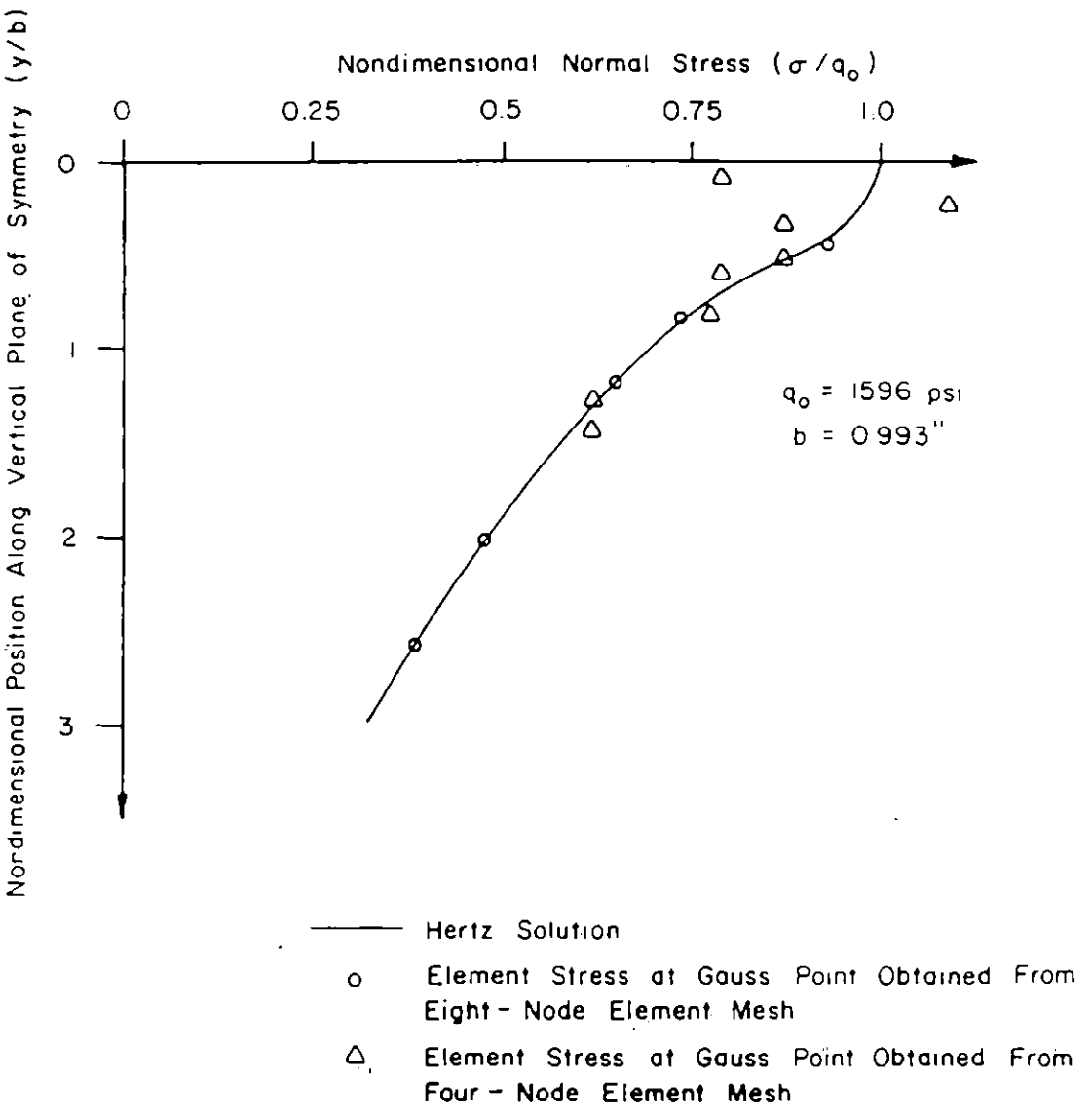

Figure 5.11: Nondimensional Normal Stress Plots Along Vertical Plane of Symmetry for Contact Between Elastic Cylinder and Block

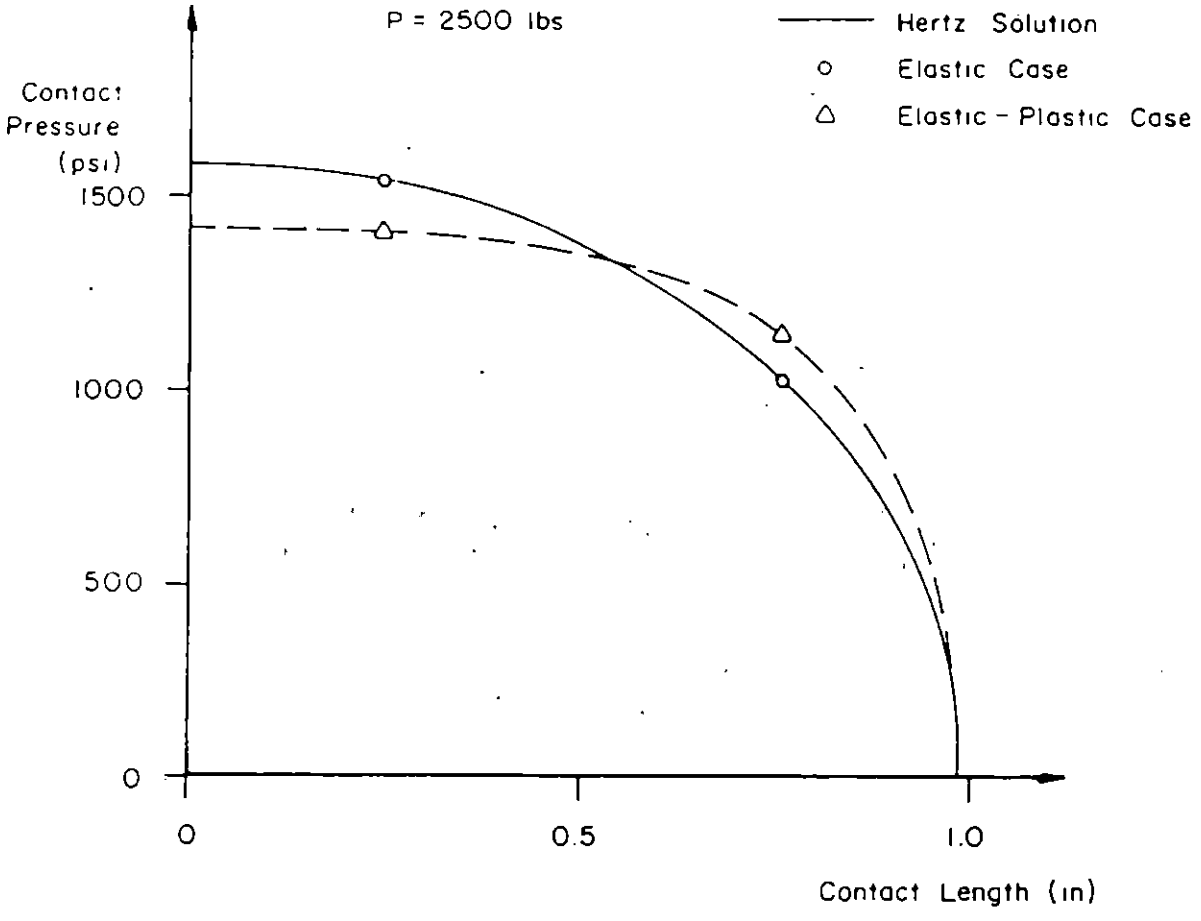

Figure 5.12: Contact Pressure Distribution for Contact Between Ealstic-Plastic Cylinder and Rigid Block

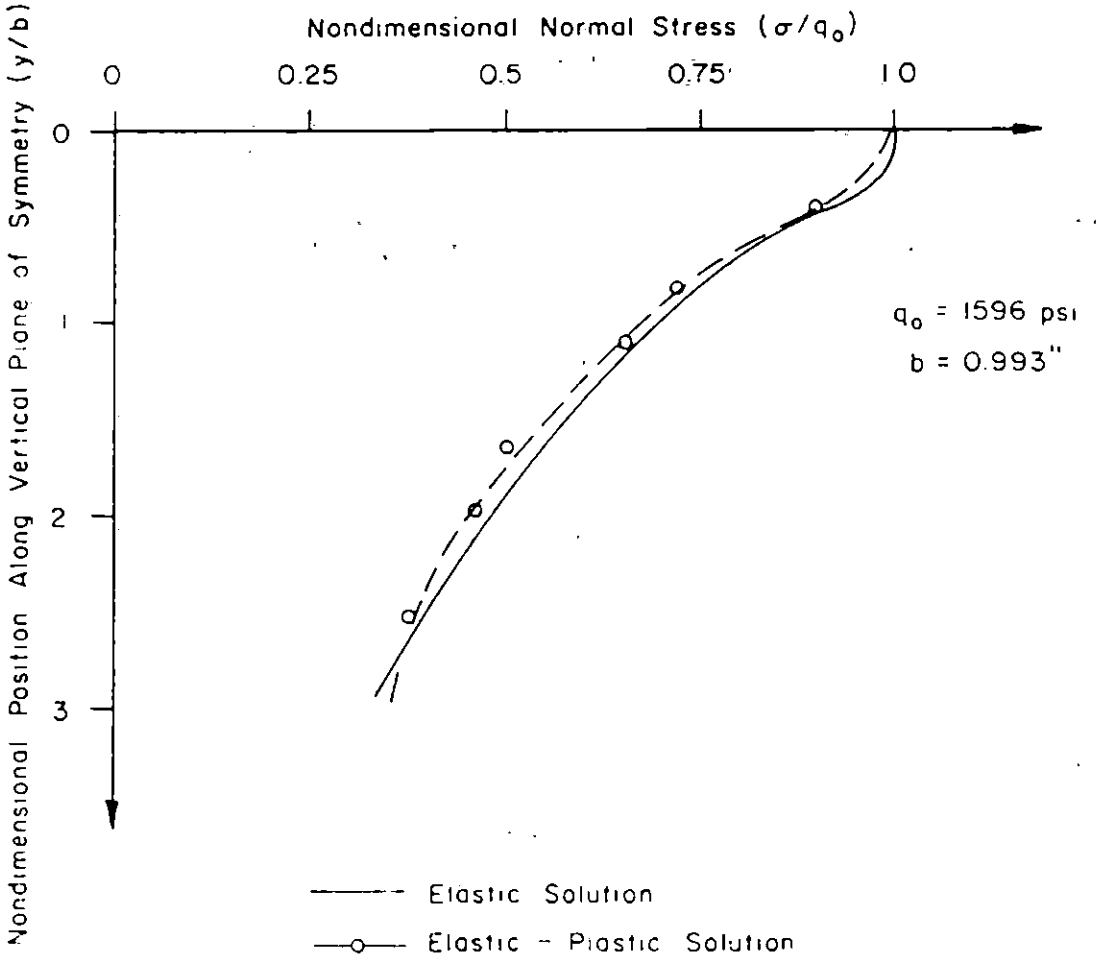

Figure 5.13: Comparison of Normal Stress Distribution Between Elastic and Elastic-Plastic Cases

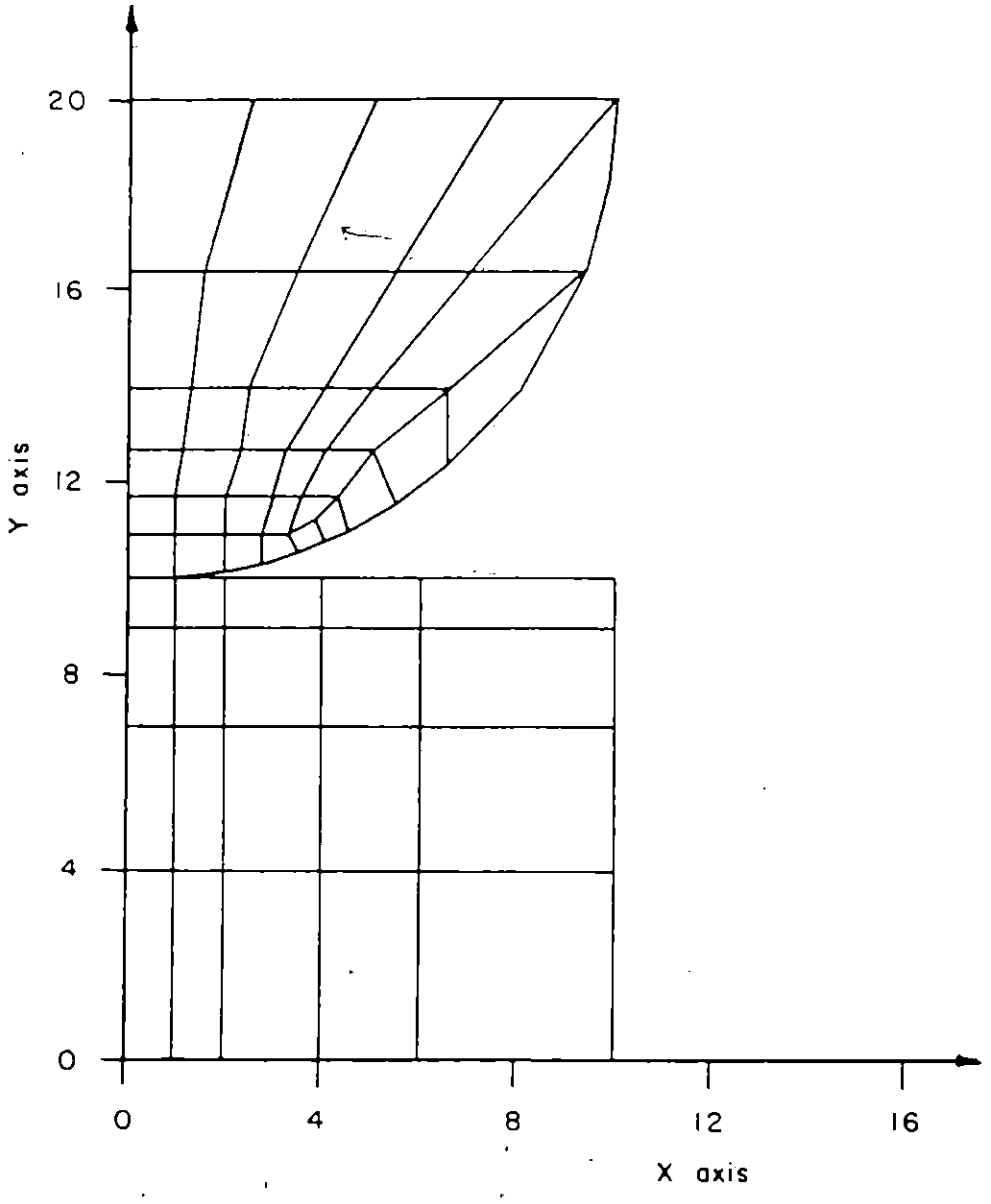

Figure 5.14: Finite Element Modeling of Elastic Cylinder and Elastic Block

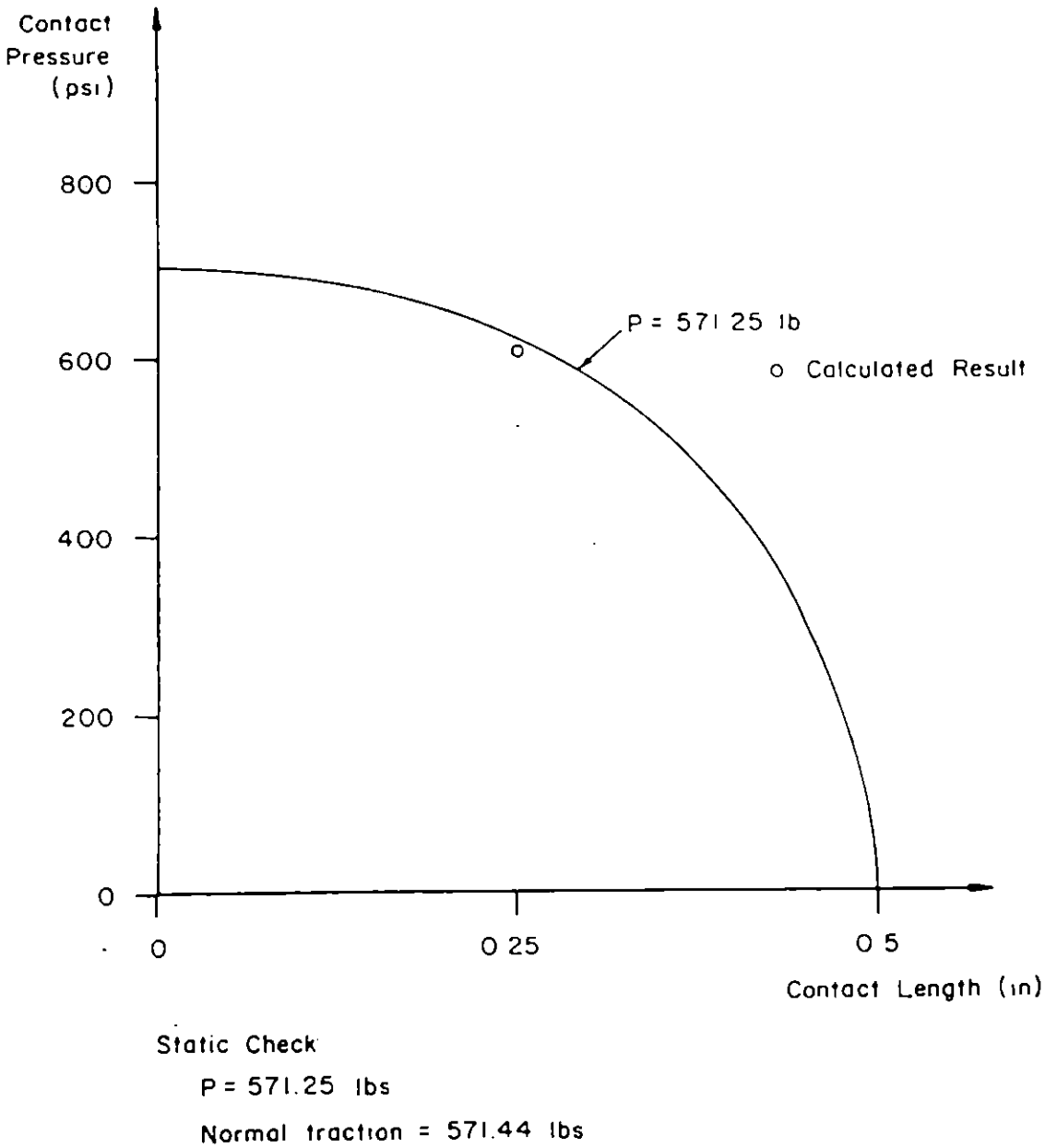

Figure 5.15: Contact Pressure Distribution for Contact Between Elastic Cylinder and Elastic Block

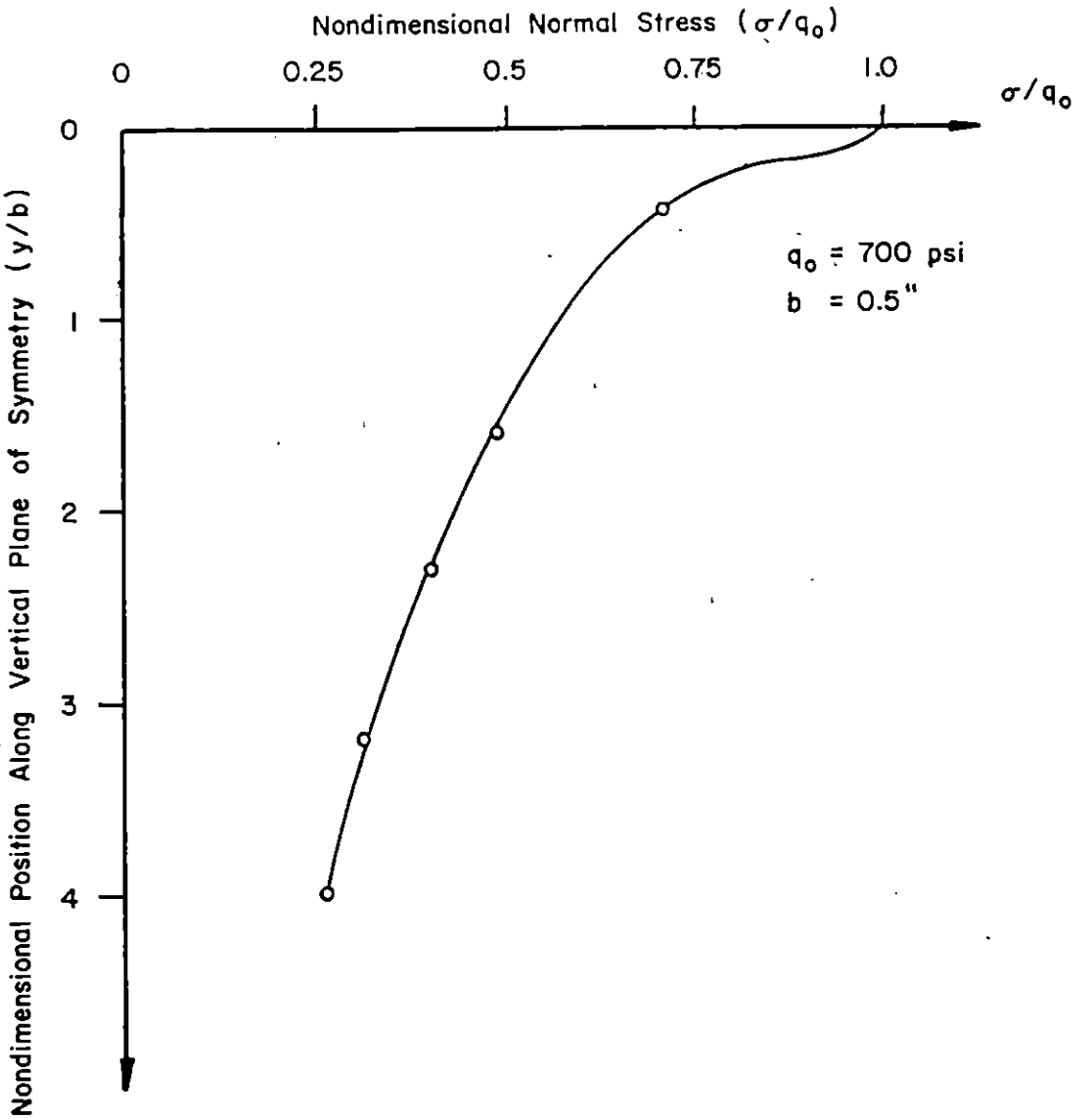

Figure 5.16: Normal Stress Distribution for Contact Between Elastic Cylinder and Elastic Block

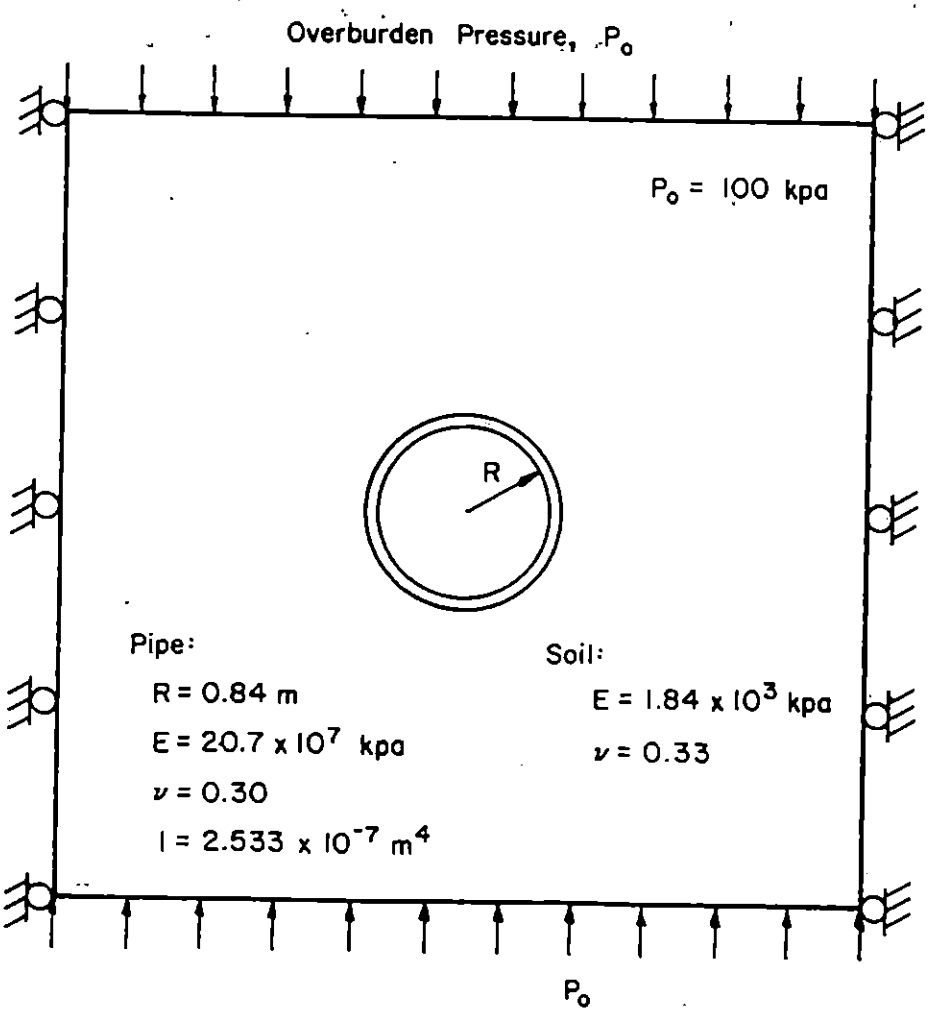

Figure 5.17: Buried Pipe Subjected to Overburden Pressure

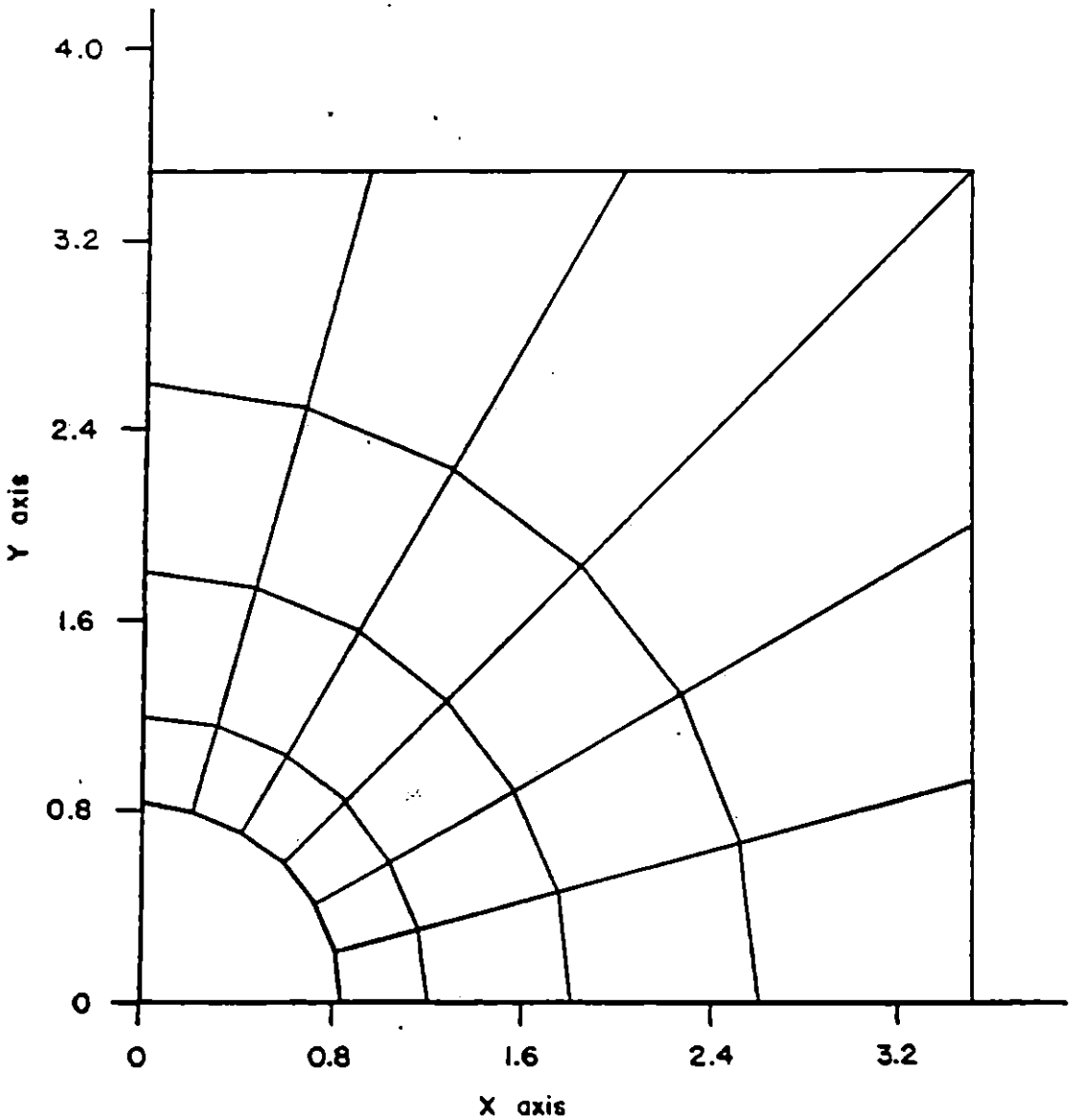

Figure 5.18: Finite Element Mesh for Analysis of Buried Pipe

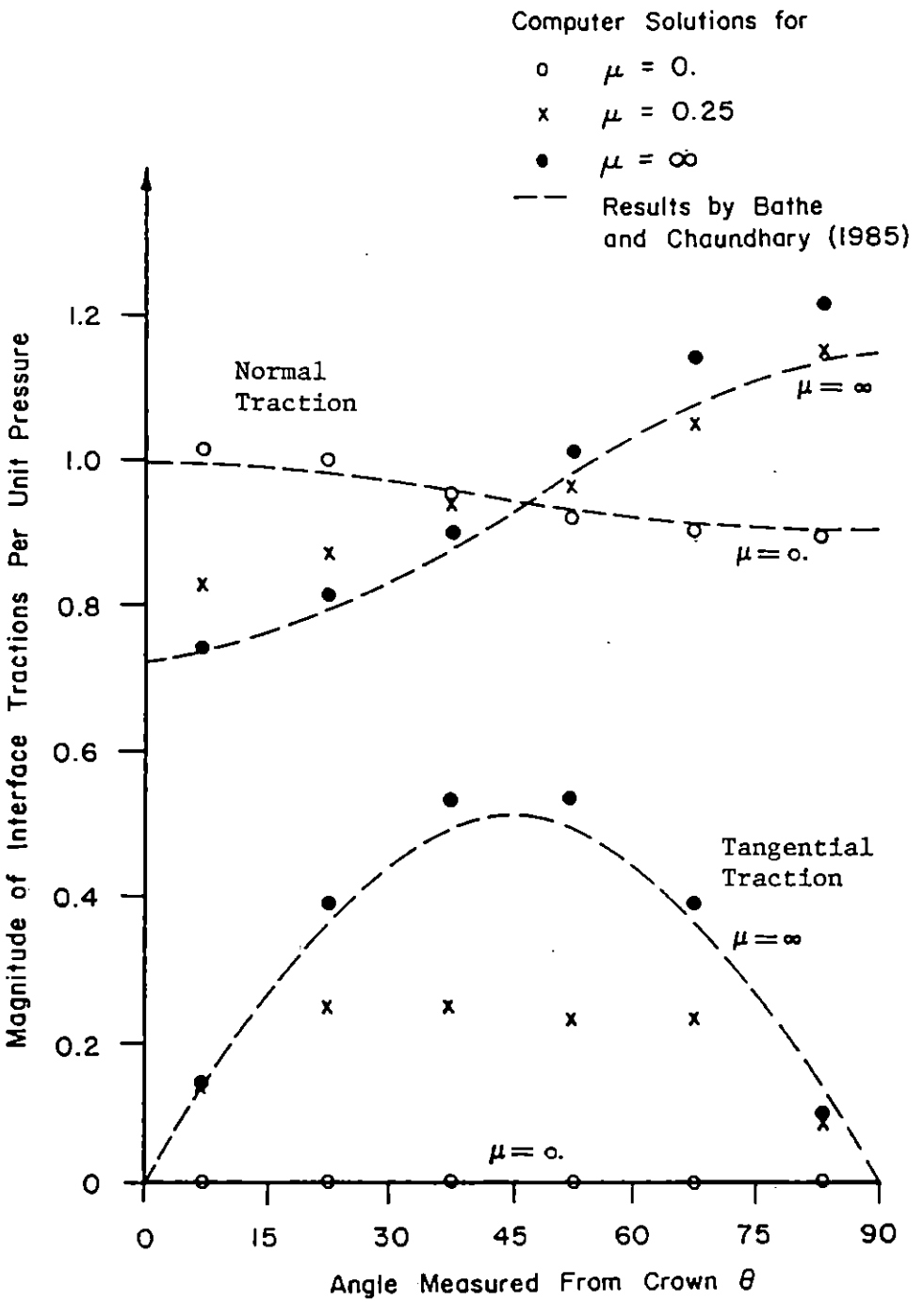

Figure 5.19: Computed Tractions Along Pipe-Soil Interface in Analysis of Buried Pipe

Chapter VI

ANALYSIS OF SHEET PILE INTERLOCKS

The computer program written is used to analyze the sheet pile interlocks. Both regular strength PS32 piles and high strength PSX32 piles are used. The analysis simulates the axially tensile pull-test performed on the sheet piles. A typical set-up for the test is shown in Figure 6.1. Making use of symmetry in the problem, only portions of the sheet piles are needed to be modeled in the two dimensional plane strain finite element analysis (Fig. 6.2). A similar model was used by Nakanishi et al (1981) and was proved satisfactory in depicting the sheet pile behavior under tensile loading. Section 6.1 presents analyses of sheet pile interlocks in which the contact points are not allowed to slip over one another. This will be denoted as Fixed case. The nonlinear formulation of the moving contact problem with elastic-plastic material response is applied to a sheet pile interlock connection in a second set of analyses. Details are given in Section 6.2.

6.1 SHEET PILE ANALYSIS WITH NO SLIDING AMONG CONTACT REGIONS

6.1.1 Description of Finite Element Model

A major concern in the analysis of the sheet pile interlocks is the variations of the interlock geometries in field condition. Since the geometry changes from one interlock to another, the as-rolled shapes of the interlocks published in the Steel Sheet Piling Handbook by United States Steel (1983) were used (Fig. 6.3). The enlarged shapes of the interlocks for both PS32 and PSX32 sheet piles were traced carefully and were used later on for finite element discretizations.

The four-node quadrilateral elements were adopted in this study to model the sheet pile interlocks. Similar element arrangements were used for both PS32 sheet piles and PSX32 sheet piles (Fig. 6.4). Both meshes were made up of 256 elements with a total of 661 degrees of freedom. Since the detailed dimensions of the interlock were not available, the coordinates of the finite element mesh were scaled from the enlarged drawing of the interlock using the known web dimension as reference. The web thickness for the PS32 and PSX32 sheet piles used were 0.5 inch and 0.45 inch respectively. Two other meshes were generated using four-node and eight-node elements to model portions of the PSX32 piles (Fig. 6.5 and 6.6). The total length of the piles is 8.656 inches

with a web thickness of 0.5 inch. In the four-node element mesh, there are 232 elements with 589 degrees of freedom while there are 124 elements with 921 degrees of freedom in the eight-node element mesh. The coordinates of the nodes were measured by an electronic digitizer which could give values up to three decimal places. The data were recorded and stored in the computer.

To obtain the material properties of the sheet piles, tension tests of steel coupons cut from the webs of both PSX32 and PS32 sheet piles were conducted (Oliver, 1984). Yield stress, ultimate stress, and Young's modulus were determined for three coupons from each grade of sheet pile. The yield stress was 44 ksi for the regular carbon steel and 50 ksi for the high strength steel. The ultimate strength was about 70 ksi for both. The average modulus of elasticity of the six coupons was 29500 ksi. In this study the modulus of elasticity was taken as 29000 ksi and Poisson's ratio was taken as 0.3 which is the typical value for steel. Since the sheet piles are expected to reach plastic range at high loading, the strain hardening characteristic of the steel is desired. A very small strain hardening modulus about 1.5 percent of the Young's modulus was used for both PS32 and PSX32 sheet piles.

6.1.2 Finite Element Analysis

Three sets of tests were carried out on the sheet pile interlocks. The first set of test used the two meshes on Figure 6.5 and Figure 6.6. A loading of 8 kips/inch was applied which would keep the interlocks within elastic range. The aim of these tests was to verify the results obtained by the four-node element mesh by a more accurate eight-node element mesh. The comparison showed that the four-node element mesh was capable of modeling the behavior of the interlocks (See Section 6.1.4) and thus was adopted for the rest of the analyses in the Fixed case. The second set of tests used the full length of the sheet piles (Fig. 6.4). The material properties mentioned in Section 4.1 were used. These tests would depict the true response of the sheet piles if there was no sliding in the contact zone. The last set of tests tried to incorporate the effect of slipping between the interlocks by using a lower value for the Young's modulus. From the experimental results obtained by Shannon and Wilson, Inc. (1983) the "effective" modulus of elasticity was chosen as approximately one-sixth of the original value. The three sets of tests are summarized in Table 6.1.

6.1.3 Results of Finite Element Analyses

One of the main objectives of the analyses is to obtain the load-displacement relationships of the sheet pile interlocks. Displacements at twelve locations on the sheet piles are observed (Fig. 6.7). In addition to displacements, the axial strains and bending strains in the webs are calculated from the test results. The axial strain is obtained as the average of the two strains at the top and bottom sides of the web while the bending strain is calculated as half the difference between the two strains. Convention of bending strain is positive when the top fibre of the web is in compression and the bottom fibre in tension. Since the computer results give strains at the Gauss points of an element, linear interpolation is used to get the strain at the top and bottom fibres of the element. To check statics, four critical sections on the sheet piles (Fig. 6.8) are investigated for their axial stress distributions. Again linear interpolations will be used when needed. Since portions of the sheet piles will behave plastically, it is important to trace the growth of plastic zone in the system. Also the equivalent stresses and equivalent strains of three of the elements are calculated in order to show the elastic-plastic response of the sheet piles. The elements are chosen from typical elements from the thumb, the finger, and the web of the sheet pile (Fig. 6.9).

6.1.4 Results of Test Set I

Recall the purpose of the test is to justify the use of the four-node element mesh for the remaining analyses of the sheet piles interlocks. Table 6.2 gives comparisons of the displacements in the X-direction for the twelve chosen points at a load of 8 kips/in. for the four-node and eight-node element meshes. The average difference between the two displacements is 7 percent.

Figure 6.10 shows the web strain distributions of the sheet piles obtained by the two meshes. Both distributions follow a very similar pattern and very good agreement is observed for the axial strain (Table 6.3). The last column in the table compares the bending strain obtained and the results seem to be quite different from each other. This is due to the fact that the differences between strains at the same Gauss point is amplified when extrapolated to the bottom and top fibres of the element. Furthermore the bending strain value is small, thus a small difference in the top or bottom fibre strains will cause a significant difference in the bending strain.

Figure 6.11 compares the stress distributions at various sections of the sheet piles. Again good agreement is found in all sections. It is also noted that excellent static checks exist for the web sections. For the thumb and finger

parts the check is reasonably well consider the fact that most of the data points shown are obtained from interpolations.

6.1.5 Results of Test Set II

In this test set, displacements at only four of the twelve points shown in Figure 6.7 are tabulated. The points are 3, 6, 8, and 10 which will provide information on displacements of the three contact regions and the maximum displacement of the sheet piles. Both displacements at X and Y directions are recorded for the three contact points. These can be found in Table 6.4 and Table 6.5 for PS32 and PSX32 sheet piles respectively. The load-displacement curves of the maximum deflection for the two types of sheet piles are plotted in Figure 6.12 and 6.13. It can be seen from Figure 6.13 that the PSX32 is well within plastic range at a load of 26 kips/in. An attempt was made to reach the guaranteed strength of 28 kips/in. but the solution failed to converge because of excess deformations on the sheet piles. For the PS32 sheet piles further increase in loading will also result in an unstable solution. To illustrate the deformations in the sheet piles, the undeformed mesh and the deformed mesh at maximum load are superimposed. Since displacement magnitudes are small compared to dimensions of the sheet

piles, an exaggeration factor of 30 is used to enlarged the deformed patterns. These meshes are shown in Figure 6.14 for PS32 and PSX32 sheet piles respectively. On these plots instead of the fixed end, the contact regions are lined up because it will give a better indication of the deformations on the sheet piles.

From the results of Test Set I, the web of the sheet pile with fixed end showed significant flexural behavior while the bending on the other web was less pronounced. Thus only the web with fixed end is investigated for axial and bending strains. Since the axial strain is almost constant along the web, a load-axial strain curve is plotted which is independent of position on web. For bending strain a family of load-bending strain curves are needed in order to show the variations of bending strain along the web. Figures 6.15 and 6.16 show the two plots for PS32 sheet piles. For PSX32 sheet piles the results are drawn in Figures 6.17 and 6.18.

For the magnitudes of loadings used in the analyses, both types of sheet piles will reach elasto-plastic range. Figures 6.19 and 6.20 show the growth of plastic zone in the interlocks with increasing loading for PS32 and PSX32 sheet piles. Both types of sheet piles have a similar plastic zone growth pattern. As expected the parts that started to yield first were the thinnest regions on the thumbs of the sheet

piles. It can be seen that the PS32 sheet piles have a larger plastic zone in the thumbs than the PSX32 sheet piles. For PSX32 sheet pile the webs will yield at a load of 26 kips/in., thus, the load resistance capacity at the thumb is not fully mobilized. Yielding of all elements is caused by a combined effect of tension and bending except for those located on or adjacent to the contact points where shearing was the major factor for yielding of the elements. Tables 6.6 and 6.7 give the stress comparisons between the two types of yielding mode for PS32 and PSX32 sheet piles. In order to look more closely at the elasto-plastic behavior of the elements, the equivalent stresses and equivalent strains (Equations 2.64 and 2.71) of three elements (Fig. 6.9) are plotted in Figures 6.21 and 6.22 for PS32 and PSX32 steels respectively.

The last result to be presented is statics check for the system. As observed from Section 6.1.4 the stress distributions obtained for the thumb and finger parts required many interpolations of stress values among different Gauss points, thus the result was not quite reliable. For this reason only the webs of the sheet piles are checked for statics for Test Set II and III. Figures 6.23 and 6.24 give the axial stress distributions for PS32 and PSX32 sheet piles. Also shown in the figures are values of the resultant

internal forces for the sections. Again a very good statics check is observed for both types of sheet pile.

6.1.6 Results of Test Set III

In Test Set III, an effective modulus of elasticity is used for the sheet pile which will try to depict the effect of slipping between the interlocks. The purpose of doing this is to obtain from the analyses the displacement magnitudes which are within the ranges measures by Shannon and Wilson (1982). Thus only the results related to displacements, shape deformations, axial strains and bending strains along web are presented. The formats of presenting these data are identical to those used in Section 6.1.5. Tables 6.8 and 6.9 give displacements at different loads in the three contact regions of PS32 and PSX32 sheet piles respectively. For the maximum tip elongations of the two types of pile, the results are shown in Figures 6.25 and 6.26. The plots of the initial and deformed meshes of the sheet piles can be seen in Figures 6.27. A magnification factor of 5 is used in both figures for drawing the deformed shapes. Figures 6.28, 6.29, 6.30 and 6.31 show the analytical results of axial strain versus load and variations of bending strain along web versus load for PS32 and PSX32 sheet piles respectively.

6.2 SHEET PILE ANALYSIS WITH SLIDING AMONG CONTACT REGIONS

6.2.1 Description of Finite Element Model

The finite element meshes used to model two sheet pile interlocks under axial tensile loading are shown in Figure 6.32. Each mesh contained 92 eight-node isoparametric elements with 771 displacement degrees of freedom and a maximum of 18 force degrees of freedom. Nine pairs of nodes were initiated as the three contact regions in the interlocks (Fig. 6.33). Futhermore the contact regions were defined by: (1) contactor nodes 2, 4, and 6 as contact segment 1, (2) contactor nodes 7, 9, and 11 as contact segment 2, and (3) contactor nodes 13, 15, and 17 as contact segment 3. They were assumed to be in sticking contact at the beginning of the solution of the incremental equilibrium equation.

In this study, both the regular strength PS32 and high strength PSX32 sheet piles were analyzed. In the field, the geometry of the interlock varies from one sheet pile to another due to rolling tolerances of the manufacturing process. As a result of the variation in the interlock geometry, two types of sliding modes were noted in the testing program by Shannon & Wilson (1983). The two modes are: (1) sliding between two thumbs of the interlocks, and (2) sliding between the thumb and the finger portion of the interlock. Since the as-rolled shapes were employed for finite

element discretization, only one sliding mode could be depicted in an analysis. In order to generate the other mode, additional constraints were added to the mesh. This will be discussed in the next section.

The material properties of the sheet piles used were same as those described in Section 6.1.1. The coefficient of friction was chosen as 0.3 for both μ_s and μ_k. This value was recommended in the report by Oliver (1985).

6.2.2 Finite Element Analysis

During the verification phase of the interlock analysis, the PS32 sheet pile model was used. It was found that sliding took place between the two thumbs of the interlocks. A second observation was that the displacements of the sheet pile in the lateral direction were significantly greater than those obtained when the contactor and target nodes were considered to be fixed to each other (Fixed case, Sec. 6.1). This required a small load increment each time for convergence to be possible. From these observations, the following three cases of analyses were performed for the PS32 sheet pile interlocks:

1. Finite element model as shown in Figure 6.32 without additional constraints.

2. The contact nodes between the two thumbs were forced to remain in contact. In addition, the last six elements in each finger of the interlock were assigned a Young's modulus of one-sixth of the original value. The choice of one-sixth follows the "effective modulus" approach used in earlier in Section 6.1.
3. To improve convergence of the problem, two lateral constraints were imposed at the tips of the two thumbs to reduce the lateral movement of the sheet piles.

From here on, these analyses will be referred to as Case 1, 2, and 3 respectively. For the PSX32 sheet piles, only the model similar to that of Case 1 was used. This will be called Case 4 in this report. The applied tensile loads in Cases 1, 2, 3, and 4 were 11.0, 8.0, 15.2, and 9.0 kips/inch respectively.

6.2.3 Results of Finite Element Analyses

One of the purposes of this study is to depict the load-deformation characteristics of the sheet pile interlocks in a pull test. Thus the maximum deflection at the end of the sheet pile on which the load is applied is plotted with the loading in Figures 6.34 and 6.35 for both PS32 and PSX32 sheet piles. In Figure 6.34, the displacements of Cases 1,

2, and 3 are compared to the previous result obtained in the Fixed case. It can be seen from the figure that the displacements increase in all three cases when sliding is allowed at contact regions. Compared to the fixed case, the increases are 27, 38, and 11 percent for Cases 1, 2, and 3 respectively. Within the range of the applied loadings, the displacement responses are linear in all cases. For PSX32 sheet pile, similar observations are noted and the increase in displacement due to sliding is 28 percent compared to the fixed case.

To investigate the sliding in the connection more closely, the displacements at the nine pairs of contactor-target nodes are recorded. For Case 1, the longitudinal displacement at contact node pairs (5,6), (11,12), and (17,18) are plotted in Figures 6.36-6.38. These plots are representatives of the results of the other six contact node pairs in the three contact segments. Similar plots are given in Figures 6.39-6.41 for Case 2. The two different modes of sliding mentioned in the last section can be observed in the two cases. For comparison, the results obtained when no sliding is allowed in all contact segments (fixed case) are also provided in the figures. For Cases 3 and 4, results are similar to those of Case 1 and are presented in Tables 6.10 and 6.11. The results of the fixed case for PSX32 sheet

pile are also listed in Table 6.11. For a pair of nodes in sticking contact, the nodal displacements are identical for the two nodes. However, a difference in value can be a result of either loss in contact or sliding between the two nodes. The contact conditions of the contact node pairs for PS32 sheet piles are given in Table 6.12. For PSX32 steel, the results can be found in Table 6.13. To further illustrate the two different sliding modes, the deformed meshes of the interlocks for Cases 1 and 2 are shown in Figure 6.42. A magnification factor of 5 is used for the nodal displacements. The figure clearly indicates the possible modes of contact failure in the interlock connection.

As mentioned in Section 6.2.2 the lateral displacements of the sheet piles in Case 1 were significantly larger than those obtained in the fixed case. To indicate this effect the lateral displacements at the nine contact pairs are given in Tables 6.14-6.15. A mean value for the lateral displacement at each contact segment is calculated by taking the average of the six nodal lateral displacements in the segment. These mean values are plotted and compared with those of the fixed case (Figs. 6.43-6.45). Because of the extra lateral constraints applied on Cases 2 and 3, these plots are omitted since the lateral displacements for both cases were about the same as those of the fixed case. Simi-

lar plots are shown in Figures 6.46-6.48 for PSX32 sheet piles. Using a least square fit on the data obtained from the analyses, two straight lines can be drawn in each figure. By comparing the slope of the fixed case to that of Case 1 or 2, this ratio thus found can be interpreted as a reduction in lateral stiffness of the sheet pile interlock connection due to sliding among the contact regions. This is similar to the E-ratio concept used by Clough and Kuppusamy (1985). The average E-ratios obtained for the range of loading are 0.058 and 0.065 for PS32 and PSX32 sheet piles respectively. To visualize the E-ratio concept, the deformed meshes for Cases 1 and 3 are shown in Figure 6.49. The applied loads in both cases are 8 kips/inch. As seen from the figure, the bending strain in the webs of Case 1 is more pronounced than that of Case 3. The comparison of bending strains in the webs of the sheet piles are illustrated in Figures 6.50 and 6.51. Each web is described by its position along the X-axis in the finite element model. Thus Web 1 is defined as the one with the fixed end while the other will be designated as Web 2 from here on. The bending strain is calculated by taking half the difference between the top and bottom fibre strains of the web. The bending strain is positive when the bottom of the web is in tension. Since Case 1 exhibited a more significant bending

behavior, only this case is studied further by plotting the change in bending strain with loading along the web portions. (Figs. 6.52 and 6.53). For Case 2, the flexural response is similar to that of Case 3 and thus will not be repeated in here. The bending strain versus load plots for PSX32 sheet pile are given in Figures 6.54 and 6.55.

A second purpose in this study is to investigate the elastic-plastic behavior of the sheet pile interlocks under tensile load. As mentioned earlier, a small load increment was required in order to reach a converged solution when the finite element model in Case 1 was used. This was especially true when the applied load becomes large which rendered the model inefficient. Thus only Case 3 was adopted to study the elastic-plastic response of the sheet piles. Figure 6.56 illustrates the growth of plastic zones in the interlocks with increase in loadings. Three different causes of yielding can be identified for those shaded zones in the figure. For the elements located on the thinnest sections of the two thumbs, yielding is initiated by direct tensile effect. For the elements on the fingers which are away from the contact regions, yielding due to flexural effect is observed. Finally, the elements around the contact regions yield mainly because of high shearing and tensile stresses. Similar observations were made from the results obtained in

the fixed case. It was also noted that when sliding occured between contact surfaces, the shearing stress of the element in contact decreases slightly. For example, in contact segment 1 at a load of 15.2 kips/in., the contactor-target node pairs start to slip. The shearing stress drops from a value of 10.82 ksi to 10.64 ksi in the element at the thumb.

As a final step to study the analytical results from the finite element program, statics checks are carried out at the web sections of the sheet piles. Typical results for all four cases are shown in Table 6.17. The table clearly indicates that excellent statics check is found on the web on which the load is applied (Section B-B). However, the resultant axial force is smaller than the applied load on the other web (Section A-A). On the average, only 95 percent of the applied load is transfered to the other web through the contact segments except for Case 2 where full transfer of the loading is observed. To look more closely at the load transfer behavior, the contact forces at each contact segment in one interlock are analyzed (Fig. 6.57). The changes in normal traction with loading in the three contact segments for Cases 1, 3, and 4 are given in Figures 6.58-6.60, respectively. The same plots are done for the tangential tractions in the contact segments (Figs. 6.61-6.63). These normal and tangential tractions are re-

solved into components in the global reference frame in order to perform statics check in the sheet pile. Typical results are provided in Table 6.18.

TABLE 6.1

Analyses on Sheet Pile Interlocks

Test Set	Mesh Used	Type of Sheet Pile	Total Length (inch)	Web Thickness (inch)	Young's Modulus (ksi)	Loading (k/in.)
I	4&8-Node Fig. 6.5 and 6.6	PSX32	8.656	0.5	29500	8
II	4-Node Fig. 6.4	PS32 PSX32	15. 16.5	0.5 0.45	29000 29000	20 26
III	4-Node Fig. 6.4	PS32 PSX32	15. 16.5	0.5 0.45	5000 4500	16 20

TABLE 6.2

Comparisons of Displacements Obtained from the Four-Node and the Eight-Node Element Meshes

Point Number	Horizontal Dsiplacement (4-node)	Horizontal Displacement (8-node)	Percent Difference
1	.001191 in.	.001287 in.	7
2	.002445 in.	.002567 in.	5
3	.002622 in.	.002703 in.	3
4	.002248 in.	.002345 in.	4
5	.002379 in.	.002557 in.	7
6	.002470 in.	.002580 in.	4
7	.002242 in.	.002317 in.	3
8	.002370 in.	.002546 in.	7
9	.003424 in.	.003739 in.	8
10	.004427 in.	.004884 in.	9
11	.004581 in.	.004923 in.	7
12	.004712 in.	.004915 in.	4

TABLE 6.3

Comparison of Axial and Bending Strains at Web (Sec. a-a) for 4-Node and 8-Node Element Meshes

Mesh	Top Fibre Strain	Bottom Fibre Strain	Axial Strain	Bending Strain
Four Node	.000628	.000402	.000515	.000113
Eight Node	.000648	.000392	.000520	.000128
Diff.	6 %	-3 %	1 %	12 %

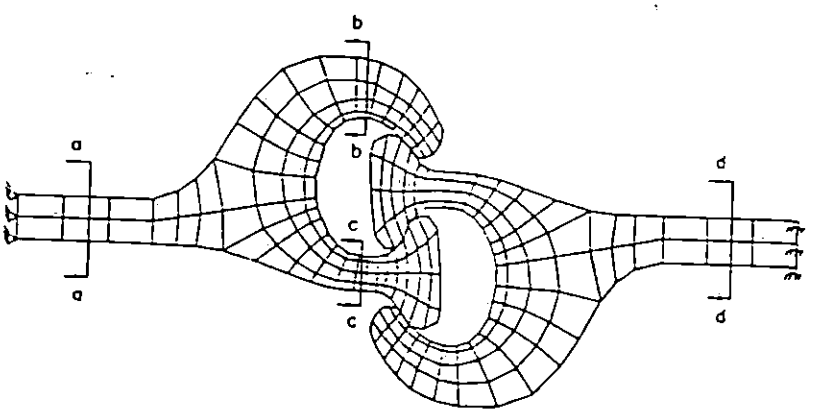

TABLE 6.4

Displacement Versus Load for Three Contact Points on PS32 Sheet Piles

Point	Load / Displ. (in)	5500. (lbs/in)	11000. (lbs/in)	16500. (lbs/in)	20000. (lbs/in)
3	X-direction	.0031737	.0062005	.0094740	.0118991
	Y-direction	.0005519	.0009963	.0014609	.0020623
6	X-direction	.0030470	.0060915	.0093095	.0118214
	Y-direction	.0004621	.0008138	.0011810	.0016952
8	X-direction	.0030357	.0045428	.0091435	.0114663
	Y-direction	.0004663	.0008220	.0011971	.0017239

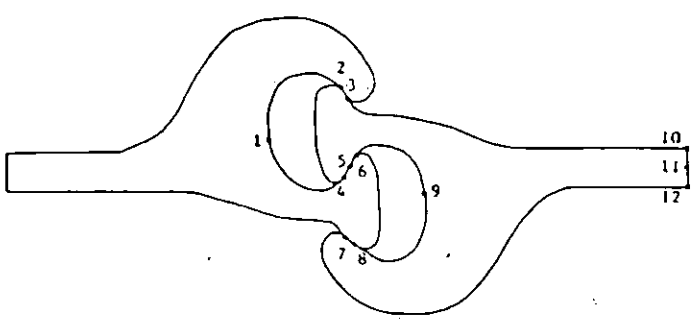

TABLE 6.5

Displacement Versus Load for Three Contact Points on PSX32 Sheet Piles

Point	Load / Displ. (in)	6500. (lbs/in)	13000. (lbs/in)	19500. (lbs/in)	26000. (lbs/in)
3	X-direction	.0036544	.0073270	.0110429	.0210442
	Y-direction	-.000933	-.001802	-.002688	-.004428
6	X-direction	.0038522	.0077073	.0115772	.0212354
	Y-direction	-.000994	-.001927	-.002882	-.004722
8	X-direction	.0039862	.0079454	.0118741	.0209675
	Y-direction	-.000973	-.001883	-.002813	-.004623

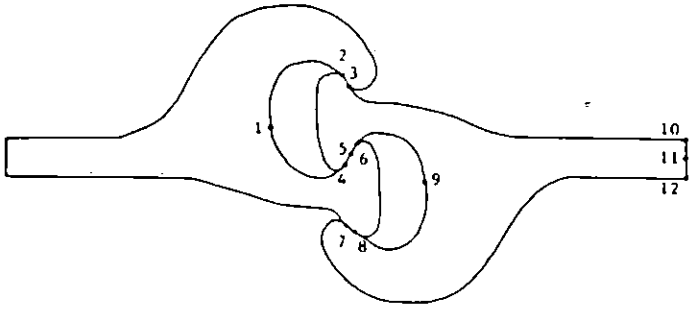

TABLE 6.6

Comparisons of Stresses for Two Elements which Exhibit Different Yielding Modes in PS32 Sheet Piles (20 k/in)

Element	Gauss Point	σ_x ksi	σ_y ksi	σ_{xy} ksi	σ_z ksi	σ_{eq} ksi
A	1	48.55	-3.32	-3.79	21.36	45.42
	2	61.65	9.51	-3.34	33.23	45.58
	3	49.50	-2.83	-1.12	21.65	45.39
	4	63.03	10.57	-0.77	33.96	45.54
B	1	20.13	8.28	23.58	8.52	42.49
	2	39.43	24.27	23.67	21.91	44.18
	3	18.48	18.03	25.09	11.19	44.03
	4	32.36	27.99	24.74	20.29	44.14

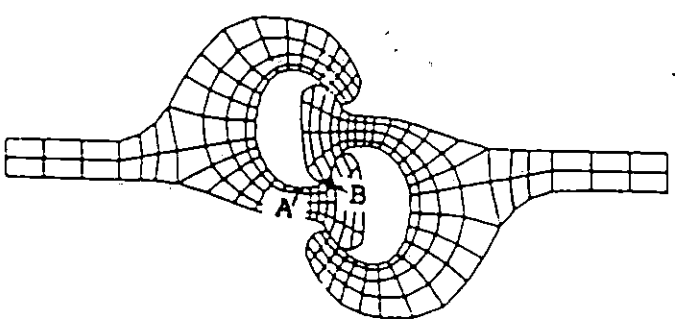

TABLE 6.7

Comparisons of Stresses for Two Elements which Exhibit Different Yielding Modes in PSX32 Sheet Piles (26 k/in)

Element	Gauss Point	σ_x ksi	σ_y ksi	σ_{xy} ksi	σ_z ksi	σ_{eq} ksi
A	1	50.90	-7.08	1.19	17.38	50.46
	2	64.01	6.13	1.78	28.43	50.66
	3	55.17	-1.36	6.20	21.04	50.46
	4	67.26	10.83	6.24	31.33	50.64
B	1	19.89	17.27	23.76	11.15	41.88
	2	49.82	32.81	26.20	26.11	50.08
	3	8.76	17.77	27.15	7.96	47.96
	4	33.59	30.16	28.09	20.33	50.09

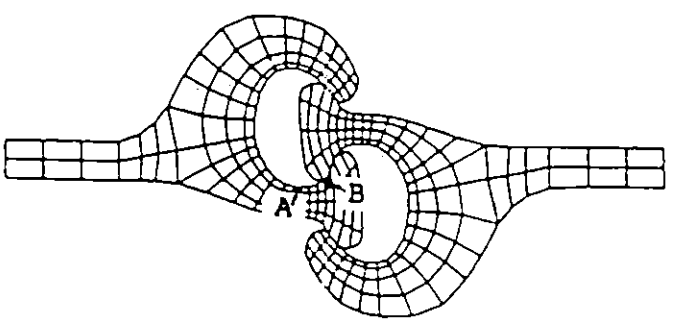

TABLE 6.8

Displacement Versus Load for Three Contact Points on PS32 Sheet Piles with Effective Young's Modulus

Point	Load / Displ. (in)	5000. (lbs/in)	10000. (lbs/in)	15000. (lbs/in)	20000. (lbs/in)
3	X-direction	.0182672	.0368029	.0554895	.0744881
	Y-direction	-.004050	-.006976	-.009194	-.011318
6	X-direction	.0191152	.0382639	.0574246	.0767044
	Y-direction	-.004370	-.007648	-.010238	-.012788
8	X-direction	.0195197	.0386096	.0574326	.0760162
	Y-direction	-.004254	-.007400	-.009848	-.012235

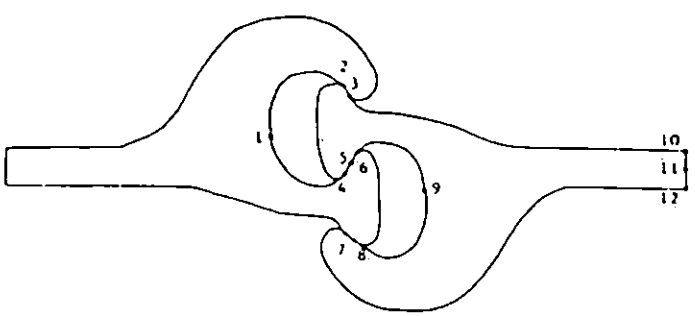

TABLE 6.9

Displacement Versus Load for Three Contact Points on PSX32 Sheet Piles with Effective Young's Modulus

Point	Load / Displ. (in)	6000. (lbs/in)	10000. (lbs/in)	14000. (lbs/in)	16000. (lbs/in)
3	X-direction	.0192515	.0322801	.0457431	.0530035
	Y-direction	.0023499	.0031268	.0037469	.0041396
6	X-direction	.0192453	.0320501	.0450446	.0519004
	Y-direction	.0017672	.0021183	.0022739	.0024323
8	X-direction	.0188386	.0310920	.0433116	.0495770
	Y-direction	.0017915	.0021588	.0022832	.0024568

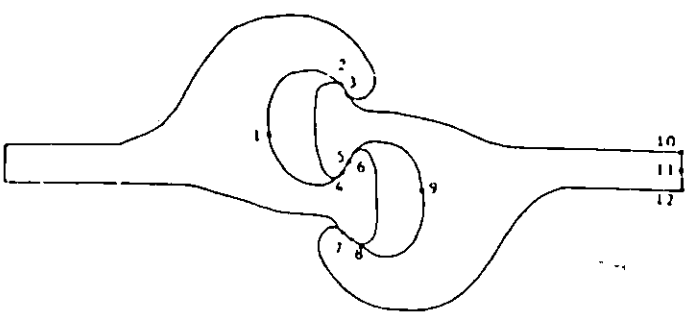

TABLE 6.10

Longitudinal Displacements at Contact Node Pairs in Case 3

Node Pair	Longitudinal Displacement at (8 kips/in)	(12 kips/in)	(15.2 kips/in)
1,2	.00381, .00381	.00581, .00581	.00771, .00771
3,4	.00401, .00401	.00610, .00610	.00818, .00818
5,6	.00430, .00418	.00652, .00634	.00858, .00827
7,8	.00472, .00376	.00700, .00566	.00853, .00716
9,10	.00471, .00375	.00697, .00562	.00849, .00714
11,12	.00474, .00371	.00702, .00557	.00859, .00711
13,14	.00473, .00460	.00704, .00685	.00881, .00856
15,16	.00498, .00498	.00741, .00741	.00927, .00927
17,18	.00528, .00528	.00787, .00787	.00983, .00983

TABLE 6.11

Longitudinal Displacements at Contact Node Pairs in Case 4

Node Pair	Longitudinal Displacement at (9 kips/in)	(Fixed Case)
1,2	.00548, .00548	.00448
3,4	.00577, .00577	.00472
5,6	.00607, .00598	.00506
7,8	.00687, .00651	.00465
9,10	.00695, .00659	.00501
11,12	.00698, .00664	.00534
13,14	.00723, .00723	.00498
15,16	.00739, .00739	.00528
17,18	.00758, .00758	.00551

TABLE 6.12

Summary of Contact Condition at Maximum Load for PS32 Sheet Piles

Node Pair	Case 1 (11 kips/in)	Case 2 (8 kips/in)	Case 3 (15.2 kips/in)
1-2	sticking	sliding	sliding
3-4	sticking	sliding	sliding
5-6	no contact	sliding	no contact
7-8	sliding	sticking	sliding
9-10	sliding	sticking	sliding
11-12	no contact	sticking	no contact
13-14	no contact	sliding	no contact
15-16	sticking	sliding	sticking
17-18	sticking	sliding	sticking

TABLE 6.13

Summary of Contact Condition at Maximum Load for PSX32 Sheet Piles

Node Pair	Case 4 (9 kips/in)
1-2	sticking
3-4	sticking
5-6	no contact
7-8	sliding
9-10	sliding
11-12	no contact
13-14	sticking
15-16	sticking
17-18	sticking

TABLE 6.14

Lateral Displacement at Contactor-Target Nodes 1-6 in Case 1

Load kip/in	Contact Node Pair (1,2)	(3,4)	(5,6)
2	.00380,.00380	.00385,.00385	.00392,.00388
4	.00827,.00827	.00836,.00836	.00851,.00842
6	.00843,.00843	.00856,.00856	.00876,.00863
8	.01010,.01010	.01116,.01116	.01143,.01125
10	.01515,.01515	.01535,.01535	.01570,.01547
11	.01682,.01682	.01701,.01701	.01742,.01714

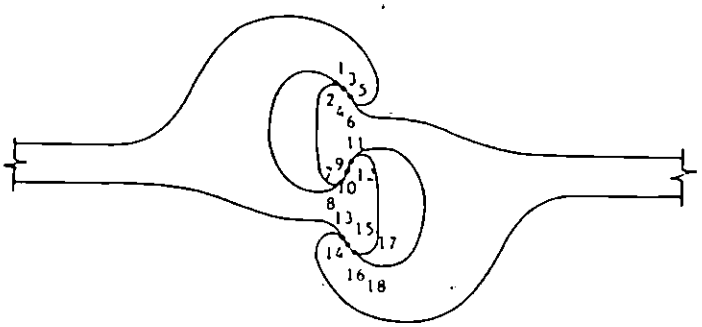

TABLE 6.15

Lateral Displacement at Contactor-Target Nodes 7-12 in Case 1

Load kip/in	Contact Node Pair (7,8)	(9,10)	(11,12)
2	.00384,.00343	.00385,.00344	.00386,.00346
4	.00834,.00752	.00837,.00754	.00839,.00759
6	.00853,.00730	.00856,.00733	.00856,.00737
8	.01112,.00947	.01115,.00950	.01116,.00957
10	.01530,.01322	.01535,.01326	.01535,.01334
11	.01695,.01487	.01700,.01491	.01699,.01499

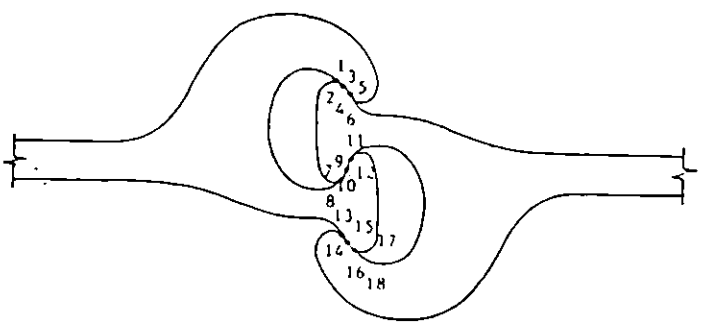

TABLE 6.16

Lateral Displacement at Contactor-Target Nodes 13-18 in Case 1

Load kip/in	Contact Node Pair (13,14)	(15,16)	(17,18)
2	.00335,.00340	.00344,.00344	.00349,.00349
4	.00737,.00745	.00753,.00753	.00765,.00765
6	.00705,.00719	.00730,.00730	.00747,.00747
8	.00913,.00932	.00946,.00946	.00968,.00968
10	.01281,.01304	.01322,.01322	.01349,.01349
11	.01442,.01466	.01485,.01485	.01515,.01515

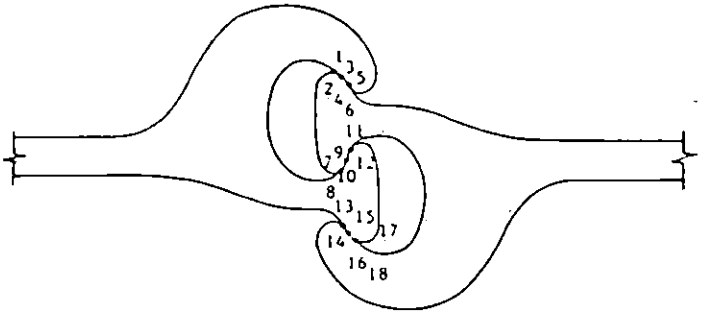

TABLE 6.17

Statics Check at Web Sections of Sheet Piles

Section A-A			
CASE No.	Applied Load	Analytical Result	Percent Different
1	11.0	10.4	5
2	8.0	8.0	0
3	15.2	14.4	5
4	9.0	8.6	4

Section B-B			
CASE No.	Applied Load	Analytical Result	Percent Different
1	11.0	11.4	0
2	8.0	8.0	0
3	15.2	15.2	0
4	9.0	9.0	0

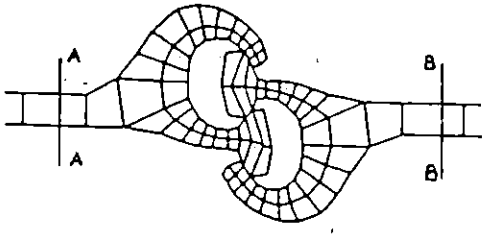

TABLE 6.18

Statics Check of Contact Forces with Loading

CASE NO.	Analytical Result (kip/in.)		Applied Load (kip/in.)		Unbalanced Load (kip/in.)	
	X	Y	X	Y	X	Y
1	-11.57	0.24	11.00	0.00	-0.57	0.24
3	-15.94	0.37	15.2	0.00	-0.74	0.37
4	-9.26	-0.28	9.00	0.00	-0.26	-0.28

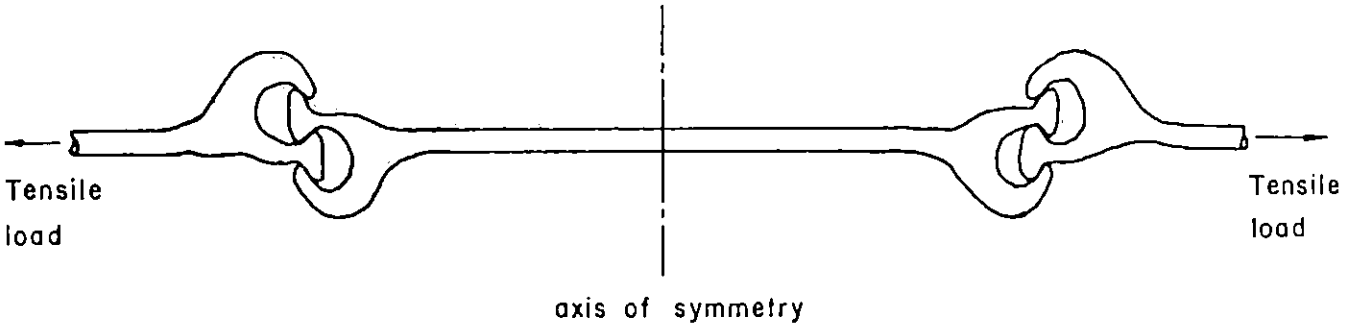

Figure 6.1: Typical Tensile Test of Sheet Pile

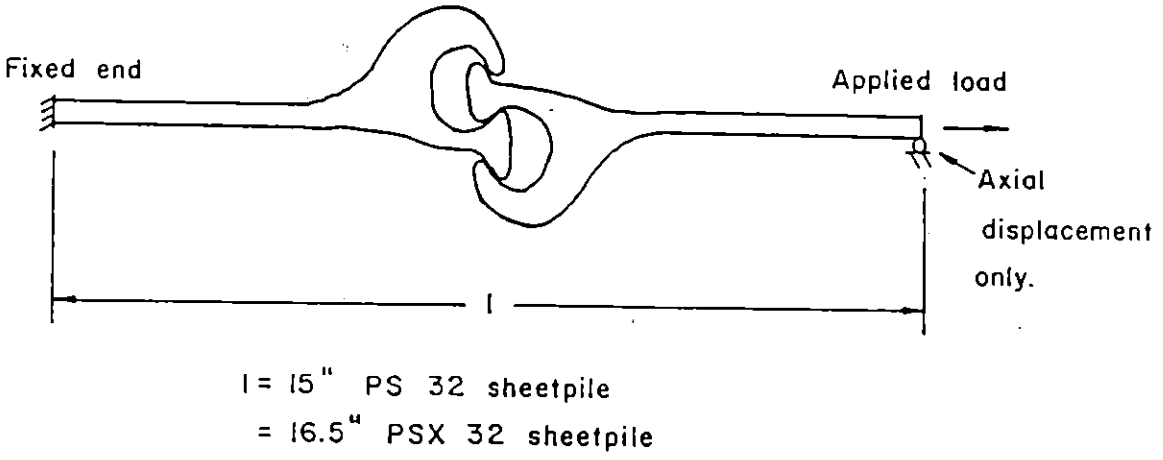

Figure 6.2: Portions of Sheet Piles Modeled for Analysis

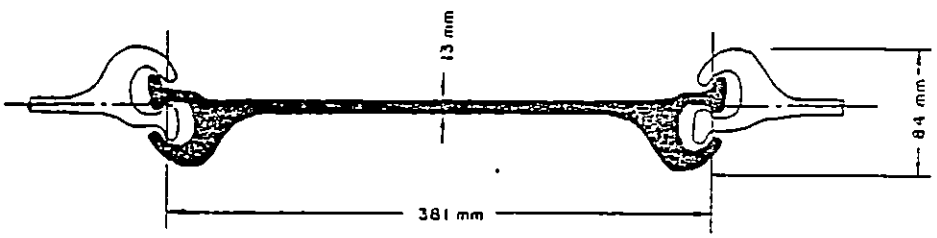

PS 32

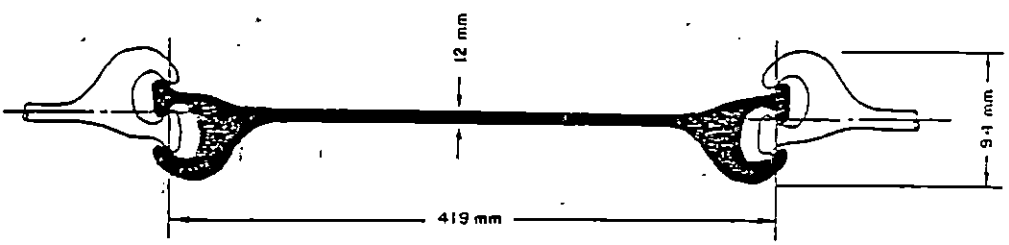

PSX 32

Figure 6.3: Details of Straight Web Piling (U.S. Steel Handbook)

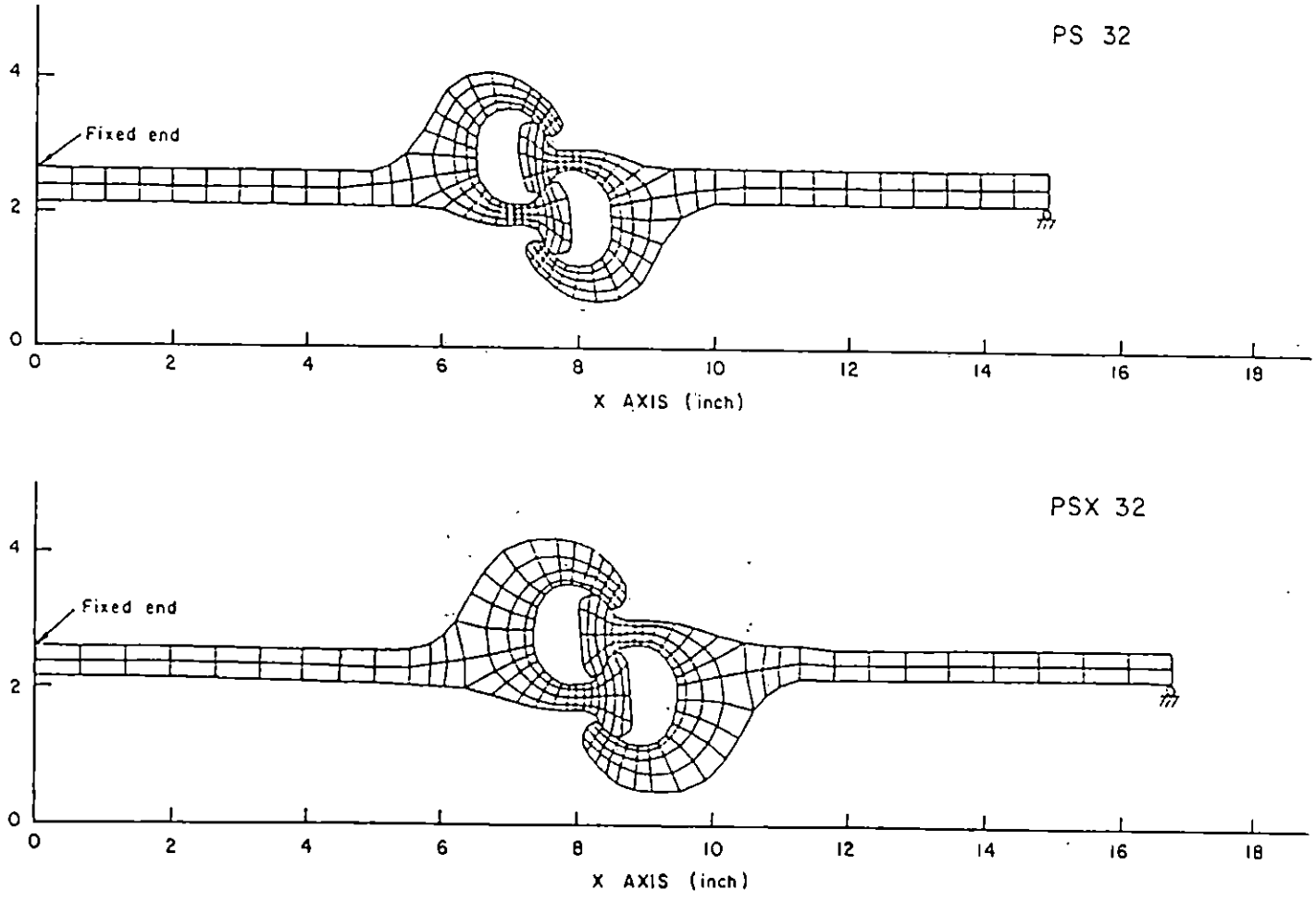

Figure 6.4: Finite Element Meshes for PS32 and PSX32 Sheet Piles

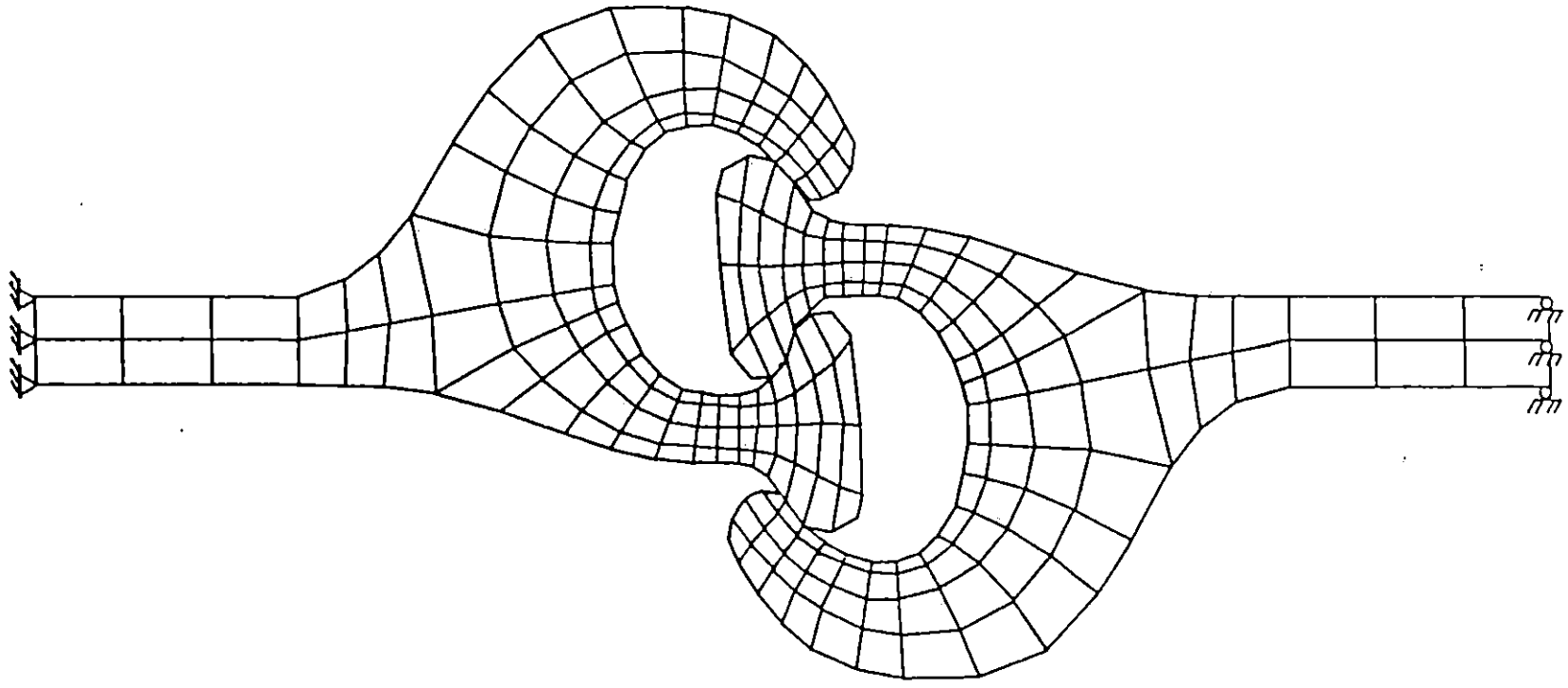

Figure 6.5: Four-Node Finite Element Mesh for PSX32 Sheet Piles

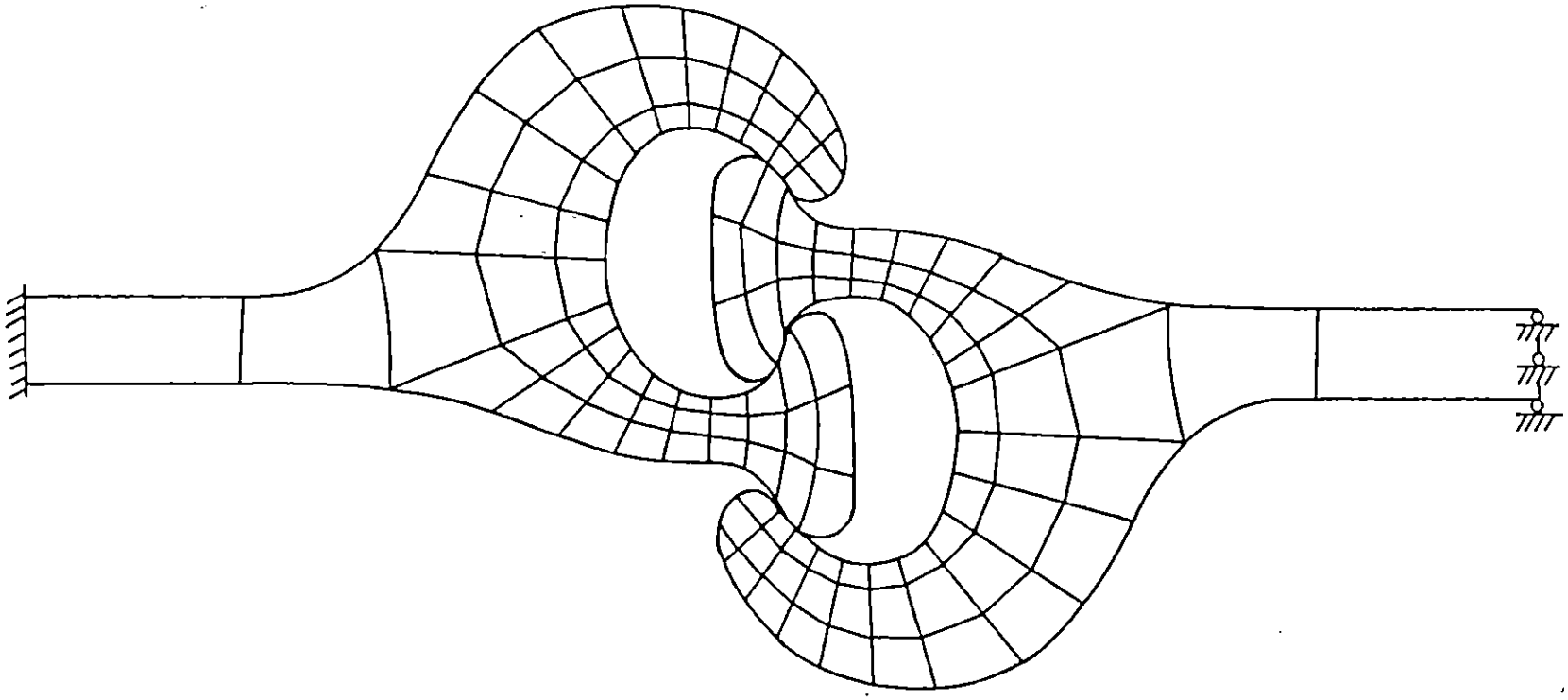

Figure 6.6: Eight-Node Finite Element Mesh for PSX32 Sheet Piles

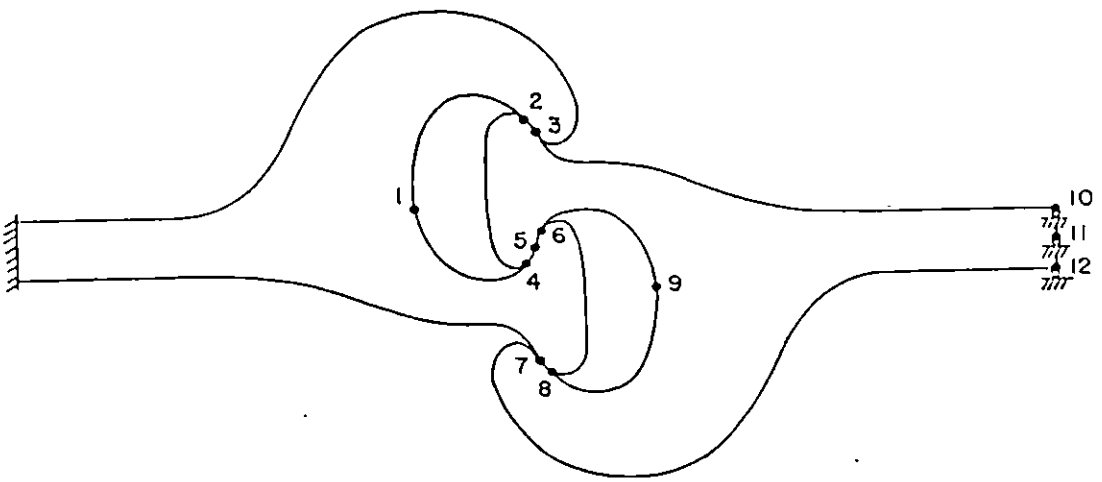

Figure 6.7: Locations in Sheet Piles at which Displacements are Tabulated

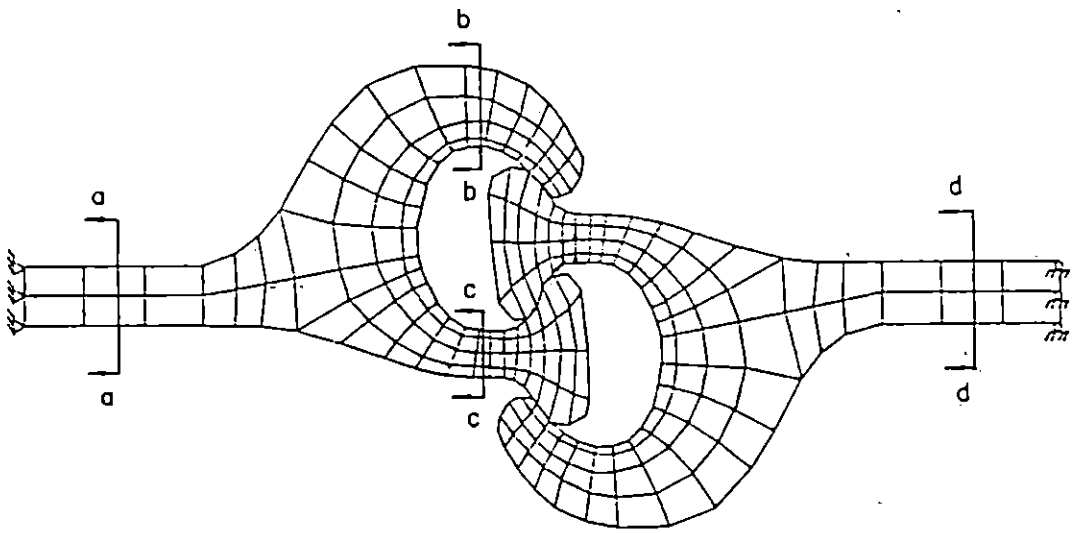

Figure 6.8: Sections on Sheet Piles for Statics Check

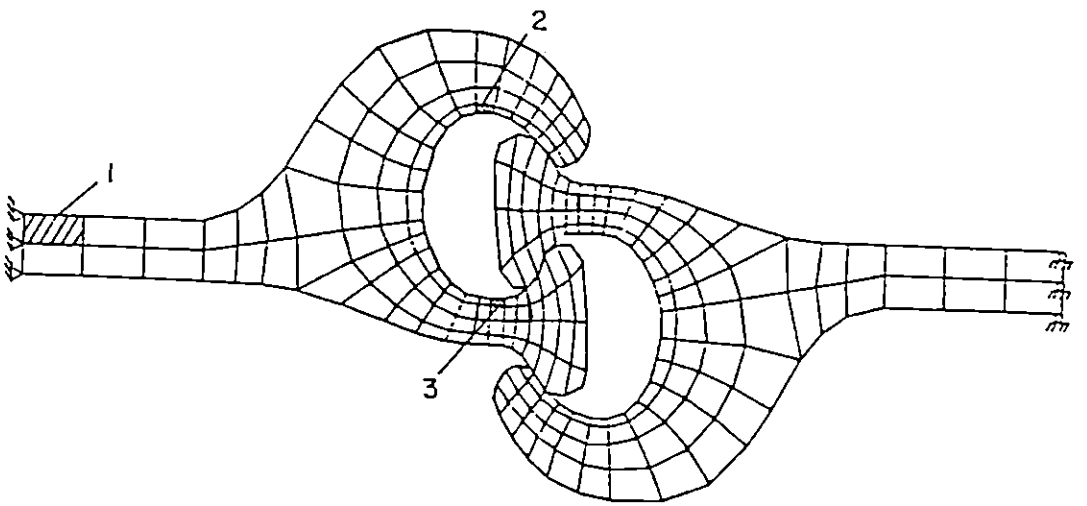

Figure 6.9: Locations of Elements in which Equivalent Stresses and Equivalent Strains are Calculated

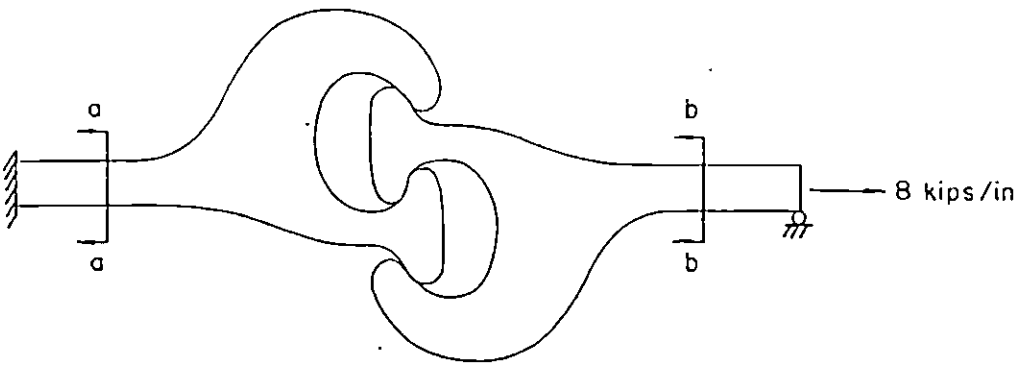

o 4-node element mesh
x 8-node element mesh

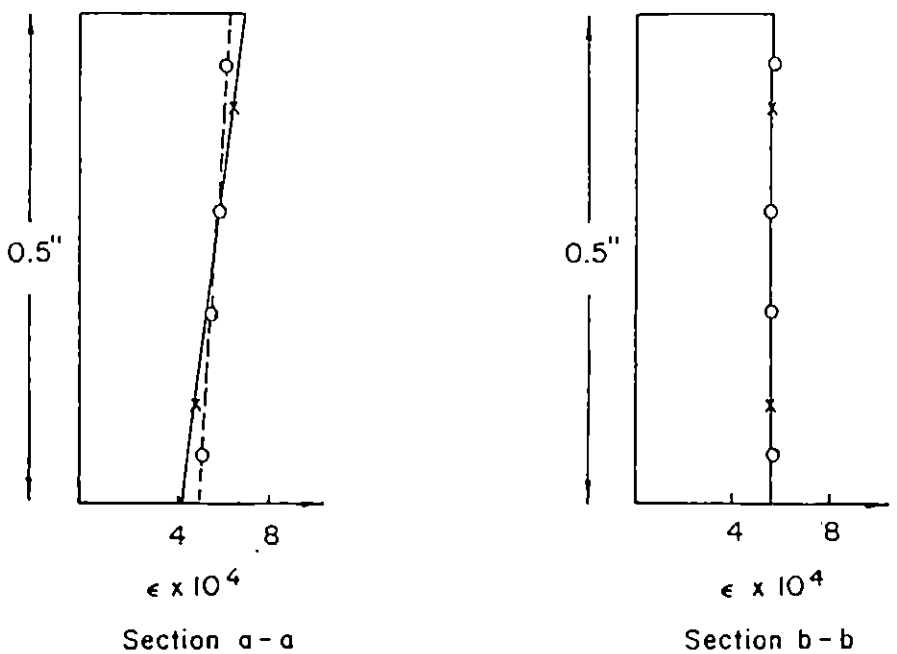

Figure 6.10: Comparison of Strain Distributions at Webs for 4-Node and 8-Node Element Meshes

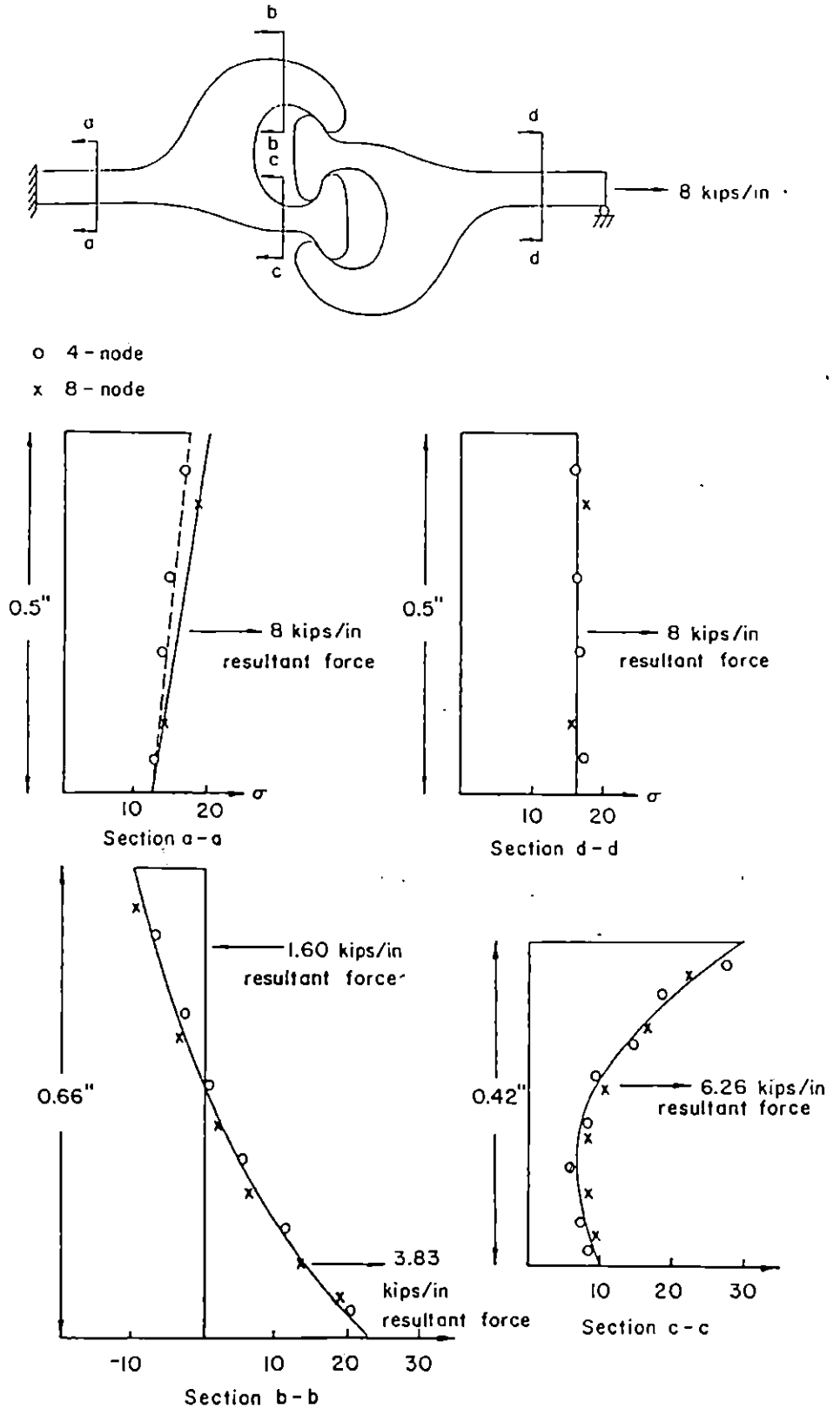

Figure 6.11: Comparisons of Stress Distributions for 4-Node and 8-Node Element Meshes

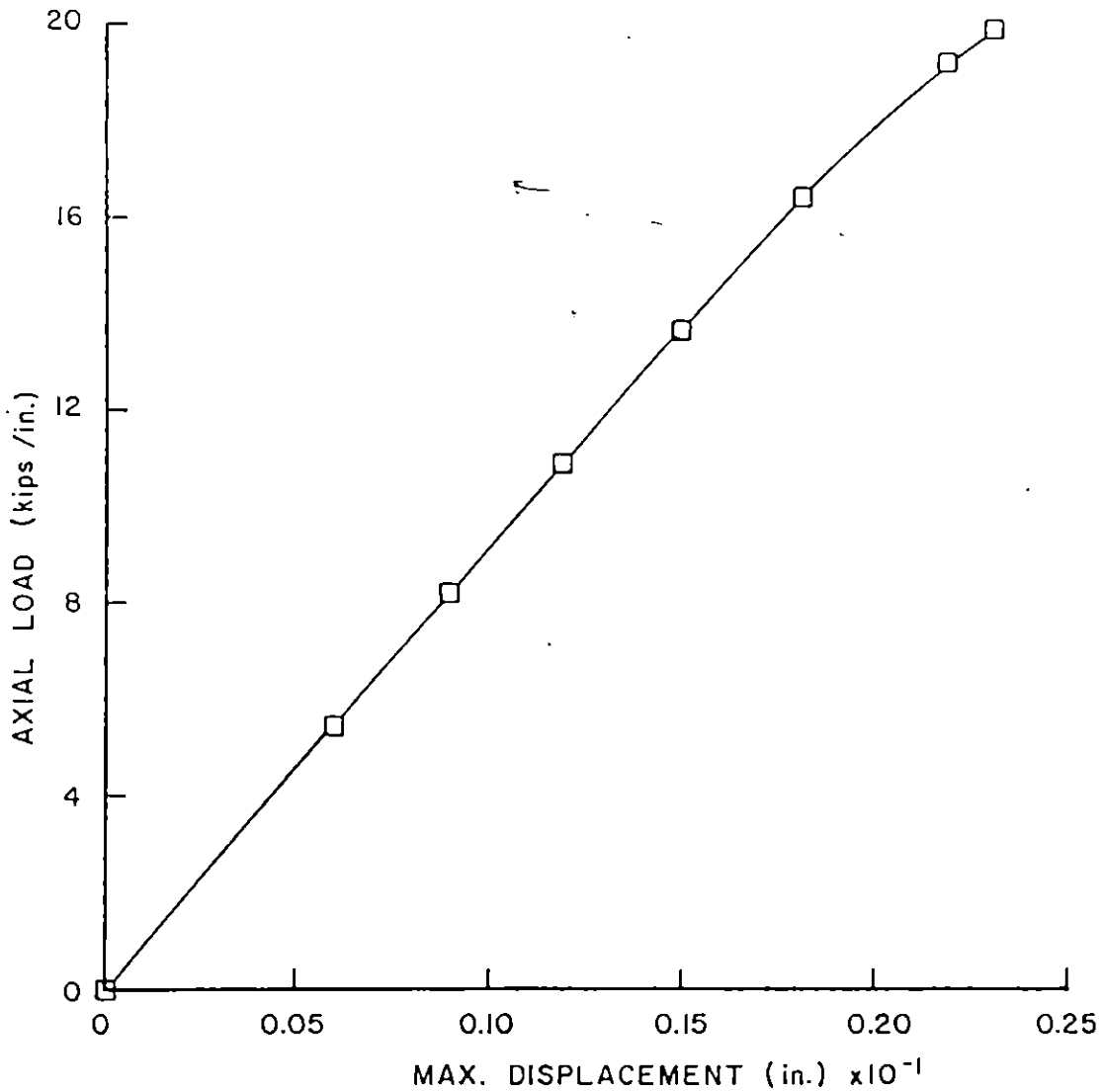

Figure 6.12: Load-Displacement Curve for Tip Deflection (Point 10) in PS32 Sheet Piles

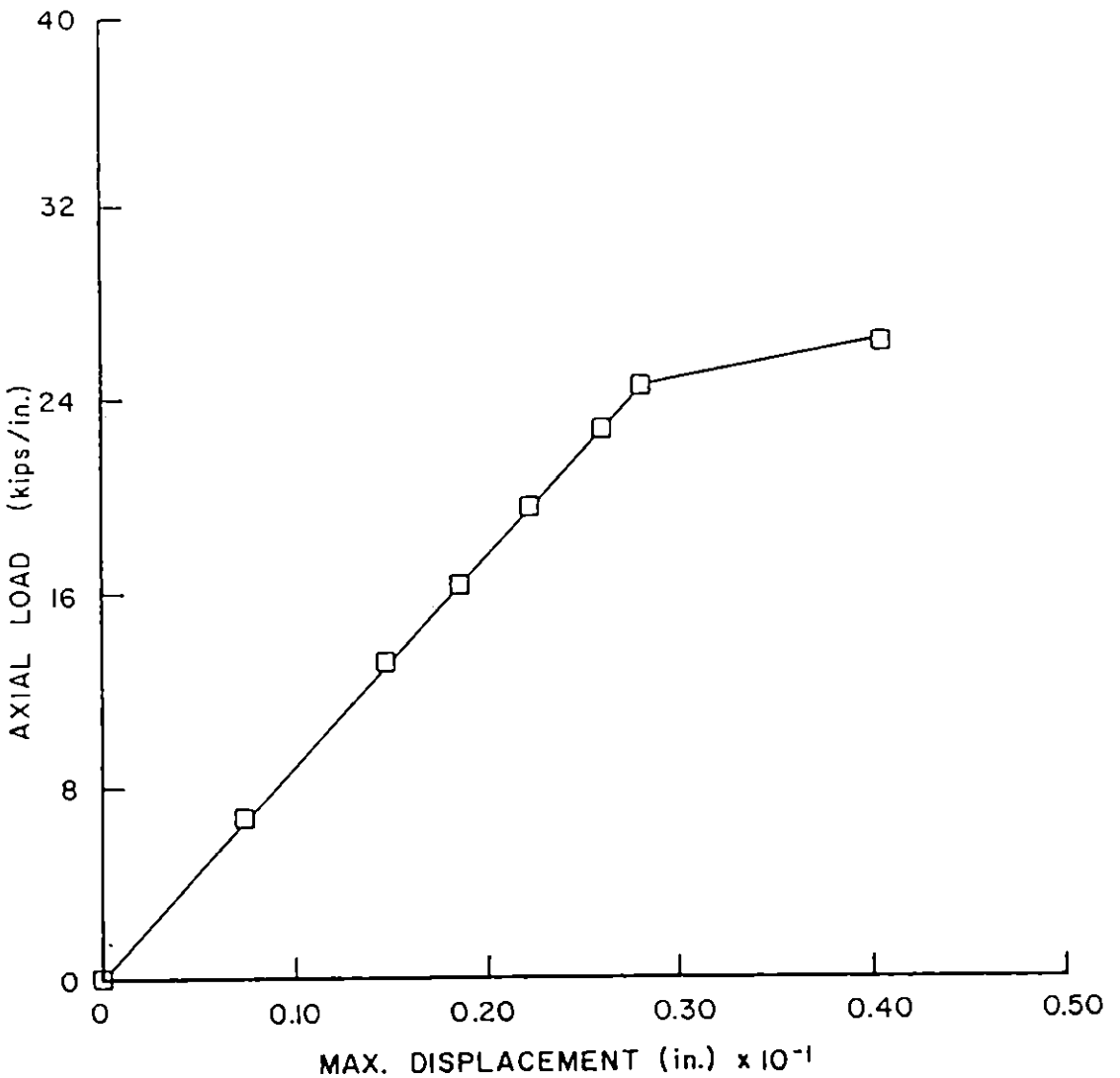

Figure 6.13: Load-Displacement Curve for Tip Deflection (Point 10) in PSX32 Sheet Piles

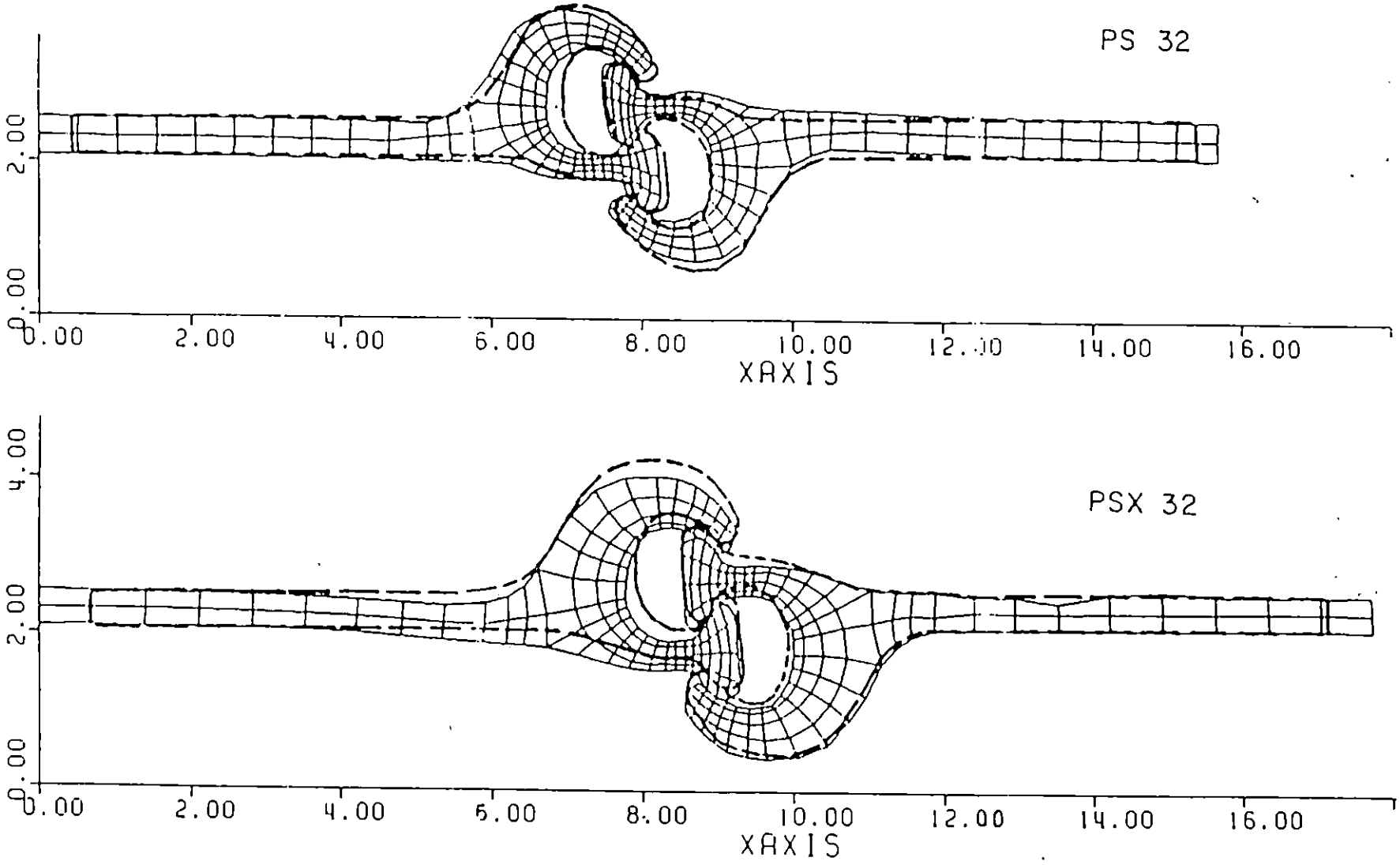

Figure 6.14: Initial and Deformed Shapes of PS32 and PSX32 Sheet Piles

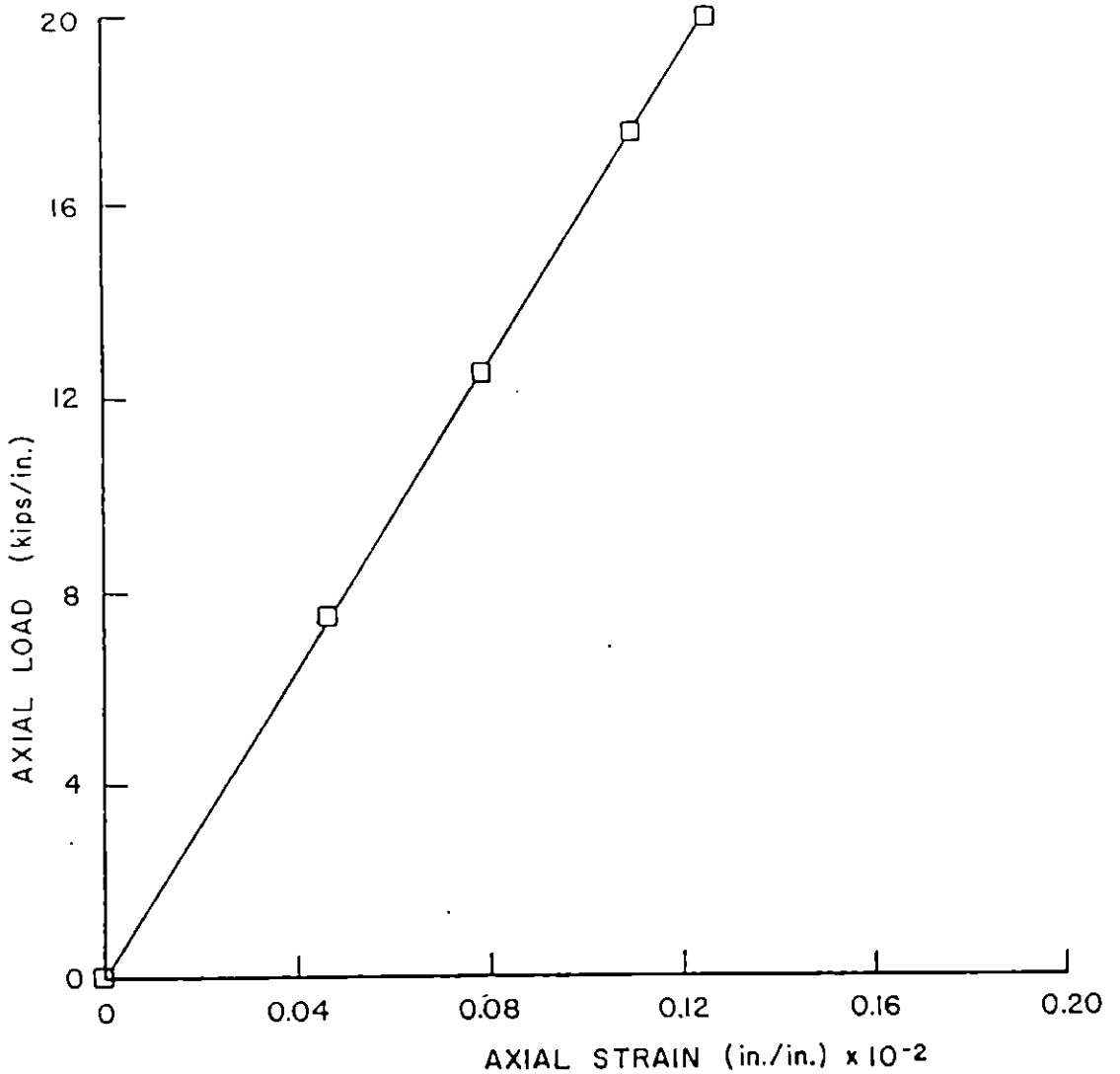

Figure 6.15: Axial Strain in Web Versus Load for PS32 Sheet Pile

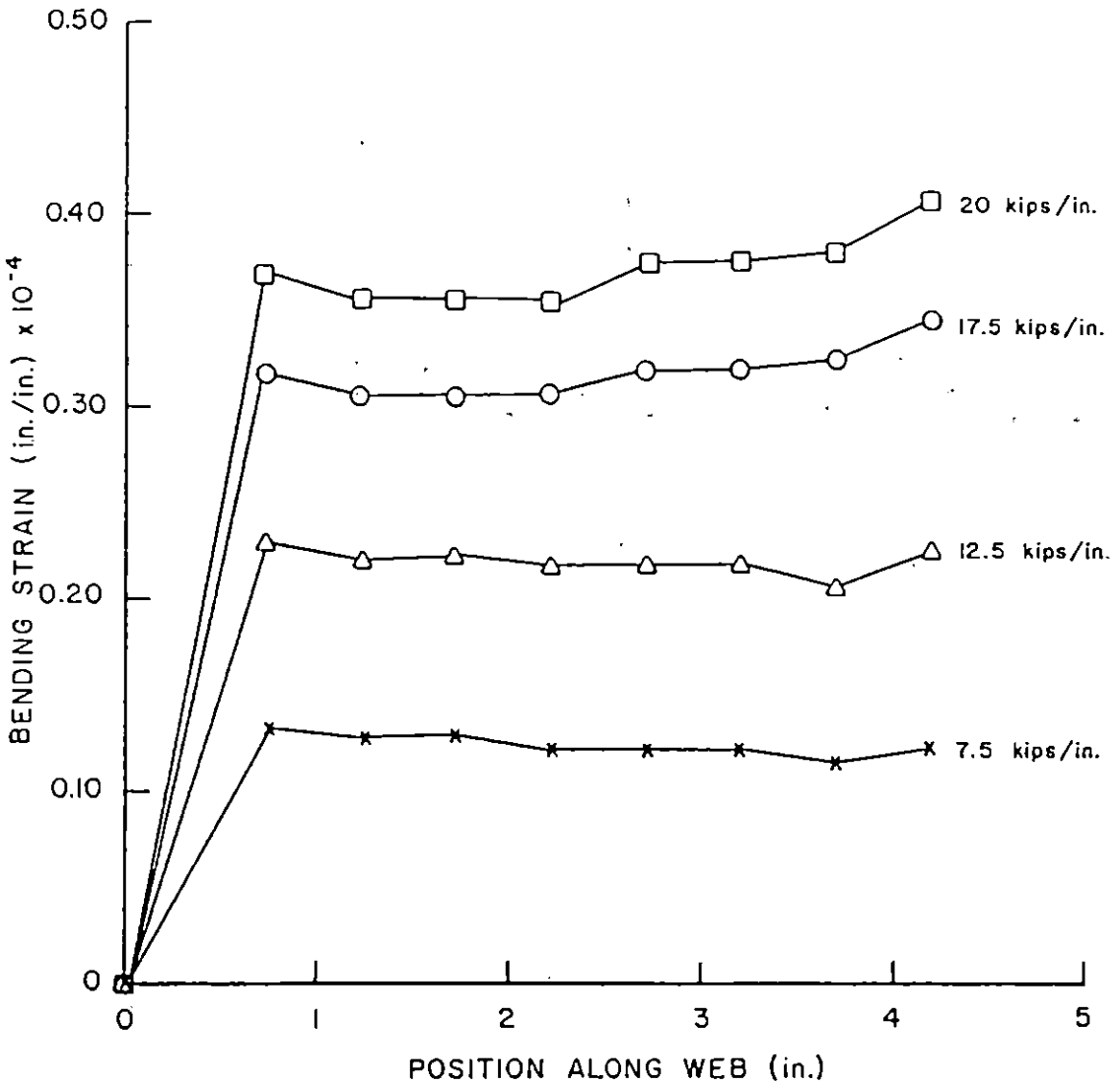

Figure 6.16: Variations of Bending Strains Along Web with Loads (PS32)

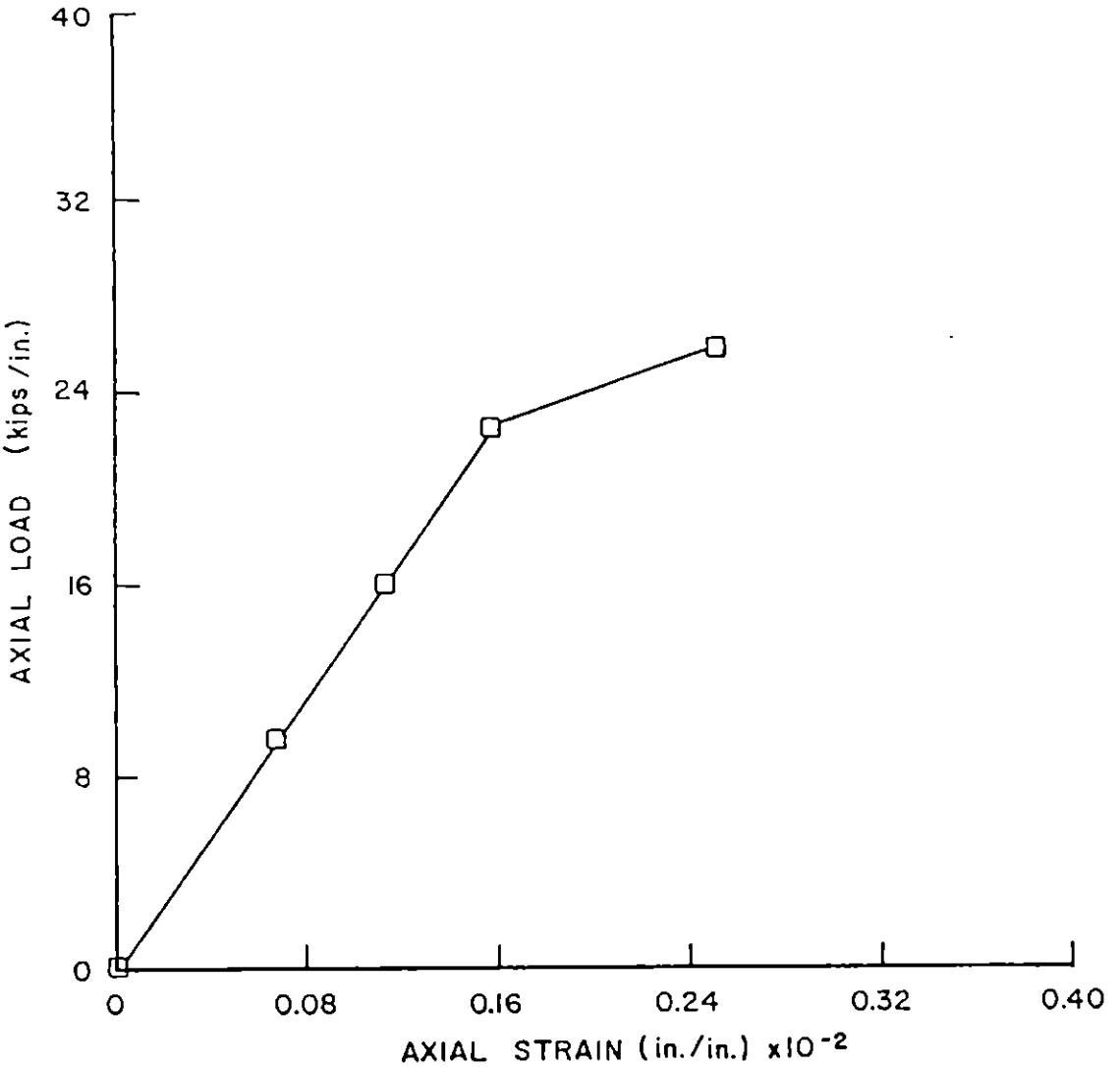

Figure 6.17: Axial Strain in Web Versus Load for PSX32 Sheet Pile

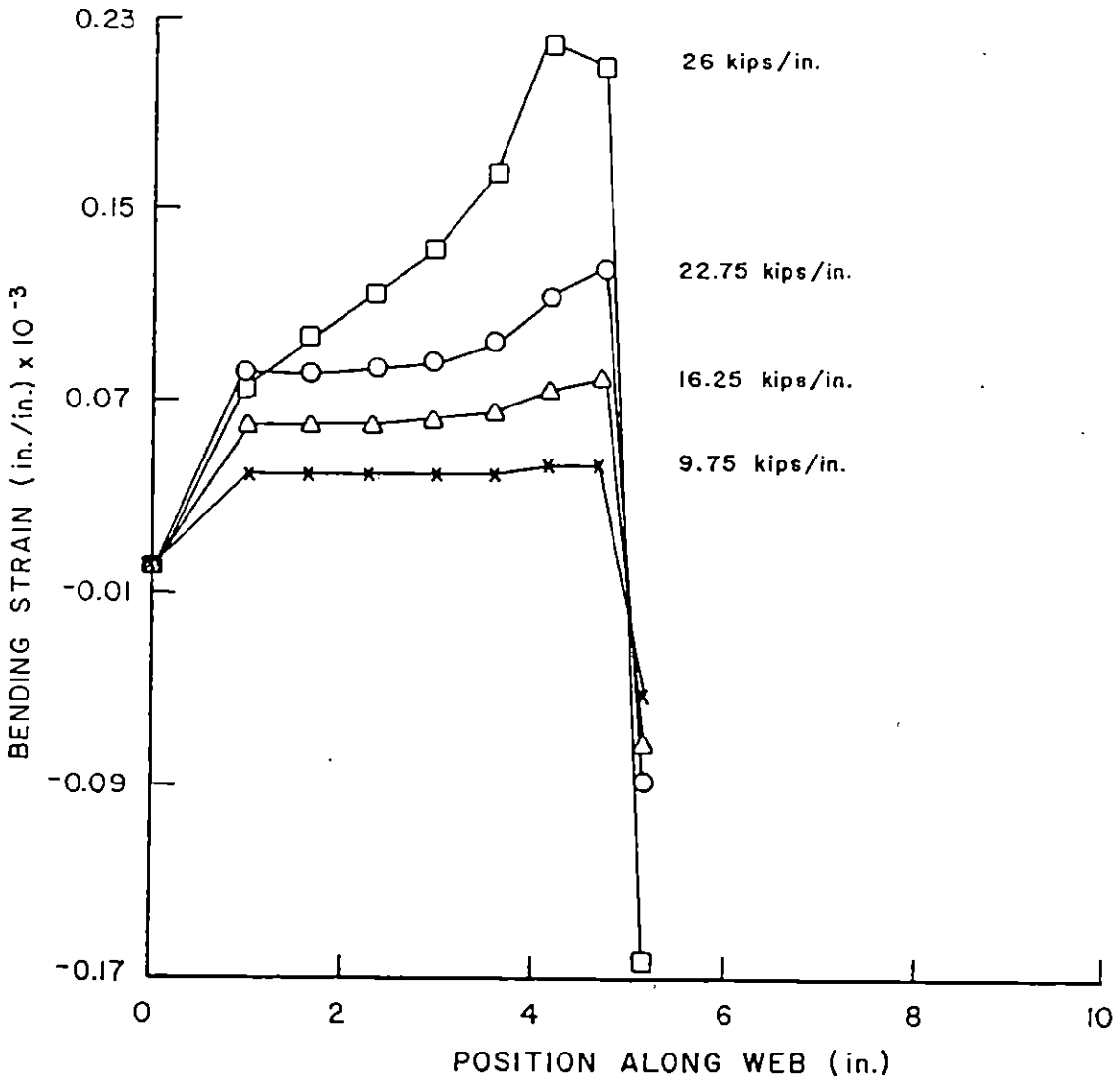

Figure 6.18: Variations of Bending Strains Along Web with Loads (PSX32)

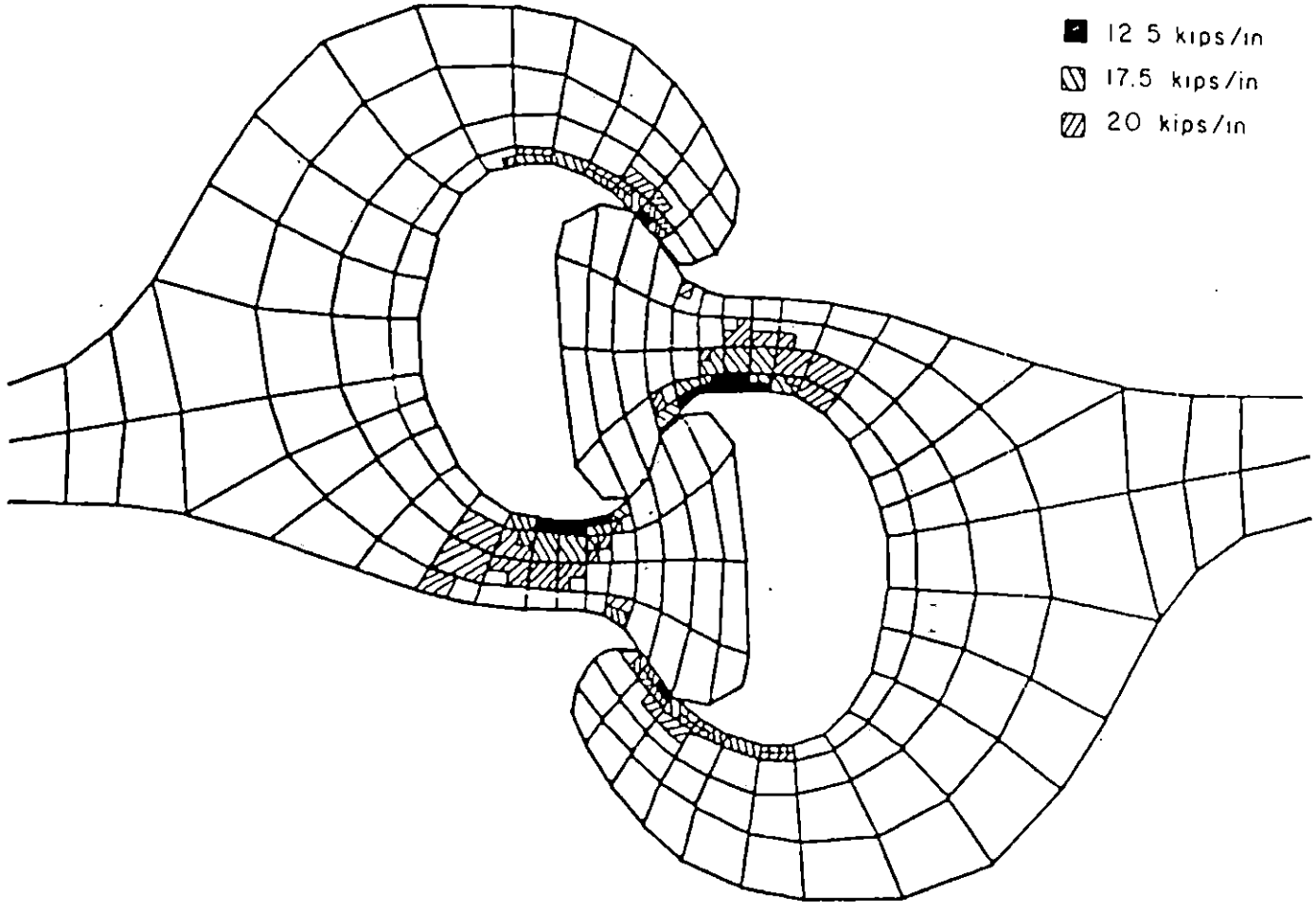

Figure 6.19: Plastic Zones on PS32 Sheet Piles at Different Loadings

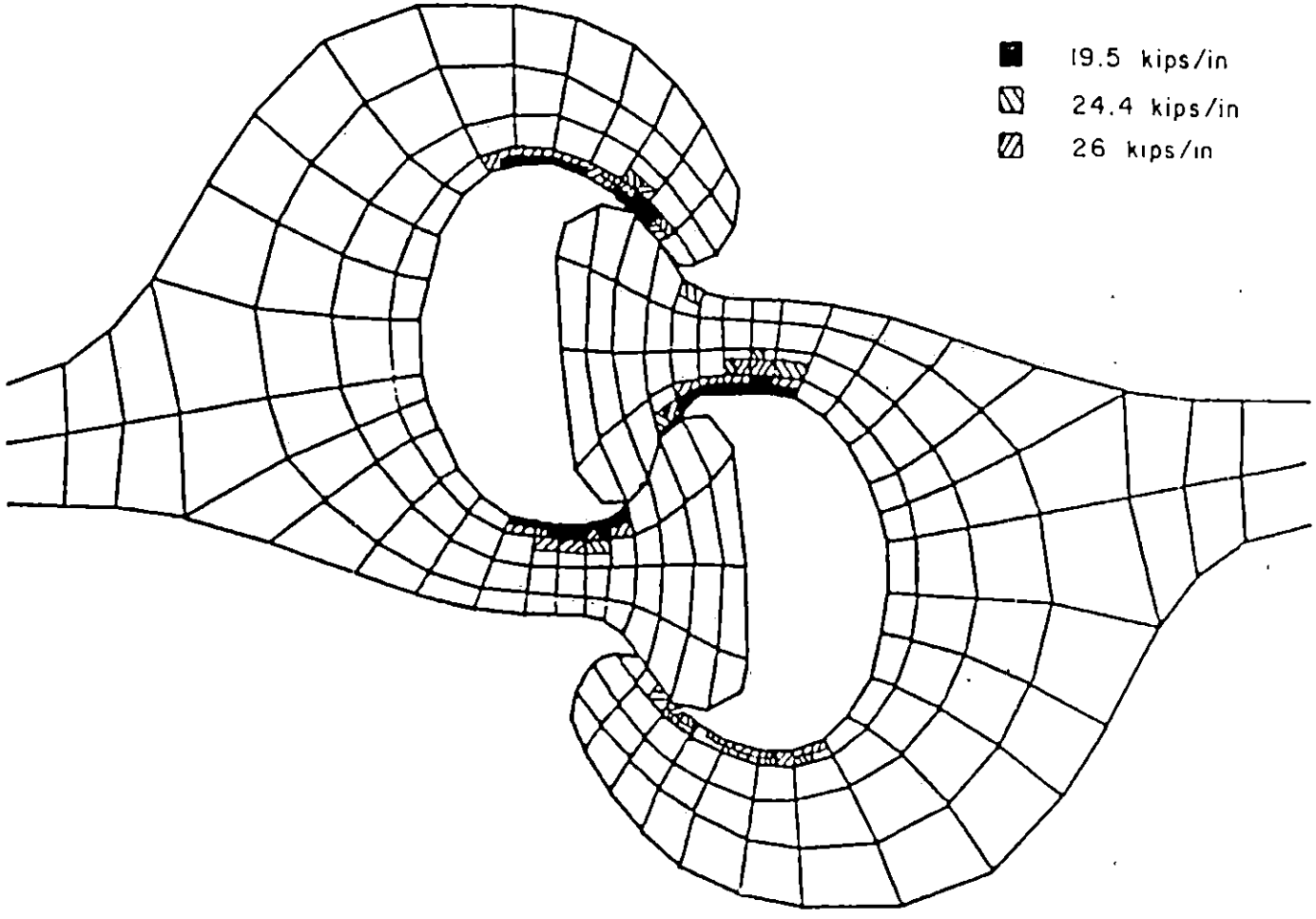

Figure 6.20: Plastic Zones on PSX32 Sheet Piles at Different Loadings

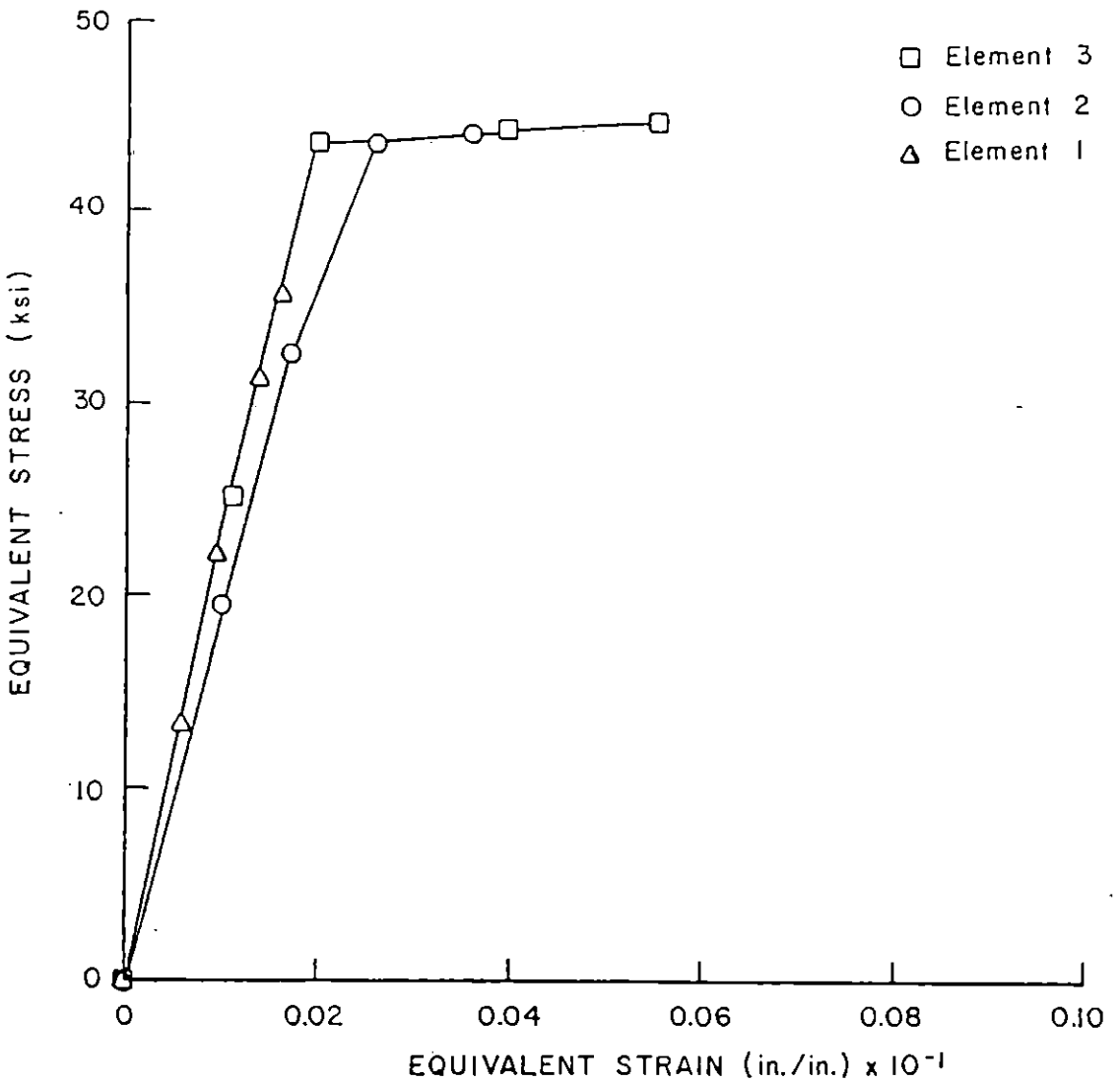

Figure 6.21: Equivalent Stress Versus Equivalent Strain Plots for Three Typical Elements on PS32 Sheet Piles Model

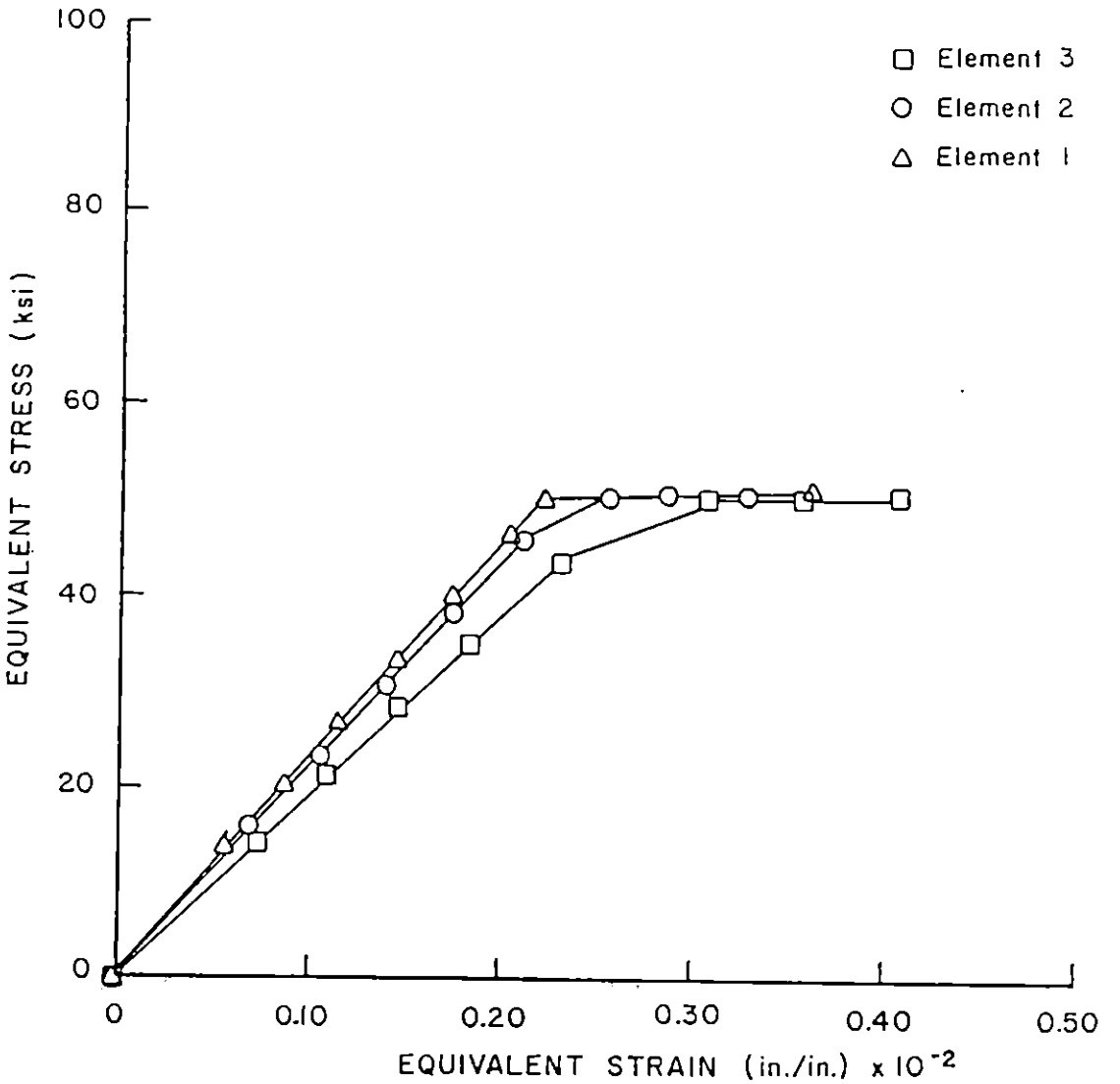

Figure 6.22: Equivalent Stress Versus Equivalent Strain Plots for Three Typical Elements on PSX32 Sheet Piles Model

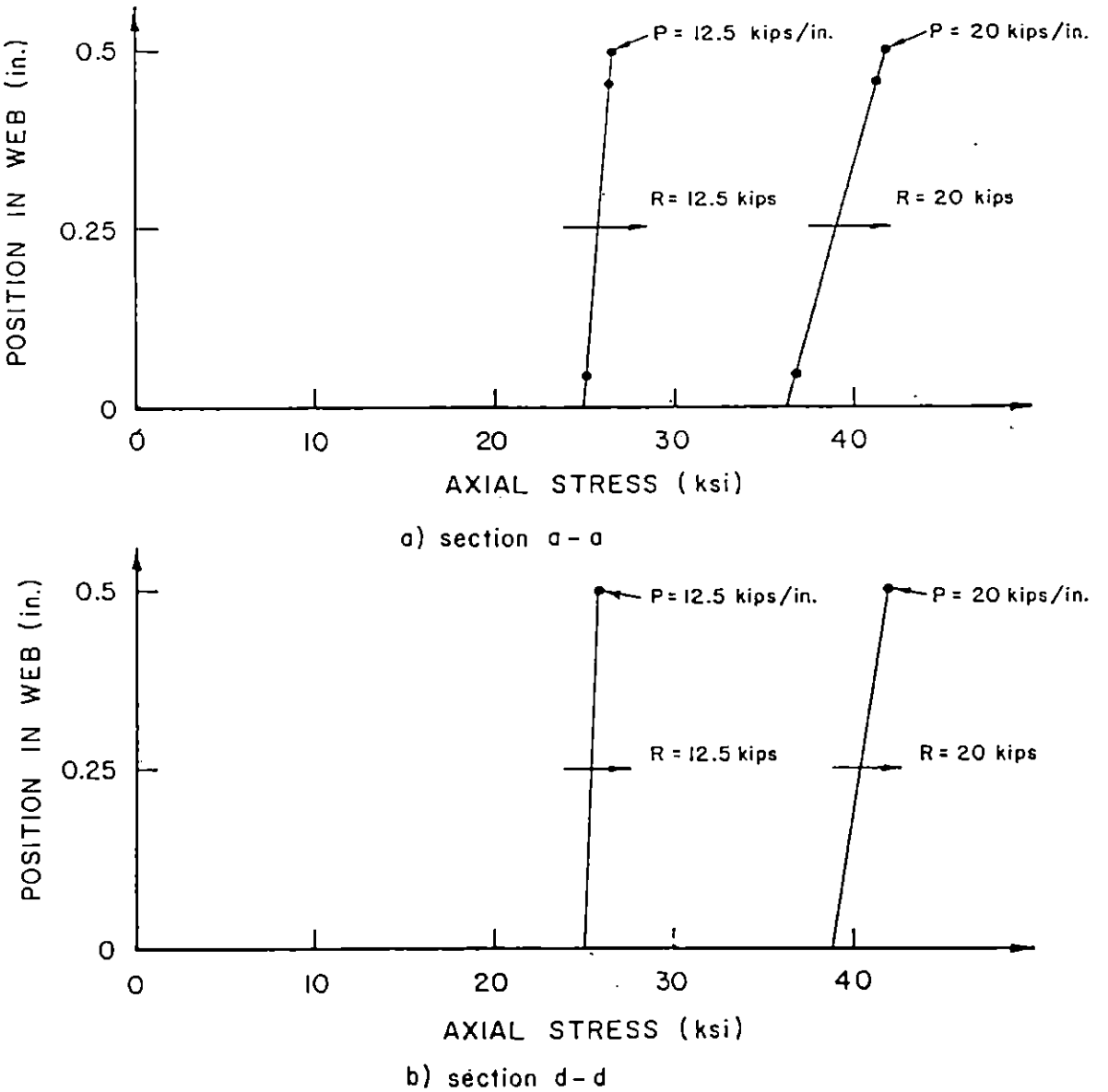

Figure 6.23: Statics Check at Web Section for PS32 Sheet Pile

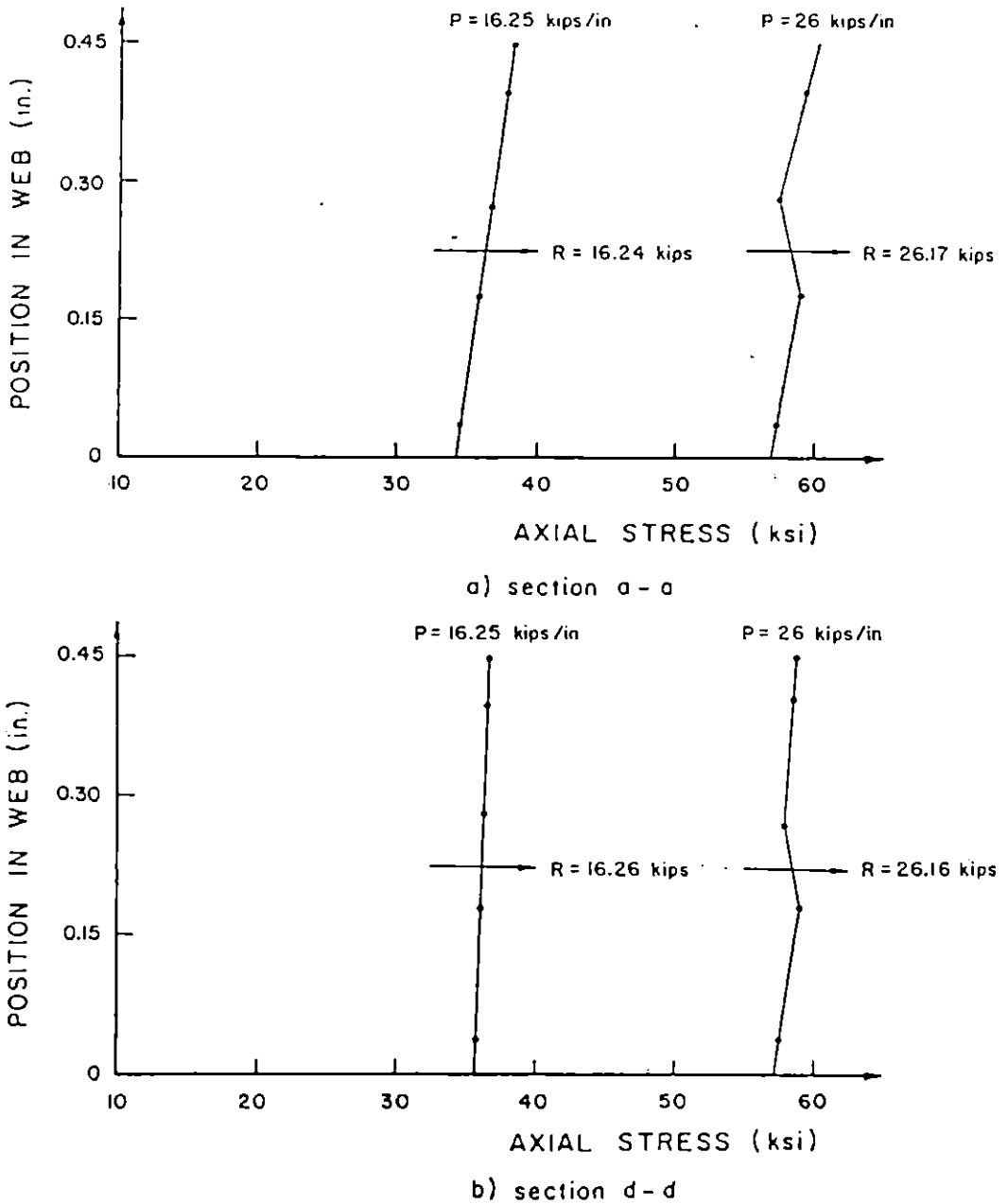

Figure 6.24: Statics Check at Web Section for PSX32 Sheet Pile

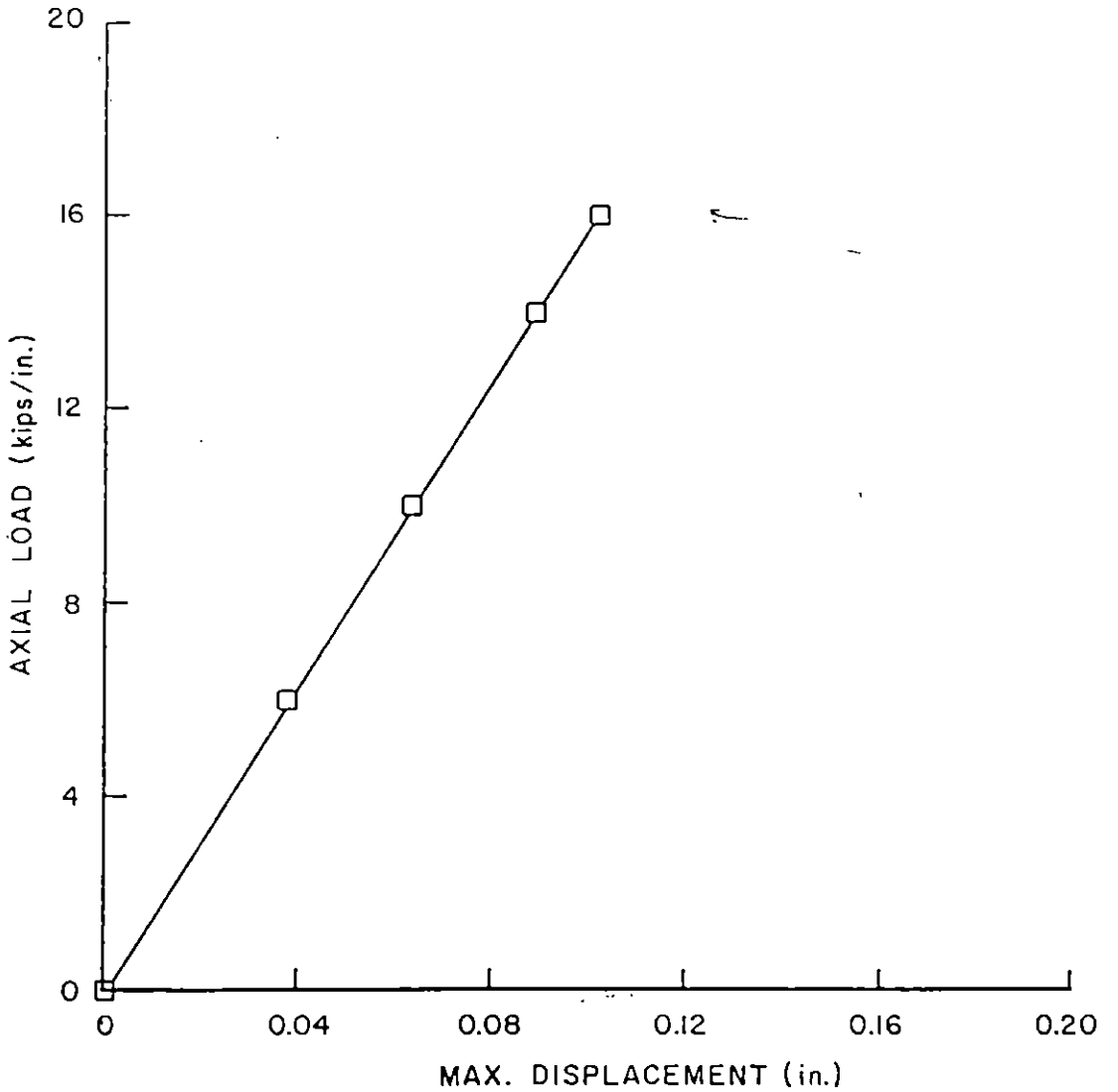

Figure 6.25: Load-Displacement Curve for Tip Deflection (Point 10) in PS32 Sheet Piles with Effective E Value

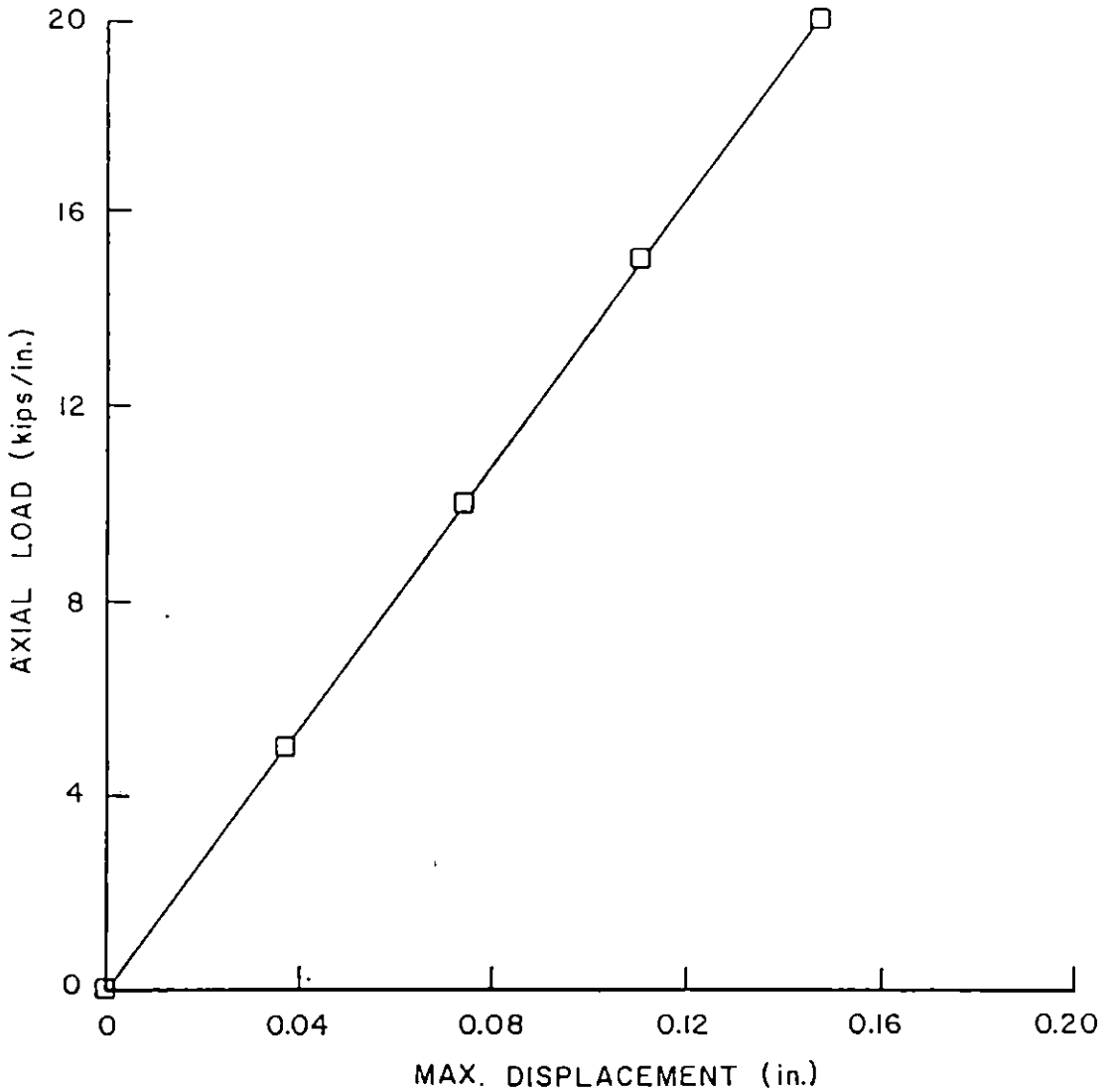

Figure 6.26: Load-Displacement Curve for Tip Deflection (point 10) in PSX32 Sheet Piles with Effective E Value

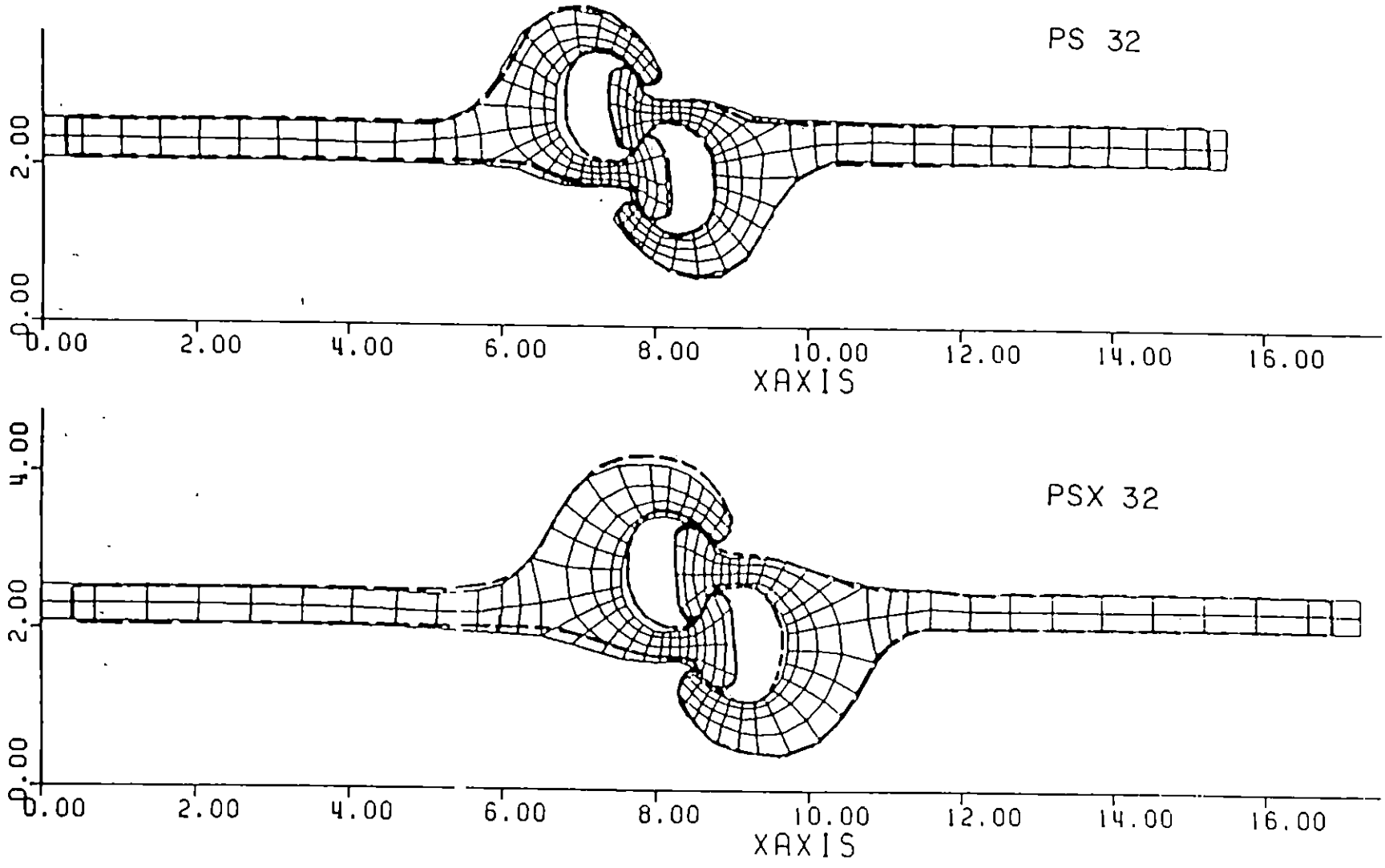

Figure 6.27: Initial and Deformed Shapes of PS32 and PSX32 Sheet Piles with Effective E Value

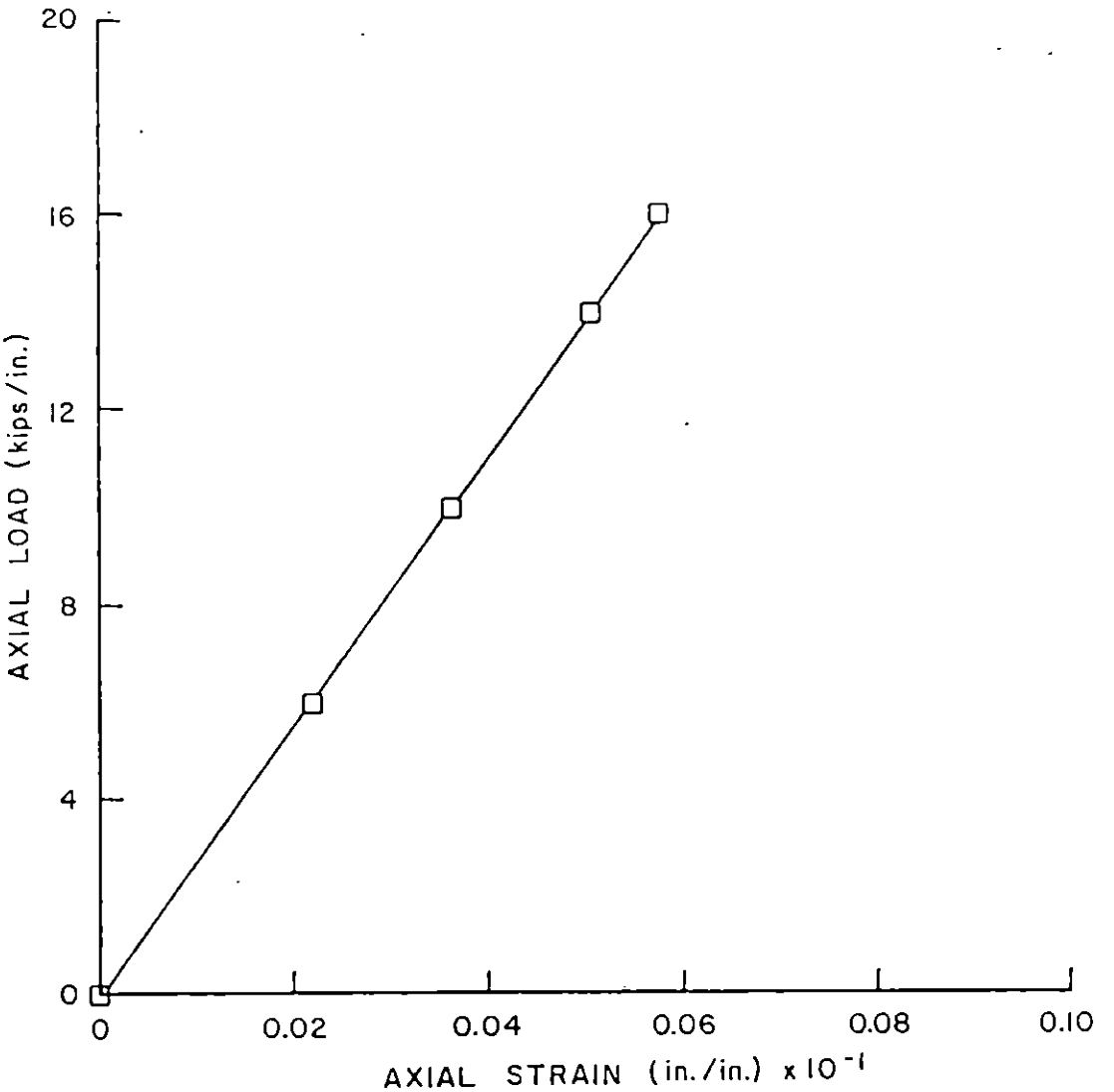

Figure 6.28: Axial Strain Versus Load for PS32 Sheet Pile with Effective E Value

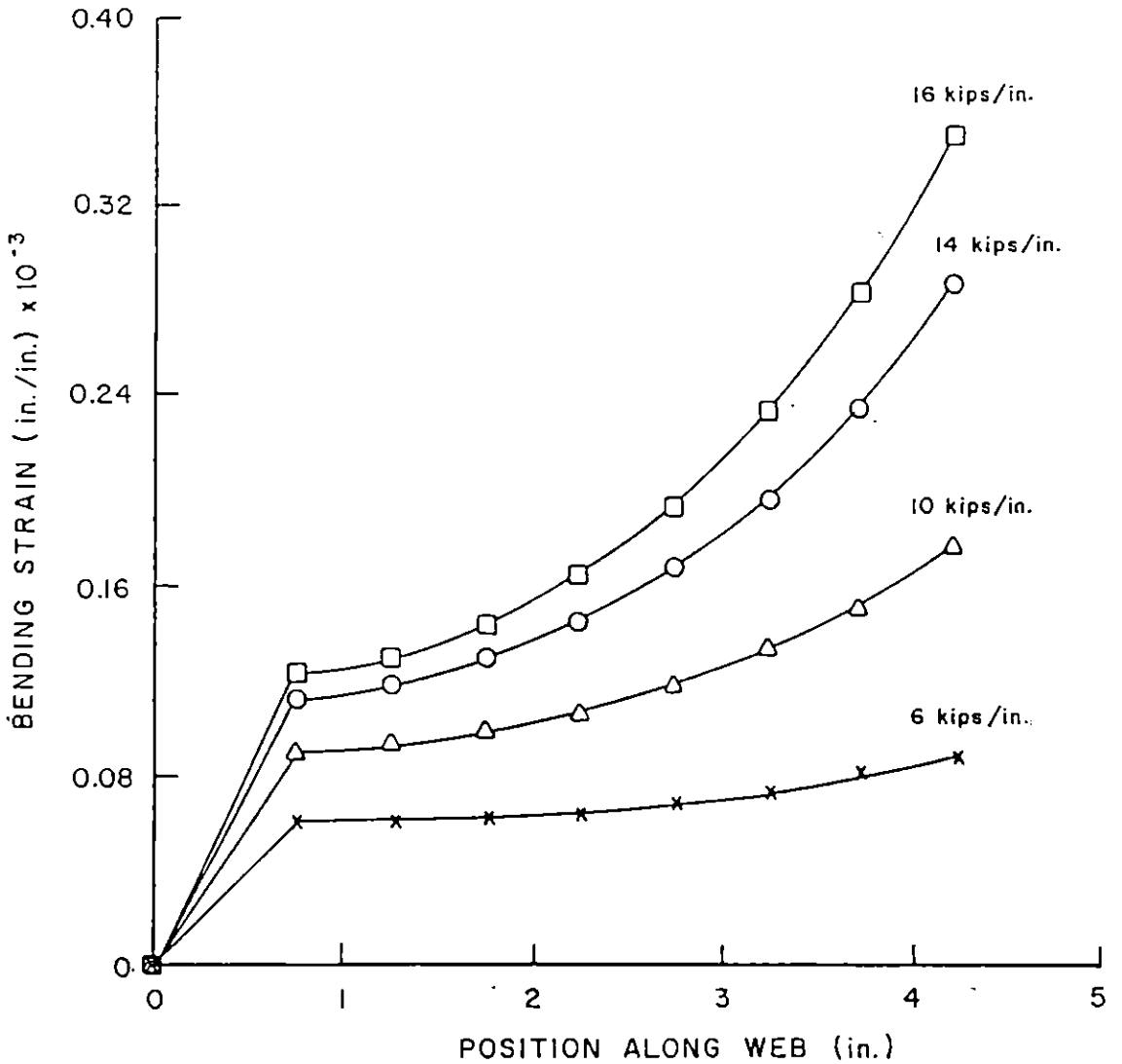

Figure 6.29: Variations of Bending Strains Along Web with Loads (PS32 With Effective E Value)

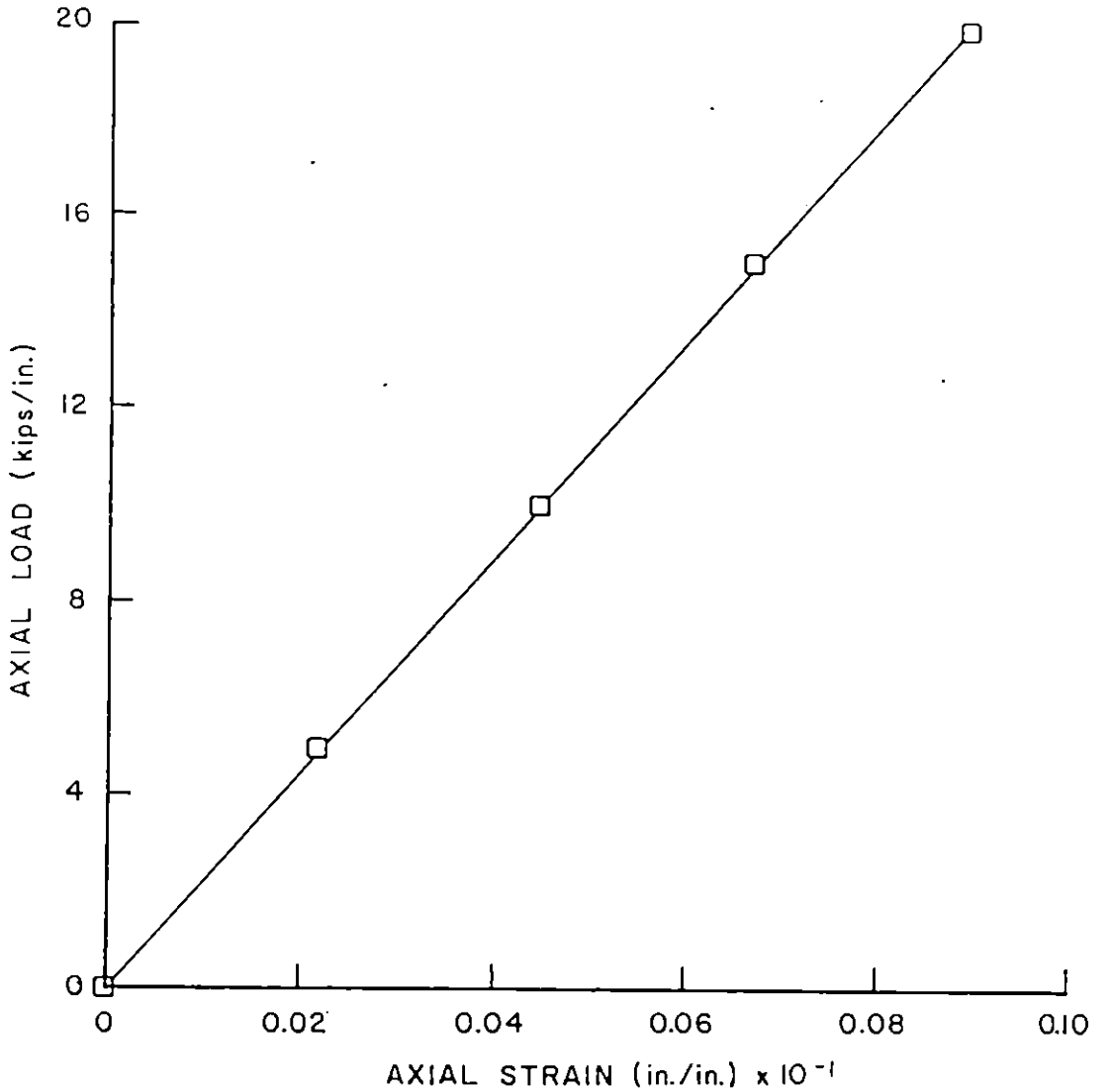

Figure 6.30: Axial Strain Versus Load for PSX32 Sheet Pile with Effective E Value

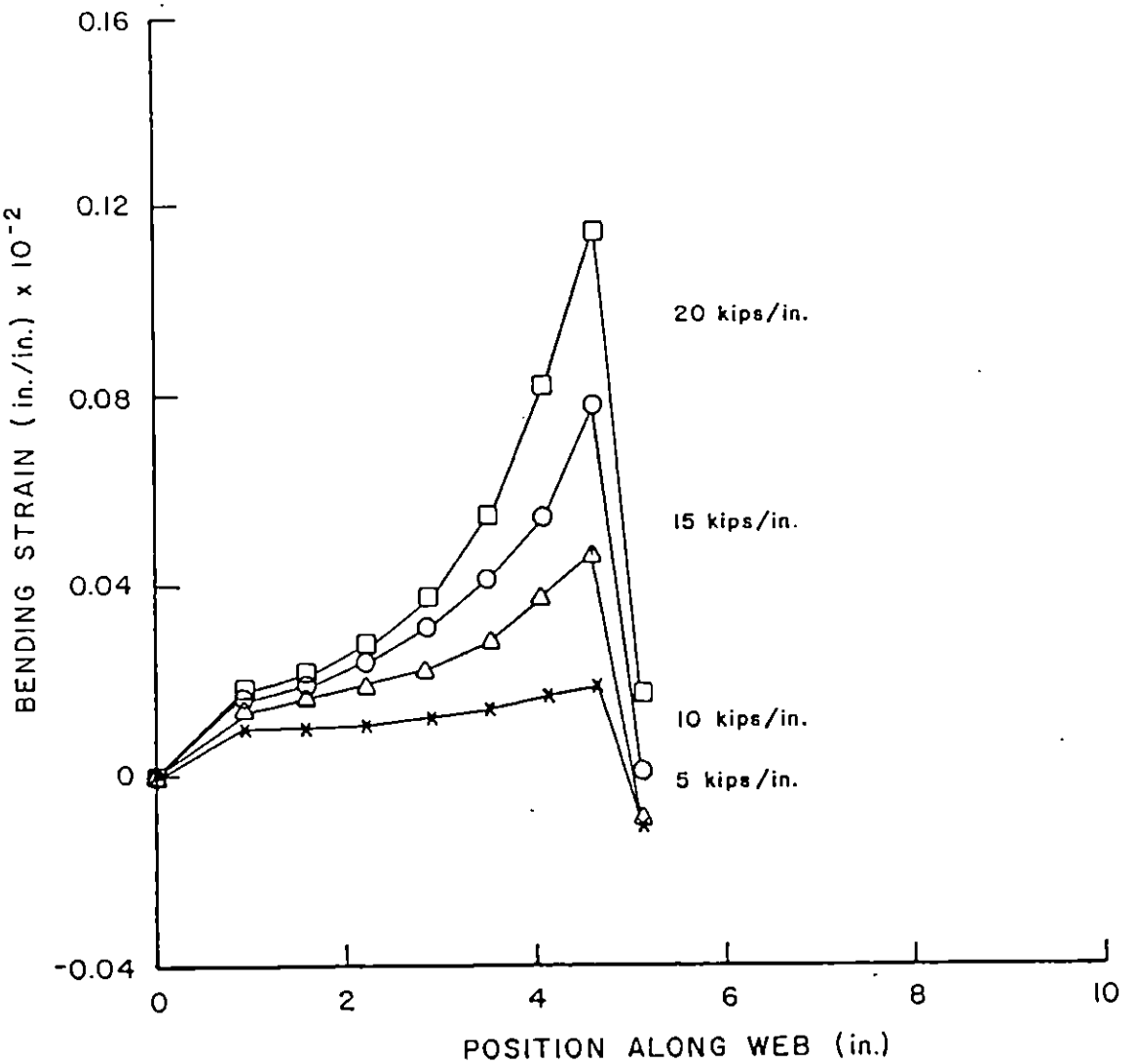

Figure 6.31: Variations of Bending Strains Along Web with Loads (PSX32 With Effective E Value)

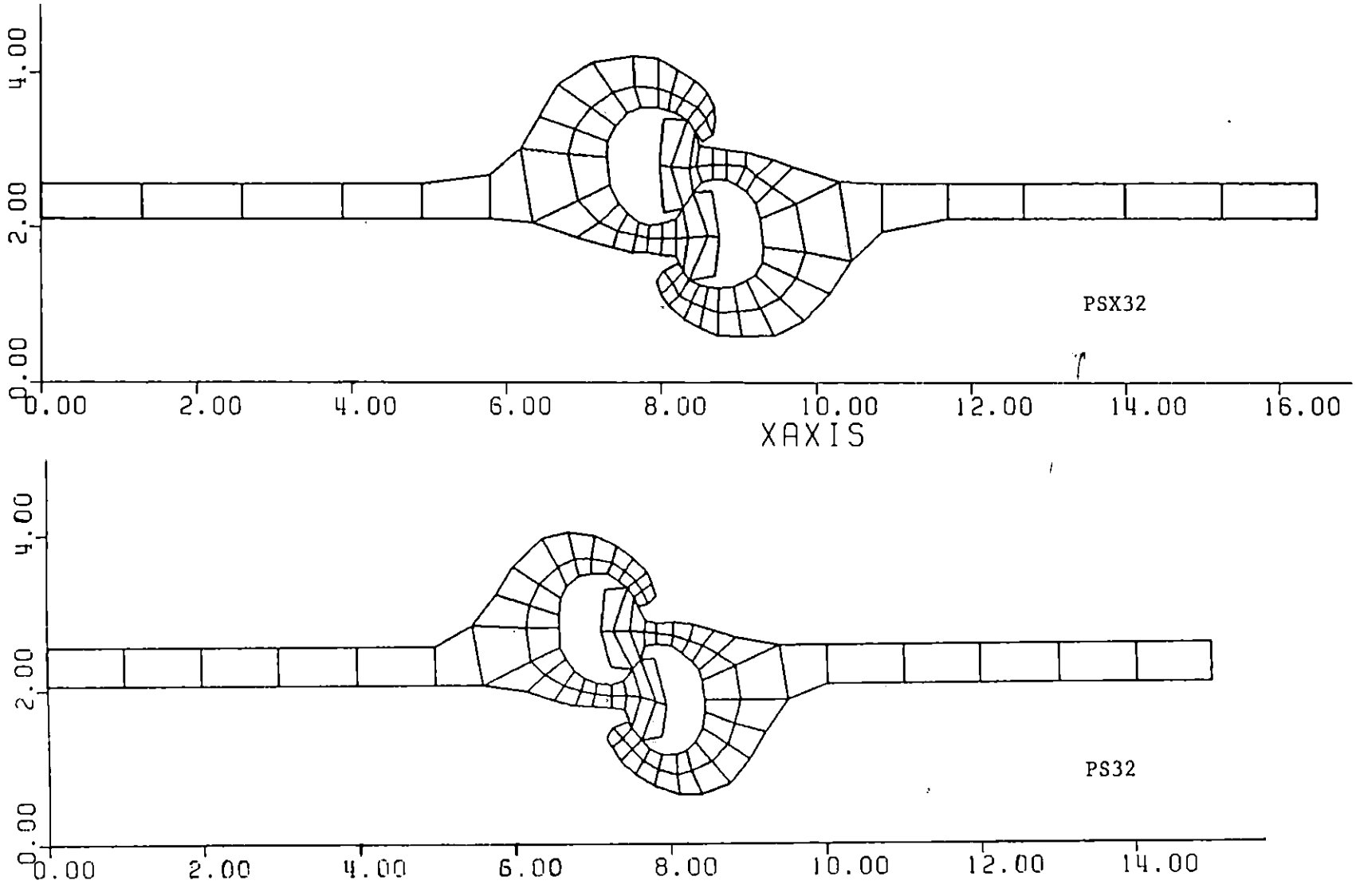

Figure 6.32: Finite Element Modeling of Sheet Pile Interlocks

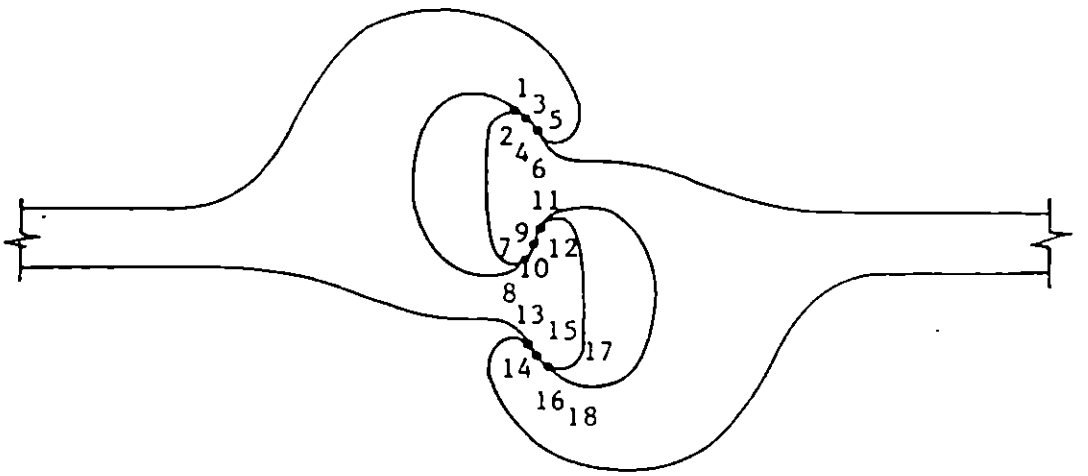

Contactor Nodes:	2,	4,	6
	7,	9,	11
	13,	15,	17
Target Nodes:	1,	3,	5
	8,	10,	12
	14,	16,	18

Figure 6.33: Contact Node Pairs in Sheet Pile Interlocks

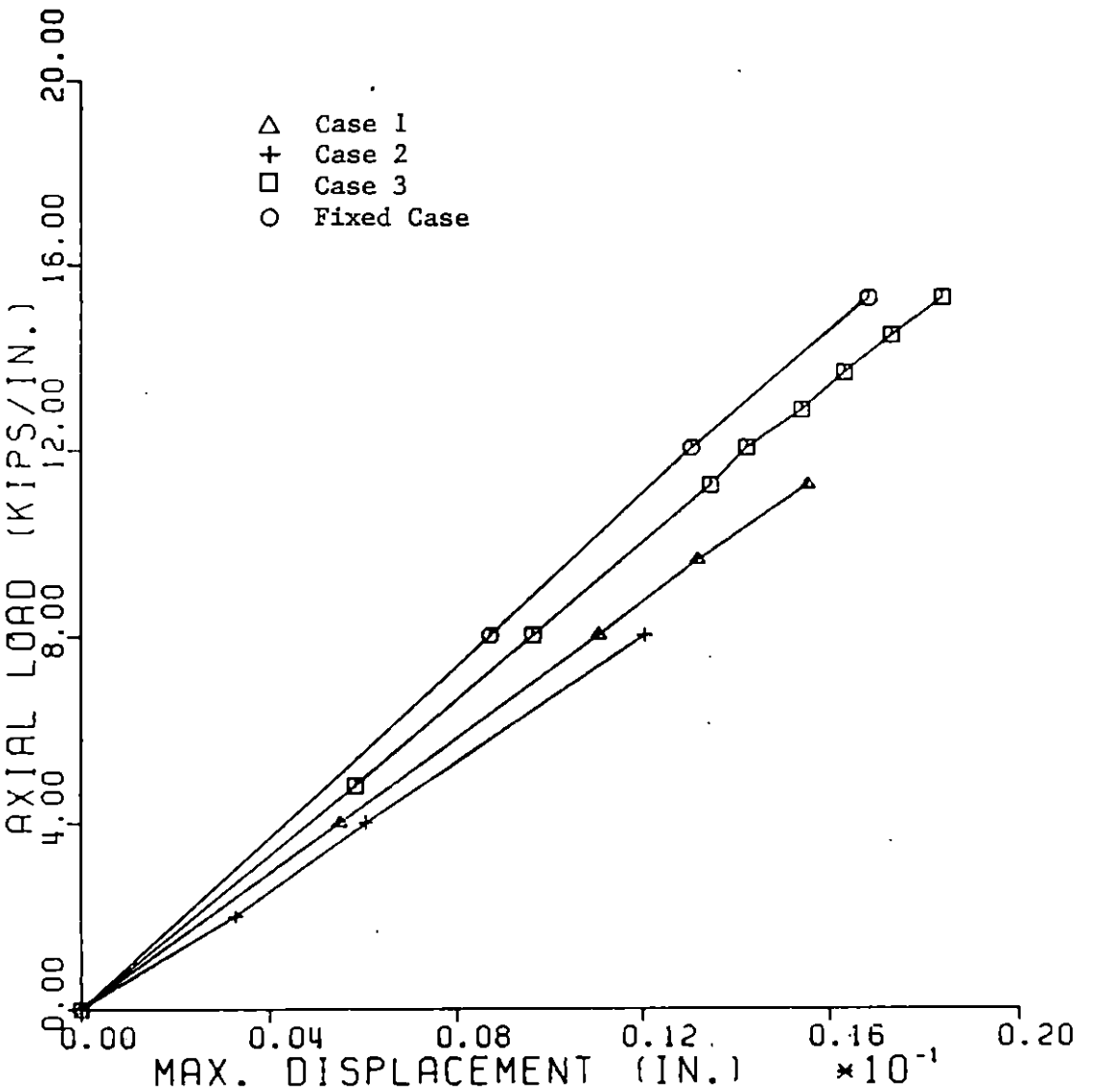

Figure 6.34: Maximum Displacement of PS32 Sheet Pile Interlocks

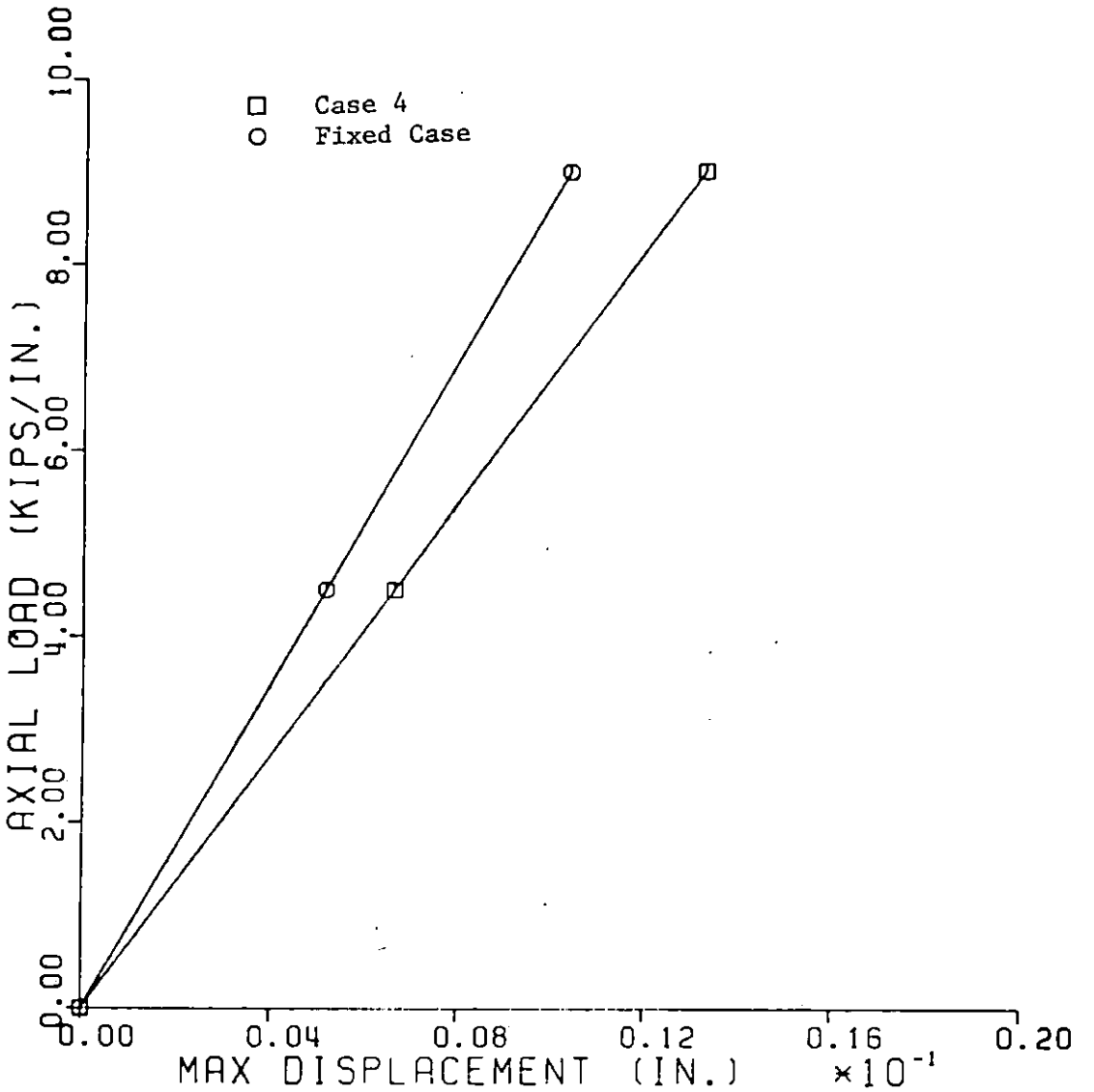

Figure 6.35: Maximum Displacement of PSX32 Sheet Pile Interlocks

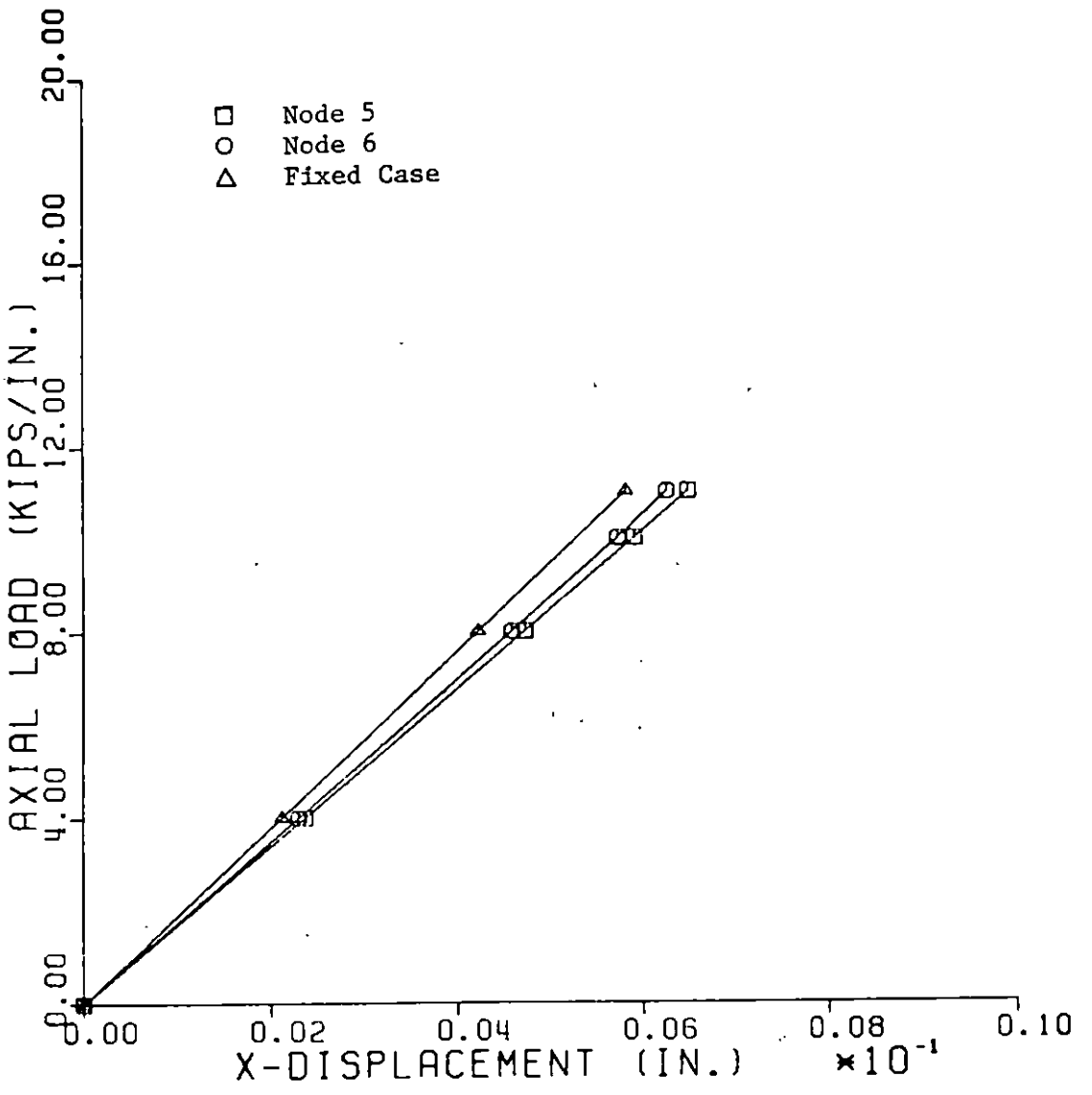

Figure 6.36: Longitudinal Displacement Versus Load Plot for Contact Node Pair (5,6) in Case 1

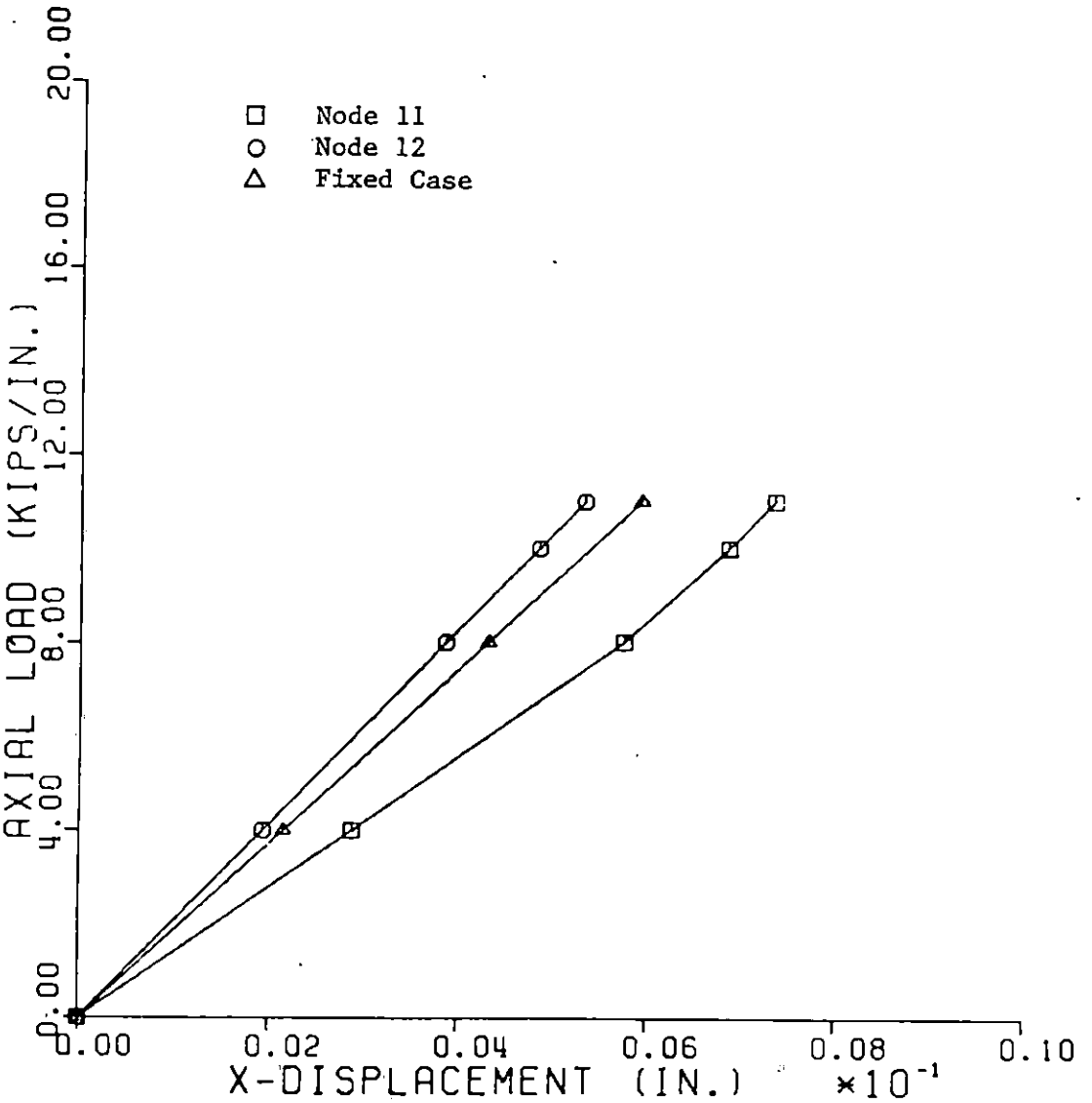

Figure 6.37: Longitudinal Displacement Versus Load Plot for Contact Node Pair (11,12) in Case 1

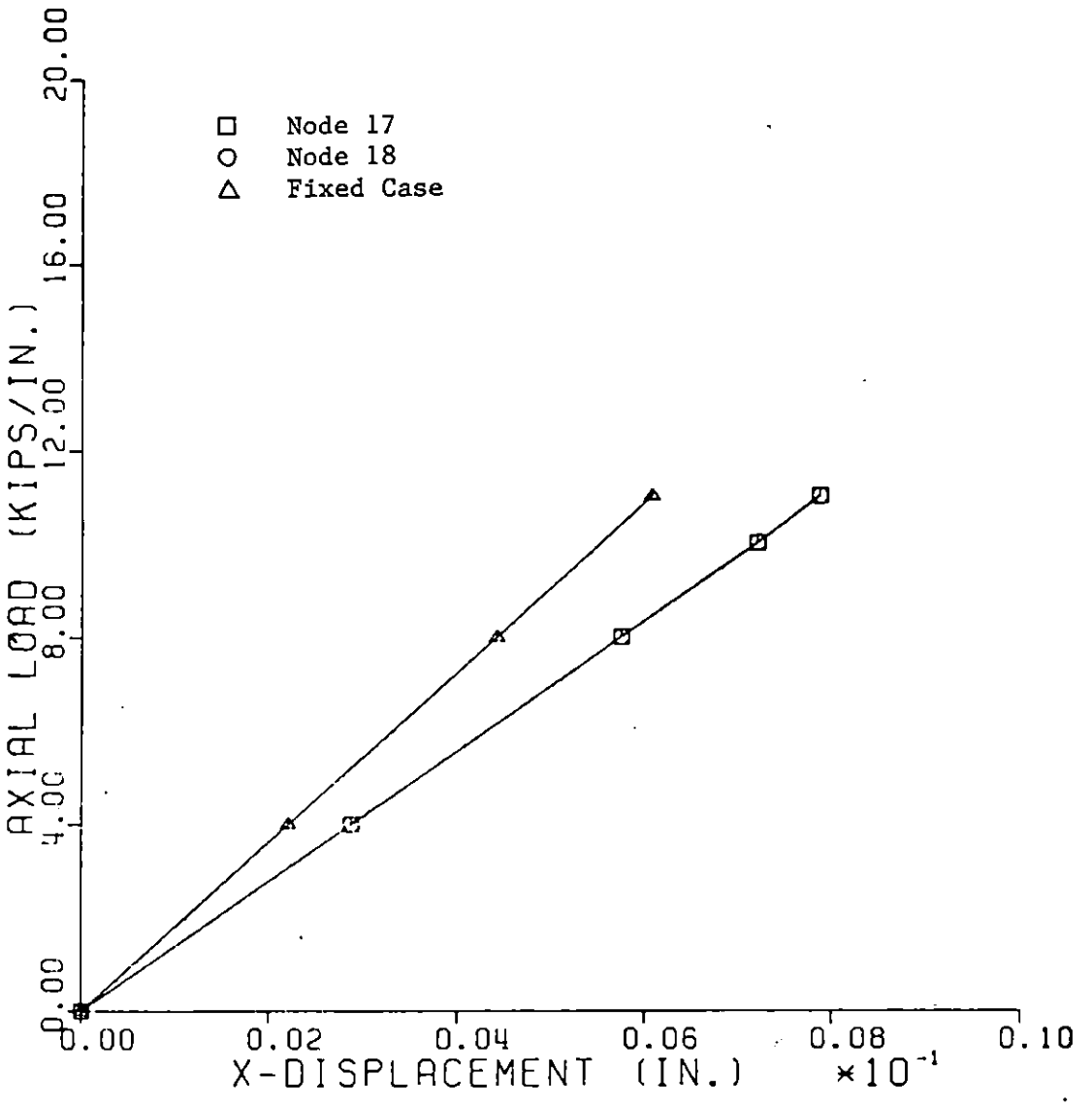

Figure 6.38: Longitudinal Displacement Versus Load Plot for Contact Node Pair (17,18) in Case 1

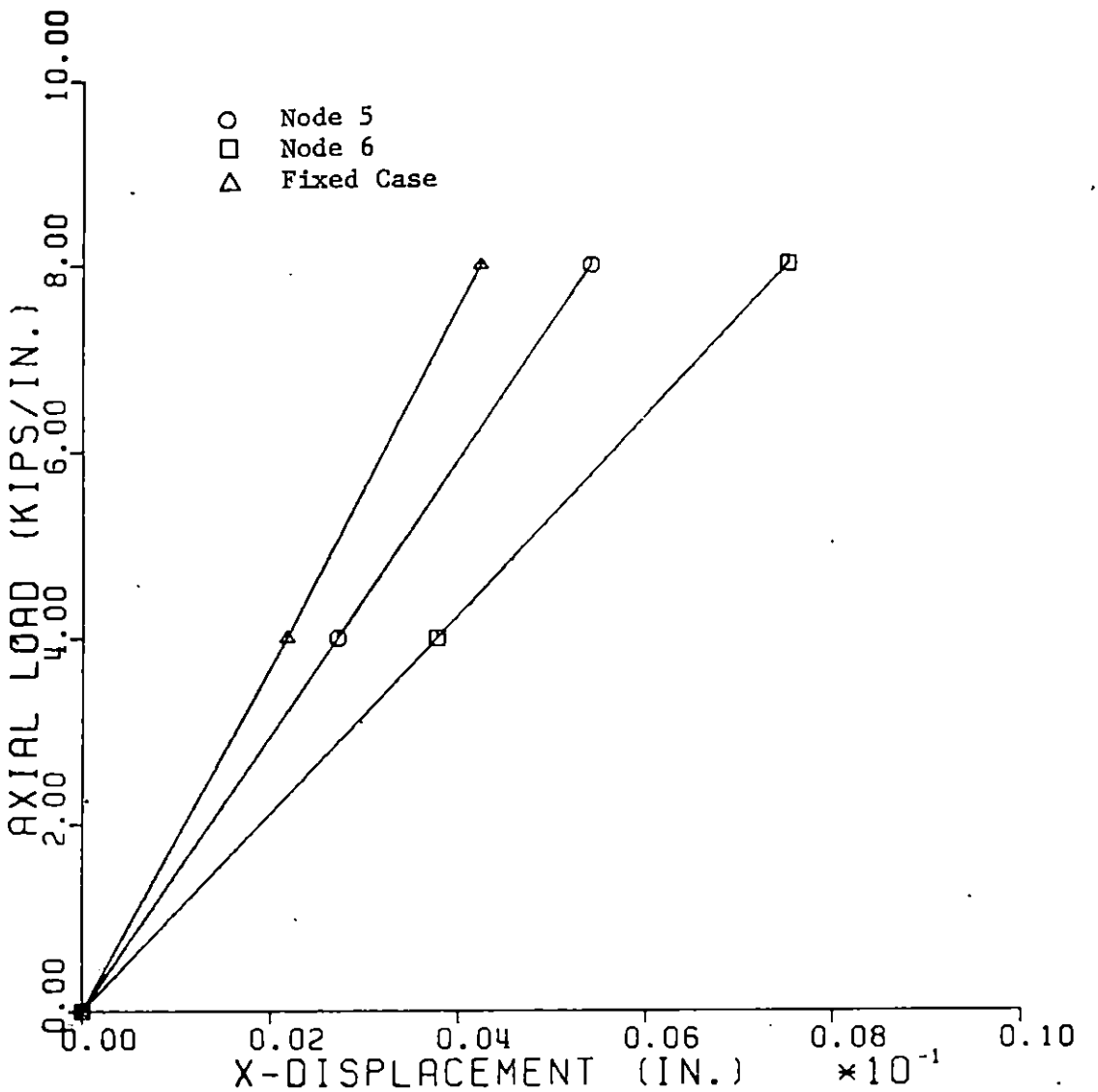

Figure 6.39: Longitudinal Displacement Versus Load Plot for Contact Node Pair (5,6) in Case 2

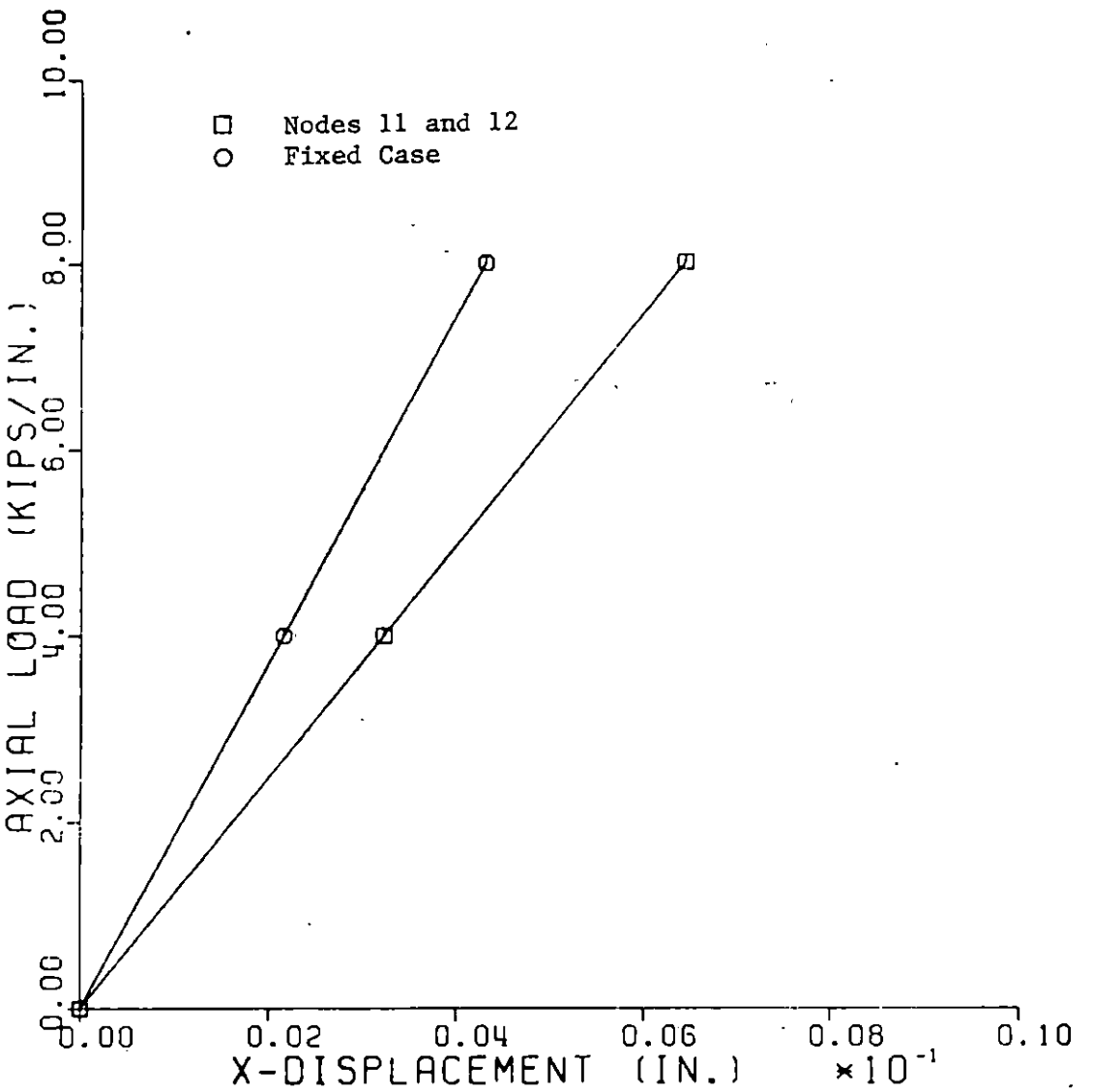

Figure 6.40: Longitudinal Displacement Versus Load Plot for Contact Node Pair (11,12) in Case 2

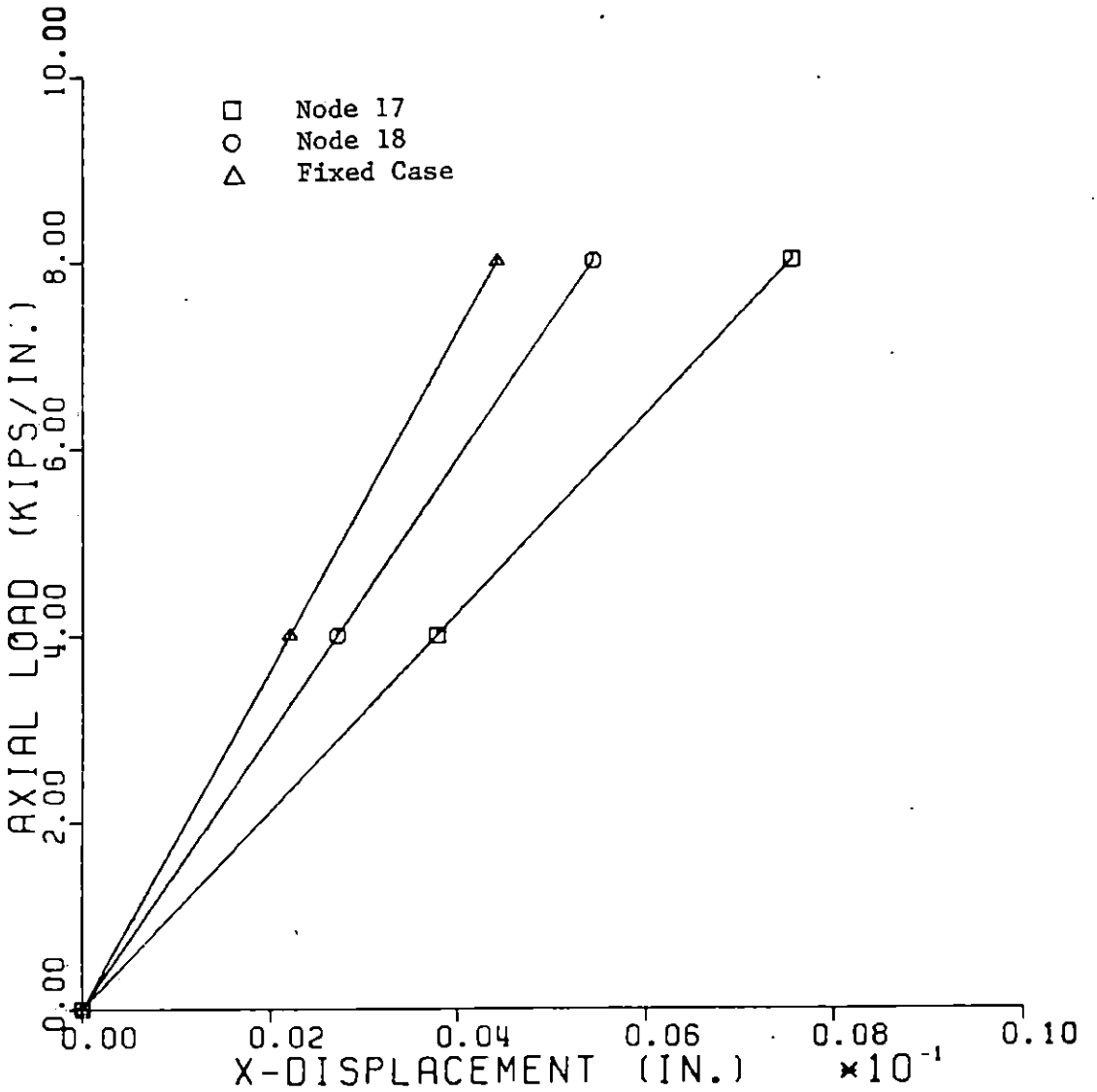

Figure 6.41: Longitudinal Displacement Versus Load Plot for Contact Node Pair (17,18) in Case 2

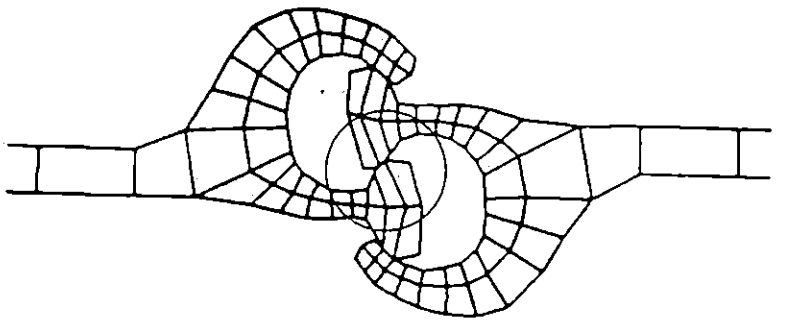

a) Sliding Between Two Thumbs of Interlocks (Deformed Shape from Case 1).

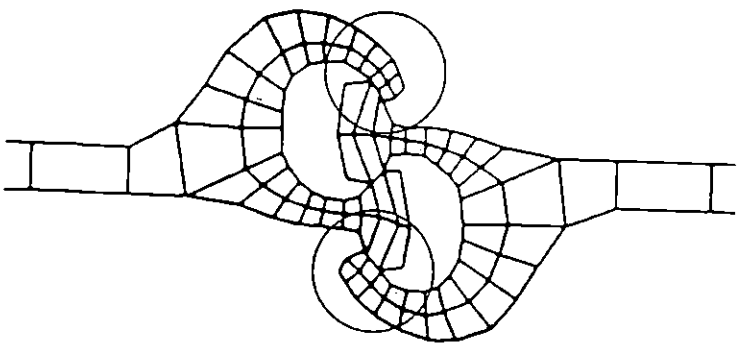

b) Sliding Between Thumbs and Fingers of Interlocks (Deformed Shape from Case 2).

Figure 6.42: Deformed Meshes Exhibiting Different Modes of Sliding

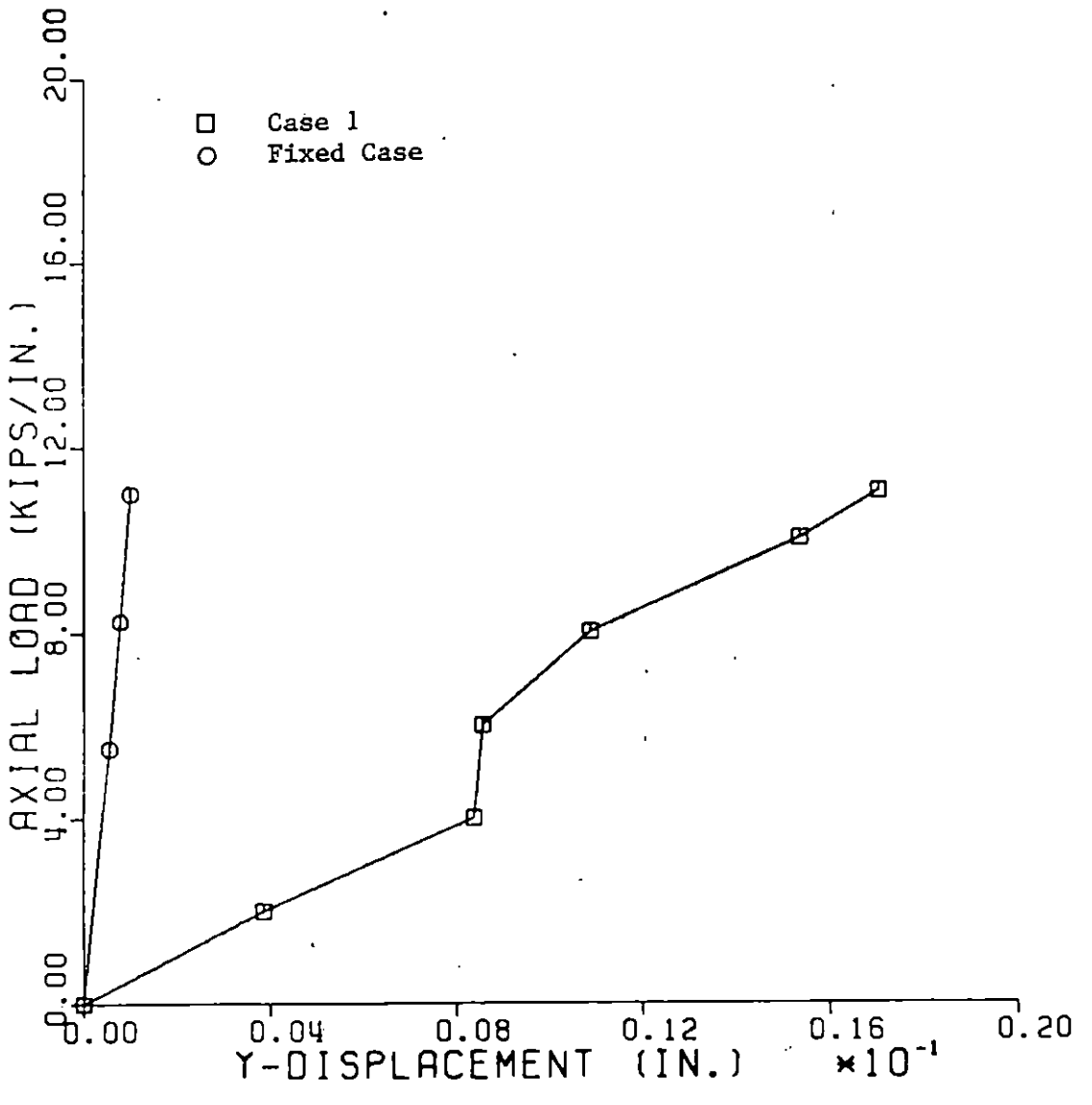

Figure 6.43: Average Lateral Displacement Versus Load Plot for Nodes 1-6 in Case 1

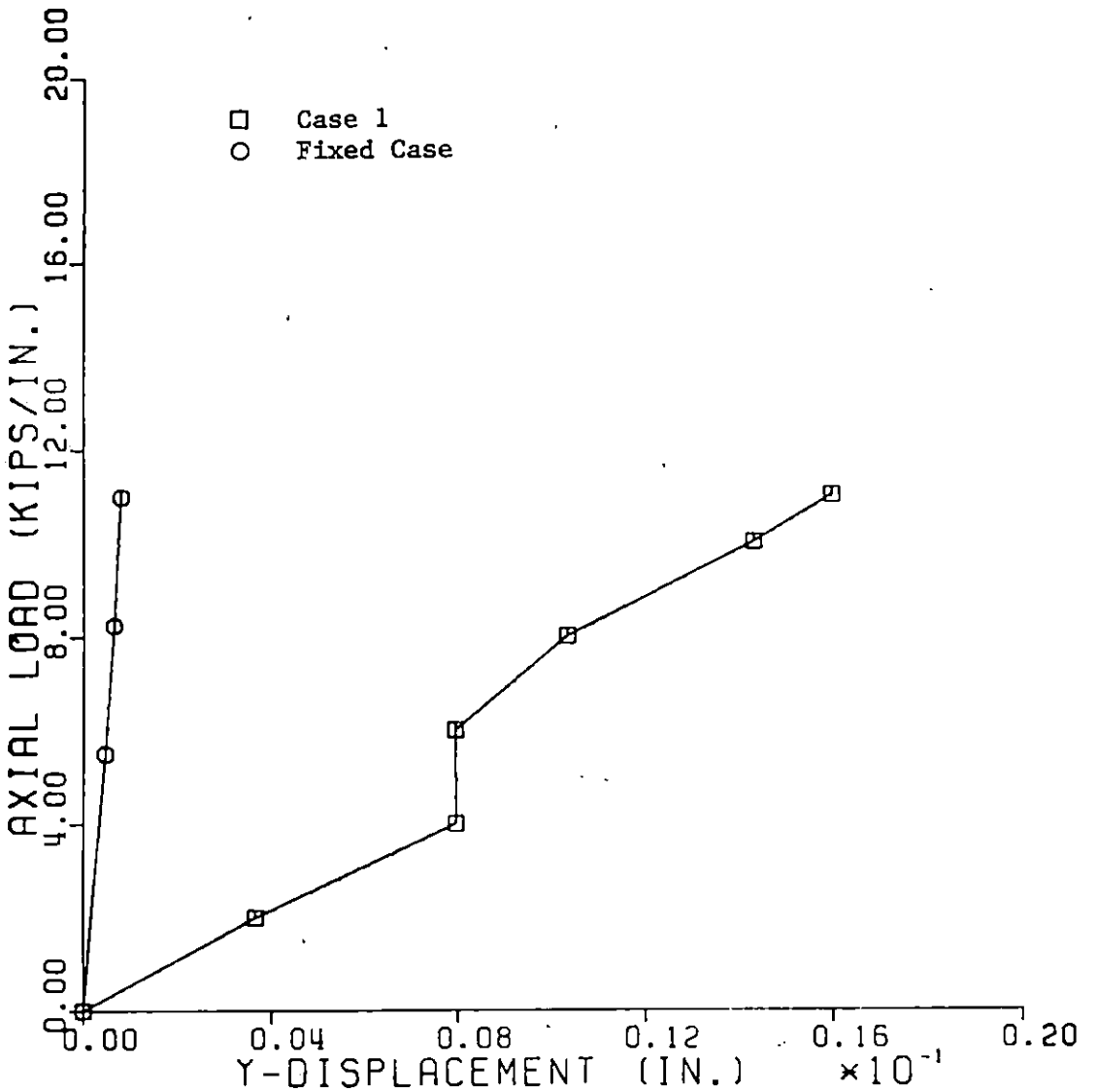

Figure 6.44: Average Lateral Displacement Versus Load Plot for Nodes 7-12 in Case 1

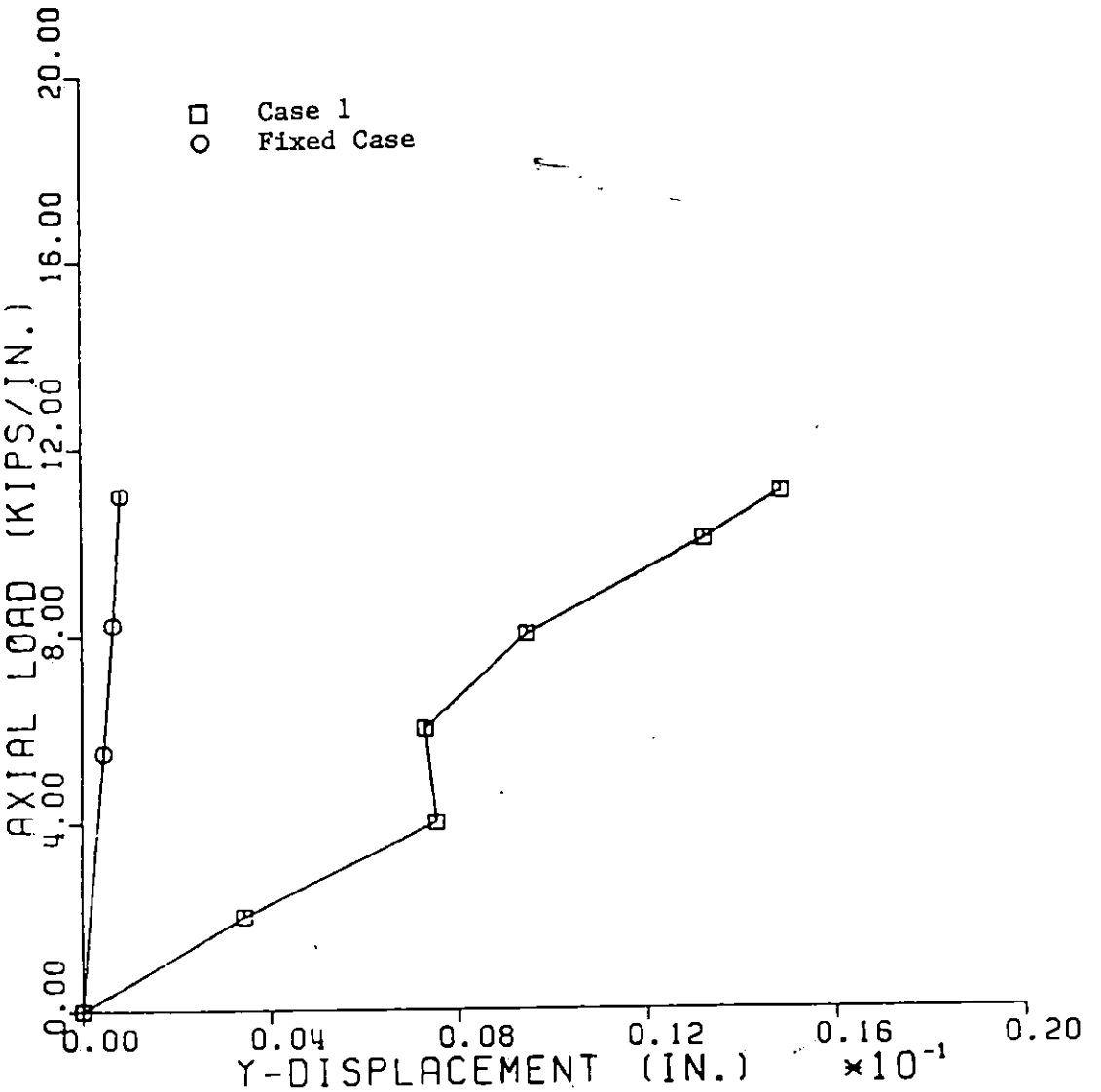

Figure 6.45: Average Lateral Displacement Versus Load Plot for Nodes 13-18 in Case 1

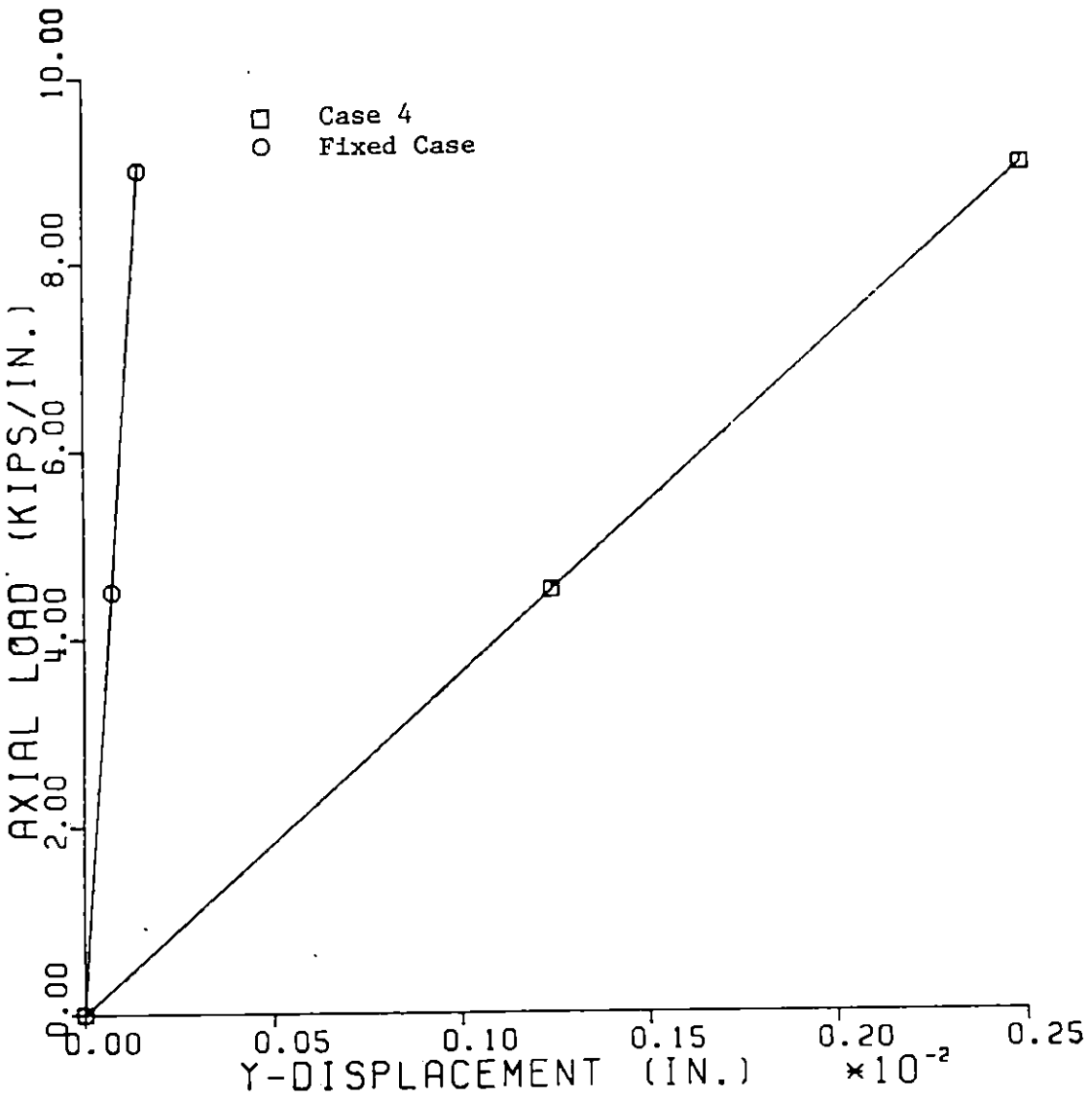

Figure 6.46: Average Lateral Displacement Versus Load Plot for Nodes 1-6 in Case 4

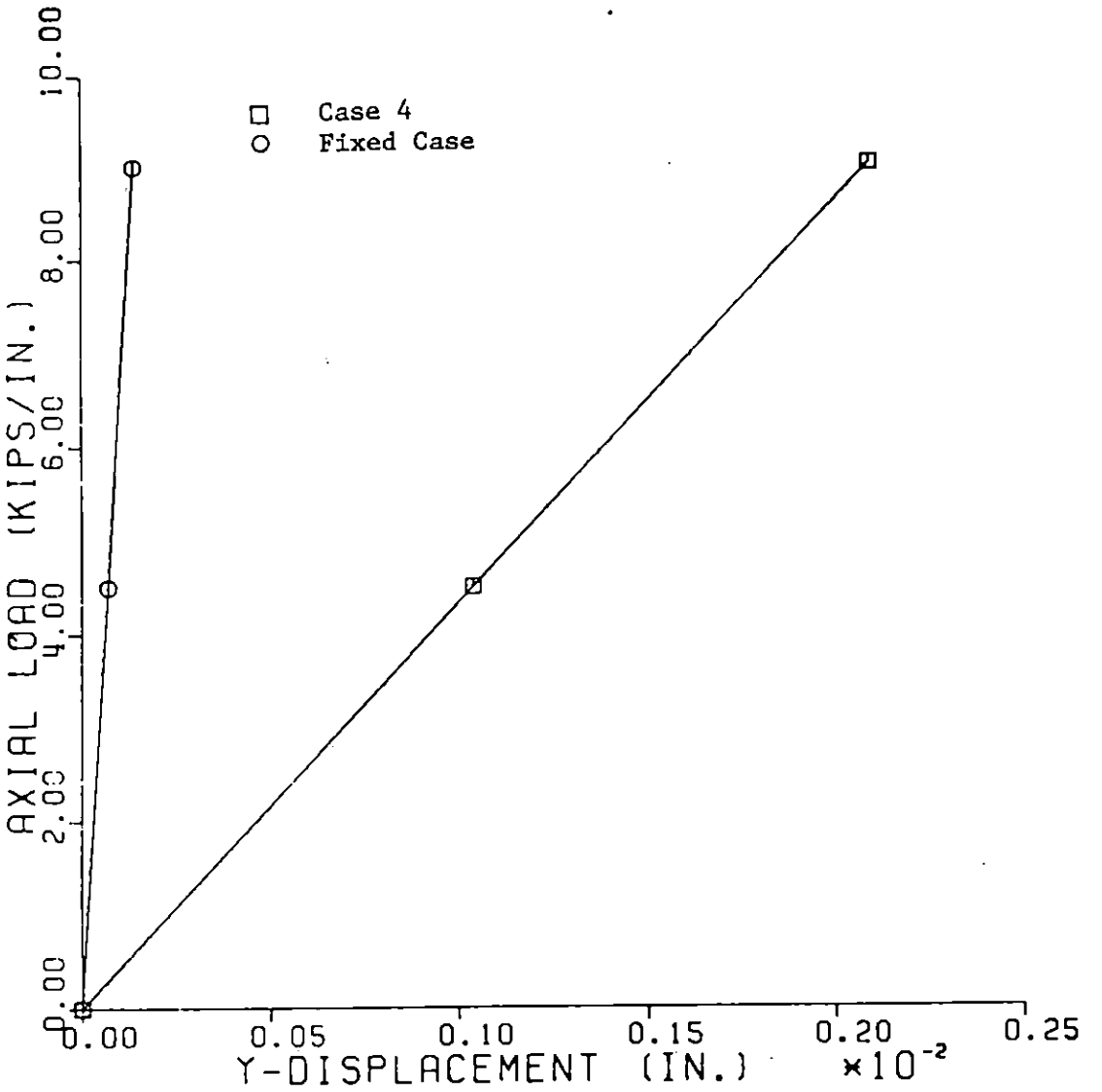

Figure 6.47: Average Lateral Displacement Versus Load Plot for Nodes 7-12 in Case 4

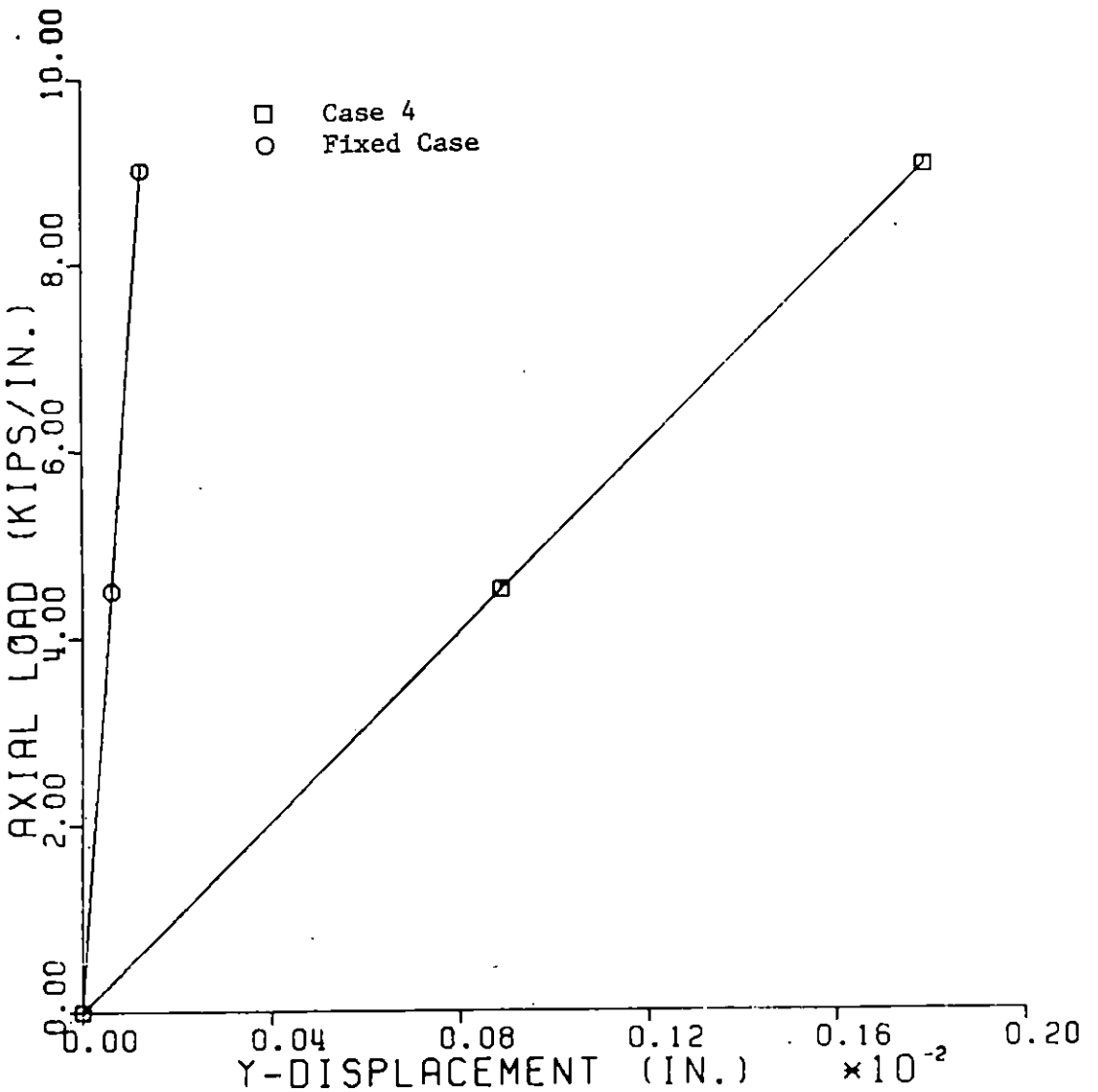

Figure 6.48: Average Lateral Displacement Versus Load Plot for Nodes 13-18 in Case 4

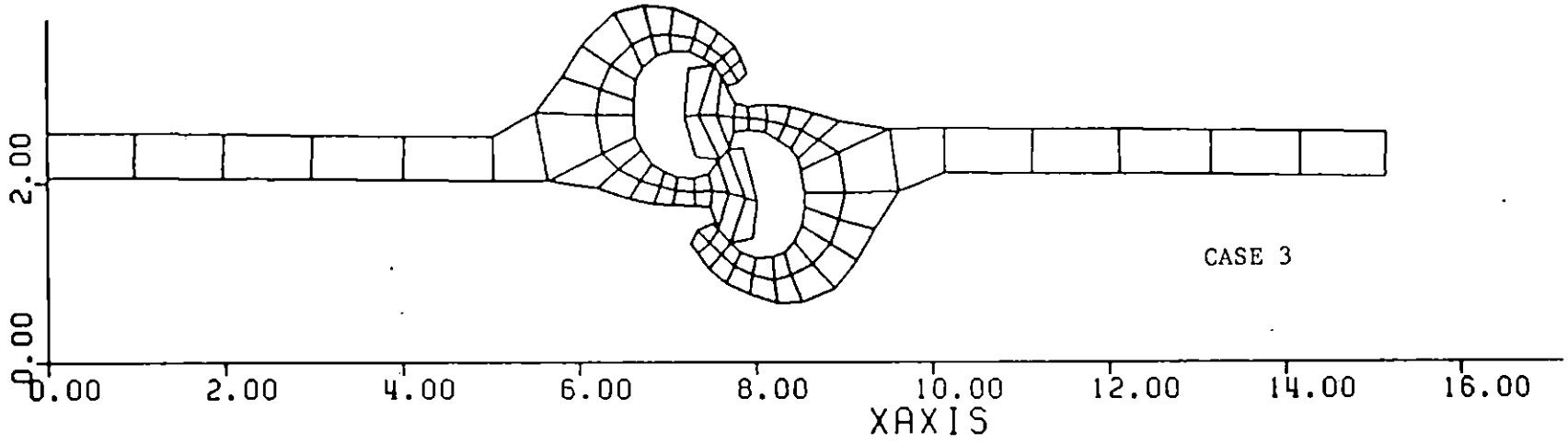

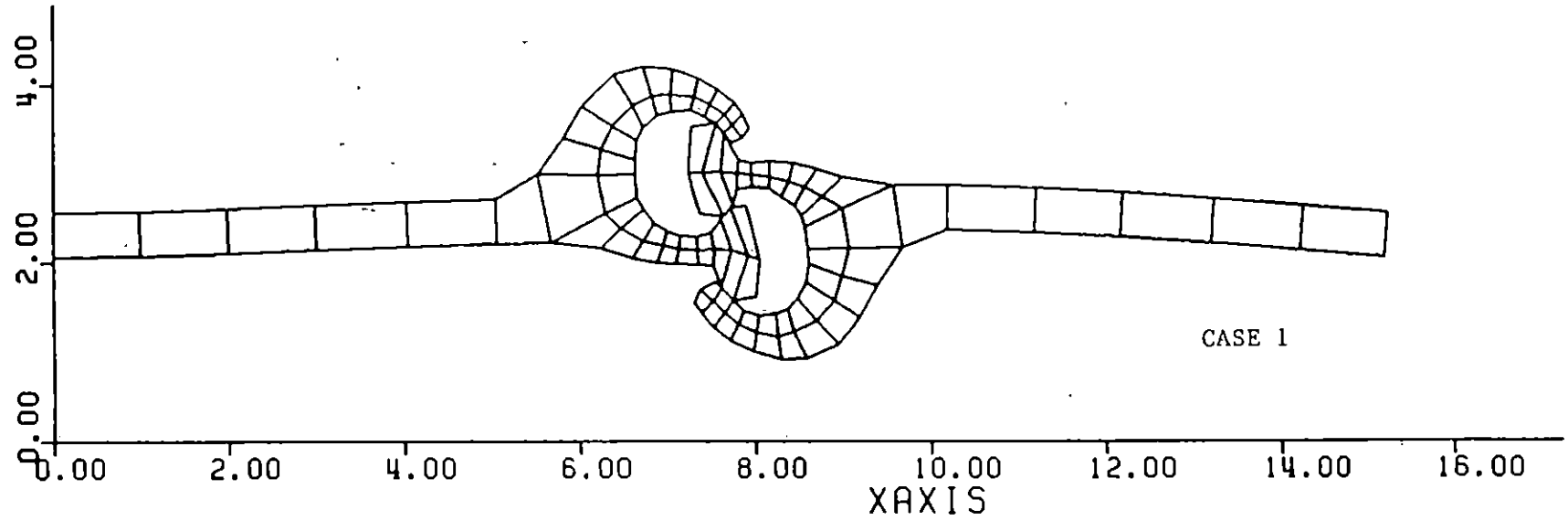

Figure 6.49: Comparison of Deformed Shapes of Sheet Pile Interlocks for Cases 1 and 3

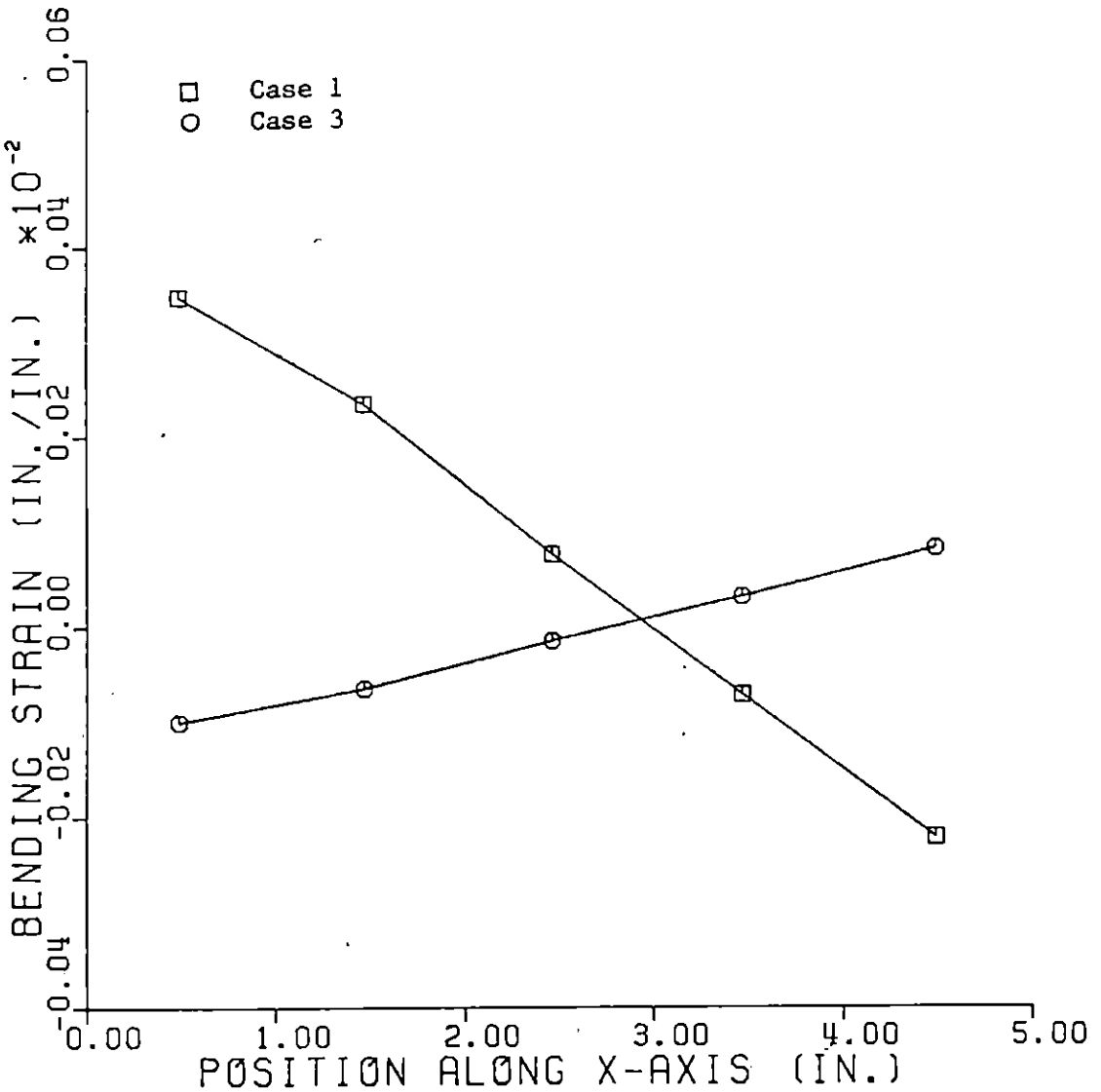

Figure 6.50: Comparision of Bending Strain in Web 1 of Sheet Piles for Cases 1 and 3

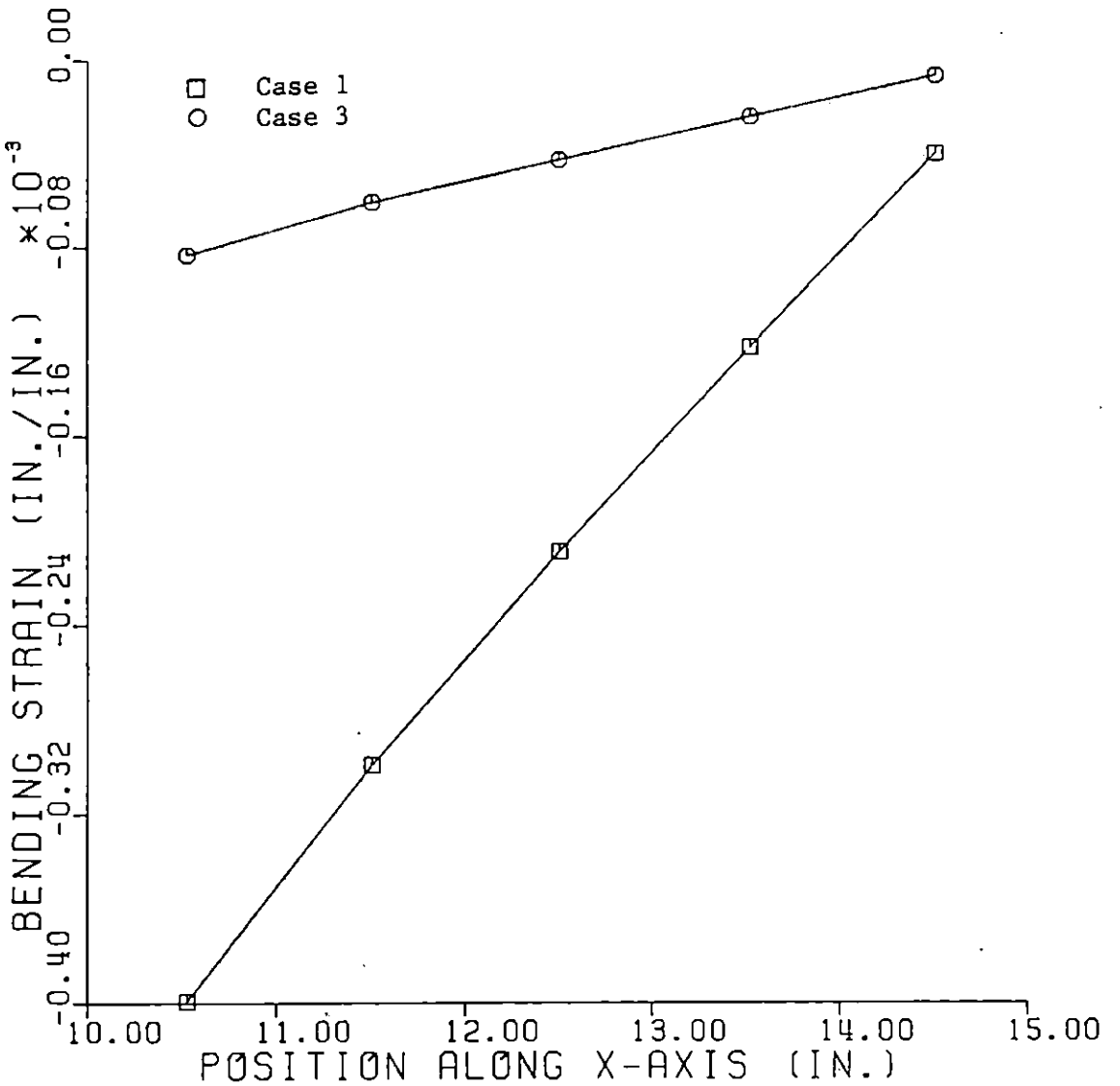

Figure 6.51: Comparision of Bending Strain in Web 2 of Sheet Piles for Cases 1 and 3

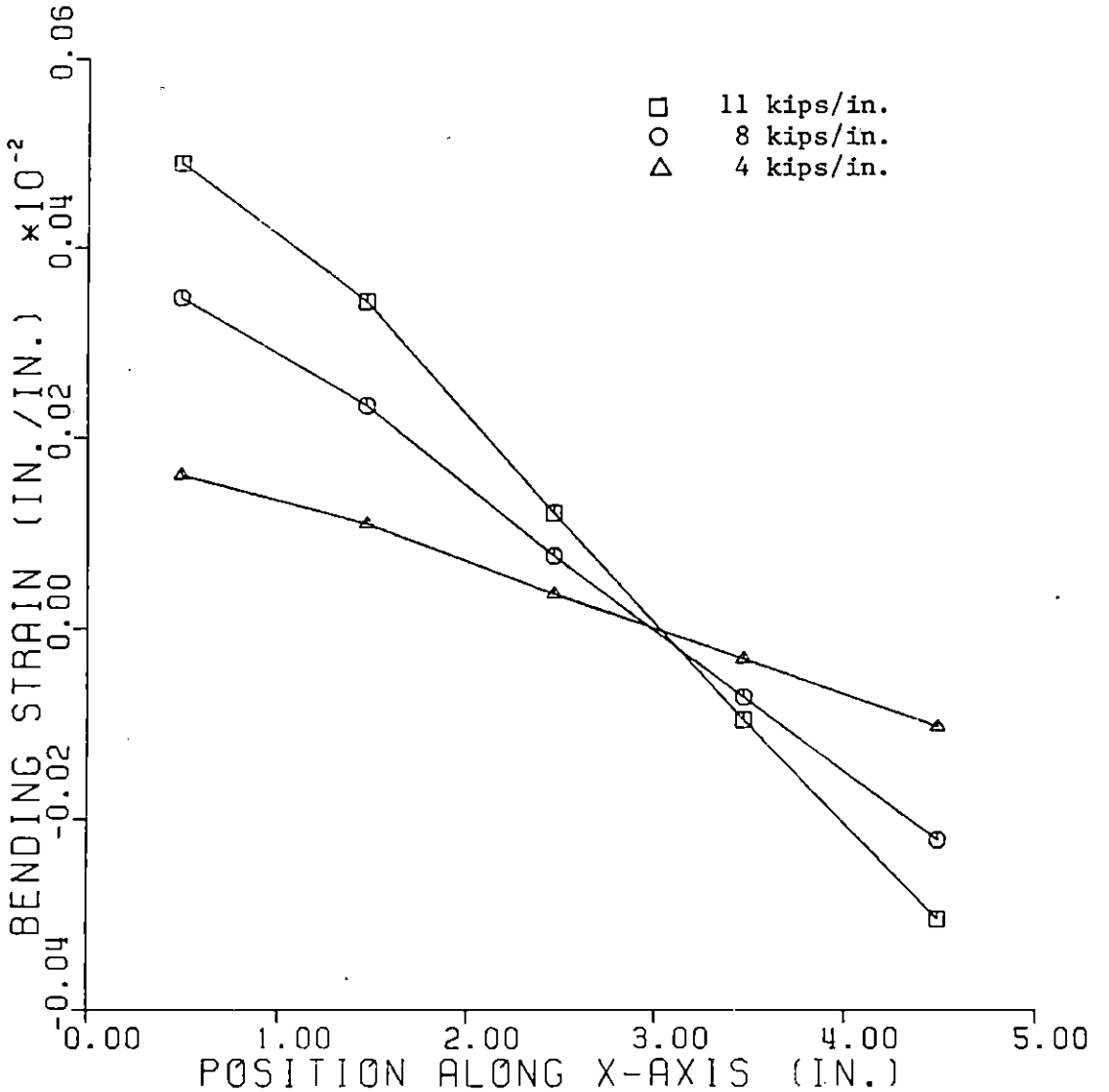

Figure 6.52: Bending Strain Versus Load Plot for Web 1 of PS32 Sheet Piles

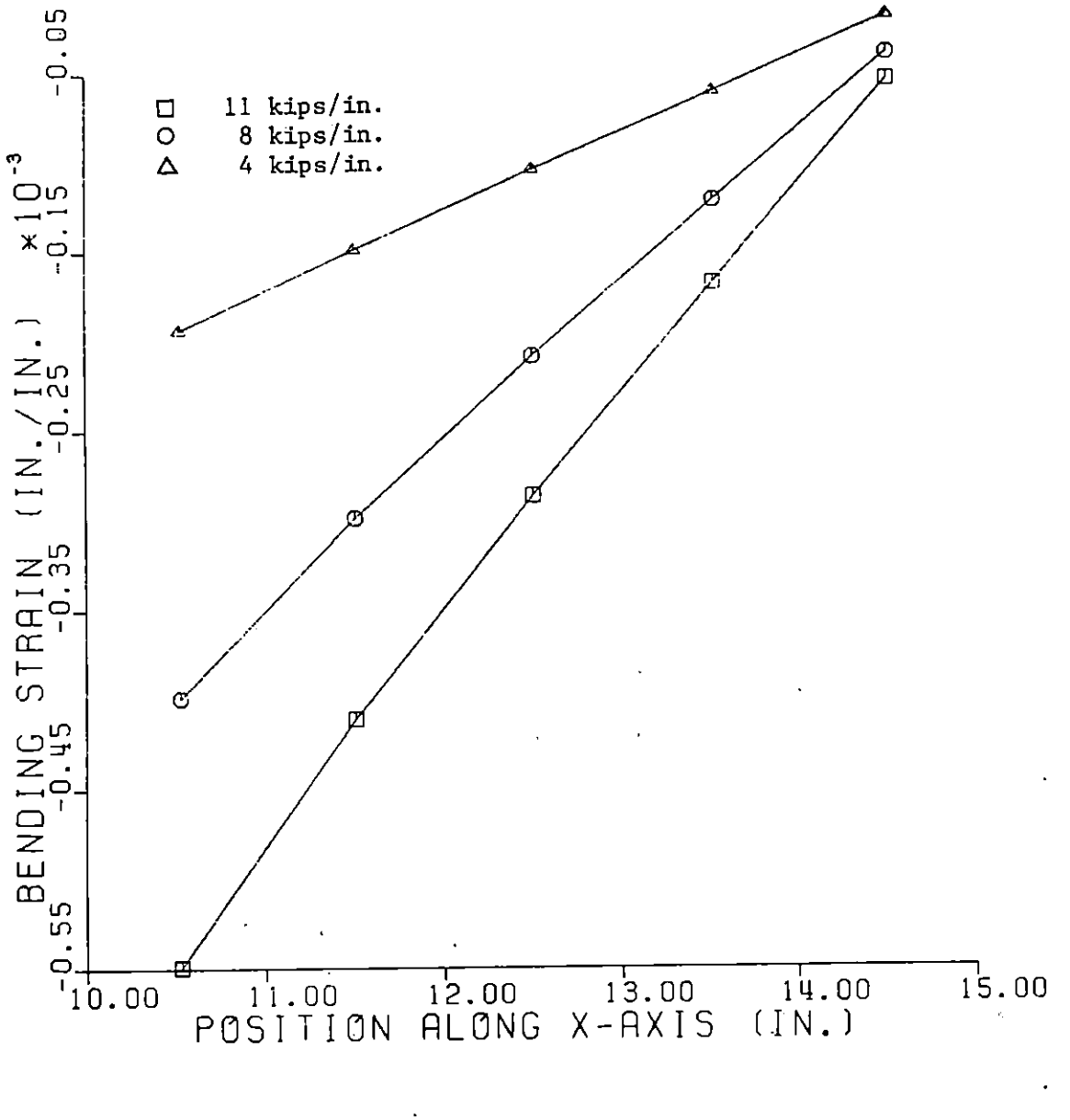

Figure 6.53: Bending Strain Versus Load Plot for Web 2 of PS32 Sheet Piles

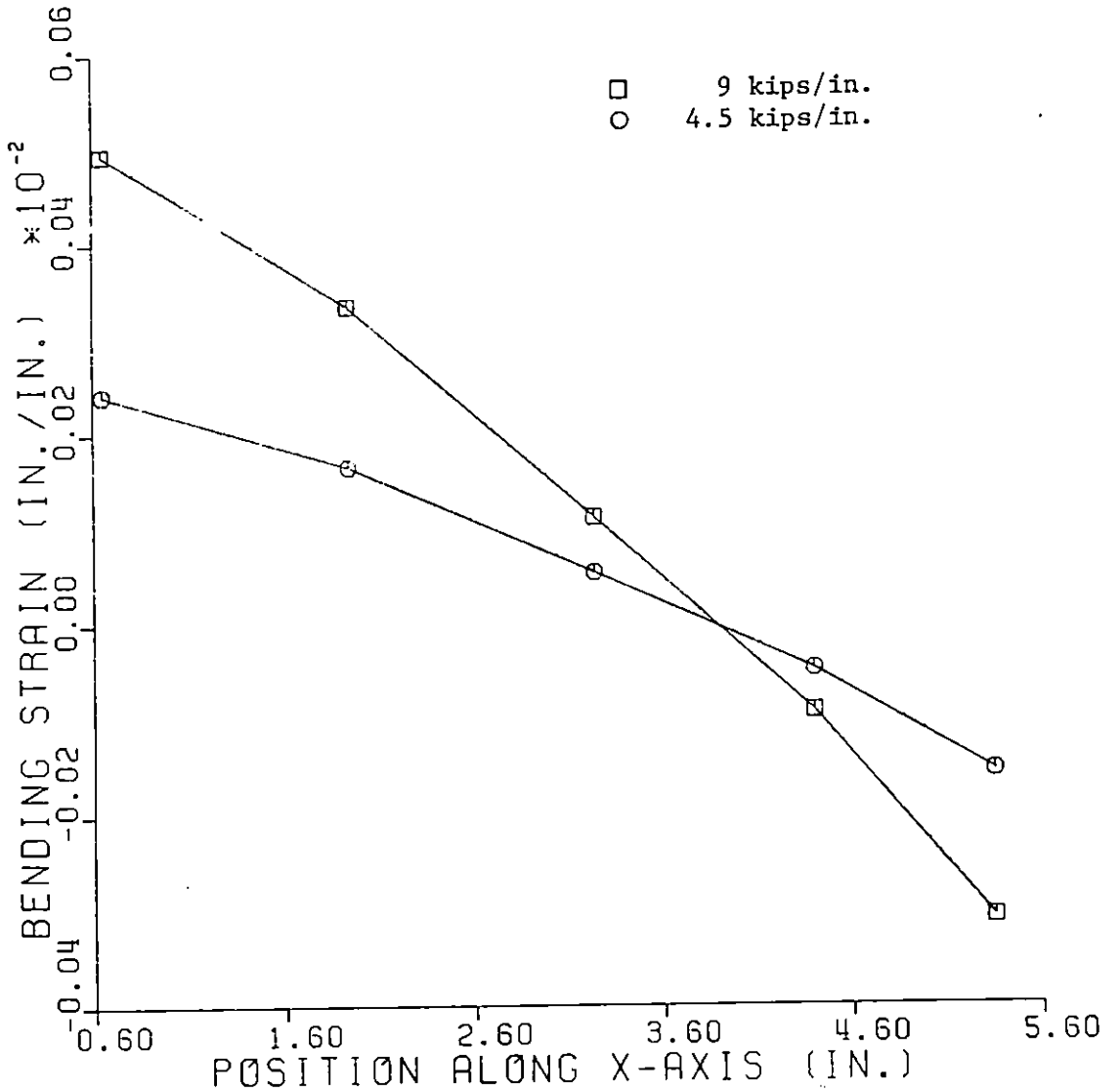

Figure 6.54: Bending Strain Versus Load Plot for Web 1 of PSX32 Sheet Piles

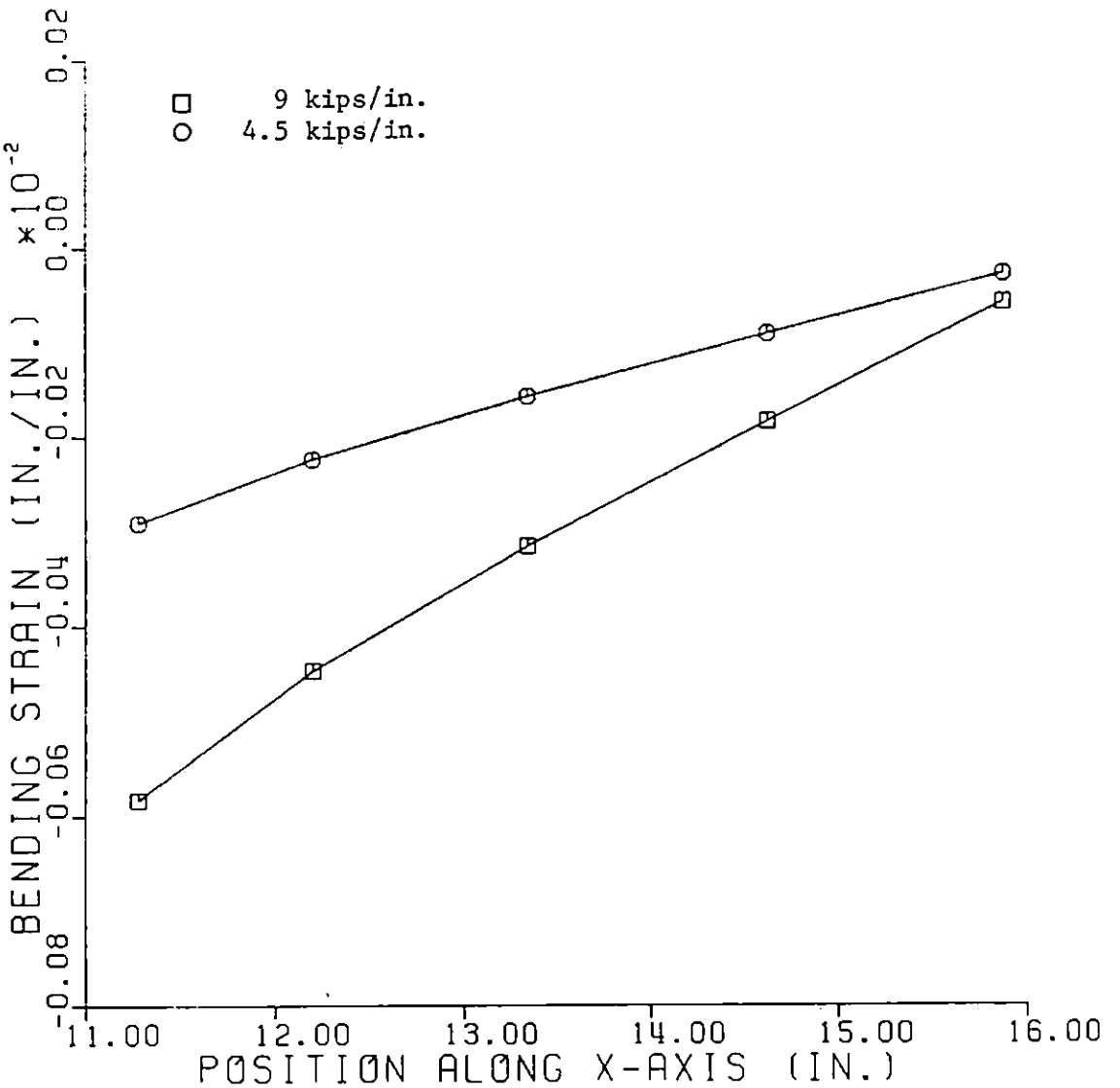

Figure 6.55: Bending Strain Versus Load Plot for Web 2 of PSX32 Sheet Piles

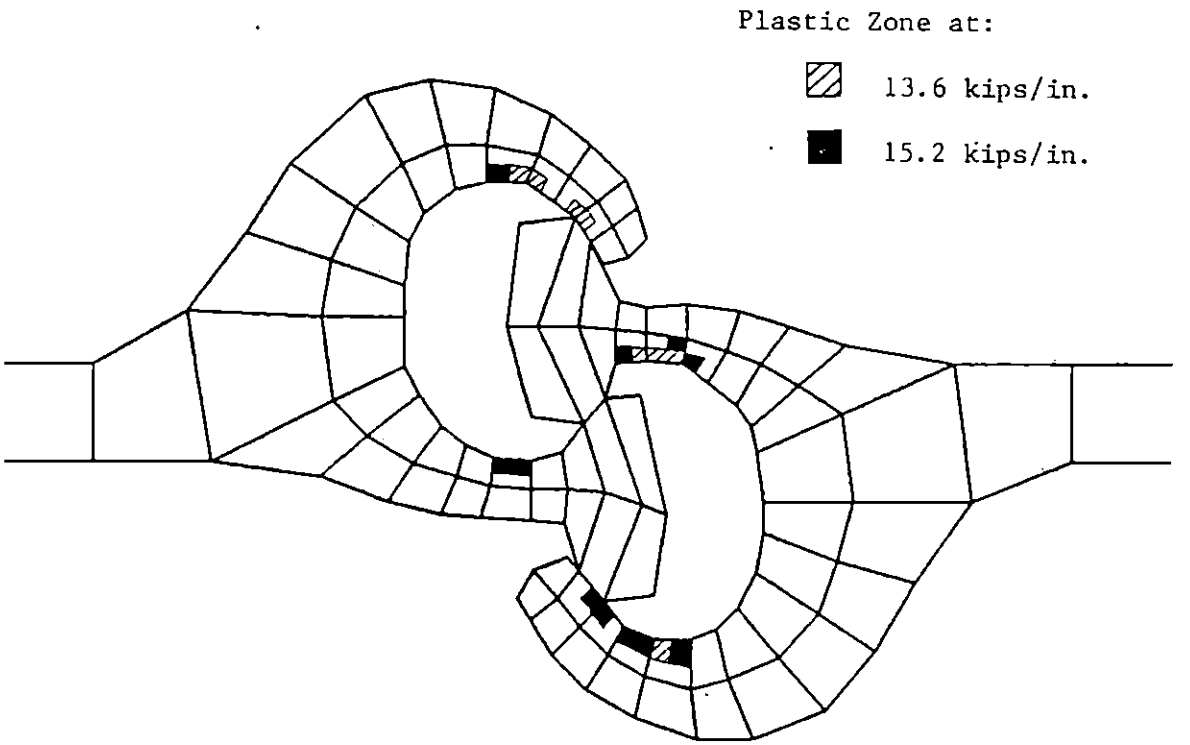

Figure 6.56: Growth of Plastic Zone in PS32 Sheet Pile (Case 3)

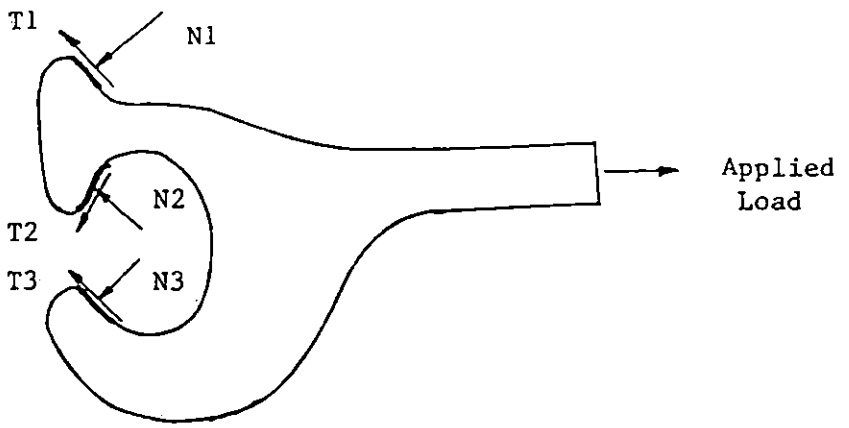

N1: normal contact force at contact segment 1

N2: normal contact force at contact segment 2

N3: normal contact force at contact segment 3

T1: tangential contact force at contact segment 1

T2: tangential contact force at contact segment 2

T3: tangential contact force at contact segment 3

Figure 6.57: Schematic Representation of Statics Check of Contact Forces in Sheet Pile

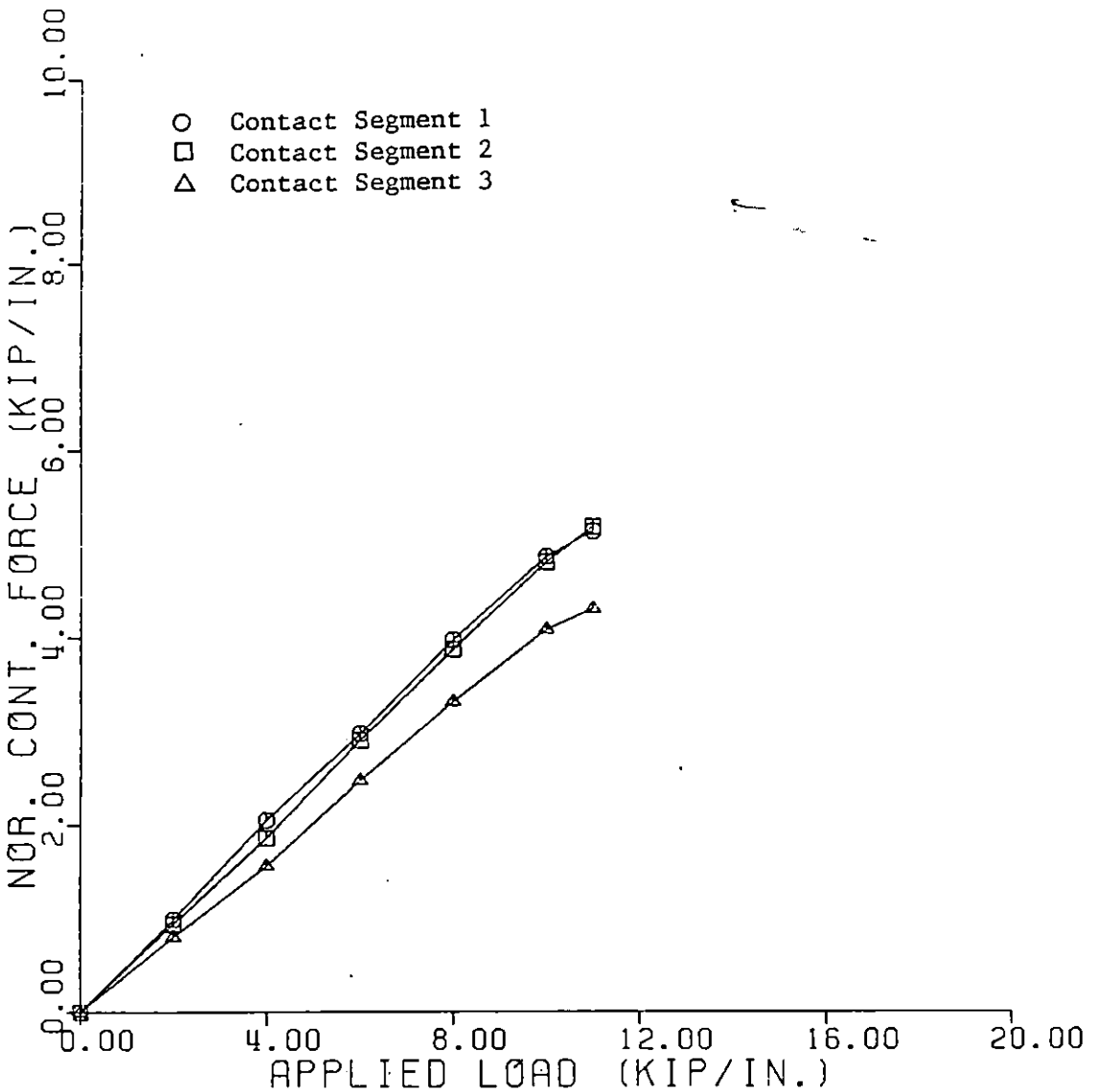

Figure 6.58: Normal Contact Force Versus Load for Case 1

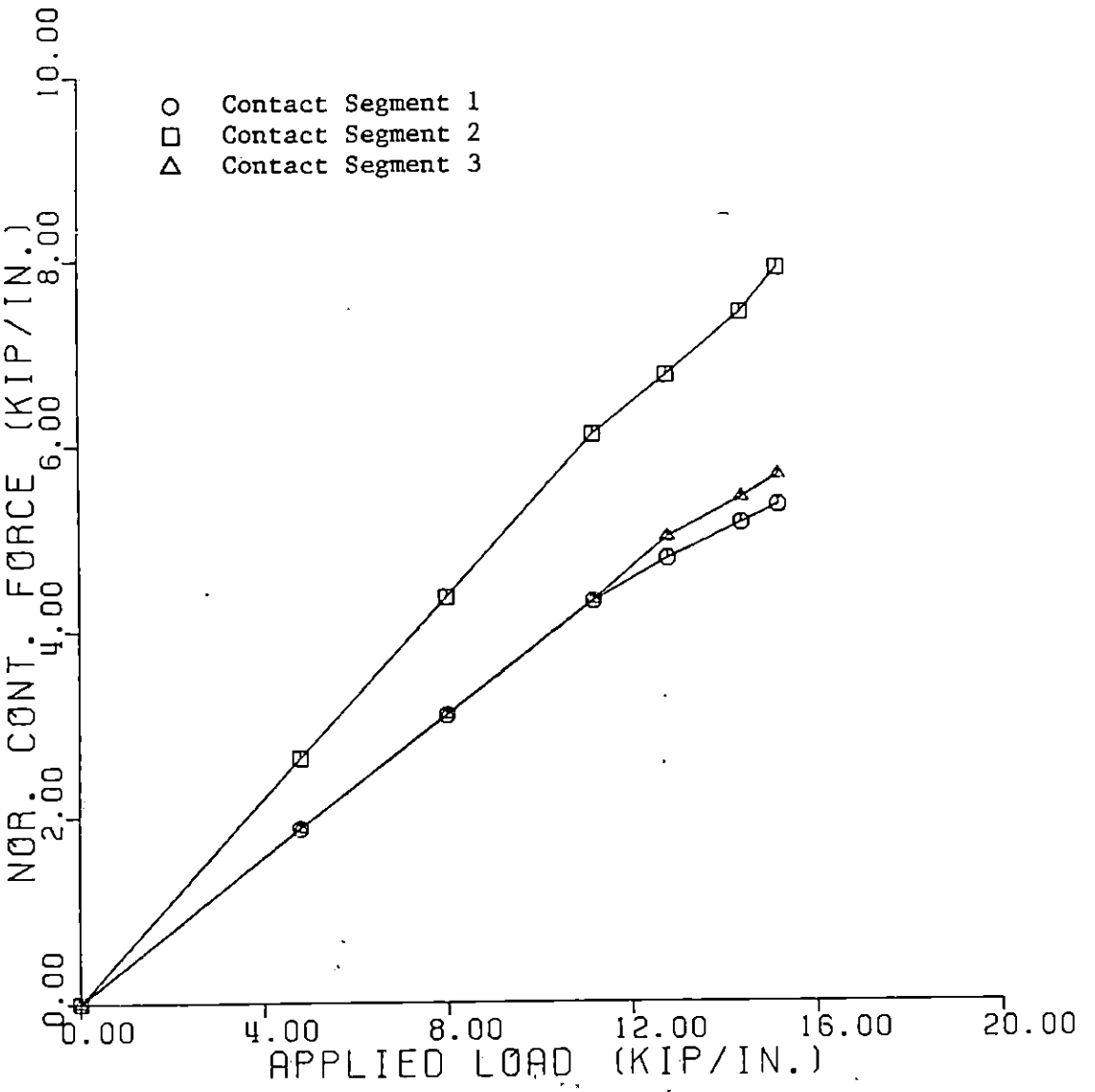

Figure 6.59: Normal Contact Force Versus Load for Case 3

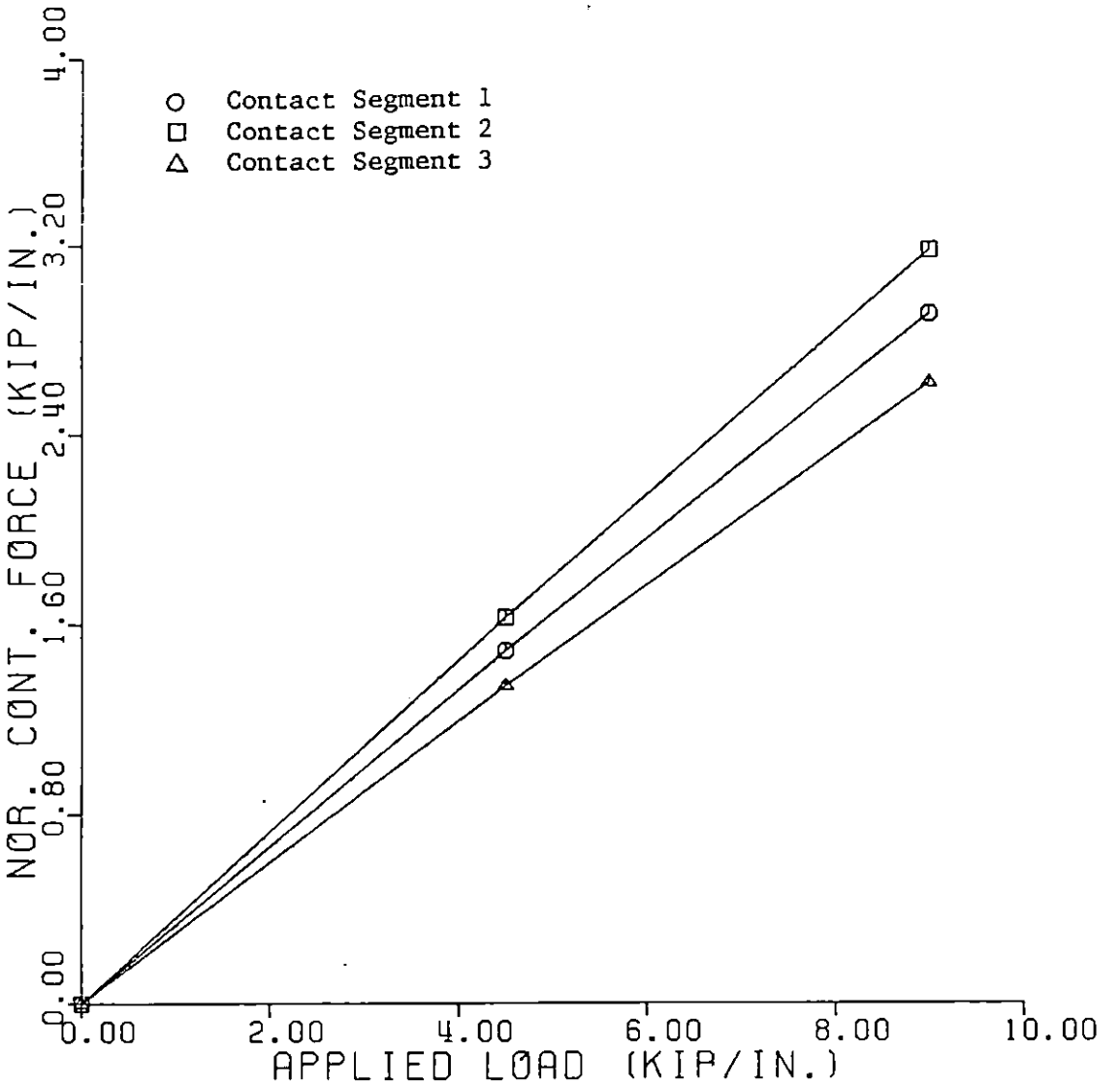

Figure 6.60: Normal Contact Force Versus Load for Case 4

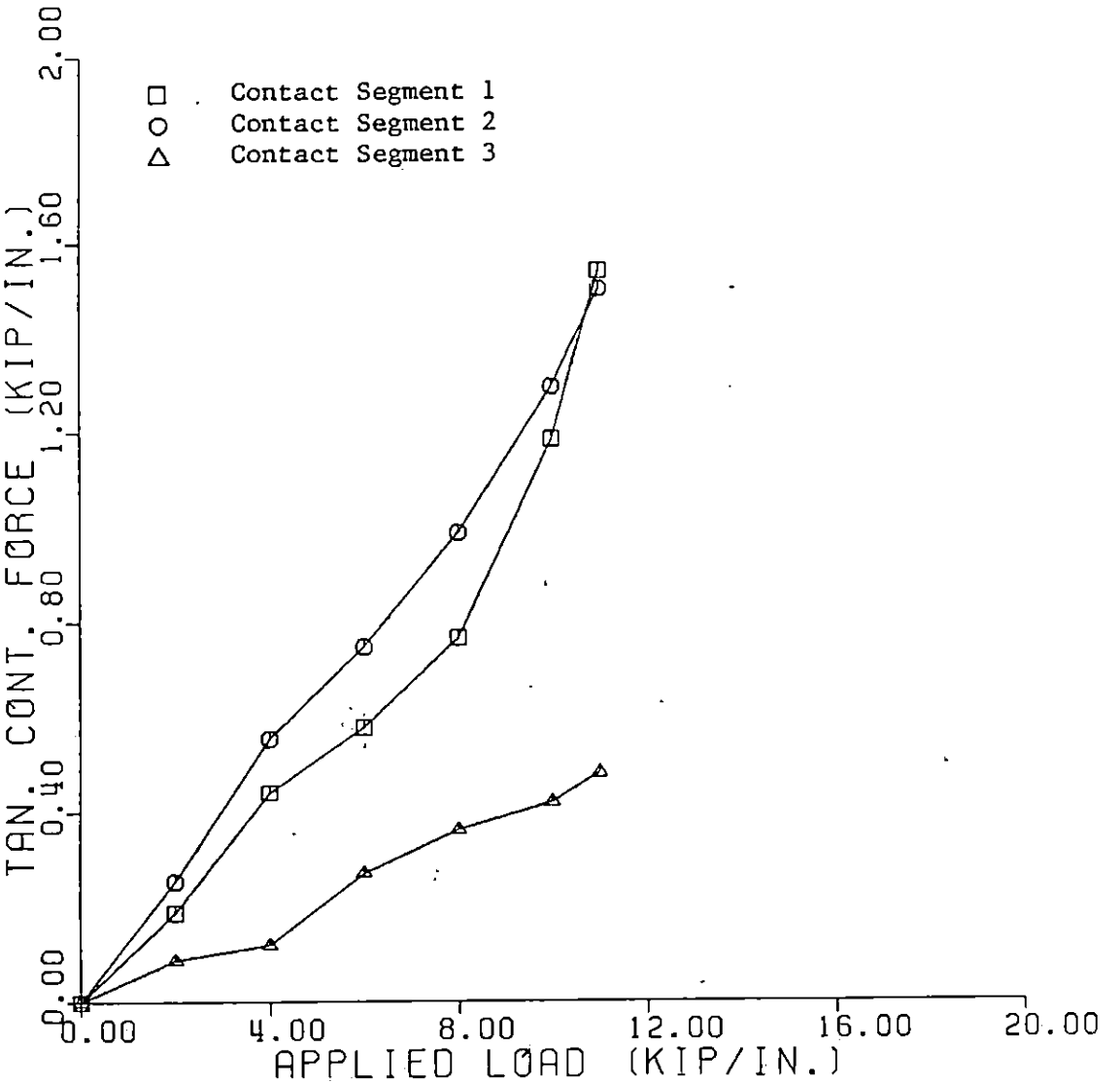

Figure 6.61: Tangential Contact Force Versus Load Plot For Case 1

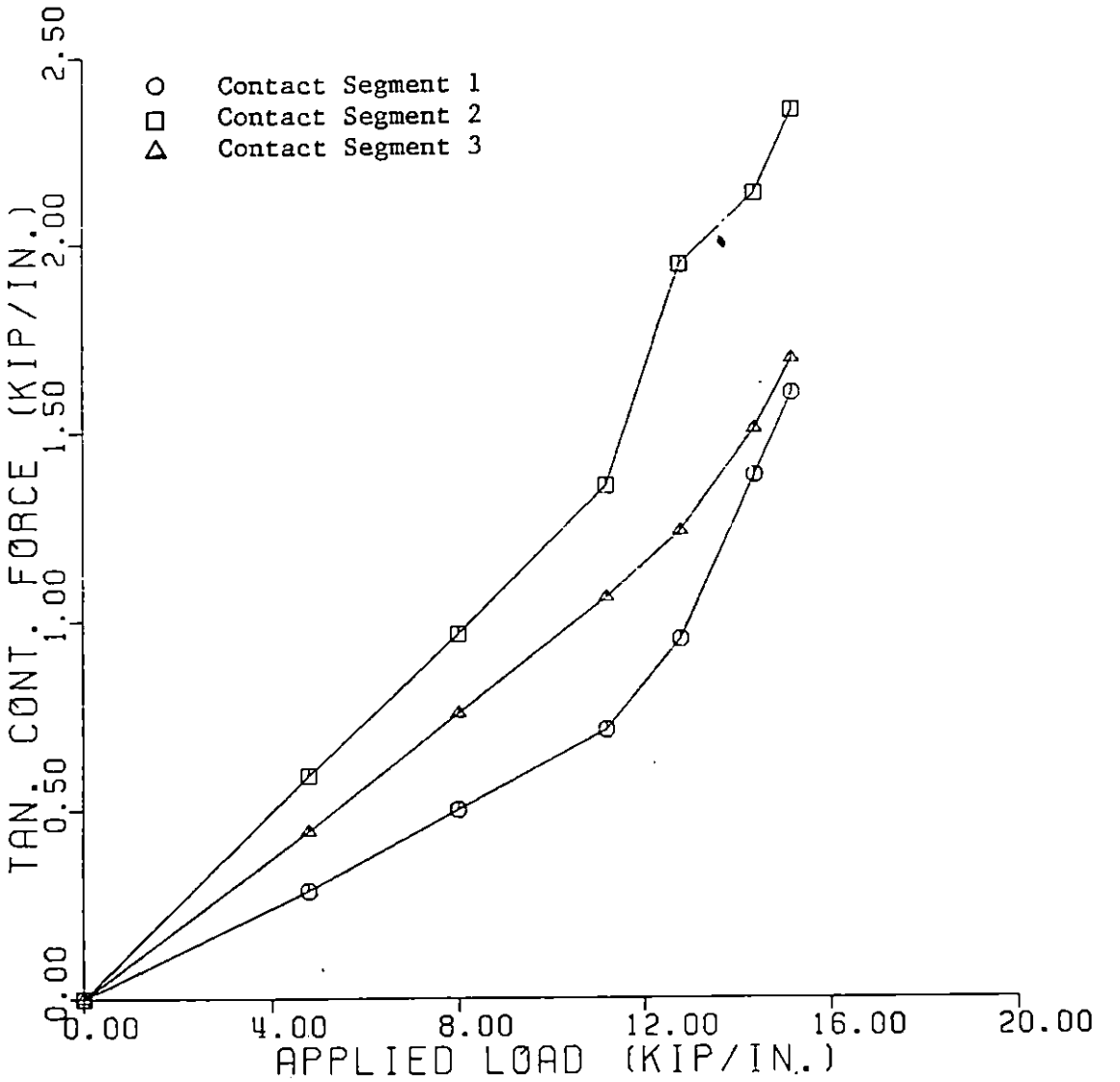

Figure 6.62: Tangential Contact Force Versus Load Plot for Case 3

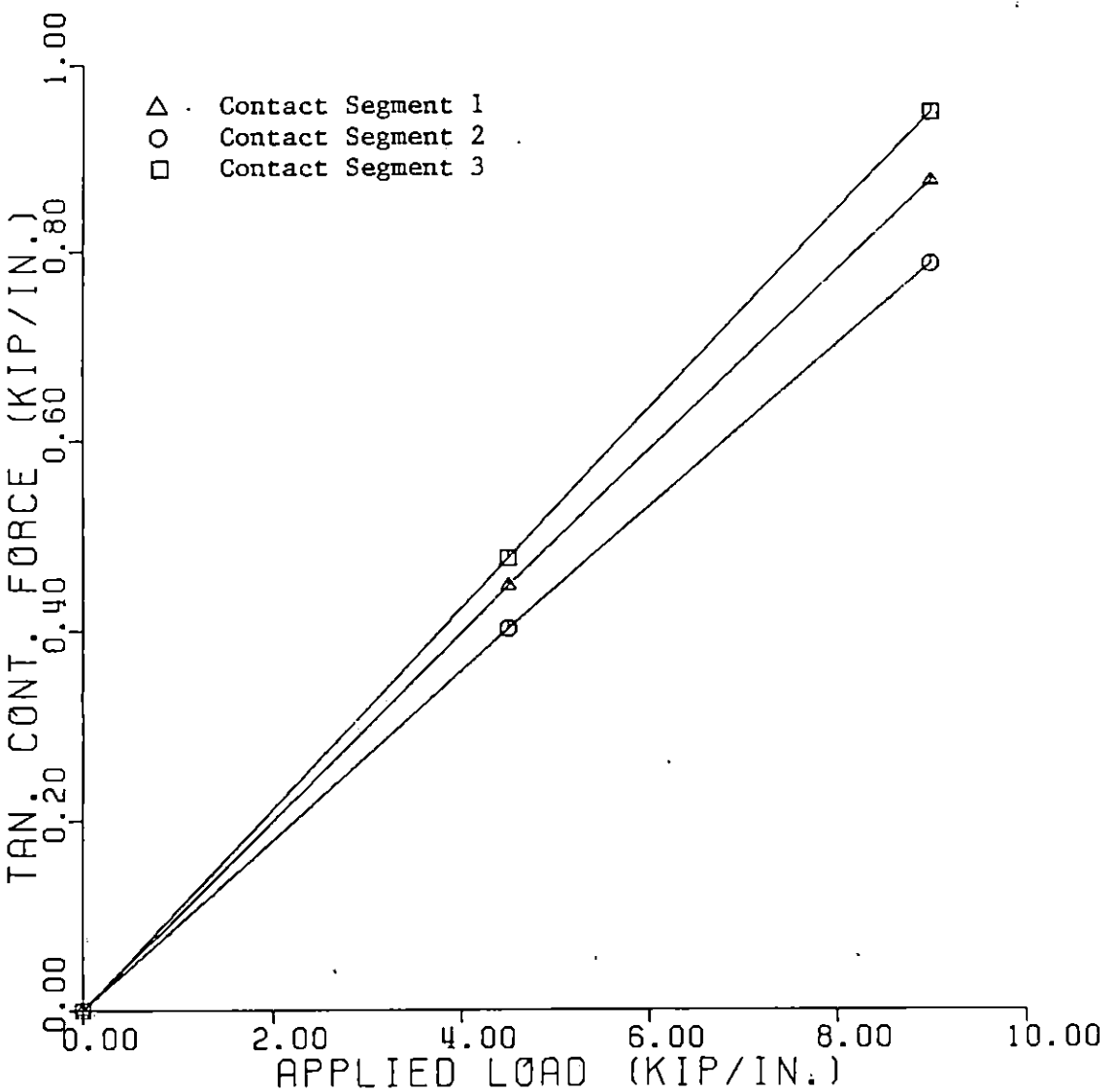

Figure 6.63: Tangential Contact Force Versus Load Plot For Case 4

Chapter VII

CONCLUSIONS, DISCUSSIONS, AND RECOMMENDATIONS

7.1 SUMMARY AND DISCUSSIONS OF SHEET PILE ANALYSIS WITH NO SLIDING ALLOWED

The purpose of this study is to investigate the behavior of sheet pile interlocks in an uniaxial pull test. The finite element models employed provide the load-displacement curves for PS32 and PSX32 sheet piles. Since the contact points in the interlocks are assumed not to slide relative to each other, the magnitudes of displacement obtained from the analyses are significantly lower than the experimental results by Shannon and Wilson (1983). With the use of "effective" modulus of elasticity for the sheet pile, the analytical results can give a reasonable estimate on the maximum elongation of the sheet pile in a pull test. Since in this study the contact points in the interlocks are fixed, additional constraints are imposed onto the system which affect the deformation pattern of the sheet piles. This is especially true for the bendings of the thumb and finger parts because of the change in load transfer positions.

However, this study does provide some insight on the properties of the interlocks. First consider the bending characteristics in the web of the sheet pile. For PS32 steel

the web will bend with single curvature while double curvatures are observed in PSX32 steel. These reflect the fact that the ratio of stiffness contributed by the web to the stiffness contributed by the interlock portion is larger in the PS32 sheet pile than the PSX32 sheet pile. Intuitively it can be seen that the interlock portion tries to move up and down as well as horizontally. This behavior depends on the ratio of the web stiffness to the interlock stiffness. If the ratio is small, as in the case of the PSX32 steel, the sheetpile will behave like a rigid mass attached on the tip of a beam. To maintain continuity in the system the slope of the end of the beam connected to the rigid mass has to be zero when the rigid mass moves vertically. Thus double curvatures result since the other end is fixed also. For PS32 sheet pile, since the stiffness ratio is high, the bending of the web will cause a rotation of the interlock portion and single curvature results.

A second observation from the analyses is the growth of plastic zones in the sheet piles. These patterns indicate the likelihood of failure mechanism in the system. The two possible failure modes are:

1. Forming of plastic hinges in the thumb and finger parts of the sheet pile.

2. Yielding of web in the sheet pile which result in excessive elongation in the system.

It can be seen from the results in this study that the regular strength sheet pile exhibits the first type of failure while the high strength sheet pile will fail by web yielding. It is also interesting to point out that in the analyses the PS32 sheet pile can reach the guaranteed interlock strength of 16 kips/in. but the PSX32 sheet pile fails to reach the guaranteed 28 kips/in. value due to yielding of the web at a lower load level.

7.2 SUMMARY AND DISCUSSIONS OF SHEET PILE ANALYSIS WITH SLIDING

The nonlinear moving contact algorithm with elastic-plastic material response and large displacement and rotation formulation is successful in modeling the tensile test of a sheet pile interlock connection. The locations of the three contact regions in the interlocks are assumed to be known a priori because of the variations in interlock geometry from one sheet pile to another. Thus the initial slacks between the interlocks are not modeled. Results of the analyses with discussions are summarized in the following:

1. The longitudinal displacements of the sheet pile interlock connection increase as a resulst of sliding among the contact surfaces. Compared to the fixed

contact case, the increase is from 11 to 38 percent depends on the finite element model used.

2. There appears to be an inherent eccentricity in the interlock connection as relatively large lateral displacements occur when it is subjected to tension in a longitudinal direction. Sliding between the thumbs prematures failure of the connection (Cases 1 and 4).
3. A second mode of failure is observed when the fingers are softened to simulate the looseness of the interlock connection caused by geomtric irregularities. With lateral displacement restrained, the interlock connection fails due to sliding of the fingers over the thumbs (Case 2).
4. As a follow-up on (2), the relatively large lateral displacement in the sheet pile indicates a reduction of stiffness in the lateral direction in comparison with that of the fixed case. The E-ratios calculated are 0.058 and 0.065 for PS32 and PSX32 sheet piles respectively. Similar results are obtained by Barker et al (1985) in a sheet pile testing program.
5. As the tensile load is increased, yielding first takes place in the stem of the thumb and then at the contact surface in the finger portion of the interlock. When sliding begins, the shearing stresses in

the contact region drop slightly. Depending on the location in the sheet pile, yielding can be initiated by either combined effect of tensile and flexural stresses or by tensile and shearing stresses.

6. The bending in the web increases significantly when the contact regions are allowed to slide over each other. For the web of the sheet pile with the fixed end, double curvature is observed while single curvature is noted on the other web.

7.3 RECOMMENDATIONS FOR FUTURE STUDIES

From the results in this study the following recommendations are made to improve the usefulness of the computer program developed and also to investigate in detail other aspects concerned with the design and analysis of sheet pile interlock systems.

1. Rigorous mathematical studies on the convergence of the solution process especially when nonlinear material response is involved. Other factors which should be investigated are size of load increment, fineness of finite element mesh, and choices on number of contactor-target pairs.
2. Modeling of lateral earth pressure against a sheet pile section in a cellular cofferdam. This will re-

quire an angle change between the axis of adjacent sheet pile segments and a follower force algorithm for tracking the normal pressures as deformation takes place. Appropriate boundary constraints are required to simulate the radial displacements in the cofferdam cell.

3. Implement three-dimensional elements in the computer program to study the frictional resistance of the sheet pile interlocks against tilting of the cell.
4. Investigate the behavior of the wye section between the main and arc cells.
5. Modeling of initial slacks in the sheet pile interlock connection by a probabilistic approach. Other numerical tools such as stochastic finite element should be looked into as an alternative to analyze the problem.
6. Perform a shape optimization on the sheet pile interlock such that all types of failure modes observed will occur simultaneously. In this manner, the capacity of the whole pile is fully mobilized.
7. Study the behavior of the sheet pile interlock subjected to cyclic or dynamic loading such as wave and earthquake forces.

REFERENCES

1. Argyris, J.H. and Chan, A.S.L., "Static and Dynamic Elasto-Plastic Analysis by the Method of Finite Elements in Space and Time," in International Symposium on Foundations of Plasticity, (Ed. A. Sawczuk), Vol. I, 1972, p. 125.

2. Argyris, J.H., Doltsinis, J.St. and Kleiber, M., "Incremental Formulation in Nonlinear Mechanics and Large Strain Elasto-Plasticity--Natural Approach," Part II, Computation Method in Applied Mechanics and Engineering, Vol. 14, 1978, p. 259.

3. Argyris, J.H. and Kleiber, M., "Incremental Formulation in Nonlinear Mechanics and Large Strain Elasto-Plasticity--Natural Approach," Part I, Computer Methods in Applied Mechanics and Engineering, Vol. 11, 1977, p. 215.

4. Atluri, S., "On the Hybrid Stress Finite Element Model for Incremental Analysis of Large Deflection Problems," International Journal of Solids and Structures, Vol. 9, 1973, p. 1177.

5. Banerjee, P.K. and Fathallah, R.C., "An Eulerian Formulation of the Finite Element Method for Predicting Stresses and Pore Water Pressures Around a Driven Pile," Proceedings of the Third International Conference on Numerical Methods in Geomechanics, 1979, pp. 1053-1060.

6. Barker, R., Lewis, C., Oliver, W., and Mould, K., "Sheet Pile Interlock Connection Testing Program," Report No. VPI/CE-ST-85/01, Dept. of Civil Engrg., Virginia Tech, Blacksburg, VA, May, 1985.

7. Bathe, K.J., Finite Element Procedures in Engineering Analysis, Prentice Hall, Inc., New Jersey, 1982.

8. Bathe, K.J. and Chaudhary, A., "A Solution Method for Planar and Axisymmetric Contact Problems," International Journal for Numerical Methods in Engineering, Vol. 21, 1985, pp. 65-88.

9. Bathe, K.J. and Cimento, A.P., "Some Practical Procedures for the Solution of Nonlinear Finite Element Equations," Computer Methods in Applied Mechanics and Engineering, Vol. 22, 1980, pp. 59-85.

10. Bathe, K.J., Ozdemir, H. and Wilson, E.L., "Static and Dynamic Geometric and Material Nonlinear Analysis," SESM Report No. 74-4, Dept. Civ. Engr., University of California, Berkeley, 1974.

11. Bathe, K.J., Ramm, E. and Wilson, E.L., "Finite Element Formulations for Large Deformation Dynamic Analysis," International Journal for Numerical Methods in Engineering, Vol. 9, 1975, pp. 353-386.

12. Bathe, K.J. and Wilson, E.L. and Iding, R., "NONSAP--A Structural Analysis Program for Statics and Dynamic Response of Nonlinear Systems," SESM Report No. 74-3, Dept. Civ. Engr., University of California, Berkeley, 1973.

13. Belz, C.A., "Cellular Structure Design Methods," Conference on Design and Installation of Pile Foundations and Cellular Structures, Ed. Fang, H.Y. and Dismuke, T.D., Lehigh University, 1970, pp. 319-338.

14. Bower, J.E., "Predicted Pullout Strength of Sheet-Piling Interlocks," Journal of Soil Mechanics and Foundation Design, ASCE, Vol. 99, Oct. 1973, pp. 765-781.

15. Chan, M. and Barker, R., "Finite Element Studies of Sheet Pile Interlock Connection," Report No. VPI/CE-ST-85/02, Dept. of Civil Engrg., Virginia Tech, Blacksburg, VA, May 1985.

16. Chan, S.K. and Tuba, I.S., "A Finite Element Method for Contact Problems of Solid Bodies--Part I. Theory and Validation," International Journal of Mechanical Science, Vol. 13, 1971, pp. 615-625.

17. Chang, S.H. and Salamon, N.J., "The Influence of Plastic Behavior on Contacting Bodies--A Finite Element Simulation," Proceedings 21st. Annual Meeting Society of Engineering Science, Blacksburg, VA, 1984.

18. Clough, G.W. and Kuppusamy, T., "Finite Element Analysis of Lock and Dam #26 Coffercam," Journal of Geotechnical Engineering, ASCE, Vol. 111, No. 4, pp. 521-541, April, 1985.

19. Cook, R.C., Concepts and Applications of Finite Element Analysis, John Wiley and Sons, Inc., London, 1974.

20. Desai, C.S., Elementary Finite Element Method, Prentice-Hall Inc., New Jersey, 1979.

21. Desai, C.S., Perumpral, J.V., Sture, S. and Phan, H.V., "Geometric and Material Nonlinear Three Dimensional Finite Element Analysis for Structures Moving in Ground," Rep. No. VPI-E 78.11, Dept. of Civil Engineering, Virginia Polytechnic Institute and State University, 1978.

22. Desai, C.S., Zaman, M.M., Lightner, J.G. and Siriwardane, H.J., "Thin-Layer Element for Interfaces and Joints," International Journal for Numerical and Analytical Methods in Geomechanics, Vol. 8, No.1, 1984, pp. 19-44.

23. Dieterich, J.H., "Time-Dependent Friction and the Mechanics of Stick-Slip," Pure Applied Geophysics, Vol. 116, 1978, pp. 790-806.

24. Drucker, D.C., Plasticity. Structural Mechanics, Ed. by Goodier, J.N. and Hoff, N.J., Pergamon Press, 1960.

25. Francavilla, A. and Zienkiewicz, O.C., "A Note on Numerical Computation of Elastic Contact Problems," International Journal for Numerical Methods in Engineering, Vol. 9, 1975, pp. 913-925.

26. Fredriksson, B., "Finite Element Solution of Surface Nonlinearities in Structural Mechanics with Special Emphasis to Contact and Fracture Mechanics problems," Computers & Structures, Vol. 6, 1976, pp. 281-290.

27. Fung, Y.C., Foundations of Solid Mechanics, Prentice-Hall, Inc., New Jersey, 1965.

28. Gadala, M.S., Dokainish, M.A. and Oravas, G.AE., "Geometric and Material Nonlinearity Problems--Lagrangian and Updated Lagrangian Formulations," Proceedings on the Second International Conference on Numerical Methods in Fracture Mechanics, Swansea, United Kingdom, 1980, p. 277.

29. Gadala, M.S., Oravas, G.AE. and Dokainish, M.A., "A Consistent Eulerian Formulation of Large Deformation Problems in Statics and Dynamics," International Journal of Nonlinear Mechanics, Vol. 18, No. 1, 1983, pp. 21-35.

30. Gaertner, R., "Investigation of Plane Elastic Contact Allowing for Friction," Computers & Structures, Vol. 7, 1977, pp. 59-63.

31. Green, A.E. and Nagdhi, P.M., "A General Theory of an Elastic-Plastic Continuum," Arch. Rat. Mech. Anal., Vol. 18, 1965.

32. Gunasekera, J.S. and Alexander, J.M., "Matrix Analysis of the Large Deformation of an Elastic-plastic Axially Symmetric Continuum," in International Symposium on Foundations of Plasticity, Ed. Sawczuk, A., Vol. I, 1972, p. 125.

33. Hatt, F., "Three-Dimensional Finite Element Analysis Including Elastic-Plastic Material Response," Ph. D. Dissertation, Virginia Polytechnic Institute and State University, Blacksburg, Virginia, July, 1974.

34. Herrmann, L.R., "Finite Element Analysis of Contact Problem," Journal of Engineering Mechanics Division, ASCE, Vol. 104, 1978, pp. 1043-1058.

35. Hill, R., The Mathematical Theory of Plasticity, Oxford Press, London, 1950.

36. Hill, R., "Some Basic Principles in the Mechanics of Solids Without a Natural Time," Journal of Mechanics, Physics, and Solids, Vol. 7, 1959, p. 209.

37. Hofmeister, L.D., Greenbaum, G.A. and Evensen, D.A., "Large Strain Elastic-plastic Finite Element Analysis," AIAA Journal, Vol. 9, 1971, pp. 1248-1254.

38. Holden, J.T., "On the Finite Deflections of Thin Beams," International Journal of Solids and Structures, Vol. 8, 1972, pp. 1051-1055.

39. Hughes, T.J.R., Taylor, R.L. and Kanoknukulchai, W., "A Finite Element Method for Large Displacement Contact and Impact Problems," Formulations and Computational Algorithms in Finite Element Analysis: U.S.--Germany Symbosium, Ed. Bathe, K.J., Oden, J.T. and Wunderlich, W., M.I.T. Press, 1977. pp.468-495.

40. Hutchinson, J.W., "Finite Strain Analysis of Elastic Plastic Solids and Structures," Numerical Solution of Nonlinear Structural Problems, Ed. Hartung, R.F., Vol. 17, ASME, New York, 1973, pp. 17-29.

41. Katona, M.G., "A Simple Contact-Friction Interface Element with Applicaitons to Buried Culverts," International Journal for Numerical and Analytical Methods in Geomechanics, Vol. 7, 1983, pp. 371-384.

42. Kumar, S., Garg, V.K. and Armigeri, B., "Adhesion and Creep Zone Investigation of Planar Elastic Steel on Steel Contacts With Friction--A Finite Element Analysis," The General Problem of Rolling Contact, Ed. Browne, A.L. and Tsai, N.T., 1980, pp. 107-119.

43. Lee, B.C. and Byung, M.K., "A Computational Method for Elasto-Plastic Contact Problems," Computers & Structures, Vol. 18, 1984, pp. 757-765.

44. Lee, E.H., "Elastic-Plastic Deformation at Finite Strains," Journal of Applied Mechanics, Trans. of ASME, Vol. 38, 1969.

45. Malvern, L.E., Introduction to the Mechanics of a Continuous Medium, Prentice-Hall, Inc., New Jersey, 1969.

46. McMeeking, R.M. and Rice, J.R., "Finite Element Formulation for Problems of Large Elastic-plastic Deformation," International Journal of Solids and Structures, Vol. 11, 1975, pp. 601-616.

47. Murray, P.W. and Wilson, E.L., "Finite Element Large Deflection Analysis of Plates," Journal of Engineering Mechanics Division, ASCE, Vol. 94, 1965, pp. 143-165.

48. Nakanishi, T., Takeda, H., Hashimoto, T., Miura, H. and Shibata, K., "Interlock Strength of Flat Type Steel Sheet Piling," Kawasaki Steel Technical Report No.2, March, 1981.

49. Nayak, G.C., and Zienkiewicz, O.C., "Elasto-Plastic Stress Analysis. A Generalization for Various Constitutive Relations Including Strain Softening," International Journal for Numerical Methods in Engineering, Vol. 5, 1972, pp. 113-135.

50. Oden, J.T., Finite Elements of Nonlinear Continua, McGraw Hill, New York, 1972.

51. Oden, J.T. and Campos, L., "Some New Results on Finite Element Methods for Contact Problems with Friction," Finite Elements, Ed. Becker, E.B., Carey, G.F., and Oden, J.T., Vol. 5, 1981.

52. Oden J.T. and Kikuchi, N., "Finite Elements for Constrained Problems in Elasticity," International Journal for Numerical Methods in Engineering, Vol. 18, 1982, pp. 701-725.

53. Oden, J.T. and Pires, E.B., "Nonlocal and Nonlinear Friction Laws and Variational Principles for Contact Problems in Elasticity," Journal of Applied Mechanics, ASME, Vol. 50, 1983, pp 67-76.

54. Ohte, S., "Finite Element Analysis of Elastic Contact Problems," Bulletine of Japan Society of Mechanical Engineers, Vol. 16, May, 1973, pp. 797-804.

55. Okamota, N. and Nakazawa, M., "Finite Element Incremental Contact Analysis with Various Frictional Conditions," International Journal for Numerical Methods in Engineering, Vol. 14, 1979, pp. 337-357.

56. Oliver, W.B. Jr., "An Experimental Investigation of the Static Coefficient of Friction for Sheet Pile Interlocks," M. S. Thesis, Virginia Polytechnic Institute and State University, Blacksburg, Virginia, January, 1985.

57. Olson, M.D., "The Mixed Finite Element Method in Elasticity and Elastic Contact Problems," Hybrid and Mixed Finite Element Methods, Ed. Atluri, S.N., Gallagher, R.J. and Zienkiewicz, O.C., 1983, pp. 19-49.

58. Osias, J.R. and Swedlow, J.L., "Finite Elasto-Plastic Deformation I: Theory and Numerical Examples," International Journal of Solids and Structures, Vol. 10, 1974, pp. 321-339.

59. Ostachowicz, W., "Mixed Finite Element Method for Contact Problems," Computers & Structures, Vol. 18, 1984, pp. 937-945.

60. Petersson, H., "Application of Finite Element Method in the Analysis of Contact Problems," Proceedings of the International Conference on Finite Elements in Nonlinear Solids and Structural Mechanics, Geilo, Norway, Vol.2, 1977, pp. 845-862.

61. Pian, T.H.H. and Kubomura, K., "Formulation of Contact Problems by Assumed Stress Hybrid Element," Nonlinear Finite Element Analysis in Structural Mechanics, Ed. Wunderlich, W. et al, Springer-Verlag,1981, pp. 49-59.

62. Popov, E.P., "Lecture Notes on Plasticity," University of California, Berkeley, September, 1981.

63. Rahman, M.U., Rowlands, R.E., Cook, R.D. and Wilkinson, T.L., "An Iterative Procedure for Finite Element Stress Analysis of Frictional Contact Problems," Computers & Structures, Vol. 16, 1984, pp. 947-954.

64. Rossow, M., "A Simple Model for Analyzing Cofferdam Sheetpile Interlock Forces," Internal Report, U. S. Corps of Engineers, St. Louis District, 1982.

65. Sachdeva, T.D. and Ramakrishnan, C.V., "A Finite Element Solution for the Two-Dimensional Elastic Contact Problems with Friction," International Journal for Numerical Methods in Engineering, Vol. 17, 1981, pp. 1257-1271.

66. Shannon & Wilson, Inc., "Sheet Pile Interlock Testing," Final Report Task 6.1 Through 6.7, Lock and Dam No. 26 (Replacement), Mississippi River--Alton, Illinois, Department of the Army, St. Louis District, Corps of Engineers, March, 1983.

67. Sharifi, P. and Yates, D.N., "Nonlinear Thermo-Elastic-Plastic and Creep Analysis by the Finite Element Method," AIAA Paper No. 37-358, AIAA/ASME/SAE 14th. Structural Dynamics and Materials Conference, Williamsburg, Virginia, 1973.

68. Simo, J.C., Wriggers, P. Schweizerhof, K.H. and Taylor, R.L., "Finite Deformation Postbuckling Analysis Involving Inelasticity and Contact Constraints," Proceedings of the International Conference on Innovative Methods for Nonlinear Problems, Ed. Liu, W.K., Belytschko, T. and Park, K.C., 1984, pp. 365-388.

69. Stricklin, J.A. and Haisler, W.E., "Formulation and Solution Procedures for Nonlinear Structural Analysis" Computers & Structures, Vol. 7, 1974, pp. 125-136.

70. Stricklin, J.A., Von Riesemann, W.A. and Haisler, W.E., "Geometrically Nonlinear Structural Analysis by Direct Stiffness Method," Journal of Structural Division, ASCE, Vol. 97, No. 9, 1971, pp. 2299-2314.

71. Stricklin, J.A., Von Riesemann, W.A., Tillerson, J.R. and Haisler, W.E., "Static Geometric and Material Nonlinear Analysis," Advances in Computational Methods in Structural Mechanics and Design, Second U. S.--Japan Seminar Matrix Methods in Structural Analysis and Design, University of Alabama Press, 1972, pp. 301-324.

72. Theocaris, P.S. and Marketos, E., "Elastic-Plastic Analysis of Perforated Thin Strips of Strain-Hardening Material," Journal of Mechanics, Physics, and Solids, Vol. 12, 1964, pp. 377-390.

73. Timoshenko, S.P. and Goodier, J.N., Theory of Elasticity, Third Edition, McGraw-Hill Book Company, 1970.

74. Torstenfelt, B., "Contact Problems in General Purpose Finite Element Computer Programs," Computers & Structures, Vol. 16, 1983, pp. 487-493.

75. Tseng, J. and Olson, M.D., "The Mixed Finite Element Method Applied to Two-Dimensional Elastic Contact Problem," International Journal for Numerical Methods in Engineering, Vol. 17, 1981, pp. 991-1014.

76. Tsuta, T. and Yamaji, S., "Finite Element Analysis of Contact Problem," Theory and Practice in Finite Element Structural Analysis, University of Tokyo Press, 1973, pp. 177-194.

77. United State Steel, Steel Sheet Piling Handbook, May, 1983.

78. Washizu, K., Variational Methods in Elasticity and Plasticity, Pergamon Press, New York, 1975.

79. Wilson, E.A. and Parsons, B., "Finite Element Analysis of Elastic Contact Problems Using Differential Displacement," International Journal for Numerical Methods in Engineering, Vol. 2, 1970, pp. 387-395.

80. Wunderlich, W., "Incremental Formulations for Geometrically Nonlinear Problems," Formulations and Computational Algorithms in Finite Element Analysis: U. S.--Germany Symposium, Ed. Bathe, K.J. et al, 1976, pp. 190-240.

81. Yaghmai, S. and Popov, E.P., "Incremental Analysis of Large Deflection of Shells of Revolution," International Journal of Solids and Structures, Vol. 7, 1971, pp. 1375-1393.

82. Yamada, Y., "Incremental Formulation for Problems with Geometric and Material Nonlinearities," in Advances in Computational Methods in Structural Mechanics and Design, Second U. S.--Japan Seminar Matrix Methods in Structural Analysis and Design, University of Alabama Press, 1972, pp. 325-355.

83. Yamada, Y., Hirakawa, T. and Wifi, A.S., "Analysis of Large Deformation and Bifurcation in Plasticity Problems by the Finite Element Method," in Finite Elements in Nonlinear Mechanics, Ed. Bergan, Pal G. et al, Vol. 1, 1977, pp. 393-412.

84. Yamada, Y. and Sakurai, T., "Basic Formulation and a Computer Program for Inelastic Large Deformation Analysis," Pressure Vessel Technology, Vol. 1, ASME, 1977, pp. 341-352.

85. Yamada, Y., Takatsuka, K. and Iwata, K., "Nonlinear Analysis by the Finite Element Method and Some Expository Examples," in Theory and Practice in Finite Element Structural Analysis, University of Tokyo Press, 1973, pp. 125-138.

86. Yamada, Y. and Wifi, A.S., "Large Strain Analysis of Some Geomechanics Problems by the Finite Element Method," International Journal of Numerical and Analytical Methods in Geomechanics, Vol. 1, 1977, pp. 299-318.

87. Yamada, Y., Yoshimura, N. and Sakurai, T., "Plastic Stress-Strain Matrix and its Application for the Solution of Elastic-Plastic Problems by the Finite Element Method," International Journal of Mechanics and Science, Vol. 10, 1968, pp. 343-354.

88. Yogeswaren, E.K., "Nonlinear Analysis of Variable Contactslip Behaviour of Structural Interfaces," M.S. Thesis, City University, London, November, 1983.

89. Zienkiewicz, O.C., The Finite Element Method, Third Edition, McGraw Hill, New York, 1977.

90. Zienkiewicz, O.C., Valliappan, S. and King, I.P., "Elasto-Plastic Solutions of Engineering Problems 'Initial Stress', Finite Element Approach," International Journal for Numerical Methods in Engineering, Vol. 1, 1969, pp. 75-100.

91. Zimmermann, T.K. and Liu, W.K., "Finite Elements for Contact Problems in Two-Dimensional Elastodynamics," Research in Nonlinear Structural and Solid Mechanics, Ed. McComb, H.G. Jr. and Noor, A.K., 1980, pp. 225-235.

Appendix A

CALCULATION OF NODAL CONTACT TRACTIONS

A "consistent" approach is used to relate the contact tractions to the nodal forces by linear interpolation. Figure A.1 illustrates a typical situation of contact tractions and nodal forces in a contact segment. For the contactor nodes, the following can be written

$$\begin{bmatrix} \Delta R_{1x} \\ \Delta R_{1y} \end{bmatrix} = h \begin{bmatrix} t_x^1 & t_x^2 \\ t_y^1 & t_y^2 \end{bmatrix} \begin{bmatrix} d_1/3 \\ d_1/6 \end{bmatrix}$$

$$\begin{bmatrix} \Delta R_{2x} \\ \Delta R_{2y} \end{bmatrix} = h \begin{bmatrix} t_x^1 & t_x^2 & t_x^3 \\ t_y^1 & t_y^2 & t_y^3 \end{bmatrix} \begin{bmatrix} d_1/6 \\ (d_1 + d_2)/3 \\ d_2/6 \end{bmatrix}$$

$$\begin{bmatrix} \Delta R_{i-1x} \\ \Delta R_{i-1y} \end{bmatrix} = h \begin{bmatrix} t_x^{i-2} & t_x^{i-1} & t_x^i \\ t_y^{i-2} & t_y^{i-1} & t_y^i \end{bmatrix} \begin{bmatrix} d_{i-2}/6 \\ (d_{i-2} + d_{i-1})/3 \\ d_{i-1}/6 \end{bmatrix}$$

$$\begin{bmatrix} \Delta R_{ix} \\ \Delta R_{iy} \end{bmatrix} = h \begin{bmatrix} t_x^{i-1} & t_x^i \\ t_y^{i-1} & t_y^i \end{bmatrix} \begin{bmatrix} d_{i-1}/3 \\ d_{i-1}/6 \end{bmatrix}$$

After assembly and by proper rearrangement, the set of equations can be formed as

$$h\begin{bmatrix} D \end{bmatrix}\begin{bmatrix} t \end{bmatrix} = \begin{bmatrix} \Delta R \end{bmatrix}$$

where h is the element thickness and D is a tridiagonal matrix. In full form, the above equation can be given as

$$h\begin{bmatrix}
d_1/3 & d_1/6 & & & & & & \\
d_1/6 & (d_1+d_2)/3 & d_2/6 & & & & & \\
 & d_2/6 & (d_2+d_3)/3 & d_3/6 & & & & \\
 & & \cdot & \cdot & \cdot & & & \\
 & & d_{i-1}/6 & d_{i-1}/3 & 0 & & & \\
 & & & 0 & d_1/3 & d_1/6 & & \\
 & & & & \text{REPEAT} & & & \\
 & & & & \text{ABOVE} & & & \\
 & & & & \text{(TRIDIAGONAL)} & & &
\end{bmatrix}
\begin{bmatrix} t_x^1 \\ t_x^2 \\ t_x^3 \\ \cdot \\ \cdot \\ \cdot \\ t_x^i \\ t_y^1 \\ t_y^2 \\ t_y^3 \\ \cdot \\ \cdot \\ \cdot \\ t_y^i \end{bmatrix} =
\begin{bmatrix} \Delta R_{1x} \\ \Delta R_{2x} \\ \Delta R_{3x} \\ \cdot \\ \cdot \\ \cdot \\ \Delta R_{ix} \\ \Delta R_{1y} \\ \Delta R_{2y} \\ \Delta R_{3y} \\ \cdot \\ \cdot \\ \cdot \\ \Delta R_{iy} \end{bmatrix}$$

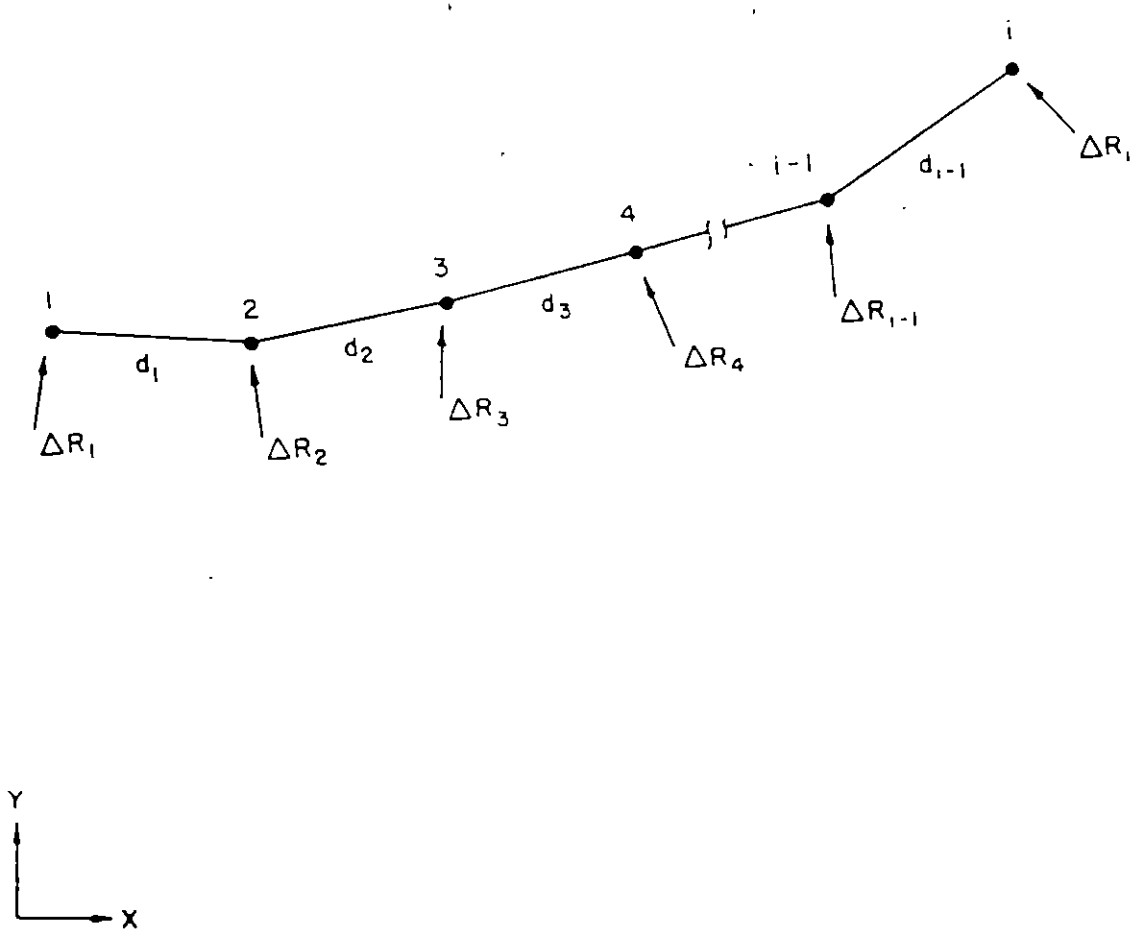

Figure A.1: Contact Tractions and Nodal Forces on a Contact Segment

The vita has been removed from the scanned document